



The University of  
**Nottingham**

UNITED KINGDOM • CHINA • MALAYSIA

# **Magnetic resonance imaging and spectroscopy of fat emulsions in the gastrointestinal tract**

Mahamoud Omar Hussein

Thesis submitted to the University of Nottingham for  
the degree of Doctor of Philosophy,

November 2012

# Dedication

This thesis is dedicated to  
my late Grandmother

Khadija Abdi Mohamed

# Abstract

The relationship between meal structure and composition can modulate gastrointestinal processing and the resulting sense of satiety. This applies also to the fat component of meals and particularly to the surface area available for digestion. The main hypothesis underpinning this thesis work was that fat emulsion droplet size has a profound effect on fat digestion and, in turn, on the gastrointestinal and satiety responses. To test this hypothesis two fat emulsion meal systems were used. They had exactly the same composition but a small (termed the Fine emulsion, with a droplet size of 400 nm) or a large (termed the Coarse emulsion, with a droplet size of 8  $\mu\text{m}$ ) emulsified fat droplet size. The two fat emulsion systems were manufactured and characterised using a range of bench techniques, in vitro digestion models and MRI techniques in vitro. The difference in microstructure caused different temporal creaming characteristics for the emulsions and different percentage hydrolysis profiles in a gastric digestion model in vitro. The Fine emulsion showed initial rapid hydrolysis whilst the Coarse emulsion showed an initial slow hydrolysis phase with the hydrolysis rate increasing at later stages. This indicated that there was indeed a droplet size effect on fat hydrolysis whereby the smaller droplet size with a larger surface area hydrolysed faster than a larger droplet size. The emulsions' performance was finally tested in vivo in healthy volunteers using MRI in a series of pilot studies leading to a main physiological study. Creaming differences in the gastric lumen were addressed by redesigning the meals using a locust bean gum (LBG) thickener that made them stable throughout the gastric emptying process. A main three-way physiological and satiety study in healthy volunteers showed that a highly emulsified, intragastrically stable emulsion delayed gastric emptying, increased small bowel water content and reduced consumption of food at the end of the study day. Finally, magnetic

resonance imaging, relaxometry and spectroscopy were further evaluated to assess fat emulsion parameters in vitro and in vivo in the gastric lumen. Main static magnetic field and droplet size effects on T2 relaxation times of the Fine and the Coarse emulsions were observed. There was reasonable correlation between m-DIXON and spectroscopy methods to quantify fat fraction both in vitro and in vivo. Differences in T2 relaxation times for different droplet sizes of 20% fat emulsions were detected in vitro. These changes were however difficult to separate from creaming effects in vivo with a view of drawing meaningful inferences on droplet sizes. The main conclusion from this work was that manipulating food microstructure especially intragastric stability and fat emulsion droplet size can influence human gastrointestinal physiology and satiety responses and that MRI and MRS provide unique non invasive insights into these processes. This improved knowledge could help designing foods with desired health-promoting characteristics which could help to fight the rising tide of obesity.

# Acknowledgements

I want to express my deeply felt thanks and everlasting gratitude to my supervisors, Professor Penny Gowland and Dr Luca Marciani. I also would like to thank Professor Robin Spiller and Dr Caroline Hoad for their endless support and guidance throughout my PhD period. I cannot explain how grateful I am to be their student and the amount of support I was given during my time of my PhD. This work would never have taken shape without their expert advices and guidance. Also, my eternal gratitude to all those people I worked with at Unilever including Dr Pip Rayment, Dr Elisabetta Ciampi (the main two supervisors at Unilever), Dr Asish Nandi (who trained me with most of the techniques that were used for sample preparation and characterisation), Dr Nick Hedges for his expert contribution and other colleague at Unilever Discover including Dr Paul Sanderson who carried out the high resolution NRM experiments for the emulsion and raw material and Dr Steve Pregent who trained me the in vitro gastric model experiments and Mr Garry Susana who helped me to run the gas chromatography (GC). Dr Gulzar Singh for running the CCK assay for me and all the BRU Nurses who helped us to do cannulation and getting blood samples from our volunteers.

Special thanks also to Dr. Harry F Peters for their expert input to this work. I would like to express my sincere thanks to Dr. Eleanor Cox, Ms Carolyn Costigan and Ms Susan Prichard for their help on scanning. Enormous thanks go to Dr. Paul Glover for doing my 2 previous vivas and giving me his view about the work and guided me how to tackle any problems. Also big thanks to Dr Elisa Placidi and Gemma Chaddock for doing double blinding for my data. Enormous thanks must go to Dr. Andrew Peters for his willing to help me through whenever I had problem with my PC. Special thanks to Dr Mary

Stephenson, Dr Samuel Wharton, Dr Kathryn Murray, Dr. Olivier Mougin and Dr. Rosa Sanchez, Dr Emma Hall and Dr Devasuda Anblagan and Dr Waldemar Senczenko, Dr Yana Yin and Dr Ian Driver for their great help and for being very special friends. I would also like to extend my thanks to all my colleagues in upstairs office past and present including Steve, Saddiq, Andre, Paula, Gerda, Glyn, Anna, Alexandra, Gregg, Karan, Ayu, Ingrid, Charlotte and James. Very special thanks go to all people in the downstairs and upstairs offices Theo, Turki, Jack, Maria, Bader, Peter, Tom, Saeed, Amul, Matthew, Chen and anyone whose name I have left out. Very warm thanks to Lesley Martin and Elizabeth Croal for their help throughout my PhD. I would like to thank all my housemates for being very supportive and helpful during the time of my PhD.

I would like to thank my family for their continuous support and help throughout my undergraduate and postgraduate degrees. Special thanks must go to my father, my mother and my aunties for devoting their lives to support me throughout my life. Also, I would like to thank my brothers Ahmed, Abdul-Aziz, Mohamed, Mustafa and my sisters Halima and Fatima.

# Abbreviations

ANOVA	Analysis Of Variance
AUC	Area under Curve
BMI	Body Mass Index
bTFE	balanced Turbo Field Echo
CSF	CerebroSpinal Fluid
CSI	Chemical Shift Imaging
CT	Computed Tomography
CV	Coefficient of Variation
DC	Descending Colon
EPI	Echo planar imaging
ETL	Echo Train Length
FDA	Food and Drug Administration
FFE	Fast Field Echo
FID	Free Induction Decay
FISP	Fast Imaging with Steady Precession
FLASH	Fast Low Angle SHot
FOV	Field Of View
FSE	Fast Spin Echo
FT	Fourier Transform
GE	Gradient Echo
GI	Gastrointestinal
GRASS	Gradient Recalled Acquisition in Steady State
HASTE	Half Fourier Acquisition Single-shot Turbo spin-Echo
HFB	HexaFluoroBenzene
IBS	Irritable Bowel Syndrome
ICJ	Ileo-Caecal Junction

IR	Inversion Recovery
LBG	Locust Bean Gum
MIP	Maximum Intensity Projection
MRI	Magnetic Resonance Imaging
MRS	Magnetic Resonance Spectroscopy
(N)MR	(Nuclear) Magnetic Resonance
NSA	Number of Signal Averages
ppm	parts per million
RARE	Rapid Acquisition with Relaxation Enhancement
PRESS	Point-Resolved Spectroscopy Sequence
RF	Radio Frequency
ROI	Region Of Interest
SB	Small Bowel
SBWC	Small Bowel Water Content
SE	Spin Echo
SEM	Standard Error of the Mean
SNR	Signal to Noise Ratio
SOP	Standard Operating Procedure
SPGR	SPOiled Gradient Recalled echo
STEAM	STimulated Echo Acquisition Mode
SVM	Support Vector Machine
TC	Transverse Colon
TSE	Turbo Spin Echo

# Symbols

$B_0$	polarising, static magnetic field
$G_z$	linear field gradient amplitude in the z direction
$\hbar$	Planck's constant divided by $2\pi$
$I$	spin quantum number
$J$	spin angular momentum
$k$	reciprocal space vector
$k_B$	Boltzmann's constant
$R^2$	correlation coefficient
$t$	time
$T_1$	spin-lattice relaxation time
$T_2$	spin-spin relaxation time
$T_{50\%}$	half emptying time for total gastric volume
w/w	weight/weight
$\gamma$	magnetogyric ratio
$\rho$	spin density
$\mu$	magnetic moment
$\omega_0$	Larmor precession frequency

# Table of Contents

1	Introduction .....	7
1.1	Background.....	7
1.2	Overall aims of this thesis .....	9
1.3	Thesis overview .....	9
2	NMR, MRI and MRS .....	12
2.1	Nuclear Magnetic Resonance .....	12
2.1.1	The nuclear spin.....	13
2.1.2	Quantisation of energy .....	13
2.1.3	Energy level populations .....	16
2.1.4	Spin and angular momentum .....	17
2.1.5	The Larmor precession .....	18
2.1.6	The Bloch equation of motion.....	19
2.1.7	Interaction with electromagnetic radiation.....	19
2.1.8	Free induction decay .....	21
2.1.9	The relaxation times $T_1$ and $T_2$ and their measurement.....	21
2.1.10	Fourier transform NMR.....	26
2.2	Magnetic Resonance Imaging.....	27
2.2.1	Linear gradients and gradient coils.....	28
2.2.2	Slice selection .....	30
2.2.3	k space .....	31
2.2.4	Imaging sequences .....	32
2.2.5	Fat suppression.....	35
2.3	Magnetic Resonance Spectroscopy .....	37
2.3.1	Chemical shift .....	38

## Table of Contents

2.3.2	Spatial localisation based on single voxel technique .....	38
2.3.3	MRS spectra quantification .....	39
2.3.4	Limitation of MRS.....	40
3	The gastrointestinal tract and its response to fat: MRI assessment.....	41
3.1	Background.....	41
3.2	Anatomy and function of the gastrointestinal tract .....	42
3.2.1	The oral cavity (mouth).....	43
3.2.2	The stomach .....	45
3.2.3	The small bowel .....	46
3.2.4	The colon .....	47
3.2.5	Gastrointestinal response to a meal .....	48
3.2.6	Gastrointestinal responses to fat .....	48
3.2.7	Fat bioavailability.....	49
3.2.8	Satiety responses.....	51
3.2.9	MRI of GI tract.....	51
3.2.10	Gastric volume measurement.....	52
3.2.11	MRI of gallbladder volume.....	53
3.2.12	MRI of small bowel water contents.....	53
4	Methods.....	55
4.1	Bench techniques at Unilever.....	55
4.1.1	Homogenisers and microfluidiser .....	55
4.1.2	Droplet size analysis .....	58
4.1.3	Rheology.....	60
4.2	MRI scanners.....	61
4.2.1	Scan day organisation.....	62
4.3	Breath test and plasma assay methods.....	63
4.3.1	IRIS Machine for breath samples .....	63
4.3.2	CCK plasma assay.....	65

## Table of Contents

4.4	Ethical approvals and GCP standards.....	67
5	Development work on fat emulsion systems and their characterisation ..	69
5.1	Background.....	69
5.2	Initial development and characterisation .....	70
5.2.1	Initial MRI assessment .....	72
5.2.2	Fat emulsions stability .....	73
5.3	<i>In vitro</i> gastric model experiment.....	81
5.3.1	Preparation of fat emulsions and LBG solutions .....	82
5.3.2	Preparation of gastrointestinal model solutions .....	82
5.3.3	Droplet size measurements.....	83
5.3.4	pH stat experiment .....	84
5.3.5	Tributylin experiment.....	87
5.3.6	Gas chromatography.....	88
5.3.7	Analysis.....	90
5.3.8	Results .....	94
5.4	<i>In vivo</i> pilot studies without thickener .....	96
5.4.1	Gastric emptying .....	97
5.4.2	Gallbladder contraction .....	100
5.4.3	Small bowel water content .....	101
5.4.4	<sup>13</sup> C breath test.....	106
5.4.5	Introducing a gum stabiliser in the emulsion.....	106
5.5	<i>In vivo</i> scouting pilot with thickener .....	107
5.5.1	Gastric emptying .....	108
5.5.2	Gallbladder contraction .....	110
5.5.3	Small Bowel water content .....	110
5.6	Discussion .....	112
5.6.1	<i>In vitro</i> bench characterisation.....	112
5.6.2	<i>In vivo</i> pilot MRI studies .....	115

## Table of Contents

5.7	Conclusion .....	116
6	Effect of fat emulsion intragastric stability and droplet size on gastrointestinal responses .....	117
6.1	Background.....	117
6.2	Specific methods and protocol .....	119
6.2.1	Fat emulsions.....	119
6.2.2	Subjects .....	121
6.2.3	MRI methods.....	123
6.2.4	Blood sampling.....	124
6.2.5	Objective pasta meal.....	125
6.2.6	Statistics.....	125
6.2.7	Safety and efficacy .....	126
6.3	Results.....	127
6.3.1	Bench checks on the test meals .....	127
6.3.2	MRI imaging.....	129
6.3.3	Gastric emptying .....	130
6.3.4	Fat/water ratio using MRS.....	130
6.3.5	Gallbladder contraction .....	133
6.3.6	Small bowel water content .....	133
6.3.7	Plasma cholecystokinin .....	134
6.3.8	Breath test.....	135
6.3.9	Satiety questionnaires .....	136
6.3.10	Objective satiety assessment.....	138
6.4	Discussion .....	139
6.5	Conclusions .....	141
7	Optimisation of fat quantification <i>in vivo</i> .....	142
7.1	Background.....	142
7.1.1	Fat fraction quantification and m-DIXON method .....	143

## Table of Contents

7.1.2	Droplet size measurements.....	145
7.2	<i>In vitro</i> studies.....	147
7.2.1	Cross field experiment.....	147
7.2.2	Dilution experiment .....	149
7.3	Results <i>in vitro</i> .....	150
7.3.1	Cross-field $T_1$ relaxation .....	150
7.3.2	Cross-field $T_2$ relaxation.....	152
7.3.3	Cross-field m-DIXON fat/water ratio .....	153
7.3.4	m-DIXON calibration for <i>in vivo</i> study.....	156
7.3.5	MRS fat fraction .....	157
7.4	Discussion: <i>in vitro</i> study.....	159
7.5	<i>In vivo</i> study.....	160
7.5.1	Aims and objectives .....	160
7.5.2	Specific methods.....	161
7.5.3	Emulsions characterisation .....	164
7.5.4	Gastric emptying .....	166
7.5.5	Gallbladder contraction .....	167
7.5.6	m-DIXON fat fraction.....	167
7.5.7	MRS fat fraction .....	169
7.5.8	Comparison m-DIXON and MRS fat fractions.....	171
7.5.9	$T_2$ relaxation times <i>in vivo</i> .....	173
7.6	Discussion: <i>in vivo</i> study .....	175
7.7	Conclusions .....	178
8	Conclusions .....	179
8.1	Brief summary of main findings.....	179
8.2	Advantages.....	181
8.3	Limitations.....	181
8.4	Future directions .....	182

## Table of Contents

9	References .....	184
10	Appendix.....	201
10.1	Specific list of materials and equipment used in Unilever .....	201
10.2	Detailed methods for preparation of emulsions .....	202
10.2.1	Area and equipment cleaning.....	202
10.2.2	Preparation of 1% LBG Solution.....	202
10.2.3	Preparation of coarse emulsion with no LBG (Coarse Control).....	203
10.2.4	Preparation of the fine emulsion.....	203
10.2.5	Preparation of the coarse emulsion with 0.5% LBG.....	204
10.2.6	Preparation of the fine emulsion with 0.5% LBG (Fine+LBG) ..	205

# 1 Introduction

## 1.1 Background

Magnetic Resonance Imaging (MRI) is based on the concept of nuclear magnetic resonance (NMR). MRI has become widely available around the globe as a non-invasive imaging modality since its inception in the 1970's by Professors Mansfield [1] and Lauterbur [2]. Since then, MRI has undergone continuous transformation and development which has made it the most versatile imaging technique for both clinical and research applications. These continuous developments were made mostly by academics from around the world innovating both the hardware and the software of the scanners. Pivotal developments have been made in signal processing, spatial resolution of scanners, speed of scan time, newly developed sequences, magnets, gradient coils, receiver coils and parallel imaging.

MRI is known for its high resolution and non-invasiveness, but hindered by its relatively low sensitivity. Recent advances in image processing, acquisition, new software and computational techniques have allowed MRI to move from anatomical applications to functional ones. MRI is not limited to clinical application but also employed in many other sectors such as pharmaceutical and food industries. This imaging modality can measure a range of powerful parameters that enable it, for example, to assess the action of new formulations in humans and to provide in-depth information about the fate of oral dosage forms [3, 4]. Nottingham is home to EPI and slice selection and

over the years the 'Sir Peter Mansfield Magnetic Resonance Centre' or 'SPMMRC' has developed many aspects of the technique of MRI. One of these key aspects is MRI of gastrointestinal function and the in-body monitoring of food components in the gastrointestinal tract and the assessment of their bioavailability and impact on gastrointestinal physiology *in vivo* [5-15]. Many of these studies were carried out both with funding from the Biological and Biotechnological Sciences Research Council (BBSRC) and in partnership with Unilever [16-22], with a particular interest in studying intra-gastric handling of fat emulsions and, in turn, its impact on gastrointestinal physiology [23-26]. Improved knowledge of the physiological and satiety responses to physical factors in foods could lead to the development of novel food products with improved health-promoting characteristics.

This is the overall background and conceptual framework behind the collaboration between the University of Nottingham and Unilever that generated and funded the joint Industrial Partnership CASE award of this studentship. Specifically for this work, there is scientific and industrial relevance in being able to carry out non-invasive monitoring of the gastrointestinal fate of fat emulsions of different temporal stability and droplet size in order to better relate the microstructure and location of different fatty food formulations with, for example, the time it takes to empty from the stomach, the levels of hormones in the blood and the sensation of satiety. This will aid not only the design of novel foods but also allow to check their predicted performance *in vivo*. The combined use of magnetic resonance imaging and spectroscopy is a novel and exciting approach to investigate the journey of fat through the gastrointestinal tract.

## 1.2 Overall aims of this thesis

The overall aim of this thesis was therefore to explore MRI and MRS methods to

- a) characterise model fat emulsion meals of different temporal stability and droplet size on the bench and
- b) study the behaviour and physiological responses to these model fat emulsion meals *in vivo* in healthy volunteers.

## 1.3 Thesis overview

The work described in this thesis was carried out at the SPMRC, School of Physics and Astronomy, University of Nottingham and Unilever Discovery at Colworth from Jan 2008 to September 2012. The research described in this thesis is original, unless otherwise stated.

The layout and content of the thesis chapters is as follows:

**Chapter 2:** This is a background chapter. The theory of nuclear magnetic resonance is introduced. The nuclear spin, the relaxation phenomena and relaxation times ( $T_1$  and  $T_2$ ) are described. The Chapter then describes the basic principles of magnetic resonance imaging including linear gradients and gradient coils, slice selection, k-space and imaging sequences. Following this, it briefly describes aspects of magnetic resonance spectroscopy (MRS) including chemical shift and spatial localisation based on single voxel techniques.

**Chapter 3:** This chapter first contains an overview of the anatomy and physiology of the gastrointestinal tract (GIT). Secondly it describes briefly how human digestion works, with particular reference to the digestion of fat and of the GI tract.

**Chapter 4:** This chapter highlights some of the methods that were used during fat emulsion sample preparation including characterisation of samples, MRI/MRS protocols and cholecystokinin (CCK) assays. The Ethics approvals and 'Good Clinical Practice' (GCP) processes are also described.

**Chapter 5:** The title of this chapter is "Development work" as it describes extensive bench work done to characterise the fat emulsion meals and to study their behaviour *in vitro*. The chapter then describes a range of pilot studies *in vivo* that were carried out in order to test fat emulsion samples and hypotheses for main studies.

**Chapter 6:** A major physiological MRI and MRS study is described here. Fat emulsions of different stability and droplet size were fed to healthy volunteers and the physiological responses measured with a range of techniques including also blood sampling and objective measures of satiety. The chapter includes methods of sample preparation, MRI protocols, results and discussion.

**Chapter 7:** Building on the experience gained, *in vitro* and *in vivo* studies were carried out to further explore and optimise intragastric monitoring of fat. This work is described in this chapter comprising relaxometry, cross-field and fat/water imaging methods such as m-DIXON.

**Chapter 8:** This final chapter contains an overall conclusion paragraph followed by a reflection on advantages and limitations of the work carried out. An outlook on possible future work is also given.

## **2 NMR, MRI and MRS**

This Chapter summarises briefly the theoretical background of nuclear magnetic resonance, magnetic resonance imaging and magnetic resonance spectroscopy as described in many standard textbooks [27-29]. This chapter is divided into 3 sections: firstly, the description of the nuclear magnetic resonance phenomenon is given in section 2.1. Secondly, magnetic resonance imaging (MRI) is briefly discussed in section 2.2 with an introduction to how an MR image is formed. Signal localization is introduced and the concept of k-space is described. Some relevant imaging pulse sequences used in the experimental work in this thesis are also briefly introduced. Finally, a concise description of magnetic resonance spectroscopy, chemical shift and chemical shift imaging are provided in section 2.3.

### **2.1 Nuclear Magnetic Resonance**

Magnetic resonance imaging also referred to as nuclear magnetic resonance imaging exploits properties of magnetism to extract images of body interiors (Table 2.1). The history of NMR goes back to as early as the 1940s, when Rabi measured more precisely the nuclear magnetic moments and then Bloch and Purcell advanced the method magnetic resonance detection.

### 2.1.1 The nuclear spin

Nuclei may possess spin angular momentum  $J \neq 0$  if the mass number and the atomic number are not both even numbers. Only nuclei with  $J \neq 0$  can give rise to NMR. Associated to this spin is a magnetic moment  $\mu$  so that

$$\mu = \gamma \mathbf{J} . \quad [2.1]$$

The vectors  $\mathbf{J}$  and  $\mu$  are parallel and the scalar constant of proportionality  $\gamma$  is called the gyromagnetic ratio.  $\gamma/2\pi$  has a value of  $42.57 \cdot 10^6$  Hz/T for protons, Nuclei of interest in biomedicine include the hydrogen proton  $^1\text{H}$ ,  $^{13}\text{C}$ ,  $^{19}\text{F}$ ,  $^{23}\text{Na}$  and  $^{31}\text{P}$ . Table 2.1 summarises some of their properties. Protons give the greatest signal (because they have the largest gyromagnetic ratio and largest abundance in biological tissues). Therefore virtually all MRI is based on proton imaging, and here only hydrogen protons (which have spin  $1/2$ ) will be considered.

### 2.1.2 Quantisation of energy

In the quantum mechanical description both  $\mathbf{J}$  and  $\mu$  are quantised. Introducing the angular momentum operator  $\mathbf{I}$  (which is dimensionless) and Planck's constant  $\hbar$ ,  $\mathbf{J}$  and  $\mathbf{I}$  can be written as

$$\mathbf{J} = \hbar \mathbf{I} . \quad [2.2]$$

In this context the z component of angular momentum  $\mathbf{I}$  along some axis z,  $I_z$ , is the observable of interest and it can have  $(2I+1)$  values as

$$I_z = \hbar m , \quad [2.3]$$

with

$$m = -I, -I+1, \dots, I-1, I. \quad [2.4]$$

Isotopes	Nuclear Spin	Gyromagnetic ratio $\gamma/2\pi$ (MHz/T)	Natural Abundance (%)
$^1\text{H}$	1/2	42.58	99.9
$^2\text{H}$	1	6.54	0.015
$^{13}\text{C}$	1/2	10.71	1.1
$^{19}\text{F}$	1/2	40.05	100
$^{23}\text{Na}$	3/2	11.42	100
$^{31}\text{P}$	1/2	17.24	100

**Table 2.1:** Properties of some nuclear isotopes used in magnetic resonance.

Therefore for a proton (for which  $I = \frac{1}{2}$ ),  $m = \pm \frac{1}{2}$ . Under normal conditions these states are degenerate with the same energy level.

The application of a magnetic field  $\mathbf{B}_0$  to the magnetic moment  $\boldsymbol{\mu}$  of an isolated nucleus produces an interaction energy  $E$  (the potential energy will be the work done to rotate the dipole in the field) given by

$$E = -\boldsymbol{\mu} \cdot \mathbf{B}_0. \quad [2.5]$$

Therefore for protons in a magnetic field, the degeneracy is removed and there are two energy levels

$$E_{\pm\frac{1}{2}} = \pm \frac{1}{2} \hbar \gamma B_0, \quad [2.6]$$

which now have a separation in energy of

$$\Delta E = \hbar \gamma B_0. \quad [2.7]$$

This energy levels structure is known as the Zeeman splitting of the energy states. This is shown in Figure 2.1.

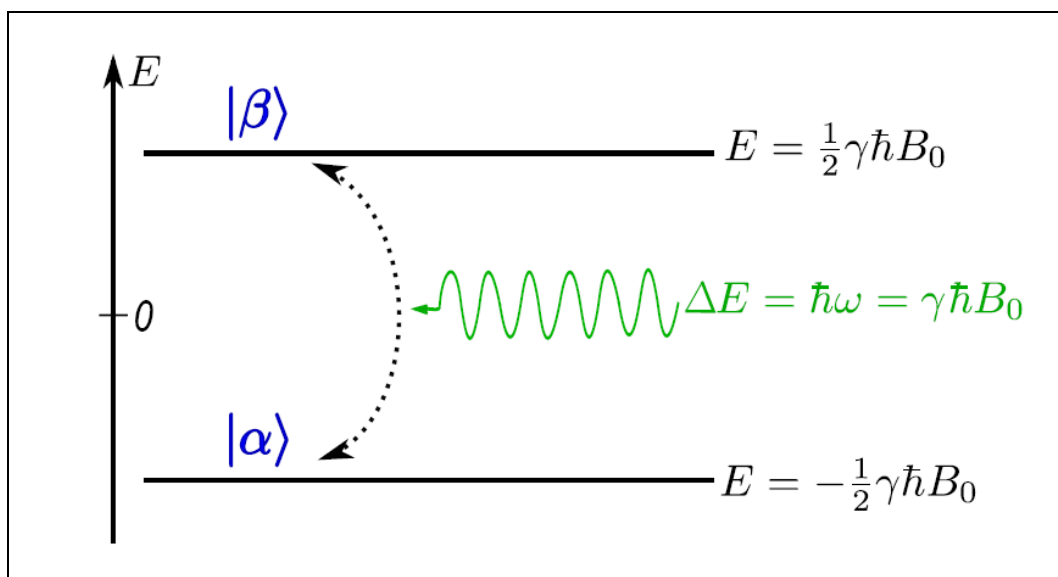


**Figure 2.1:** Energy level diagram of the hydrogen nucleus (spin  $\frac{1}{2}$ ) in a magnetic field  $B_0$ . Transitions can be induced between the spin states by adding energy  $\Delta E$ , equal to the difference between energy levels of the split, to the system

Applying radiation of frequency  $\nu$  will cause a transition between the two energy levels provided that

$$\Delta E = h\nu = \hbar \omega = \gamma \hbar B, \quad [2.8]$$

$$\text{i.e. } \omega = \gamma B, \quad [2.9]$$

which is the Larmor equation.

This frequency of precession is known as the Larmor frequency. Radiation applied at the Larmor frequency ( $\omega_L$ ) will be just as likely to cause a flip up as down, therefore for absorption to occur there must be a net difference in population of the two energy levels.

### 2.1.3 Energy level populations

Considering a spin system at thermal equilibrium, the spins will be distributed between the two Zeeman energy levels,  $n_\uparrow$  parallel ('up' and low energy aligned state) and  $n_\downarrow$  antiparallel ('down' and higher energy state) to  $B_0$  respectively, separated by  $\Delta E$  and governed by a Boltzmann distribution such that

$$\frac{n_\downarrow}{n_\uparrow} = e^{-\frac{\Delta E}{k_B T}}, \quad [2.10]$$

where  $\Delta E$  is the energy difference between the two Zeeman levels,  $k_B$  is the Boltzmann's constant and  $T$  is the absolute temperature. Given that there are only two states, the total number of spins  $n$  is such that  $n = n_\uparrow + n_\downarrow$ , then the difference in population (or polarisation of the sample) can be written as

$$n_\uparrow - n_\downarrow = n \frac{1 - e^{-\frac{\hbar \gamma B_0}{k_B T}}}{1 + e^{-\frac{\hbar \gamma B_0}{k_B T}}} = n \tanh\left(\frac{\hbar \gamma B_0}{2k_B T}\right). \quad [2.11]$$

The energy splitting of the levels is small compared with  $k_B T$  (a quantum of thermal energy), thus Eq. 2.11 can be approximated to

$$n_\uparrow - n_\downarrow = n \frac{\hbar \gamma B_0}{2k_B T}. \quad [2.12]$$

This polarisation can then be written as a net magnetisation  $M_0$  as

$$M_0 = (n_{\uparrow} - n_{\downarrow}) \frac{\gamma \hbar}{2} = \frac{\gamma^2 \hbar^2 B_0 n}{4k_B T}. \quad [2.13]$$

#### 2.1.4 Spin and angular momentum

Although the nature of the NMR phenomenon requires a quantum mechanical description, the use of a semi-classical, phenomenological approach is adequate when a large number of non (or weakly) interacting spins is considered. This is the case for the water protons, with which the work described in this thesis is concerned.

Equation 2.9 does not contain Planck's constant. This suggests that a semi-classical approach to describe the motion of the magnetic moment vector should prove satisfactory. Consider a magnetic moment  $\boldsymbol{\mu}$ . The angular momentum  $\mathbf{J}$  is a colinear vector so that

$$\boldsymbol{\mu} = \gamma \mathbf{J}. \quad [2.14]$$

When placed in a uniform magnetic field  $\mathbf{B}$ ,  $\boldsymbol{\mu}$  will experience a torque  $\boldsymbol{\Gamma}$  given by

$$\boldsymbol{\Gamma} = \boldsymbol{\mu} \times \mathbf{B}. \quad [2.15]$$

The angular momentum  $\mathbf{J}$  must satisfy the equation

$$\frac{d\mathbf{J}}{dt} = \boldsymbol{\Gamma}, \quad [2.16]$$

therefore, substituting equations 2.14 and 2.15 into 2.16, the rate of change of the magnetic moment is given by

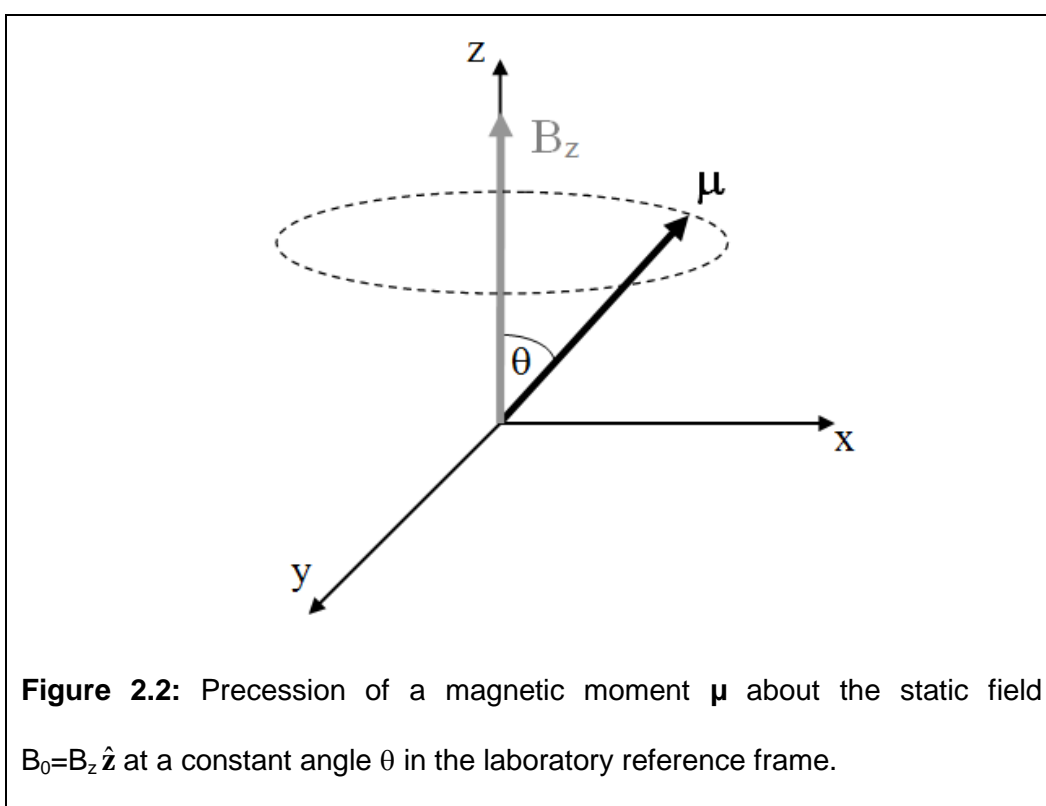
$$\frac{d\boldsymbol{\mu}}{dt} = \gamma \boldsymbol{\mu} \times \mathbf{B}. \quad [2.17]$$

This shows that the rate of change of  $\boldsymbol{\mu}$  is always perpendicular to both  $\boldsymbol{\mu}$  and  $\mathbf{B}$ .

### 2.1.5 The Larmor precession

If  $\mathbf{B}$  is time independent and directed along  $\hat{z}$  this will result in a precession of  $\boldsymbol{\mu}$  around the  $\mathbf{B}$  axis at a fixed angle  $\theta$  between  $\boldsymbol{\mu}$  and  $\mathbf{B}$  (Fig. 2.2) with a Larmor precession frequency given by

$$\omega_0 = -\gamma B_z. \quad [2.18]$$



The minus sign indicates that the Larmor precession is anticlockwise for a positive  $\gamma$ . There is a conventional coordinate system used in NMR: the z-axis is aligned with the applied ( $B_0$ ) field and equilibrium bulk magnetisation.

This is known as the longitudinal direction. The xy-plane is perpendicular to  $B_0$  and is known as the transverse plane.

### 2.1.6 The Bloch equation of motion

In reality not one single spin, but a large ensemble of spins  $\mu_i$  will be under examination in a sample. Introducing the vector  $\mathbf{M}$ , sum of all the magnetic moments so that

$$\mathbf{M} = \sum_i \mu_i, \quad [2.19]$$

the Bloch equation of motion becomes

$$\frac{d\mathbf{M}}{dt} = \gamma \mathbf{M} \times \mathbf{B}. \quad [2.20]$$

### 2.1.7 Interaction with electromagnetic radiation

Radiofrequency (RF) magnetic fields of appropriate energy (frequency) are applied to excite transitions between the Zeeman energy levels. These magnetic fields are conventionally known as  $B_1$  fields and are not static (but time-dependent, i.e. they are a vector  $\mathbf{B}_1(t)$ ). Let  $\mathbf{B}_0 = B_0 \hat{\mathbf{z}}$  and  $\mathbf{B}_1(t)$  be applied perpendicular to the  $\hat{\mathbf{z}}$  axis in the laboratory reference frame and rotating in the x,y plane at a frequency  $\omega$  so that  $\mathbf{B}_1(t)$  can be written as

$$\mathbf{B}_1(t) = B_1 (\hat{\mathbf{x}} \cos \omega t + \hat{\mathbf{y}} \sin \omega t). \quad [2.21]$$

Eq. 2.21 shows that  $B_1(t)$  is now rotating at the same frequency as the precessing magnetisation. The total magnetic field applied to the magnetisation  $\mathbf{M}$  is the sum of  $B_0$  and  $B_1(t)$ . Substituting into Eq. 2.20, the Bloch equation of motion becomes

$$\frac{d\mathbf{M}}{dt} = \gamma \mathbf{M} \times (B_0 \hat{\mathbf{z}} + \mathbf{B}_1). \quad [2.22]$$

The term in parenthesis is called the effective field  $\mathbf{B}_{\text{eff}}$  applied to  $\mathbf{M}$  in the laboratory reference frame. Equation 2.22 shows that the additional effect of  $B_1(t)$  is to tip the magnetisation vector away from the  $\hat{z}$  axis.

It is convenient now to transform the laboratory reference frame  $x,y,z$  into a frame  $x',y',z'$  rotating about  $\hat{z}$  at the frequency  $\omega$  to achieve an easier visualisation of the precession of  $\mathbf{M}$ . In the rotating reference frame the field  $B_1$  appears stationary and directed along the  $\hat{x}'$  axis (Figure 2.3a).

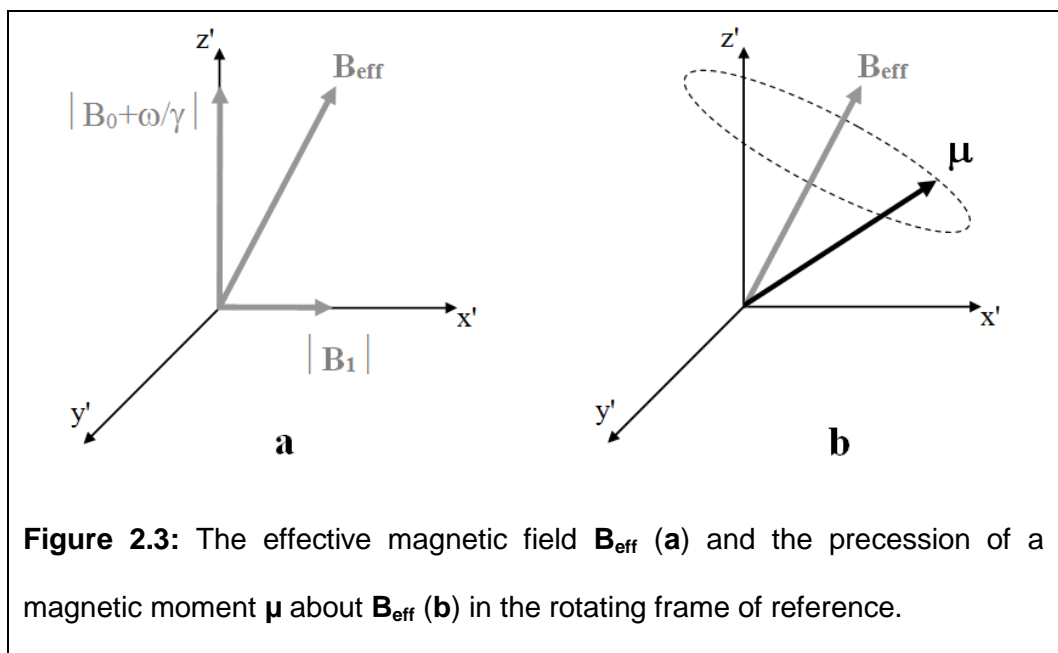


**Figure 2.3:** The effective magnetic field  $\mathbf{B}_{\text{eff}}$  (a) and the precession of a magnetic moment  $\boldsymbol{\mu}$  about  $\mathbf{B}_{\text{eff}}$  (b) in the rotating frame of reference.

Hence, by choosing a rotating frame with  $\omega = -\gamma B_0$  the equation of motion of the magnetisation in the rotating frame of reference becomes simply

$$\frac{\partial \mathbf{M}}{\partial t} = \gamma (\mathbf{M} \times \mathbf{B}_1), \quad [2.23]$$

showing that  $\mathbf{M}$  precesses now about the direction of  $B_1$  (Fig 2.3.b).

The field  $B_1$  is usually applied as a short burst of radiofrequency (called a RF pulse). If a RF pulse of magnitude  $B_1$  is applied only for a period  $t_p$  then the angle of precession  $\theta$  about the  $z$ -axis is given by

$$\theta = \gamma B_1 t_p. \quad [2.24]$$

A RF field that rotates the equilibrium magnetisation to the y axis is called a  $90^\circ$  or  $\pi/2$  pulse, and one that rotates the magnetisation to the  $-z$  axis is called a  $180^\circ$  or  $\pi$  pulse.

### 2.1.8 Free induction decay

After a  $90^\circ$  RF pulse the magnetisation vector has been tipped into the x-y plane and at this moment all the spins are in phase with no difference in population between the states 'up' and 'down'.

When the RF pulse is switched off, this xy magnetisation will now precess about the main field  $B_0$  at the Larmor frequency. This rotating magnetisation can induce an oscillating field in a receiver coil which is detected via a phase sensitive detector. The initial amplitude of the induced electromagnetic field will be proportional to the bulk nuclear magnetisation  $M_0$ , yet many nuclear and chemical interactions in the sample will reduce the signal over time with a characteristic decay envelope. This signal decay is called the Free Induction Decay.

### 2.1.9 The relaxation times $T_1$ and $T_2$ and their measurement

The semi-classical approach described so far applies to an ensemble of isolated spins in a magnetic field  $B_0$ . In reality the spins will be part of a molecular sample structure (lattice) and interacting with it. When the difference in the Boltzmann population of the states is perturbed by a RF pulse, the spins will return to the thermal equilibrium state by interactions with their surroundings, particularly with magnetic fields arising from the surrounding

dipoles via dipole-dipole interactions. The magnetisation of the spins therefore relaxes back to its equilibrium state along the  $\mathbf{B}_0$  field with a first-order process at a rate characterised by the time constant  $T_1$  (called the spin-lattice or longitudinal relaxation time).

This is described by the Bloch equation

$$\frac{dM_z}{dt} = -\frac{(M_z - M_0)}{T_1}, \quad [2.25]$$

which has the exponential solution

$$M_z(t) = M_z(0)e^{-\frac{t}{T_1}} + M_0\left(1 - e^{-\frac{t}{T_1}}\right). \quad [2.26]$$

The application of a RF pulse tips the magnetisation away from the z axis, hence a transverse component of the magnetisation is also produced in the x-y plane. Such component decays exponentially as well, but the decay mechanism is now due to irreversible and random dephasing of the spins (loss of phase coherence). The relaxation of the transverse magnetisation is generally complex and cannot be described with a single time constant. However, in the liquid phase the mechanism simplifies and can be described with a first-order process characterised by a single time constant called spin-spin relaxation time (or transverse relaxation time)  $T_2$ . The Bloch equations describing this process are

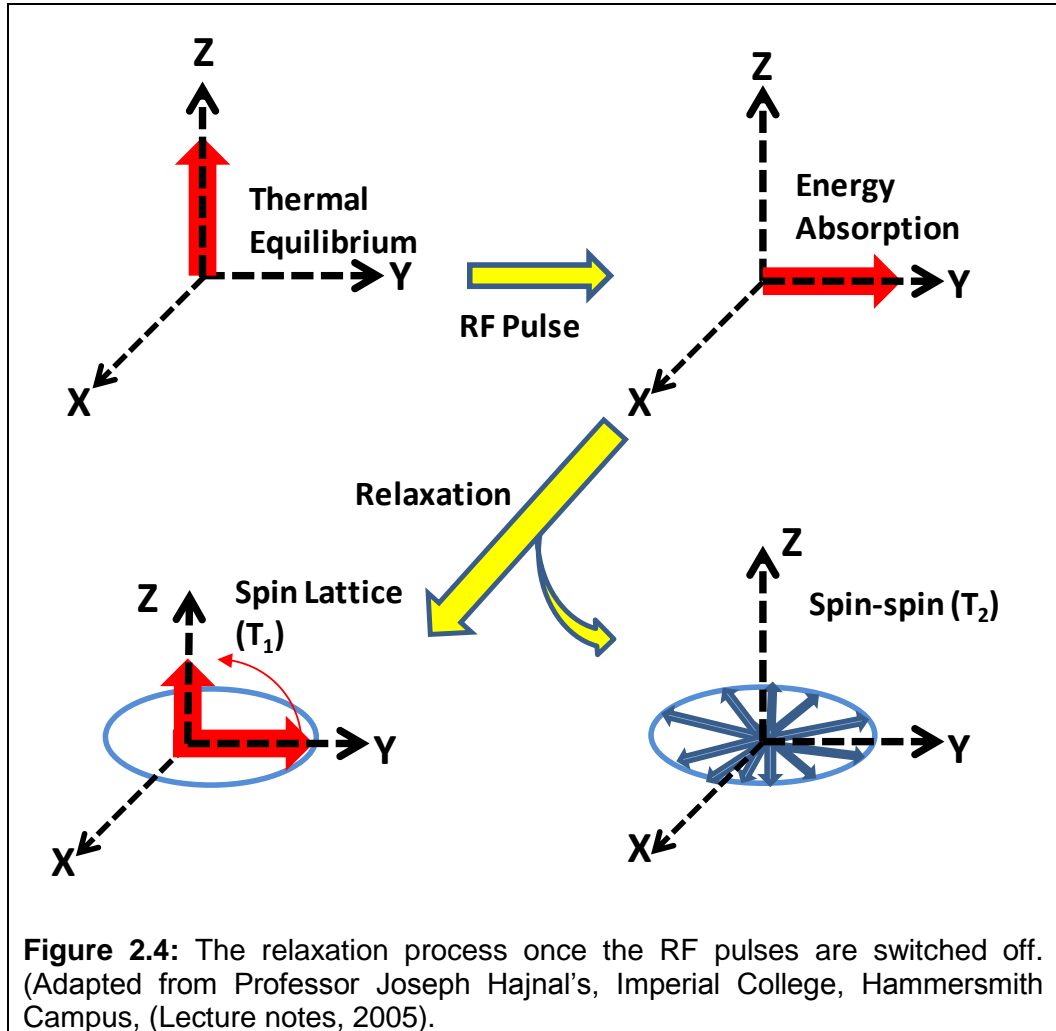
$$\frac{dM_{x,y}}{dt} = -\frac{M_{x,y}}{T_2}, \quad [2.27]$$

which have exponential solutions

$$M_{x,y}(t) = M_{x,y}(0)e^{-\frac{t}{T_2}}. \quad [2.28]$$

Figure 2.4 represents schematically the  $T_1$  and  $T_2$  relaxation processes. Various physical processes determine the relaxation rates  $T_1$  and  $T_2$ , but in

general:  $T_2 < T_1$ ;  $T_2 \sim T_1$  in systems in which the molecules are highly mobile (such as water);  $T_2 \ll T_1$  in solids.

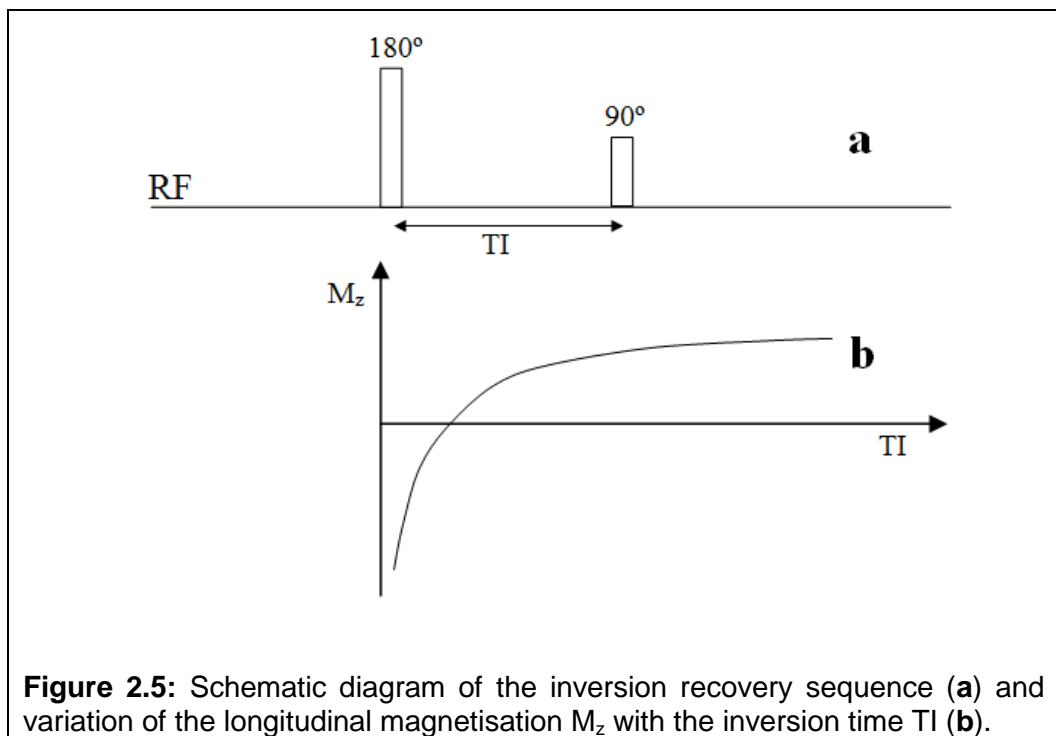


The incoherent dephasing effects by static field inhomogeneities can be reversed in the transverse plane using the spin-echo method introduced by Hahn (Figure 2.5). The excitation  $90^\circ$  pulse is followed, after a time delay  $TE/2$ , by a  $180^\circ$  pulse. The effect of the  $180^\circ$  pulse is to invert (neglecting spin diffusion) any phase evolution that the spin may have gained in the transverse plane during the interval  $TE/2$ . Hence this action will cancel out the incoherent phase accumulation and produce, at a further time interval  $TE/2$  after the  $180^\circ$

pulse (the time after the  $90^\circ$  pulse at which the spin-echo is formed is called the echo time TE), an echo which purely reflects a  $T_2$  decay process.

The relaxation time  $T_1$  may be measured using the Inversion Recovery (IR) pulse sequence (Fig. 2.5.a). The initial  $180^\circ$  pulse rotates the equilibrium magnetisation along the  $-z$  axis. Hence no transverse component is generated. A purely longitudinal (spin-lattice) relaxation is allowed to take place for an interval TI (inversion time) after which a  $90^\circ$  pulse tips the remaining longitudinal magnetisation into the transverse plane where it can be measured. From Eq. 2.26, with  $M_z(0) = -M_0$ , the initial amplitude of the corresponding FID is given by

$$M_z(\text{TI}) = M_0 \left( 1 - 2e^{-\frac{\text{TI}}{T_1}} \right). \quad [2.29]$$



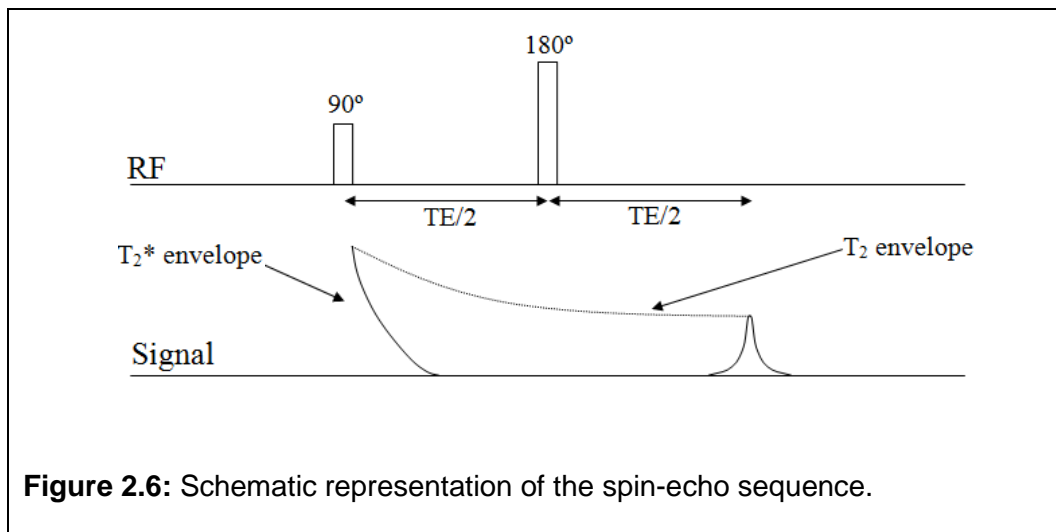
The sequence is then repeated with increasing TI. Providing that a sufficient repetition time TR ( $TR > 5 T_1$ ) is allowed between each repetition to allow full recovery of the initial magnetisation, the curve of the variation of  $M_z$  with TI (Fig. 2.5b) can be plotted and fitted to Eq. 2.29 to obtain the value of  $T_1$ .

The transverse relaxation time  $T_2$  can be measured using a simple Hahn spin-echo sequence as described in Fig 2.6.

For a given echo time TE the initial amplitude of the FID can be described by

$$M(TE) = M_0 e^{-\frac{TE}{T_2}} \quad [2.30]$$

The spin echo experiment is then repeated for increasing values of TE (allowing again a time  $TR > 5 T_1$  between experiments). The curve of the variation of M with TE can be fitted to Equation 2.30 to provide the value of  $T_2$ .



The spin echo measurement of  $T_2$  described above is made under the assumptions that no spin diffusion or movement occurred during the measurement. Spin diffusion or RF imperfections will affect the spin echo  $T_2$

measurement. Various modifications of these basic techniques for measuring relaxation times, have been introduced to improve speed and reduce systematic errors. Other interactions can affect the characteristics of the NMR signal and provide valuable information on the spatial and physico-chemical properties of the system.

### 2.1.10 Fourier transform NMR

The FID signal obtained irradiating a group of spins with a 90° RF pulse may be written as

$$S(t) = a e^{i\phi} e^{i\Delta\omega t} e^{-\frac{t}{T_2^*}}, \quad [2.31]$$

where  $a$  is a constant (depending on the instrumental gain and on the sample),  $\phi$  is the receiver phase and  $\Delta\omega$  is the resonant offset so that  $\Delta\omega = \omega_0 - \omega_{\text{ref}}$ .

This time signal can be represented in the frequency domain by use of a Fourier transform (FT) so that

$$H(\omega) = \int_0^{\infty} S(t) e^{-i\omega t} dt = a e^{-i\phi} \frac{T_2^*}{1 + i(\Delta\omega - \omega)(T_2^*)^2}. \quad [2.32]$$

This gives the real and imaginary components of the spectrum as

$$\text{Re}[H(\omega)] = a e^{-i\phi} \frac{T_2^*}{1 + (\Delta\omega - \omega)^2 (T_2^*)^2} \quad \text{and} \quad [2.33]$$

$$\text{Im}[H(\omega)] = -a e^{-i\phi} \frac{(\Delta\omega - \omega)(T_2^*)^2}{1 + (\Delta\omega - \omega)^2 (T_2^*)^2}. \quad [2.34]$$

Equation 2.33 and 2.34 describe, respectively, the absorption and the dispersion spectra. Usually, only the absorption spectrum is of interest. It has

a Lorentzian shape peak centred at  $\Delta\omega$ , with a full width at half maximum of  $2/T_2^*$ .

Figure 2.7 below summarises the entire NMR process.

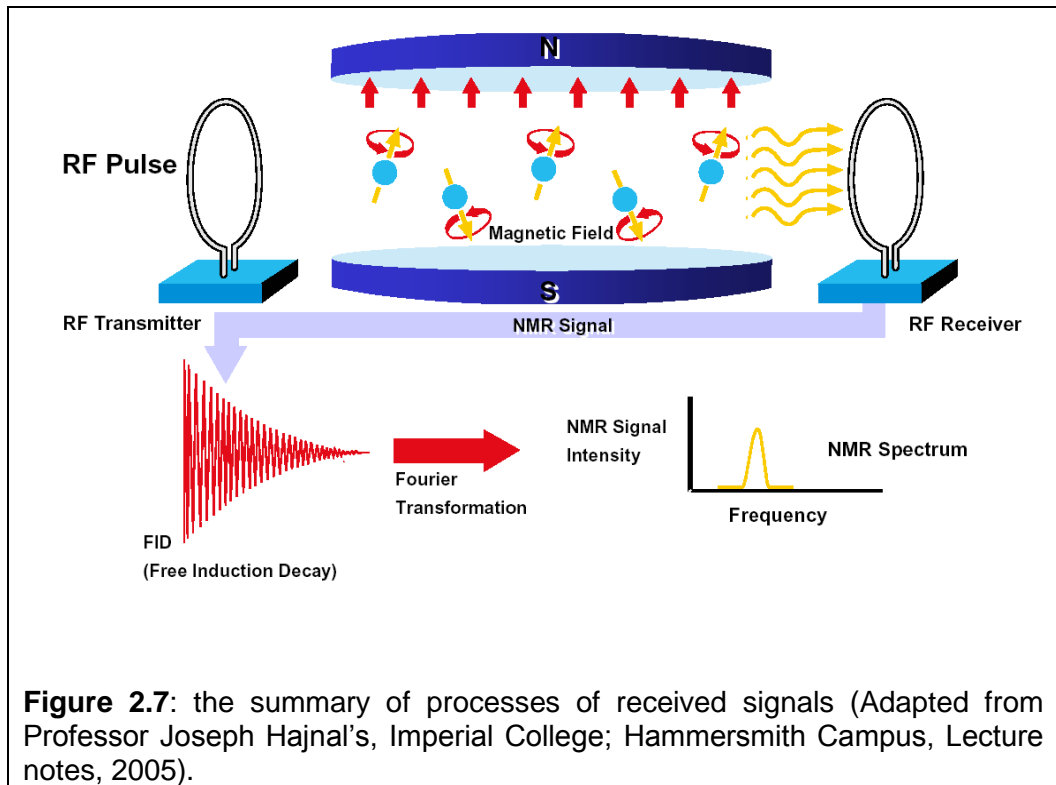


**Figure 2.7:** the summary of processes of received signals (Adapted from Professor Joseph Hajnal's, Imperial College; Hammersmith Campus, Lecture notes, 2005).

## 2.2 Magnetic Resonance Imaging

The previous section (section 2.1) described the basic principles of nuclear magnetic resonance. From 1950 until early 1970 NMR was used for chemical and physical molecular analysis. MRI was invented independently by Lauterbur and Mansfield. In 1973, Paul Lauterbur proposed imaging using gradients in the magnetic field such that a 2D image of a sample can be produced by applying a linear gradient at different angles to a sample and combining these projections using a back-projection reconstruction method [2]. In the same year, Peter Mansfield proposed spatial discrimination by use

of gradients and based on diffraction principles (Section 2.3 below). Ernst's group proposed the first Fourier imaging using non-selective excitation [1, 30]. In 1977 Mansfield introduced the ultra-fast imaging technique known as echo Planar imaging (EPI). In 1977 the first magnetic resonance imaging was performed on a human. In 2003 Lauterbur and Mansfield were rewarded with a Nobel Prize in 'physiology or medicine' for their contribution to the discovery of MRI [31]. Magnetic resonance imaging is growing fast and there have been many developments in the last 4 decades. MRI has become one of the most powerful imaging techniques and there are numerous research centres around the globe who dedicate themselves to further developments and improvements.

This section introduces the basic principles of magnetic resonance imaging which are extensively described in a number of text books and other publications [32-37].

### **2.2.1 Linear gradients and gradient coils**

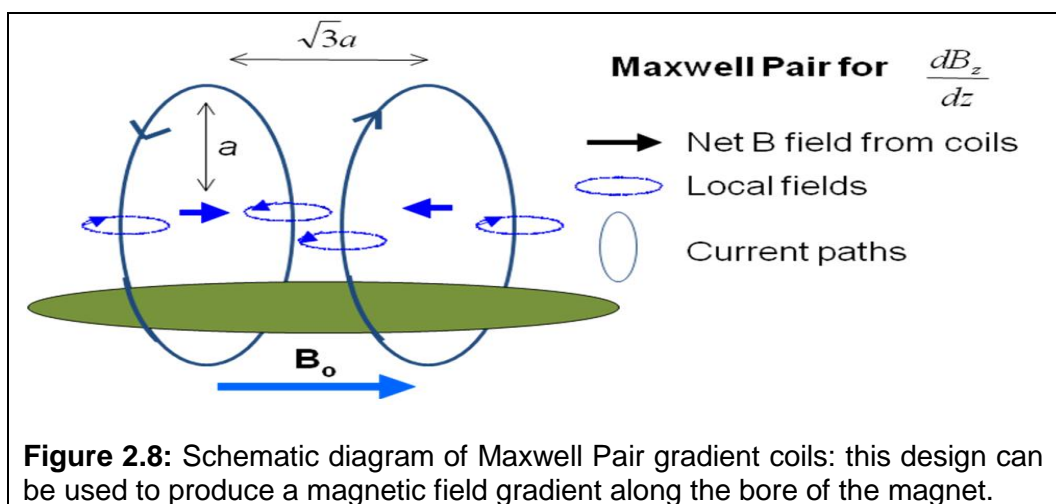
In the NMR experiment described above, the signal is produced by the spins in the sample, precessing at approximately the same frequency, with no spatial information. To obtain a spatially resolved map of the spins in the sample one needs to make the Larmor frequency spatially dependant. This is usually done on all modern scanners by varying spatially the main static magnetic field  $\mathbf{B}_0$  because Equation 2.18 shows that the Larmor frequency depends linearly on the applied polarising, homogeneous field  $\mathbf{B}_0$ . This implies that the superimposition of a linearly varying spatial magnetic field gradient  $\mathbf{G}$  to  $\mathbf{B}_0$  will apply a predictable spatial variation in the Larmor frequency of the spins. The Larmor frequency at a position  $\mathbf{r}$  may then be written

$$\omega(\mathbf{r}) = \gamma B_0 + \gamma \mathbf{G} \cdot \mathbf{r}. \quad [2.35]$$

Equation 2.35 shows that the scalar product  $\mathbf{G} \cdot \mathbf{r}$  defines planes normal to  $\mathbf{G}$  in which  $\omega$  is constant. The gradient  $\mathbf{G}$  is generally a tensor. However, one is generally only interested in the  $B_z$  components ( $\partial B_z / \partial x$ ,  $\partial B_z / \partial y$  and  $\partial B_z / \partial z$ ), so the tensor may be reduced to a vector and Eq. 2.35 may be reduced to

$$\omega(\mathbf{r}) = \gamma B_0 + \gamma \left( \frac{\partial B_z}{\partial x} x + \frac{\partial B_z}{\partial y} y + \frac{\partial B_z}{\partial z} z \right). \quad [2.36]$$

This represents the starting point of the process of two-dimensional MR imaging. Magnetic field gradient coils are designed to produce linearly-varying magnetic fields. One of the simplest coil designs for use with a cylindrical whole body imaging system is shown in Figure 2.8. The movement of the gradient coil wires in the magnetic field as strong electric currents are pulsed through them is the reason that MRI is so acoustically noisy. Because of the high current carried by coils during an imaging sequence (600 A), the coils are often water cooled to prevent overheating.



### 2.2.2 Slice selection

In order to produce a two-dimensional MR image of a desired plane within a three-dimensional object, the spins in a given plane need to be prepared first for a subsequent planar encoding. This is achieved using the process of slice selection, as indicated originally by Garroway, Grannell and Mansfield in 1974. This process is based on the application of a RF pulse with a limited bandwidth in conjunction with a linear magnetic field gradient, applied in a direction orthogonal to the slice.

The diagram in Fig 2.9 illustrates this concept. Consider a cylindrical object filled with water and positioned with its axis along a polarising field  $\mathbf{B}_0 = B_0 \hat{z}$ . Let a linear magnetic field gradient  $G_z$  be applied along the z axis.  $G_z$  will cause the Larmor frequency of the spins to vary linearly along z according to Eq. 2.36, hence every plane perpendicular to the z axis will have a constant  $\omega(z)$ .

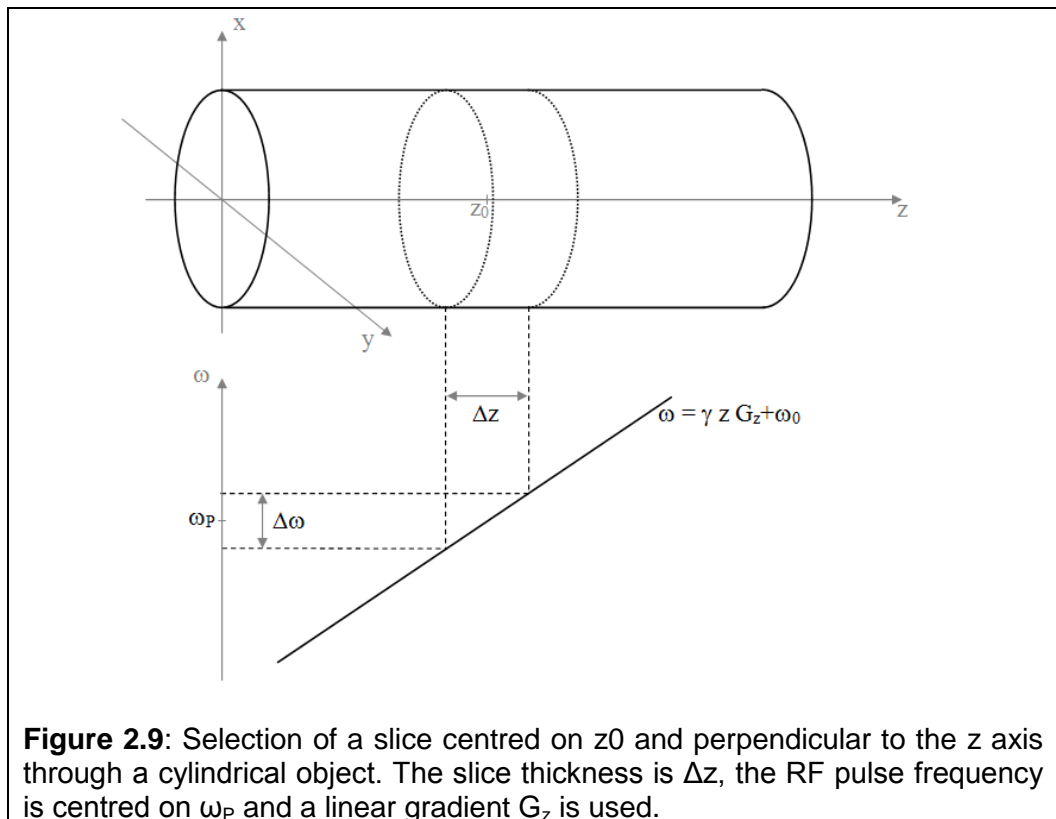


**Figure 2.9:** Selection of a slice centred on  $z_0$  and perpendicular to the z axis through a cylindrical object. The slice thickness is  $\Delta z$ , the RF pulse frequency is centred on  $\omega_p$  and a linear gradient  $G_z$  is used.

The resonant frequency is then given by

$$\omega_p = \gamma [\mathbf{B}_0 + G_z(z) z]. \quad [2.37]$$

If a RF pulse with a limited bandwidth is now applied along the x axis in conjunction with the gradient  $G_z$ , only spins near its centre frequency  $\omega_p$  will be excited. Neglecting relaxation effects, Eq. 2.37 describes then the selective excitation of a finite slice of the sample perpendicular to the polarising field and centred on the position  $z_0$ , corresponding to the RF carrier frequency (Fig. 2.9).

### 2.2.3 k space

Consider now a slice of an object of spin density  $\rho(\mathbf{r})$ , which has been selected perpendicular to the z axis. The FID signal  $s(t)$ , demodulated at the reference frequency, may be written as a spatially varying phase evolution

$$s(t) = \int \rho(\mathbf{r}) e^{i\gamma \mathbf{r} \cdot \int_0^t \mathbf{G}(t') dt'} d\mathbf{r}, \quad [2.38]$$

where  $\mathbf{G}$  is a linearly varying gradient applied for a time  $t$  and  $d\mathbf{r}$  is a volume of integration. This equation highlights the relationship between the spin density  $\rho(\mathbf{r})$  and the time signal  $s(t)$  as a Fourier pair. It is convenient now to introduce the reciprocal space vector  $\mathbf{k}$  (also called spatial frequency, with units of  $\text{m}^{-1}$ )

$$\mathbf{k}(t) = \gamma \int_0^t \mathbf{G}(t') dt', \quad [2.39]$$

and to substitute  $\mathbf{k}$  in Eq. 2.38, thus obtaining

$$s(\mathbf{k}) = \int \rho(\mathbf{r}) e^{i\mathbf{k} \cdot \mathbf{r}} d\mathbf{r}. \quad [2.40]$$

This “k-space” description was first introduced by Mansfield and Grannell in analogy with optical plane wave scattering. The “MRI wave” is fictitious but has an effective wavelength  $\lambda$  given by

$$\lambda = \frac{2\pi}{|\mathbf{k}|}. \quad [2.41]$$

In analogy with the wave vector in optics, the MRI resolution  $\Delta r$  that can be achieved in the direction  $r$ , using a gradient of intensity  $G_r$ , applied for a time  $t_G$ , will be determined by the maximum value of  $\mathbf{k}$ ,  $k_{r(\max)}$ , as

$$\Delta r = \frac{2\pi}{k_{r(\max)}} = \frac{2\pi}{\gamma G_r t_G}. \quad [2.42]$$

The Fourier transform of Eq. 2.40 becomes

$$\rho(\mathbf{r}) = \int s(\mathbf{k}) e^{-i\mathbf{k}\cdot\mathbf{r}} d\mathbf{k}. \quad [2.43]$$

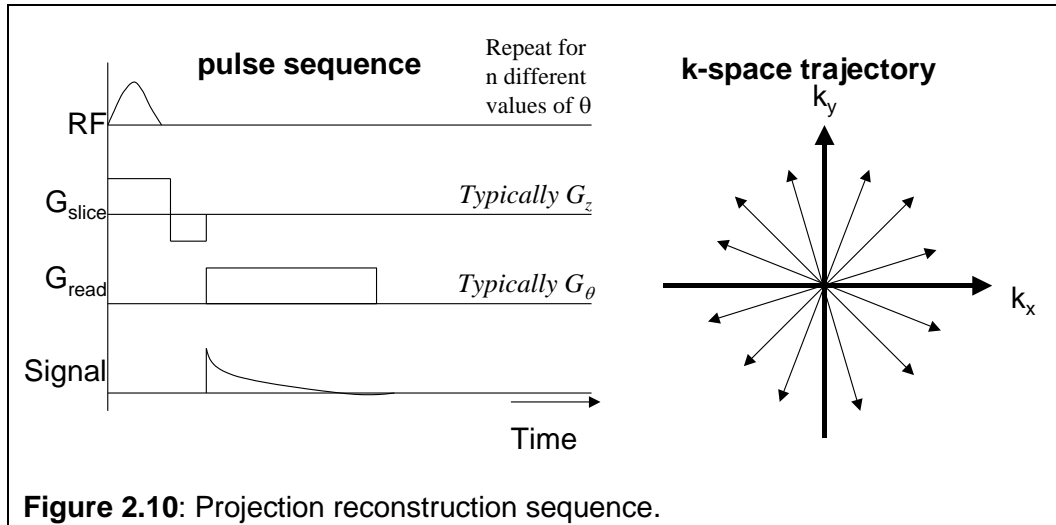
In analogy with the scattering of X-rays, the MRI signal,  $s(\mathbf{k})$ , is the reciprocal lattice of  $\rho(\mathbf{r})$ . Hence, sampling the k-space map of an object and calculating the Fourier transform of  $s(\mathbf{k})$  will yield the spin density map  $\rho(\mathbf{r})$  of the object, which is its MRI image.

The k-space description simplifies the analysis of any MRI technique. Having selected a slice through the object of interest, the direction of the x and y components of the  $\mathbf{k}$  vector are determined by the direction of the x and y components of the gradient vector  $\mathbf{G}$  respectively.  $S(\mathbf{k})$  may thus be plotted as a function of  $k_x$  and  $k_y$  drawing a trajectory in k-space.

#### 2.2.4 Imaging sequences

The ability to select a slice within an object and to manipulate the signal spatial dependence using linear gradients, opened the possibility to acquire two-dimensional planar MR images of the spin density within a reasonable

experimental time. There are many ways of producing an image in MRI, and just a few of them will be considered here.

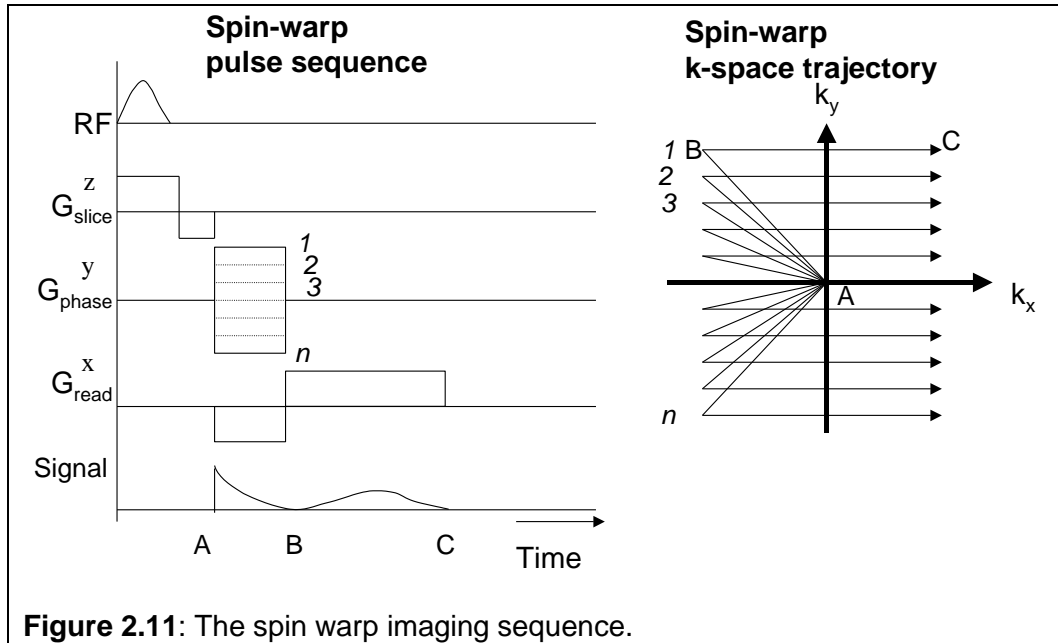


The projection reconstruction imaging method is shown in Figure 2.10. This shows the time course of the gradient and RF waveforms. The first line shows the slice selective RF pulse, and the second line shows the slice selection gradient. The third line shows the image encoding (frequency encoding/ readout) gradient. The fourth line shows the magnitude of the signal that will be acquired.

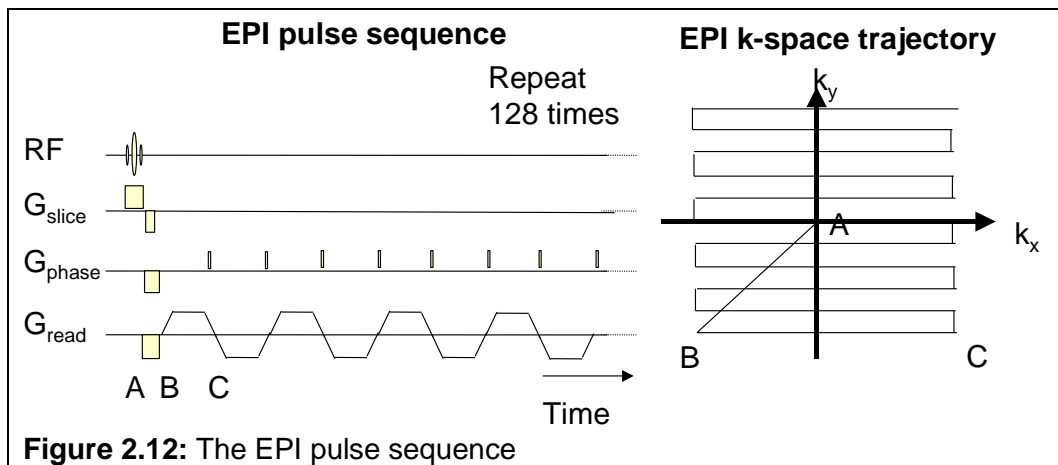
Using this method one can take images by sampling very quickly after excitation, hence projection reconstruction is useful for imaging samples with a short  $T_2^*$  (for example the lungs) however scanning times may be long.

Another method is Spin Warp imaging whereby k space is sampled on a regular grid. Figure 2.11 shows a diagram of the Spin Warp method. This was introduced by Edelstein, who proposed increasing the amplitude of the gradient  $G_y$  whilst keeping constant the time it is applied. In this way, each line in k-space is sampled at constant time intervals, consequently minimising differences in phase shifts due to  $B_0$  variations and relaxation weighting. This

is one of the most widely used sequences though it has relatively long imaging times and suffers from motion-related artifacts.



Another method is Echo planar imaging. This was invented by Professor Sir Peter Mansfield in Nottingham. EPI uses a single RF excitation followed by a very rapid, full sampling of k-space, using one of the orthogonal gradients to recall the magnetisation each time a line in k-space is swept, and the other gradient to pace consecutive phase encoding steps as shown in Figure 2.12.



EPI is so fast there are virtually no motion artifacts, it therefore can scan dynamic physiological processes very well and is particularly suited to measure quantitative parameters such as  $T_1$  and  $T_2$ . EPI has also some limitations such as low spatial resolution and is very sensitive to distortion.

### **2.2.5 Fat suppression**

The signal from fat in  $^1\text{H}$  MRI images can provide valuable information but is often undesired because it can cause artifacts (such as ghosting and chemical shift) and it had a high signal on  $T_1$  weighted images due to its short relaxation times so it can obscure tissues of interest. To overcome this problem various fat suppression techniques have been developed, such as fat saturation, inversion-recovery imaging, and opposed-phase imaging.

#### **2.2.5.1 Fat saturation**

This fat suppression technique uses a frequency selective RF saturation pulse with the same resonance frequency as the frequency of fat and it is applied to each slice selection. The advantages of this method are that it is lipid specific, it provides good contrast of  $T_1$  weighted images and it is very useful for tissue characterisation especially in areas with a large amount of fat. This method is also useful for avoiding chemical shift misregistration artifact. However, there are a number of disadvantages associated with this method. In order to achieve fat saturations the frequency of the frequency-selective pulse must be equal to the resonance frequency of lipid. However this is often not the case because of inhomogeneities of static magnetic field, for instance due to local magnetic susceptibilities. Such inhomogeneities will reduce the efficiency of fat saturation.

### 2.2.5.2 Inversion recovery imaging

This fat suppression technique is based on the fact that the  $T_1$  of the tissue or sample of interest can be different from the  $T_1$  of the fat around it. Some tissues such as adipose tissues have shorter  $T_1$  than the  $T_1$  of water. After a  $180^\circ$  inversion pulse is applied, the longitudinal magnetisation of adipose tissue will recover faster than water. However, if a  $90^\circ$  excitation pulse is used at the null point of fat,  $T_{1null}$  (Figure 2.13), then the adipose tissue will provide no signal whilst water has not been nulled and will continue to produce signals.

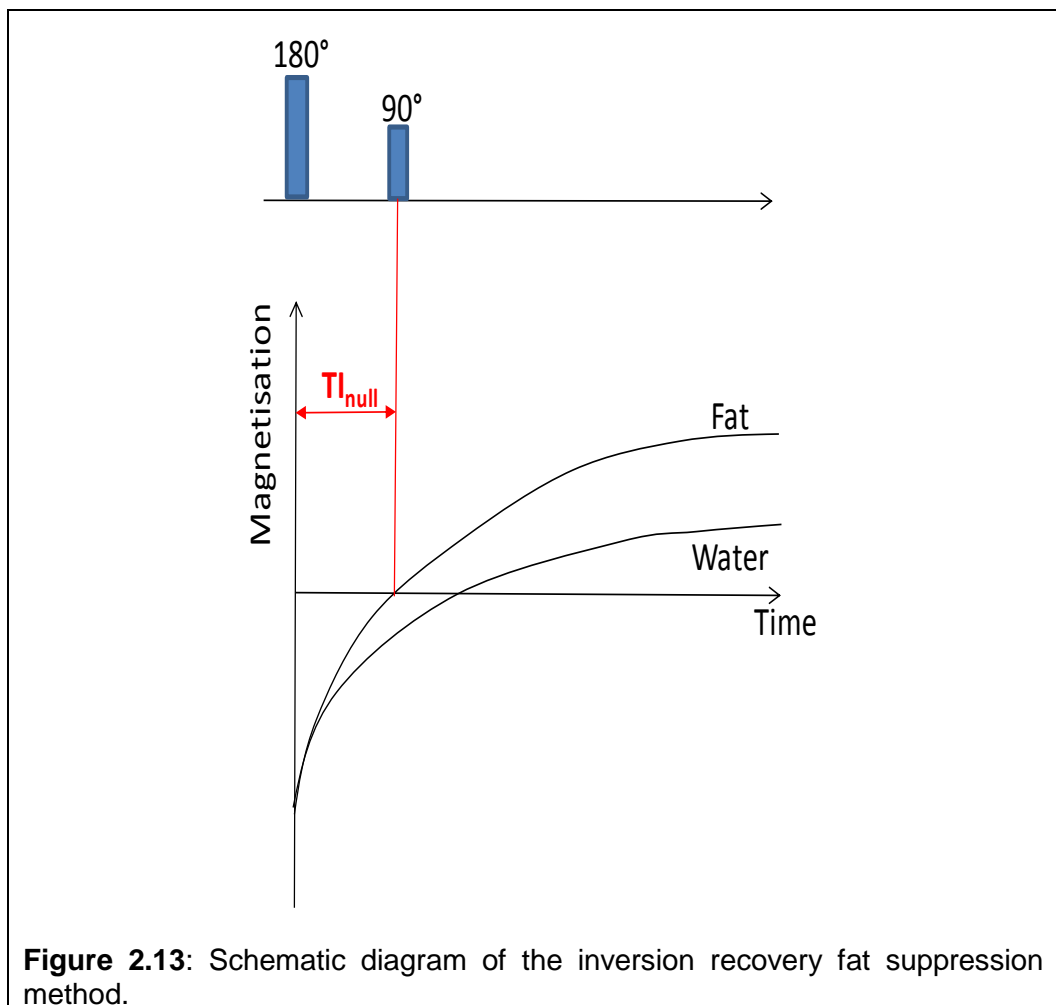


**Figure 2.13:** Schematic diagram of the inversion recovery fat suppression method.

Fat  $T_1$  is short so this means that in order to achieve good fat suppression; one has to use a shorter  $T_1$  inversion recovery. This is also known as STIR (Short  $T_1$  inversion recovery) and it is based on fast spin echo readout sequences. STIR has an important advantage over other fat saturation techniques as it is insensitive to magnetic field inhomogeneities. This technique works best with both long  $T_1$  and  $T_2$  values of the sample of interest and it is good for tumour detections.

### **2.2.5.3 Opposed phase imaging**

This is another technique used for fat suppression. This method uses the difference between resonance frequencies of the fat protons and the water protons as the phases of these protons relative to each other change after the initial excitation. Therefore, immediately after the excitation the lipid proton and water protons are in phase but the water protons precess faster than lipid protons. It is therefore possible to take images of the water and fat protons in phase or out of phase by simply varying the TE. This method is very simple, fast and available on every MRI system. The main disadvantage of this technique is that it does not suppress the signal from adipose tissue. There are specific versions of this such as m-DIXON which is described in more detail in Chapter 7.

## **2.3 Magnetic Resonance Spectroscopy**

Magnetic resonance spectroscopy is a specialised technique complementary to MRI as a non-invasive imaging modality. There are many biorelevant nuclei that MRS can monitor such as  $^{31}\text{P}$  and  $^{13}\text{C}$ . The most widely used however is the proton ( $^1\text{H}$  MRS) with which the work described in this thesis is concerned.

The first MRS *in vivo* brain spectra was published in the 1980s. The first studies *in vivo* were performed on patients who had stroke or brain tumour.  $^1\text{H}$  MRS has become clinical routine in neurology applications [38]. The reasons for this are not only because of the clinical/academic relevance: the brain is nearly spherical and suffers from minimal motion. Proton MRS is also particularly suited to assess the amount of fat in sample and body organ. MRS of fat fraction has recently become popular for the study of the liver [39] but it has not been applied yet to study *in vivo* the intragastric fat component of foods.

### **2.3.1 Chemical shift**

The resonance frequency of different metabolites in a MRS spectrum (also called their chemical shift) depends on the physicochemical environment of those metabolites. This modifies the individual resonance frequency for each species and allows them to be separated and measured. The historical definitions of the 'direction' of the scale in parts per million (ppm) arose from the time when the field was changed in continuous wave spectrometers and is programmed into the scanners. A negative frequency shift is a positive shift in ppm and is referred to as being 'up field'.

### **2.3.2 Spatial localisation based on single voxel technique**

The simplest way to acquire a spectrum of a region of the human body is to use a surface coil which will probe a small volume of approximately the same dimensions as the coil itself. It is of course desirable to be able to localise small volumes within the human body more precisely and this can be achieved using different methods to localize a discrete spatial voxel region. One method

is single volume spectroscopy with STimulated Echo Acquisition Mode (STEAM) [40]. The method involves the use of gradients to localise a volume of interest within a sample in conjunction with three  $90^\circ$  pulses.

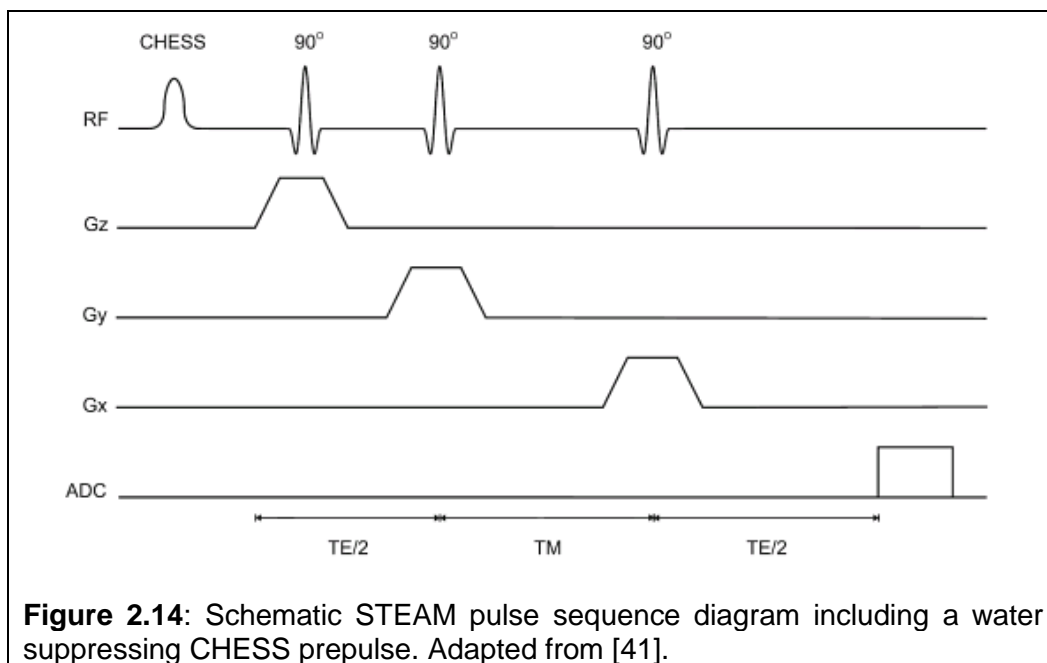


**Figure 2.14:** Schematic STEAM pulse sequence diagram including a water suppressing CHES prepulse. Adapted from [41].

In the work described in this thesis the STEAM method was used. Figure 2.14 shows a schematic STEAM pulse sequence diagram.

Multivoxel methods are an attractive methodology to perform Chemical Shift Imaging (CSI) also known as magnetic resonance spectroscopic imaging (MRSI).

### 2.3.3 MRS spectra quantification

In an ideal situation the area under the peaks of a MRS spectrum will reflect directly the concentration of the metabolites scanned. However the different relaxation times of different species and possible field inhomogeneities can affect quantitation. Phantom work, assessment of the spectral changes with varying TEs and knowledge of the relaxation times of the various species can improve quantitation methods. In reality spectral width, shimming and

relaxation limit the resolution of individual metabolites. However the water and the fat peak (including CH<sub>2</sub> and other lipid resonances) of samples like the fat emulsions used in this work are separated well enough to allow measurement.

#### **2.3.4 Limitation of MRS**

NMR spectroscopy *in vitro* usually is performed at very high field (10T-14T), in small *ex vivo* samples spinning rapidly in very homogeneous fields. MRS *in vivo* is instead performed at medium field strength (e.g. 1.5T-3T) with limited field homogeneity due to the nature of the human sample, power deposition limits and low signal to noise ratio. The spatial resolution is limited to volumes of a few cm<sup>3</sup>.

## **3 The gastrointestinal tract and its response to fat: MRI assessment**

This chapter describes briefly the anatomy and function of the gut and its response to food, with particular reference to the gastrointestinal response to fat. Magnetic resonance imaging of the gastrointestinal response to food is also summarised here.

### **3.1 Background**

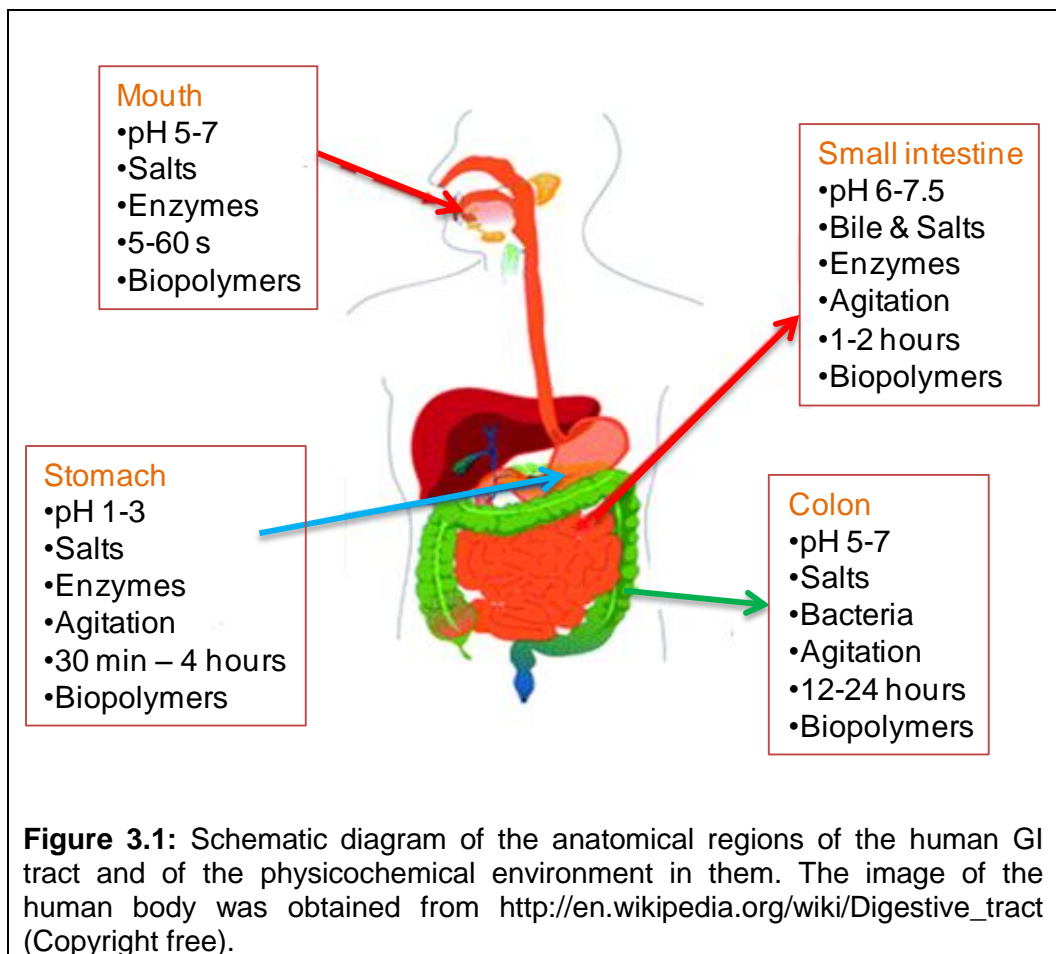
The gastrointestinal (GI) tract is the part of the human body dedicated to processing food. In the GI tract food undergoes mechanical grinding, dilution, chemical breakdown, mixing and transport and absorption. During these processes the GI tract sends key feedback signals that determine the sense of satiety and subsequent food intake. Most of the GI tract is difficult to access in order to study function and many old reports in the literature were based on invasive intubation studies or animal models. Imaging methods provide a clear advantage though ultrasound suffers from air/liquid interfaces and gamma scintigraphy provides poor resolution and cannot detect any secretions added to the chyme. Magnetic resonance imaging has many advantages over such techniques and in the last 15 years it has provided unique insights in gastrointestinal physiology and the processing of food.

This chapter describes briefly the anatomy and function of the gut and its response to food, with particular reference to the gastrointestinal response to

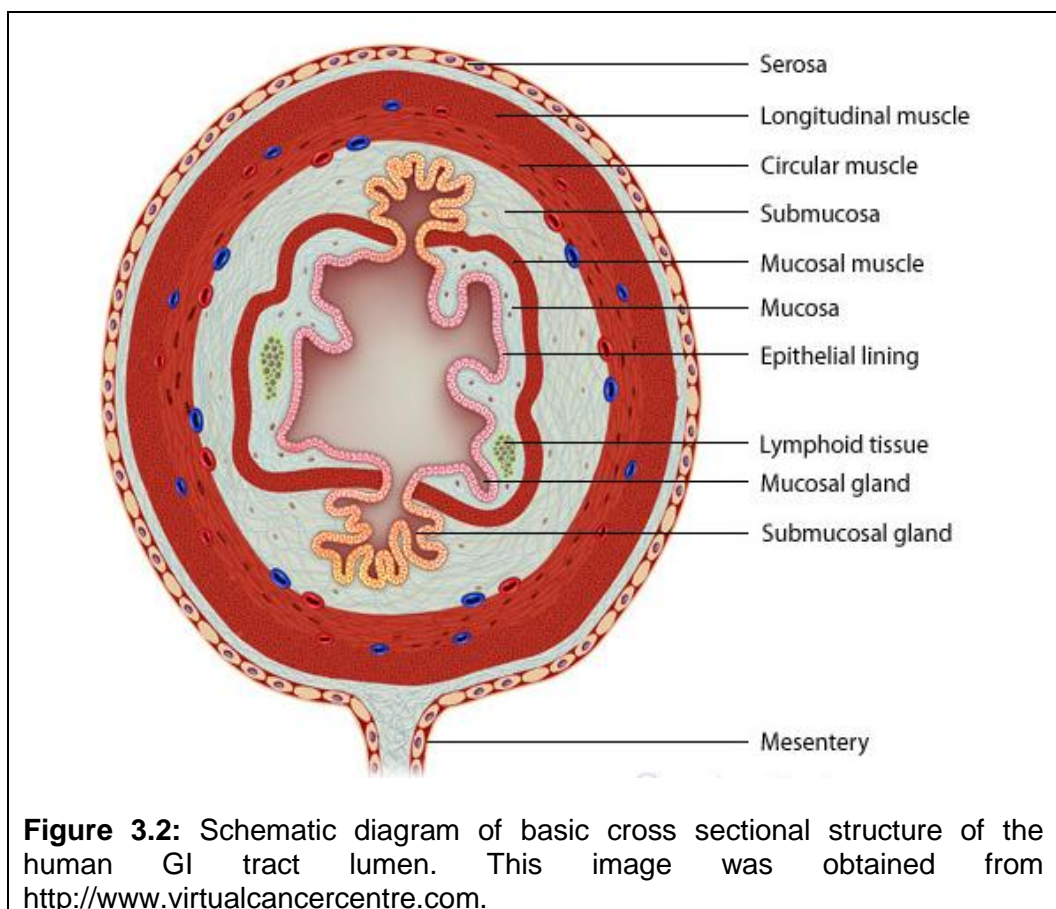
fat. Advances in magnetic resonance imaging of the gastrointestinal response to food are subsequently summarised.

### 3.2 Anatomy and function of the gastrointestinal tract

The gastrointestinal tract consists of four main anatomical regions: the oral cavity (mouth), the stomach, the small bowel or intestine and the large intestine or colon (Figure 3.1). From the anatomical point of view, the GI tract is a muscular tube lined by a mucous membrane starting from the oral cavity to the rectum and anus. The epithelium of the GI tract consists of 4 main areas: the mucosa, the submucosa, the muscularis and the serosa.



The physiological structure of the cells (Figure 3.2) is quite similar along the GI tract. However some local variations occur in the different and more specialised parts. Of particular importance are the villi in small intestine which are finger-like structures in the mucosa wall. These cell types increase the surface area and blood supply of the small intestine which ultimately increases capacity for absorption of nutrients in the small intestine.



### 3.2.1 The oral cavity (mouth)

From the anatomical point of view the mouth can be divided into three main areas: an epithelial surface, the lamina propria which is a supporting connective tissue and the muscularis mucosa which is a thin smooth muscle layer responsible for local movement and folding. The functions of the mouth

can be summarised as trituration, digestion, articulation and swallowing. Here the roles of ingestion and initial fragmentation of food will be considered.

In the mouth complex physiochemical and physiological processes take place. This part of the GI tract is responsible for converting the food into a form that suitable for swallowing. Food type can be liquid, semi-liquid or solid. The mouth has a set of glands that release saliva with digestive enzymes such as lingual lipase, amylase and protease as well as electrolytes and glycoprotein. These initiate food digestion in a very efficient way [42]. The teeth are responsible for chewing and the tongue movement allows interaction of the secreted saliva and foods. The pH of human saliva is around 5.5 to 6.1 when the body is fasting and this can drift more towards neutral (between 7 and 8) after food ingestion [43]. The human body can secrete around 500 to 1500 ml of saliva a day. The mucus contents of the saliva are capable of inducing flocculation and coalescence of ingested lipid droplets, whereas the protein fraction plays a major role in food digestion. This is complex and contains many different kinds of proteins, each with its own roles and functionalities [43, 44]. Foods spend only a relatively short amount of time in the mouth, but there are many physiochemical and physiological processes that occur during that time [45]. These processes will very much depend on the nature of ingested materials. There are various taste receptors in the oral cavity and some studies have indicated that the mouth actually contains receptors that are capable of detecting lipids [46]. Minimal food absorption takes place in the oral cavity. However, there is the possibility that small molecules could be absorbed via the oral epithelium by either the paracellular route (between cells) or the transcellular route (through the cells by passive diffusion).

### 3.2.2 The stomach

The stomach is a reservoir that serves as temporary storage for food. Here complete food fragmentation occurs and food digestion progresses. The human stomach can be divided into 3 main physiological function regions: the upper region known as the cardia, the middle region divided in the stomach fundus and the stomach body which are responsible for storage and releasing the digestive enzymes and gastric juice and acids; and the lower region known as the antrum provides the mechanical forces for mixing and allows regulated stomach content transportation down to the small intestine for absorption [47]. The pH of the stomach depends on whether the person is fasting or fed and ranges from pH 1-3 under fasted condition and up to pH 6 for the fed stomach [48, 49]. There are a number of substances that are secreted in the stomach including gastric lipase, hydrochloric acid, pepsin and various minerals and mucus. Each one of these molecules has its own role of function for food digestion [48]. Gastric lipase binds to the surface of the lipid droplets, where it converts the encapsulated triacylglycerols (TAG) into diacylglycerols (DAG), monoacylglycerols (MAG), and free fatty acids (FFA). This process is called triglyceride hydrolysis or lipolysis in which the triglyceride molecule is broken down into FFA, MAG and DAG to complete the lipid digestion and ultimate absorption of fat. There is a minimal to zero absorption in stomach and the small intestine is the main absorption site for food and other active compounds/substances. Around 30-40% of lipid hydrolysis is achieved in the stomach and the reason for the hydrolysis not exceeding 40% is due to the droplets' surface. The droplets' surface becomes covered with free fatty acids and therefore the lipase cannot access the TAG in order to complete the hydrolysis. The physicochemical mechanism for the inhibition of gastric lipase by fatty acids is believed to be the trapping of the lipase within a colloidal

structure (200 nm) that is comprised of FFA, DAG, MAG and phospholipids [50, 51].

### **3.2.3 The small bowel**

The small intestine is the mid-region in the GI tract between stomach and large intestines (colon). It can be considered to be a tube-like structure (about 2.5 to 3 cm in diameter) consisting of three major regions: duodenum (about 26 cm long), jejunum (about 2500 cm long) and ileum (about 3500 cm long). However, the actual total surface area of the small intestine in humans is much greater due to the presence of villi and microvilli which increase the surface area to approximately 200 m<sup>2</sup>. This large surface area makes the small bowel the main absorption site of the GI tract [52]. The pH of the small intestine varies from one region to another: it is around 5.8-6.5 at the duodenal site and increases to pH 7 at the lower part of the small intestine. The reason is that the duodenum is slightly more acidic because it is closer to the stomach where the pH is around 1-3 where pancreatic enzymes work effectively. Also, the bile salts and phospholipids from the gallbladder act as a surface acting agent to emulsify any TAG fat constituents of the food. Bile salts are extremely important for lipid digestion and absorption processes. As mentioned earlier, bile salts are surface acting molecules that adsorb to the oil water interface and form micelles and colloids in water. Bile salts are synthesised from cholesterol in the liver. Their chemical structure consists of a hydrophobic site, that interacts with molecules which are non-polar such as oil and an hydrophilic site, that interacts with polar molecules such as water.

### 3.2.4 The colon

The large intestine, also known as the colon, has 3 main physiological regions: the ascending colon, the transverse colon and the descending colon. There are also other regions known as the caecum (this is a small region including the appendix and is located between the ascending colon and the end of the small intestine) and the sigmoid colon and anorectum regions at the other side. Overall, the length of human colon is approximately 1.5m long and around 7.5cm in diameter. Cell types in the colon are the same as those in the rest of the GI tract except that the small intestine villi are not present in the stomach nor in the colon. There are 3 major functions of the colon including: collecting all unabsorbed materials from GI tract to form a solid waste (faeces), re-absorption of minerals (such as vitamins, water, salts and sugars) and bacterial digestion. In summary, the colon absorbs and secretes fluid and thereby maintains normal salt and water homeostasis [52].

The colon is considered to be the most difficult region of the GI tract to simulate due to variations in bacterial populations that exist in different parts of the colon. The caecum and ascending colon are the areas of the intestine where microbial activity is higher [53]. The microbes in the large intestine digest food residues such as carbohydrates and proteins. Bacteria in this region of the GI tract are responsible for breaking down organic matter by anaerobic reaction or fermentation whereby these microorganisms gain energy [54]. There is limited absorption in the colonic region of the GI tract, however throughout the fermentation short chain fatty acids go through their final stage the digestive process. Bacteria in the colon deconjugate bile acids and modify steroid which comes back to the liver via the enterohepatic circulation [33, 55].

### **3.2.5 Gastrointestinal response to a meal**

There are numerous activities taking place in the GI tract in response to meal arrival, however the discussion in this section will briefly concentrate on three main responses which can be summarised as:

- Physical response: for example the GI tract can accommodate large volumes of food in the stomach, can transfer chime material to the small intestine and colon and can collect waste at the end of the colon for excretion.
- Physicochemical response: where a wide range of chemical reactions takes place from mouth to colon. This chemical reaction/interaction includes fermentation, emulsification, conjugation and more.
- Hormonal and secretory response: the gut releases hormones and enzymes at each stage of digestion along the tract. For example lipase and pepsin in stomach, bile salts in small intestine, the peptide response to feeding such as the relevant cholecystinin (CCK) responses to feeding, and the physiologic role of CCK in gallbladder contraction.

### **3.2.6 Gastrointestinal responses to fat**

Fat is one the major components of our diet, it is a source of energy (phospholipids, triglycerides etc) and can be obtained from animals or plants directly or indirectly. Fats are incorporated into many processed foods in order to improve the texture, taste, appearance and palatability. The complex mix proteins, carbohydrates, vitamins and micronutrients that make up a meal may impact positively on stability, solubility and absorption of fat [56-58]. It is well documented that food ingestion triggers many stimuli within the GI tract that

modulate motility, salivary secretion, appetite and releasing gastrointestinal hormones such as CCK, peptide YY (PYY) and glucagon-like peptide (GLP) [59]. There are 2 major GI tract responses to nutrient intake and these are: the cephalic response (a number of vagal cholinergic activities initiated by smell, thought, sight and taste etc); and intestinal phase response where ingesting fat will stimulate the secretion of CCK, PYY and GLP, which eventually inhibit gastric emptying and appetite. Dietary fat, specifically the free fatty acids (FFAs), interact with the oral cavity and small intestine in order to adjust energy intake [60, 61]. Sensing of nutrients in the small intestine plays an important role in the regulation of GI tract function and energy intake [62]. Manipulation of the formulation of fat emulsions can modulate these responses. One possibility is to reduce the fat droplet size which will allow the lipase to have enough surface areas to bind [63]. This will allow FFA to be delivered into the small intestine and control gastric emptying. Another possibility is to change intragastric spatial distribution of the fat [64].

The consumption of high fat levels has been linked to medical conditions such as obesity and cardiovascular diseases.

### **3.2.7 Fat bioavailability**

The term “bioavailability” is primarily used by pharmaceutical and food industries to estimate the effect of an active ingredient in a formulation. According to Taylor & Lloyd [65], the term bioavailability is defined as “the rate and the extent to which an active ingredient is absorbed and becomes available at the site of action and therefore gives a therapeutic response or nutrient effect”. There are other terms relating to bioavailability including relative bioavailability (this is comparing the rate and extent of two similar formulations e.g. standard product and test product) and absolute

bioavailability (this is comparing the same formulation in different delivery routes). There are number of physiological factors that can influence fat bioavailability including [65-68]:

- Gastrointestinal motility including: segmentation, tonic contractions and peristalsis.
- The pH in the GI tract which varies from one region to another. For example; low pH in the stomach (around pH 1 to 2) and high pH in small intestine and colon (at around pH 5-7).
- Metabolism: this is complex and involves the interplay of many aspects, from enzymes (such as Cytochrome P450 3A4) to first-pass metabolism in the liver.
- Individual variation: there are variations between individuals such as gender, age, race and disease state that can affect the oral bioavailability.
- Other contents of gut including secretions and bile salts.

The physiological factors are not the only aspects that influence oral bioavailability; however there are many other factors that can affect oral bioavailability such physicochemical factors including pKa, lipid solubility and partition coefficient and solubility. Other important factors that can affect oral bioavailability are particle size, droplet sizes and additives [3, 65].

In order to determine bioavailability it is necessary to measure the amount of active ingredient in the blood plasma. This is normally done by taking blood samples which can be time consuming, inconvenient to many and it may also deter people from participating in studies. Therefore, an alternative way for measuring the bioavailability of formulations becomes an interesting topic of research. Non-invasive techniques such as magnetic resonance imaging

(MRI) and magnetic resonance spectroscopy may provide us with a method of monitoring the transit of food components through the gastrointestinal track to target organs such as the liver and muscles.

### **3.2.8 Satiety responses**

The satiety response to fat may start well before ingesting food and the impact of this may last hours after the ingestion of fatty food. There are many cephalic responses such as the smell, thought and taste of food which influence the absorption and utilised nutrient through the vagal cholinergic activity [62]. When fat is emptied from the stomach into the small intestine the small bowel releases hormones such as CCK to slow gastric emptying and signal satiety. It is also reported that carbohydrates behave similarly to fat by releasing these hormones to delay gastric emptying [59]. However, the length of chain of free fatty acids can modulate both energy intake and suppression of hunger. The gold standard method for assessing satiety is a self-report visual analogue scale (VAS) technique. This is difficult in terms of its accuracy due to subject to subject variation as well the physiological response.

### **3.2.9 MRI of GI tract**

MRI of the GI tract initially developed slowly compared to MRI of other organs due to artifacts caused by respiratory movement (breathing) and peristaltic motion. The first gastrointestinal MRI papers were published in the late 1980s to early 1990s [69, 70]. These early MRI images of the GI tract were acquired using EPI. EPI at low field (0.5 T) was well suited for dynamically assessing gastric physiology [71] and imaging the stomach contents with excellent contrast between water based meals and the surrounding tissues [69]. EPI

acquires images very rapidly (in under 130 ms) overcoming artifacts due to abdominal motion. Furthermore, the EPI pulse sequence gives intrinsically  $T_2^*$  weighted images, and hence provides excellent contrast between water-based liquid meals and surrounding tissues, and between the liquid and solid components of a meal [69, 72], without the need for the addition of MRI contrast agents. Over recent years there has been considerable progress and most modern imaging sequences can take good quality images of the abdominal organs at 1.5T and also 3T.

A number of physiological parameters can be obtained using these techniques on the GI tract such as gastric emptying (gastric volume with time), stomach spectroscopy, gallbladder contraction (volume with time), liver volume assessment, liver spectroscopy, small bowel water contents (SBWC) and colon volumes and assessing its functions or motility.

### **3.2.10 Gastric volume measurement**

MRI is capable of providing good contrast between the stomach contents and the stomach wall as well as the surrounding areas (organs such as spleen, liver, heart). Therefore, it is easy to visualise the stomach contents over time. Gastric volume measurement were validated with gold standard methods such as gamma scintigraphy and intubation and both correlated well with MRI gastric emptying measurement [73, 74]. The rate of gastric emptying depends on the type of food, calorie load and its structural formation. For example liquids like water and beverages empty relatively rapidly compared to fat and solid food. The SPMRC has published several papers on MRI of gastric emptying of a variety of food types [75-77].

### **3.2.11 MRI of gallbladder volume**

The gallbladder is small organ that is adjacent to the liver, links with the pancreas by the pancreatic duct and also links with the duodenum by the bile duct. The content of the gallbladder is mainly bile salt produced by the liver and used for fat digestion. Using the bTFE sequences provides good contrast for the liquid in the gallbladder against the surrounding organs, and can be processed similarly to the stomach volumes. Gallbladder contraction can be considered as a biomarker for fat digestion. Therefore, there are many publications that highlight the link between gallbladder contraction, satiety hormones such as cholecystinin (CCK) and fatty foods [78, 79]. Cholecystinin cells are located in the small intestine, specifically in the duodenum and jejunum, but not in the ileum. CCK is release from these cells when they sense fat [80-82].

### **3.2.12 MRI of small bowel water contents**

The small bowel is subject to large fluxes of fluid (on the order of 6-8 litres daily) and this fluid is crucial for the digestion and transport of nutrients. Secretion and absorption vary with different foods and disease. Therefore, there is a need to visualise and measure the state of small bowel water content as this may affect digestion. Monitoring of bowel fluid can be done by intubation but this is very unpleasant for the subjects and can sample only limited segments of the bowel. The anatomical details of the small bowel can be visualised non-invasively by using MRI sequences without using contrast agents or intubation. The SPMRC developed a method to evaluate the amount of free water in the small bowel. This was developed and validated by Dr Caroline Hoad [83]. The method is based on using strongly T<sub>2</sub> weighted

HASTE or RARE sequences (similar to magnetic resonance cholangiopacreatography or MRCP). The fluid signal is normalised against cerebrospinal fluid (CSF) because it is relatively free water and is in the centre of the field of view inside the subject, which has many advantages over external phantoms. In order to quantify the free water in the small bowel, we use in-house software written in IDL (Research Systems Inc. Boulder, Colorado, USA) by this group. The operator needs to set their threshold by using the spine fluids and select the ROI of small bowel segment filled with water. This method assumes that only pixels with a signal bigger than the threshold contain water, which can lead to an underestimation of the amount of free water because of partial volume effects.

In summary the GI tract is presently poorly understood and MRI provides a non-invasive method of studying its function in health and disease.

## 4 Methods

This chapter provides some more details of the equipment and methods that were used in the studies described in the following chapters and/or provides brief additional descriptions of techniques which were not given in those chapters due to size and logical flow. This chapter is divided into 4 main areas: Bench techniques at Unilever, MRI scanners, breath test and CCK plasma assay methods and ethical approvals and GCP standards.

### 4.1 Bench techniques at Unilever

There were number of techniques and equipment that were used in order to carry out sample preparation, sample characterization and routine checks of samples' specifications: droplet size and rheology assessments.

#### 4.1.1 Homogenisers and microfluidiser

Two homogenisers were used to prepare emulsion samples for both *in vitro* and *in vivo* studies. These were the Ultra-Turrax and the Silverson (Figure 4.1 and Figure 4.2 respectively). The Ultra-Turrax is a rotor/stator system. Shear force and inert force in turbulent flow are the cause for the breakdown of the droplets, resulting in homogenisation. The machine has available five crushing

rotors, three types of seals and several special dispersing elements to adapt to a variety of applications. For this work all *in vivo* emulsions were prepared using an Ultra-Turrax (Model IKA T25BS2).



**Figure 4.1:** an Ultra-Turrax (Model IKA T25BS2), image taken from the manufacturer's website.

The Silverson is another mixer homogeniser which can produce a very unified particle size mixture. This uses and generates exceptionally high shear rates in a three stage mixing/homogenising process: the high speed rotor, the centrifugal force and hydraulic shear. The Silverson homogeniser can produce a fat emulsion droplet size at around 2 microns and above. This instrument has different meshes and variety of speed ranges for range of applications. This type of homogeniser (Silverson: model L5R) was used for Cross-field Coarse emulsion and preparations of locust bean gum (LBG) solutions.



**Figure 4.2:** the Silverson L5R homogeneiser, image taken from the manufacturer's website.

The Microfluidizer is based on a high pressure emulsification system. It consists of a high pressure pump and a high pressure dispersal unit as shown in Figure 4.3.



**Figure 4.3:** The Microfluidiser 110S® (Quelle).

The mixed compounds are put into the storage tank (A), which is connected with the reservoir (B). From there it is pressed into the interaction chamber (C) where the main reduction of the droplet size takes place. Within the interaction chamber the stream of fluid is separated by a barrier, creating two streams of fluid. These are then recombined at high speed and during this collision the droplets break-up and reduce their size. This instrument applies high pressure (range 3,000 psi to 23,000 psi) and was used to produce the Fine emulsions for these studies.

#### **4.1.2 Droplet size analysis**

There are number of instrumental methods available for particle size measurement. Laser diffraction methods were used to measure fat emulsions droplet sizes in this work.

Laser diffraction is usually the preferred method to carry out particle size analysis because it offers a short analytical time, robustness, high precision, reproducibility, wide measurement range and flexibility of operation using liquid, spray and dry dispersion attachments. The instrument used was the Malvern Mastersizer 2000 (Malvern, Worcestershire, UK) as shown in Figure 4.4.

The Mastersizer 2000 uses laser diffraction to measure the size of particles/droplets by measuring the intensity of light scattered as the laser beam passes through the sample.

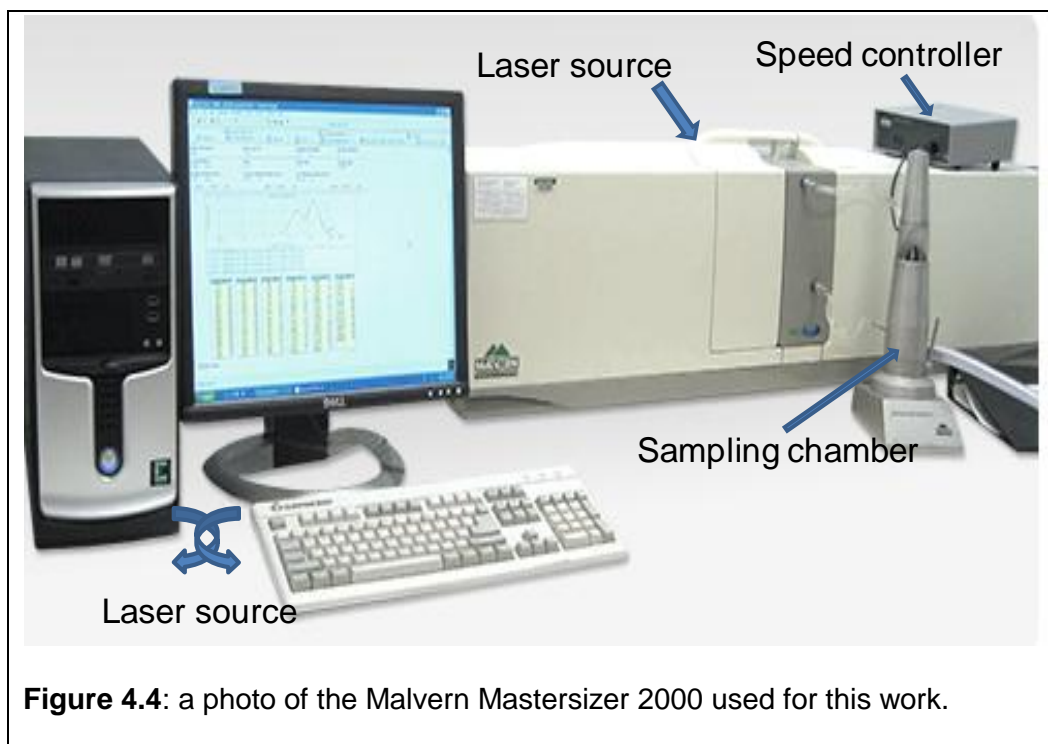


**Figure 4.4:** a photo of the Malvern Mastersizer 2000 used for this work.

The refractive index of sunflower oil and water were selected to model the data. The name of the tested samples and the average of number of cycles were documented. Initially, the stirred regulator was set at 2000 rpm. The emulsion sample was dispersed into the sample chamber in re-circulating water in the 'Hydro SM' measuring cell until an obscuration rate of 12– 14% was obtained. The dispersed sample was stirred until homogeneous dispersion without agglomeration was achieved. The sample was then pumped through the measuring zone (the laser beam zone without bias or distortion) and it was circulated again for further measurement. The mean emulsion droplet size is commonly reported as  $D[3,2]$  (the surface area mean diameter) or  $D[0,5]$  (a mass median diameter). The measurement was carried out in triplicate on each emulsion. The results were represented as particle size distribution. The instrument was then cleaned using distilled water at maximum speed until the desired cleanness was achieved before proceeding with a new sample.

### 4.1.3 Rheology

Rheology is defined as the study of deformation of solid matter and flow of liquid materials. The main interest for solid material rheology is based on its elasticity whereas the rheology of liquids is based on its viscosity measurement. Rheology measurement of the properties of food materials is important for the food industry because it allows design, monitoring and quality control of food. The most common viscometers are the steady shear and the oscillatory types. The rheometer that was used for this work was an Anton Paar Physica MCR 501 Rheometer as shown in Figure 4.5. All samples were measured at 37°C in small amplitude oscillatory shear with 17 mm diameter parallel plates on the Anton Paar MCR (cc17-0.25). The amount of sample loaded was 3 ml for each emulsion.



**Figure 4.5:** an Anton Paar Physica MCR 501 Rheometer (image taken from AntonPaar.com).

## 4.2 MRI scanners

This section describes briefly the MRI methods used for this work which was carried out using state of the art, research dedicated Philips Achieva machines at 1.5T and 3T. The work that was carried out on the 3T Philip Achieva scanner was the pilot work (described in Chapter 5) and part of the *in vitro* Cross-field experiment (described in Chapter 7). All other work was carried out on the 1.5T MRI scanner shown in Figure 4.6. For the *in vivo* experiments at 1.5T a range of abdominal scans were acquired in ~15 minutes.

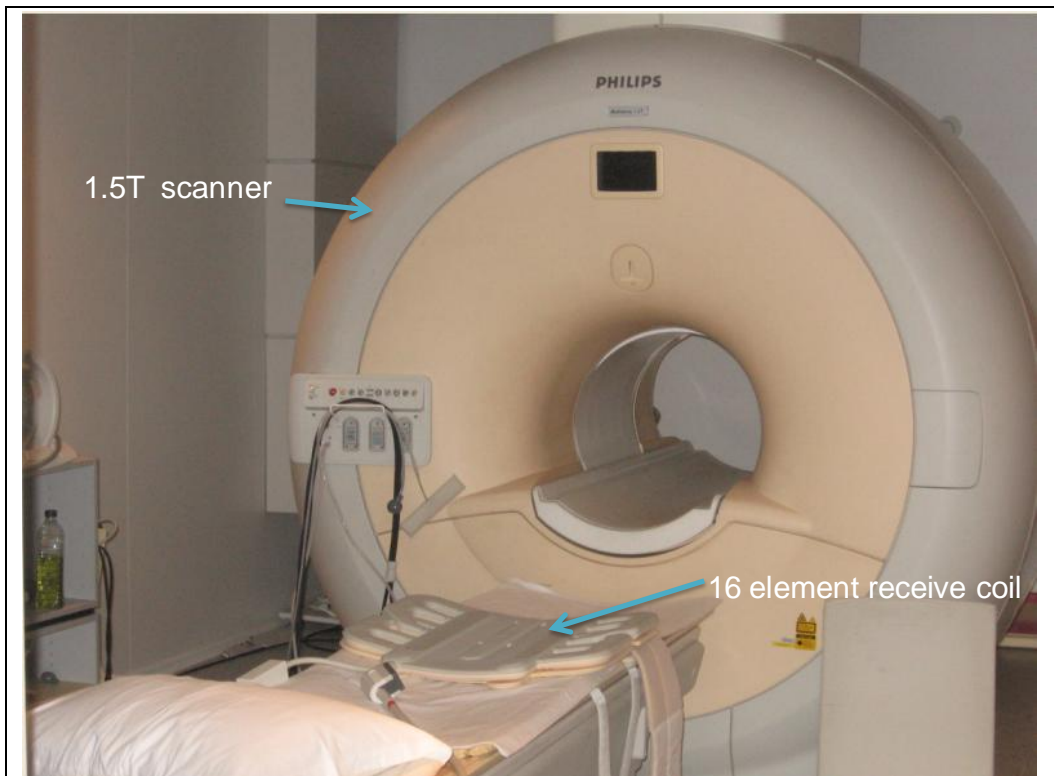


**Figure 4.6:** The Philips Achieva 1.5T scanner. The top half of the 16 element parallel receiver coil used for this work can be seen, the other half is below the bed padding.

**4.2.1 Scan day organisation**

The organisation of the study days on healthy volunteers was optimised to make best use of the expensive machine time. Two to three volunteers were interleaved per day and various staff including the research radiographer and, when necessary, the research nurses followed a printed day sheet which contained the timed interventions to be carried out such as taking breath or blood samples, preparing test meals and MRI scans. An example of such a day sheet is given in Figure 4.7.

	Subject A	Subject B	Subject C
Time			
Adjust the 2 study clocks in both rooms NOW to 8.30 am <input type="checkbox"/>			
8.30	2 x breath bags baseline <input type="checkbox"/> A baseline1 and A baseline2		
	Scan baseline <input type="checkbox"/>		
	Questionnaire <input type="checkbox"/>		
8.50	Insert venflon <input type="checkbox"/>	2 x breath bags baseline <input type="checkbox"/> B baseline1 and B baseline2	
	Blood baseline <input type="checkbox"/> ..... - 01	Scan baseline <input type="checkbox"/>	
		Questionnaire <input type="checkbox"/>	
9.10		Insert venflon <input type="checkbox"/>	2 x breath bags baseline <input type="checkbox"/> C baseline1 and C baseline2
		Blood baseline <input type="checkbox"/> ..... - 01	Scan baseline <input type="checkbox"/>
			Questionnaire <input type="checkbox"/>
9.15	Feed fat emulsion <input type="checkbox"/> Leftover emulsion weight (g) .....		
9.30	Breath bag t=0 min <input type="checkbox"/> A1		Insert venflon <input type="checkbox"/>
	Blood t=0 min <input type="checkbox"/> ..... - 02		Blood baseline <input type="checkbox"/> ..... - 01
	Scan t=0 min <input type="checkbox"/>		
	Questionnaire t=0 min <input type="checkbox"/>		
9.35		Feed fat emulsion <input type="checkbox"/> Leftover emulsion weight (g) .....	
9.45	Breath bag t=15 min <input type="checkbox"/> A2		
9.50		Breath bag t=0 min <input type="checkbox"/> B1	
		Blood t=0 min <input type="checkbox"/> ..... - 02	
		Scan t=0 min <input type="checkbox"/>	
		Questionnaire t=0 min <input type="checkbox"/>	
9.55			Feed fat emulsion <input type="checkbox"/> Leftover emulsion weight (g) .....

**Figure 4.7:** an example of a page of a daily scan sheet for the main physiological study at Chapter 6.

### 4.3 Breath test and plasma assay methods

#### 4.3.1 IRIS Machine for breath samples

Stable isotopes such as  $^{13}\text{C}$  are safe to use for non-invasive diagnosis. A  $^{13}\text{C}$  substrate can be ingested with a meal and metabolised and excreted in the breath. This can be collected and analysed using infrared methods such as the infrared isotope analyzer IRIS® (Wagner Analysen Technik, Bremen, Germany), which allows a precise determination of the two isotopes,  $^{13}\text{CO}_2$  and  $^{12}\text{CO}_2$ . This was used in these studies. The results are presented as delta-over baseline values (DOB) which indicates the change in the  $^{13}\text{CO}_2/^{12}\text{CO}_2$  ratio brought about by the metabolic activity induced by the administration of the labelled substrate. The breath samples were collected by using breath bags (Figure 4.8) designed for the Infra Red ISotope Analyser (IRIS) machine (Wagner Analysen Technik, Bremen, Germany) shown in Figure 4.9.

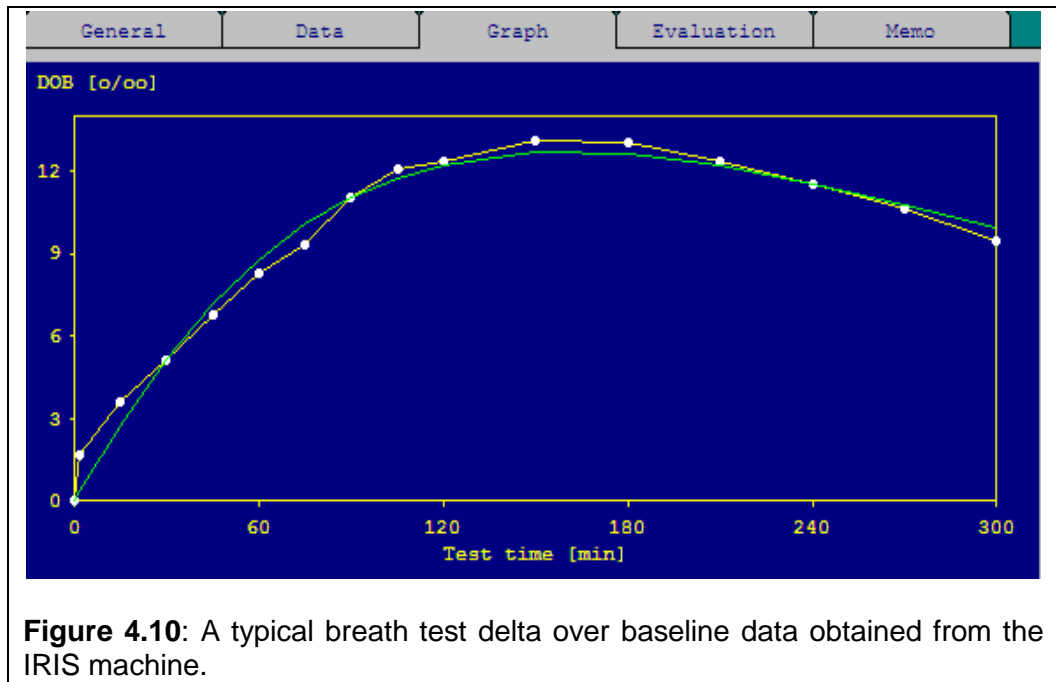


**Figure 4.8:** Image of the breath bag that was used to collect breath samples.

Two  $^{13}\text{C}$ -labelled compounds were used for this work and they were  $^{13}\text{C}$ -triolein and  $^{13}\text{C}$ -Octanoic acid for pilot work and the main physiological study (Chapters 5 and 6 respectively). The volunteers were asked to breathe into the bag at an initial baseline and at regular intervals for 4-5 hours depending on the study. These breath samples were then analyzed by using the IRIS machine shown in Figure 4.9. The output from the IRIS machine consists of a plot of the delta over baseline (Figure 4.10), a fit to the data and a calculation of  $T_{1/2}$ ,  $T_{\text{lag}}$  and % of  $^{13}\text{C}$  metabolised during the time experiment.



**Figure 4.9:** a photo of the IRIS machine used to analyse breath samples.



#### 4.3.2 CCK plasma assay

The volunteers were cannulated in a forearm vein by a qualified research nurse as shown in Figure 4.11. 10 venous blood samples (6.5 ml) were collected by syringe at 30-min intervals for the first 2 h and 60-min intervals afterward up to 5 h. The blood was quickly transferred into chilled blood collection tubes containing 0.3 ml EDTA and 5,000 KIU aprotinin. The samples were cooled in an ice bath immediately. The plasma was readily separated by centrifugation (Figure: 4.12) at 4°C, and the plasma snap-frozen in liquid nitrogen and then stored at -70°C until assayed by Dr. Gulzar Singh at the School of Biomedical Sciences as described previously [26].

Briefly, the methods were as follows. The plasma samples were extracted before assay to eliminate nonspecific interference from plasma proteins. One ml of plasma was added to 2 ml of 96% ethanol, vortex mixed in a glass tube. The tubes were allowed to stand on the bench for 10 min, before centrifugation at 3000 g for 10 min. The supernatant containing CCK was

decanted into another glass tube and evaporated to dryness in vacuum before being re-dissolved in 1 ml of phosphate buffer.



**Figure 4.11:** shows the cannulation in a forearm vein of the volunteers and sample taking.



**Figure 4.12:** The fisher refrigerated centrifuge used to separate the plasma in the blood and all the blood tubes set-up for a study day.

The concentrations of CCK were then measured by radioimmunoassay (RIA) with commercially available kits according to the manufacturer's instructions (EURIA-CCK, Euro-Diagnostica, obtained from Immunodiagnostic Systems, Ids, Tyne and Wear, UK). Briefly, the samples and the standards competed with <sup>125</sup>I-CCK-8 sulfate in binding to antibodies of CCK-8 sulfate. The antibody bound with <sup>125</sup>I-CCK-8 sulfate was separated from the unbound fraction by using a double-antibody solid phase. The radioactivity of the bound fraction was then measured in a gamma counter. The minimum detectable concentration for CCK was 0.3 pmol/l of sample with intra- and interassay variations less than 6 and 15%, respectively. The antibody was highly specific, cross reactivity being <0.01% to CCK-(26-33) nonsulfated, CCK-(30-33) and gastrin-17, nonsulfated, 0.5% to gastrin-17, sulfated compared with CCK-(26-33) sulfate (CCK-8).

#### **4.4 Ethical approvals and GCP standards**

Each study received full ethics approval from the local University of Nottingham Medical School Research Ethics Committee. Informed written consent was obtained from each subject participating in the study. The approval numbers were B/11/2008 for the initial pilot studies and the main physiological study and C10052012 for the final quantification phase.

All human studies were conducted in compliance with their protocols, the Declaration of Helsinki and the principles of Good Clinical Practice. These include

- keeping the rights, safety, and well-being of the trial subjects as the most important consideration

- recording, handling and storing all study information in a way that allows its accurate reporting, interpretation and verification (e.g. using Case Report Forms and Trial Master Files)
- implementing systems and standard operating procedures that assure the quality of every aspect of the study

After the initial pilot phase for which the data were processed in 'open label' fashion, the human studies were carried out to clinical trial standard. The test meals were given to the volunteers following a latin square randomisation schedule to avoid order effects. The volunteers were kept blind to the test meal type. The author prepared the meals and knew the randomisation schedule but after this one member of the team who was not involved with this study subsequently blinded the data file names according to approved standard operating procedures for analysis hence the trial become a double-blind. A formal blind data review was carried out both at Nottingham by the study team and at Unilever and all data queries were answered before breaking the blind codes.

## 5 Development work on fat emulsion systems and their characterisation

This thesis chapter describes the development and characterisation of two fat emulsion meal systems (with a small and large droplet size) using a range of bench and MRI techniques and *in vitro* digestion models. The emulsions' performance was finally tested *in vivo* in healthy volunteers using MRI.

### 5.1 Background

The relationship between meal structure and composition, the way the meal is handled by the body and the resulting sense of satiety are critical to improve understanding of how to control and reverse the rising tide of obesity. This is particularly true with respect to fat which is a highly palatable and highly caloric component of food, often added in marked amounts to pre-processed foods in the western world. Magnetic resonance imaging (MRI) can monitor non-invasively and in a single study session many parameters of gastrointestinal (GI) function [84], including the spatial distribution of fat and water in the stomach separately [23, 25, 85] and these parameters can be related to hormonal responses and the sense of satiety [23, 26] in complex physiological studies on healthy volunteers, of which the Nottingham group has a long and successful track record.

One question remains unanswered thus far from previous experiments: for a given amount of fat in a well characterized, model fat emulsion meal, what is the effect of the fat emulsion droplet size on the gastrointestinal physiological responses and the resulting sense of satiety?

The work described in this chapter aimed to provide an answer to this research question. Two sunflower oil fat emulsion model meals developed initially by colleagues in Unilever were used. These fat emulsion meals have the same volume, amount of fat and taste but two markedly different fat droplet sizes, one of the order of 400 nanometers (called here throughout the **Fine** emulsion) and one of the order of 8 micrometers (called here throughout the **Coarse** emulsion). After an initial MRI assessment these emulsions were characterised *in vitro* in the Unilever laboratories using a range of techniques such as bench rheology for viscosity profiles, laser diffractometry for droplet size and *in vitro* digestion models with gas chromatography / mass spectrometry (GC-MS) for fat hydrolysis. The performance of the two emulsion systems was subsequently assessed *in vivo* in a limited series of pilot studies in healthy volunteers.

## 5.2 Initial development and characterisation

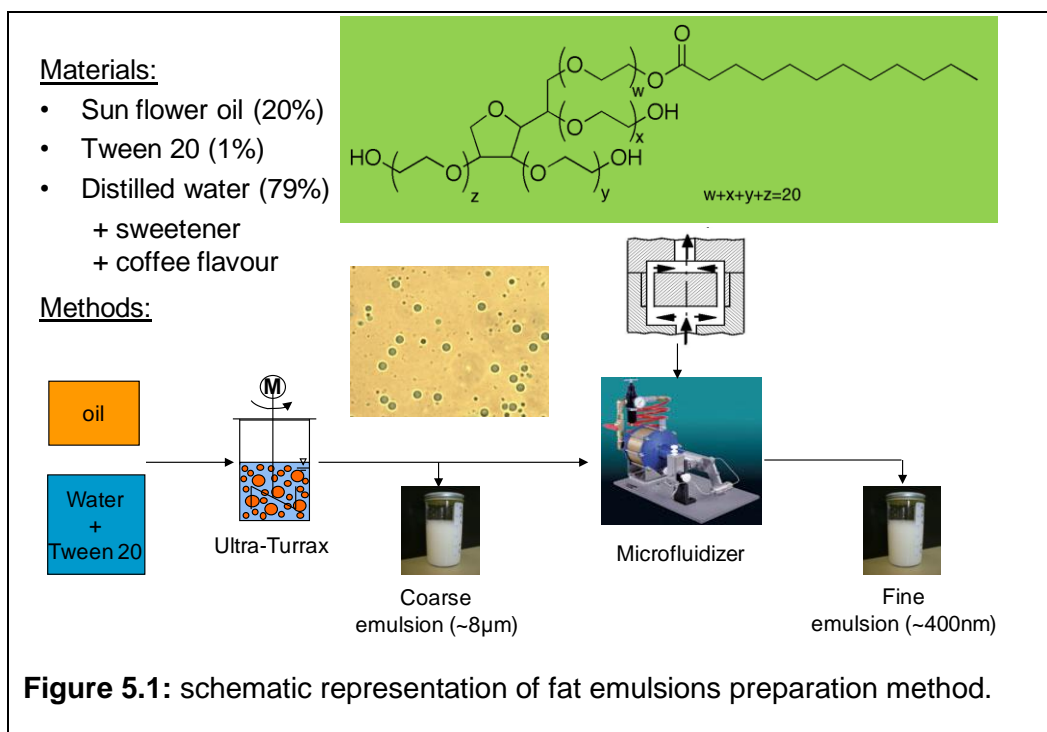
The emulsions were made of 79% distilled water, 20%, sunflower oil and 1% Tween20. Two tablets of sweetener (Hermesetas mini sweetener) and 1.5g coffee flavour (Dr. Oetker coffee flavouring) were added in order to improve the taste of the emulsion.

The main two fat emulsion to be investigated were:

- a Coarse emulsion with a mean diameter of approximately 8  $\mu\text{m}$  (the **'Coarse'** emulsion)

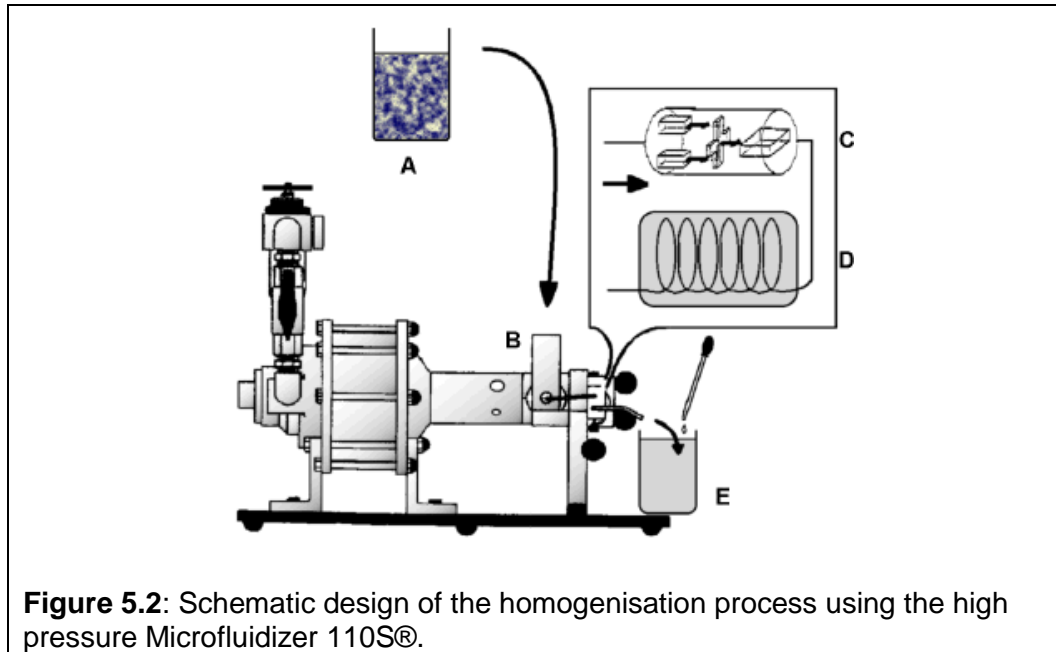
- a Fine emulsion with a mean diameter of approximately 0.4  $\mu\text{m}$  (the 'Fine' emulsion).

The overall preparation procedure for the emulsions is shown schematically below in Figure 5.1. To produce the Coarse fat emulsion an Ultra-Turrax was used. The Ultra-Turrax is a rotor/stator system where shear force and turbulent flow cause the breakdown of the droplets, resulting in homogenisation. The Coarse emulsion was produced using the Ultra-Turrax for 20 minutes with a rotation speed of 13,500 rpm. To produce the Fine emulsion the Ultra-Turrax was used again for 20 minutes with the same rotation speed. After this step the emulsion was passed through a Microfluidizer. The Microfluidizer as shown previously in paragraph 4.1.1 is based on a high pressure emulsification system. It consists of a high pressure pump and a high pressure dispersal unit (Figure 5.2).



The emulsion was passed through the system with a pressure of 1 bar at the inlet, which corresponded to 233 bar in the interaction chamber. The mixed

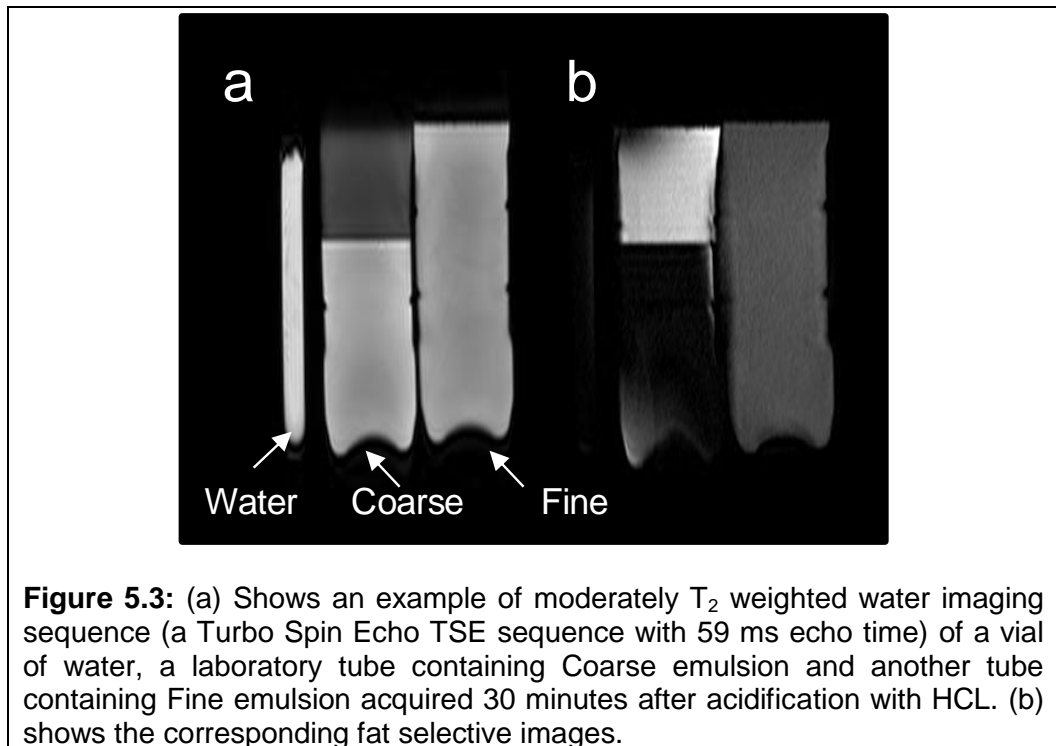
compounds were put into the storage tank (A), which was connected with the reservoir (B). From there it was passed into the interaction chamber (C) where the main reduction of the droplet size took place. There the stream of fluid is separated by a barrier, creating two streams of fluid which are subsequently recombined at high speed. During this collision the droplets break-up and reduce their size.



### 5.2.1 Initial MRI assessment

Figure 5.3 shows examples of the initial MRI images of the fat emulsion systems. This initial assessment was undertaken to verify *in vitro* that the emulsions could actually be imaged well before progressing their detailed bench characterisation. Such images showed that the Coarse emulsion, acidified with HCl to mimic stomach conditions, rapidly separated into two layers (fat creaming towards the top and water at the bottom due to density) whilst the Fine emulsion remained homogeneous as predicted. The  $T_2$  relaxation times were measured to give an idea of the range of  $T_2$ s in the two

fat emulsion systems and this is shown in Figure 5.4. These initial  $T_2$  measurements were carried out with the Philips proprietary T2CALC sequence. This generates automatically a  $T_2$  map using a spin echo type of sequence with an EPI readout. It acquires 5 echoes for 40 transverse slices with  $0.90 \text{ mm} \times 0.90 \text{ mm} \times 3 \text{ mm}$  resolution. The acquisition lasts about 6 minutes. This initial MRI experience was positive and showed that the two fat emulsions should provide good imaging characteristics *in vivo*.

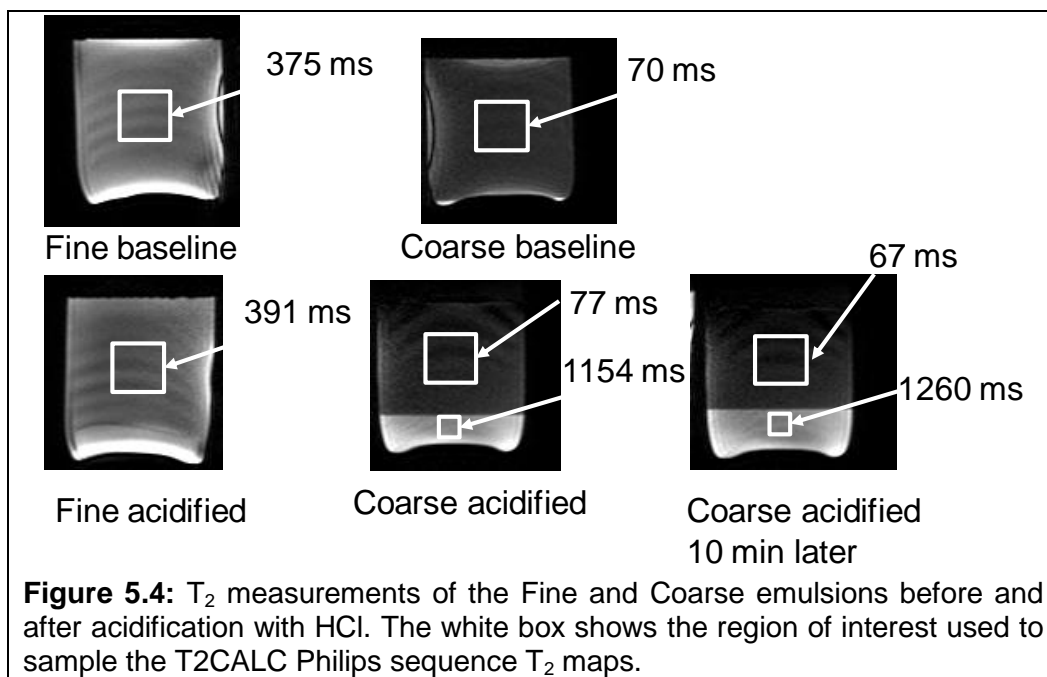


## 5.2.2 Fat emulsions stability

### 5.2.2.1 Introduction to emulsion stability work

Having reflected on the differences in creaming observed in the initial fat emulsion systems it was decided to evaluate thickened fat emulsion systems (containing Coarse and Fine fat emulsions) that will empty the fat phase from the stomach at the same rate. This would allow testing of the hypothesis that the GI/small bowel effects observed depend on surface area of the droplets

and not on differences in gastric emptying due to creaming of the Coarse emulsion. A number of thickening food materials were investigated including guar gum (GG), locust bean gum (LBG), citrus fibres and xanthan gum (XG).



Most of these are common food thickeners and all showed to be unstable in gastric condition due to impurities such as protein and other compounds. However the pure LBG from CPKELCO (Denmark) performed very well so an assessment of the concentrations needed to make the Coarse emulsion stable was made. The aim was to stabilize the emulsion for a period of several hours without compromising the texture i.e. viscosity and acceptability for our volunteers. In other words the aim was to prepare emulsions that were minimally thickened but stable (no creaming) throughout the gastric emptying process.

### **5.2.2.2 Specific methods for LBG concentrations**

3 different emulsions with different LBG concentration (0.3%, 0.5% and 0.7%) were prepared. The LBG was incorporated with both the Coarse (creaming in GI tract) and Fine emulsions. For example, to obtain a final 0.5% w/w LBG/water solution, 5 g of LBG powder was weighed in a weighing boat and dispersed in 495g of boiling water whilst stirring using a Silverson blender. Any aggregates were manually dissolved using a clean spatula and dispersed whilst stirring for 5 minutes. After this, H<sub>2</sub>O (101.5g) + Tween 20 (3.5g) + LBG (175g of 1%LBG) solution were placed in 600ml glass beaker and mixed well (due to thickness of the solution). Then the sunflower oil (70g) was added in and the mixture was placed in an Ultra-Turrax for 5 minutes at high speed. This yielded a final 0.5% LBG fat emulsion.

### **5.2.2.3 Specific methods for preparation of gastric solutions**

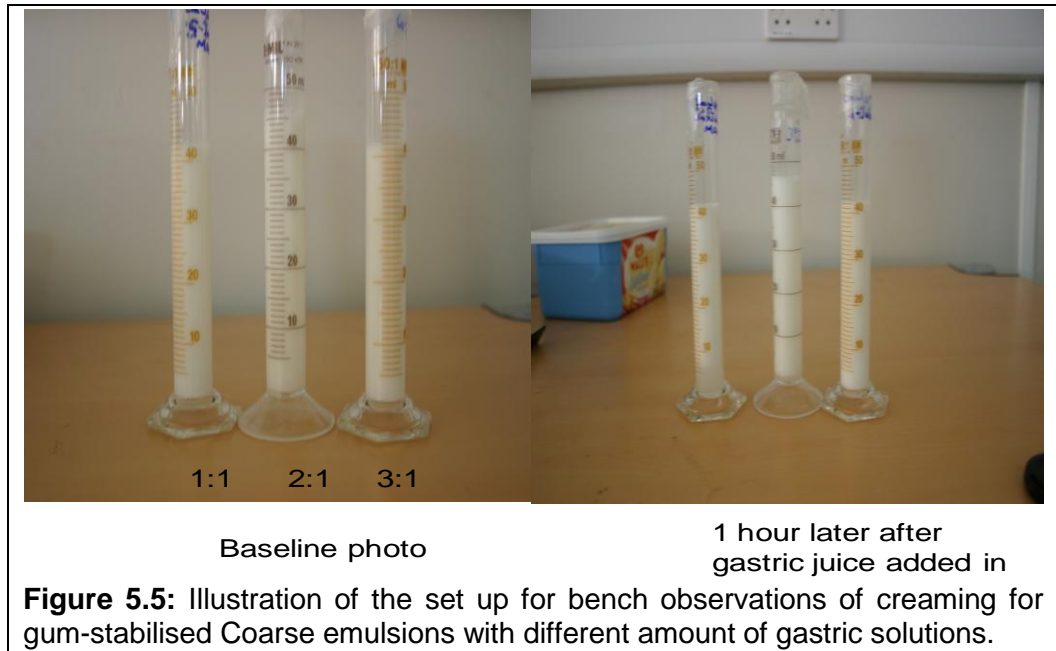
The stomach environment is acid and gastric secretion contain salts so in order to dilute the fat emulsion systems in a biologically relevant manner simulated gastric solution and not distilled water should be used. Dilution of the fat emulsions systems will be important to assess and predict intragastric stability. For this purpose in this work the gastric solution was prepared by dissolving the salts in distilled water to 200ml in a volumetric flask. The amounts and the type of salts added are listed in Table 5.1. The solution was then acidified with HCL as needed to reach pH=2.

Salts	Mw (g/mol)	Concentration (mM)	% Concentration (w/w)	Mass of Salt (g in 200ml)
KCl	74.55	5	0.037	0.075
CaCl <sub>2</sub> ·2H <sub>2</sub> O	147.01	5	0.074	0.147
NaCl	58.44	150	0.877	1.753

**Table 5.1:** Salts used to prepare the gastric solution

#### 5.2.2.4 Stability test

Different ratios of emulsion to gastric solution were used. These ratios were 1:1, 1:2 and 1:3 gastric solution:emulsion as shown on Figure 5.5. For example to prepare a 3:1 ratio (emulsion: gastric solution): 30g of emulsion was placed in a 50ml measuring cylinder and (10g) of simulated gastric solution was added in. The mixture was shaken until an homogenized solution was achieved. Then the cylinder was placed in an oven at 37°C. Visual observations of the creaming layer appearance and height in cm were subsequently made and recorded on the lab book every hour for 6 hours and the following day at the 24 hour time point. The same procedure was repeated for different ratios and emulsions (Coarse and Fine). The movement of the creaming part of the emulsions were measured hourly for 24 hours.



### 5.2.2.5 Results

Figure 5.6: shows the laser diffractometry data for 5 emulsions: 4 Coarse emulsions were shown to have similar droplet sizes whereas the Fine emulsion showed a smaller droplet size. The data are reported in Table 5.2.

Figure 5.7 shows the height of the aqueous phase for three different ratios of 0.5% LBG Coarse emulsion to gastric solution. The 1:1 ratio showed fast creaming. When the gastric solution ratio was reduced this slowed the emulsion creaming process. A simple calculation at  $t=6$  hour (assuming linearity) shows that the 1:1 ratio emulsion creamed at a rate of  $5.2 \text{ cm}^3/\text{h}$ , the 2:1 ratio emulsion creamed at a rate of  $3.2 \text{ cm}^3/\text{h}$  and the 3:1 ratio emulsion creamed at a rate of  $1.7 \text{ cm}^3/\text{h}$ . Figure 5.8 shows the experimental set up for these observations.

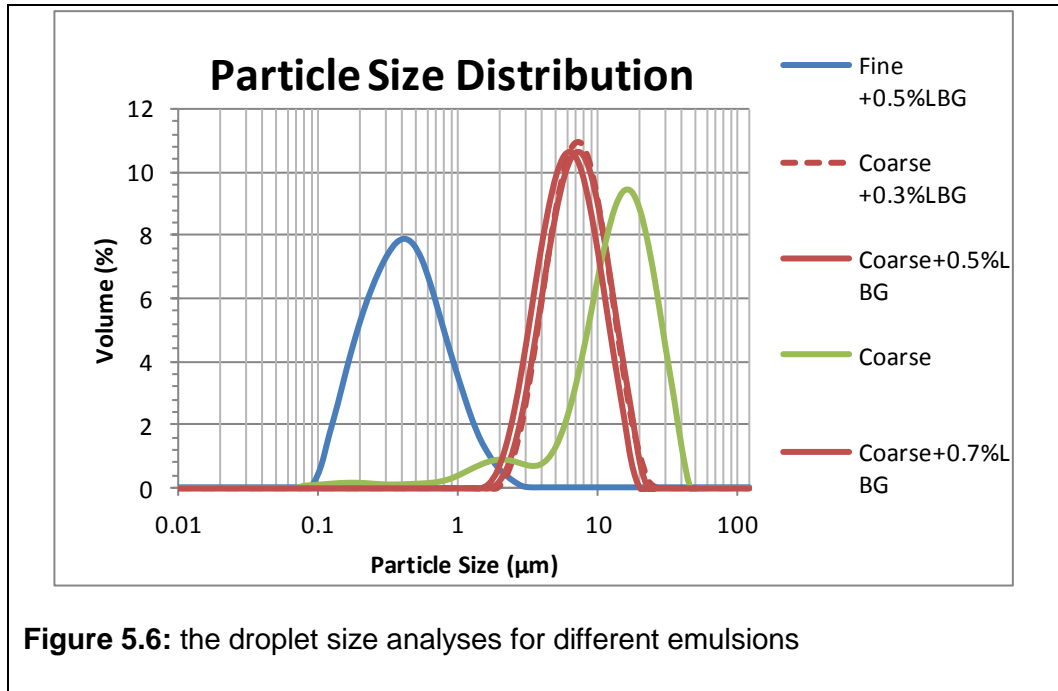


**Figure 5.6:** the droplet size analyses for different emulsions

	<b>Fine +0.5% LBG</b>	<b>Coarse +0.3% LBG</b>	<b>Coarse +0.5% LBG</b>	<b>Coarse +0.7% LBG</b>	<b>Coarse no LBG</b>
Measurements	Mean (micron)	Mean (micron)	Mean (micron)	Mean (micron)	Mean (micron)
D [3, 2]	0.43	6.92	7.01	6.58	8.10
D [4, 3]	0.59	4.21	8.14	4.58	14.12
D [0, 5]	0.45	5.45	6.47	6.41	7.12

**Table 5.2:** Summary of laser diffractometry data for the 5 emulsions used in the stability studies. The table reports the emulsion droplet size using the most commonly reported measures: D[3,2] (the surface area mean diameter), D[4, 3] (a volume mean diameter) and D[0,5] (a mass median diameter).

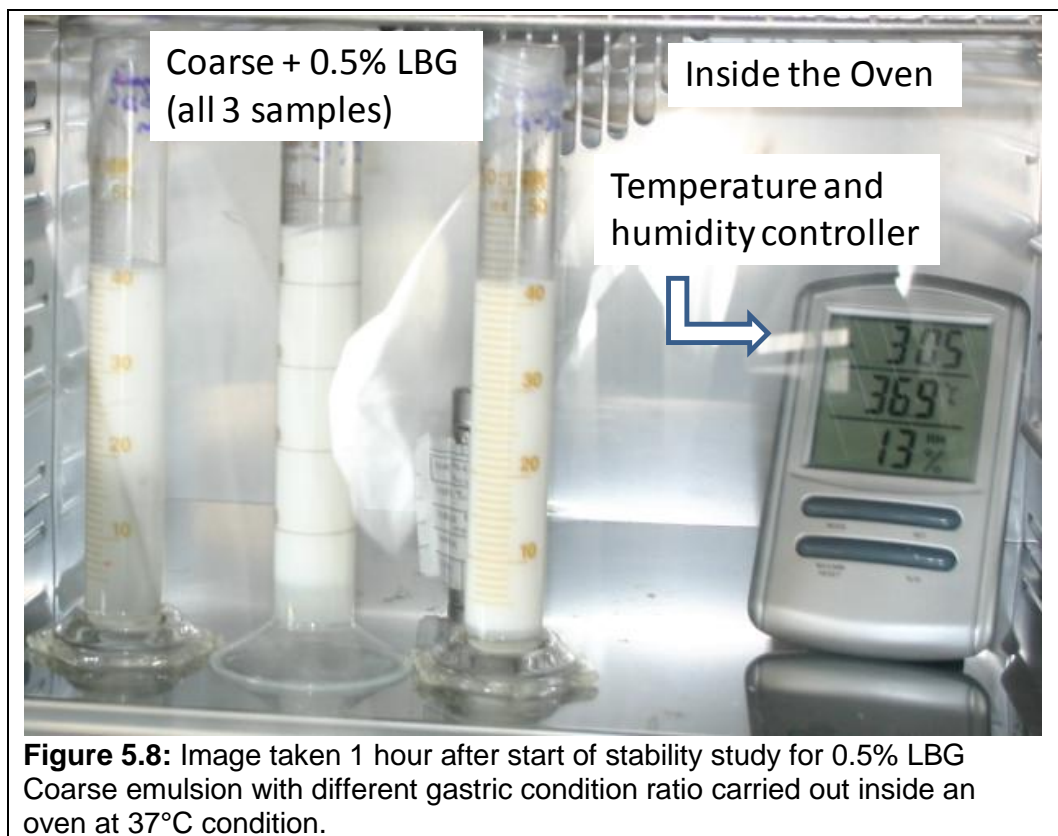
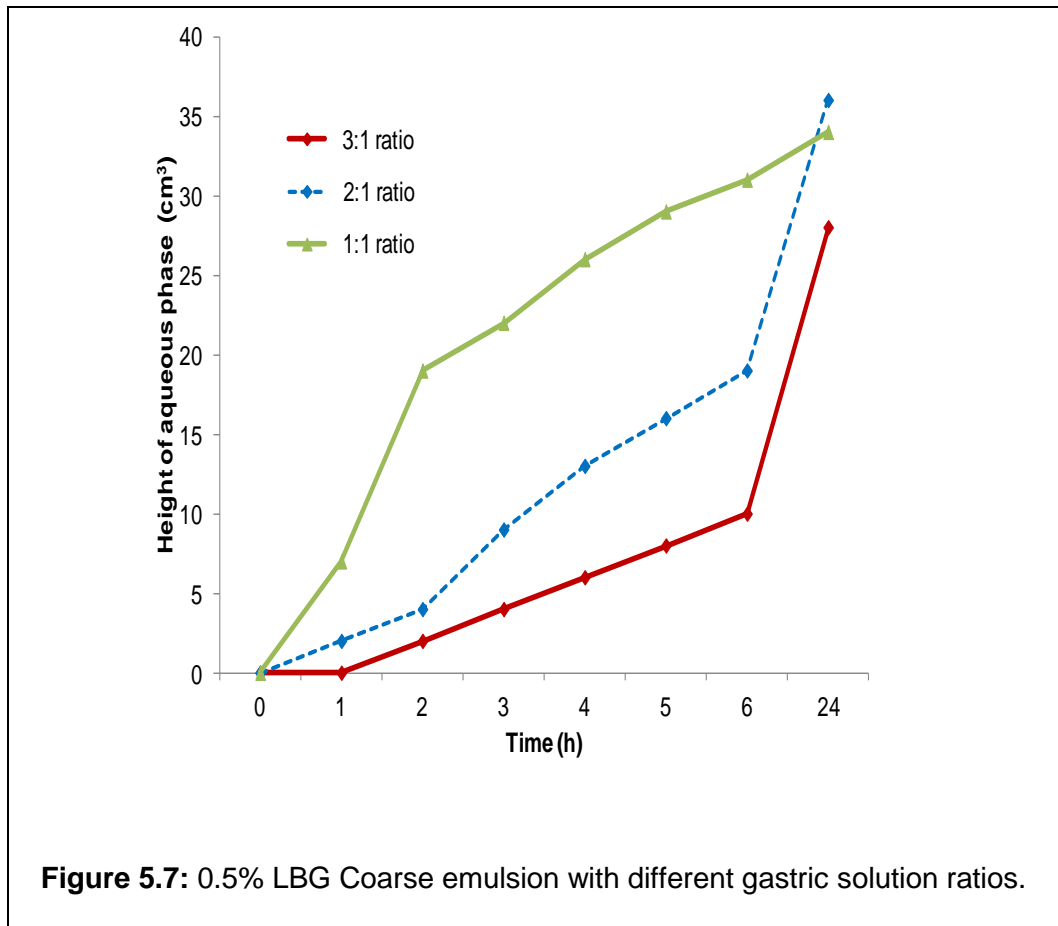
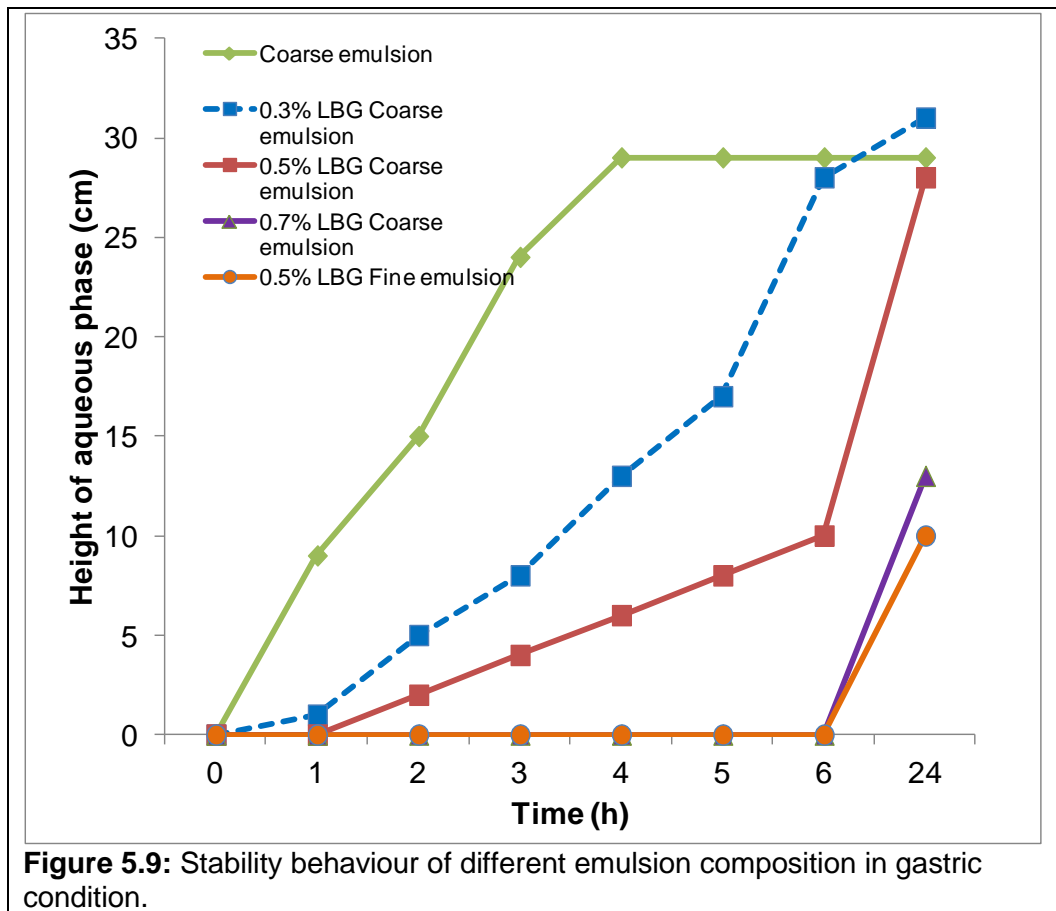
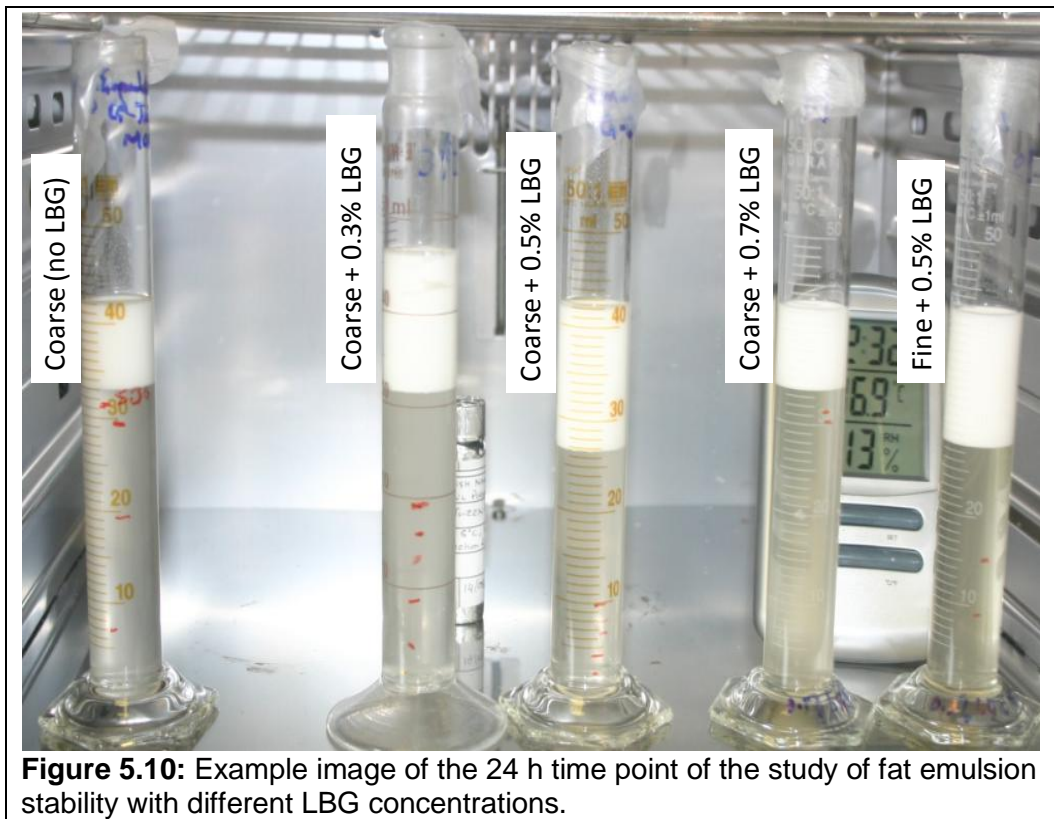


Figure 5.9 plots the data for the stability tests of different emulsions as shown in Figure 5.10, namely a Coarse emulsion (without LBG), a Coarse emulsion with different LBG concentration and a Fine emulsion with LBG. The ratio of emulsion to gastric solution used was 3:1. Figure 5.9 shows that the Coarse emulsion without stabiliser creamed up very rapidly whereas the introduction of LBG in the emulsion caused it to cream slower (the highest LBG concentration that was used was 0.7% which behaved the same as the Fine emulsion, with no creaming observed for more than 6 hours). The drawback of this was that the emulsion became very viscous which might make it difficult for the volunteers to consume. Therefore the maximum thickener to be used was chosen as a compromise to be 0.5% LBG.





**Figure 5.10:** Example image of the 24 h time point of the study of fat emulsion stability with different LBG concentrations.

### 5.3 *In vitro* gastric model experiment

Fat hydrolysis in the stomach is key to fat digestion. An *in vitro* gastric model of lipolysis was used in the Unilever laboratories, with the help of several colleagues there, to investigate the Fine and Coarse fat emulsions' hydrolysis. This may help in the prediction of the likely % hydrolysis of triglycerides in the subsequent *in vivo* studies and it will be useful in order to assist in the interpretation of the *in vivo* study data.

The main outcome here was the measure of the % hydrolysis of triglycerides of the Fine and Coarse droplet size fat emulsions. The aim was to understand whether emulsion droplet size and/or LBG addition could influence the rate and extent of hydrolysis. Also of interest was the comparison of the % of TG

hydrolysis values obtained from two different methods, namely the “pH stat” method (which measures the product of fat digestion soluble in the aqueous phase and titrable by NaOH only), and the “Gas Chromatography (GC)” method (which extracts the total hydrolysed products, aqueous and oil phases).

### 5.3.1 Preparation of fat emulsions and LBG solutions

There were 4 different droplet sizes, sunflower oil-Tween20 emulsions prepared for this task, namely:

- a) **Fine** (without LBG) - 350g o/w-emulsion with 20% sunflower oil/1% Tween20, with 0.4 $\mu$ m mean droplet size.
- b) **Coarse** (without LBG) - 350g o/w-emulsion with 20% sunflower oil/1% Tween20, with ~8 $\mu$ m mean droplet size.
- c) **Fine + LBG** - 350g o/w-emulsion with 20% sunflower oil, 1% Tween20, with 0.4 $\mu$ m mean droplet size with 0.5% Locust Bean Gum
- d) **Coarse + LBG** - 350g o/w-emulsion with 20% sunflower oil/ 1% Tween20, with ~8 $\mu$ m mean droplet size with 0.5% Locust Bean Gum

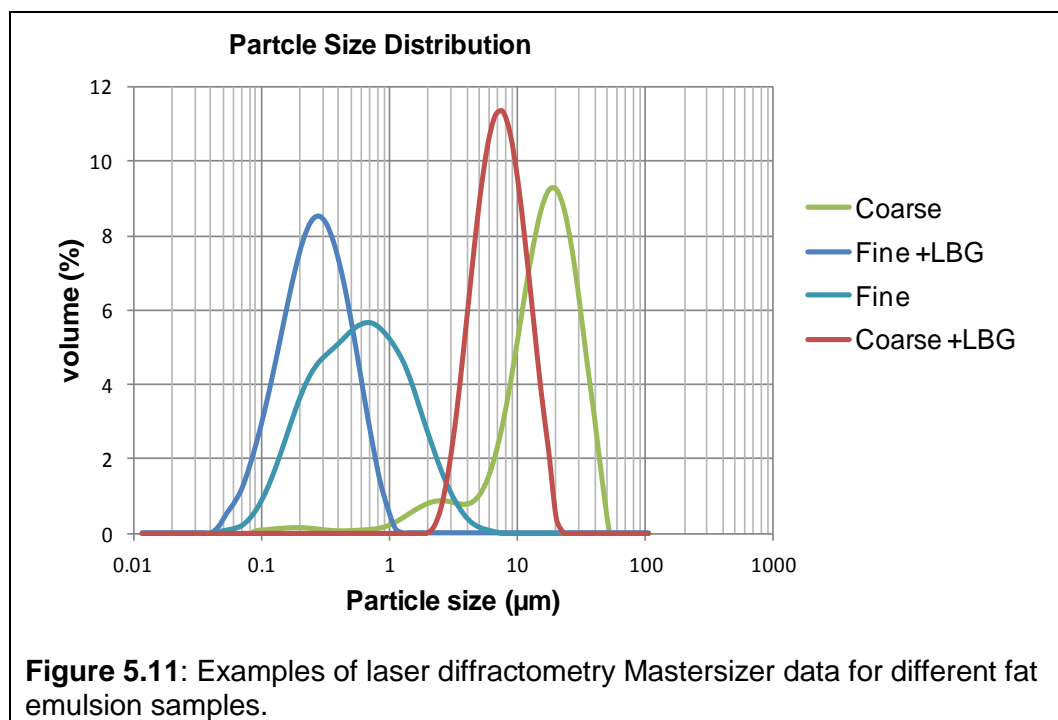
### 5.3.2 Preparation of gastrointestinal model solutions

The gastrointestinal model solution was prepared by dissolving the salts in distilled water to 200ml in a volumetric flask. The amount and the type of different salts added were listed in Table 5.1 above. 25mg of lipase RO and 60mg of pepsin were each dissolved in 2ml of gastric solution. The pH of the pepsin solution was approximately 4.25 whereas the pH of the lipase solution was approximately 3.80. The pH stat titrator is very sensitive when the pH of the mixture is below the predetermined pH and may cause overshooting of

NaOH when lipase and pepsin solution are added to the emulsion mixture in the pH stat sample chamber. Thus the pH of the lipase and pepsin solutions was adjusted to the desired pH using 0.1M NaOH before adding them to the emulsion mixture. The pH was adjusted between 5.5 and 6.5 (approximately 1-3 drops of NaOH solution were required depending on the pH needed).

### 5.3.3 Droplet size measurements

The droplet size of the emulsion was measured with laser light scattering using a Mastersizer 2000 (Malvern, Worcestershire, UK) using known refractive index of sunflower oil and water. Before the sample was dispersed into the sample chamber, the stirred regulator was set at 2000rpm. The emulsion sample was dispersed in re-circulating water in the Hydro SM measuring cell until an obscuration rate of 12– 14% was obtained.



The dispersed sample was stirred and pumped through the laser beam measuring zone. The mean emulsion droplet size is reported here as the surface-weighted mean diameter  $D[3,2]$ . The measurement was carried out in triplicate on each emulsion. The mean droplet sizes  $D[3,2]$  for Fine + LBG and Fine control was of the order of 400 nm, where the Coarse + LBG and Coarse Control were of the order of 7  $\mu\text{m}$ . The Fine emulsion had a broad peak compared to Fine+LBG emulsion. The Coarse and Coarse+LBG emulsions were similar apart from the Coarse+LBG emulsion size distribution was shifted slightly to larger values (green line on the right hand side of Figure 5.11). The data for the droplet size measurements are given in Table 5.3.

	<b>Fine+LBG</b>	<b>Coarse+LBG</b>	<b>Fine</b>	<b>Coarse</b>
Measurements	Mean (micron)	Mean (micron)	Mean (micron)	Mean (micron)
D [3, 2]	0.45	6.47	0.43	7.48
D [4, 3]	0.69	7.82	0.56	12.14
D [0, 5]	0.42	6.12	0.48	14.21

**Table 5.3:** Summary of laser diffractometry data for Fine+LBG, Coarse+LBG, Fine and Coarse emulsions for the gastric solution studies. The table reports the emulsion droplet size using the most commonly reported measures:  $D[3,2]$  (the surface area mean diameter),  $D[4, 3]$  (a volume mean diameter) and  $D[0,5]$  (a mass median diameter).

#### 5.3.4 pH stat experiment

The pH stat experiment is an established method to measure the hydrolysis of fat emulsions under continuous titration of the pH of the solution. The T70 titrator in Figure 5.12 allows simulation of the change in pH to maintain or

“stat” pH during lipolysis. In simulated gastric conditions, the pH is first adjusted to 6.0 where lipase and pepsin are added. The fungal lipase used is not active at low pH and therefore the pH stat experiments were conducted at pH 6. This value of pH may appear high compared to acid stomach secretion but is nevertheless relevant for pH conditions within the stomach during fed conditions [48].

The pH stat method used followed established laboratory procedures. Briefly, 3g of the emulsion was weighed out and placed in a 100 ml beaker. 53g of gastric solution were added into the emulsion and transferred into the sample holder of the pH stat titrator instrument. The sample holder with the mixture was attached to its position and the experiment was started by adjusting both the temperature ( $37.0 \pm 0.2$  °C) and pH ( $6 \pm 0.2$ ) for five minutes. After titration optimisation was achieved, the pepsin solution was added followed by the lipase solution. Then the baseline sample was collected and samples were taken every 15 minutes for two hours (except the 2 Coarse formulations as they were slow to be hydrolysed and therefore sampling intervals were changed accordingly).

The data in Figure 5.13 is the % hydrolysis calculated from the raw pH stat data: Coarse (Figure 5.13a) shows 3 phases, an initial short lag phase followed by a faster hydrolysis up to approximately 20 minutes and then a slower hydrolysis phase reaching approximately 5% hydrolysis after 2 hours.

The Fine emulsion (Figure 5.13b) shows initial rapid hydrolysis which slows after approximately 30 minutes, reaching >25% hydrolysis after 2 hours. The Coarse + 0.5% LBG (Figure 5.13c) shows an initial slow hydrolysis phase followed by an increased hydrolysis rate at later stages.

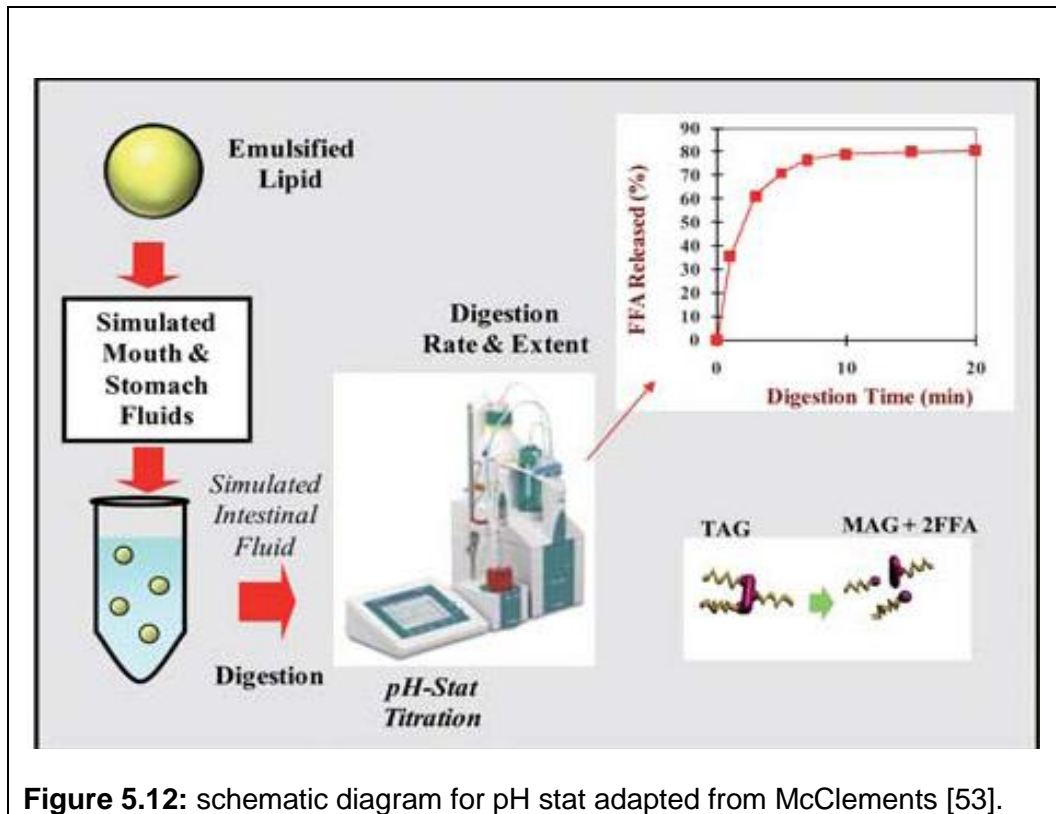
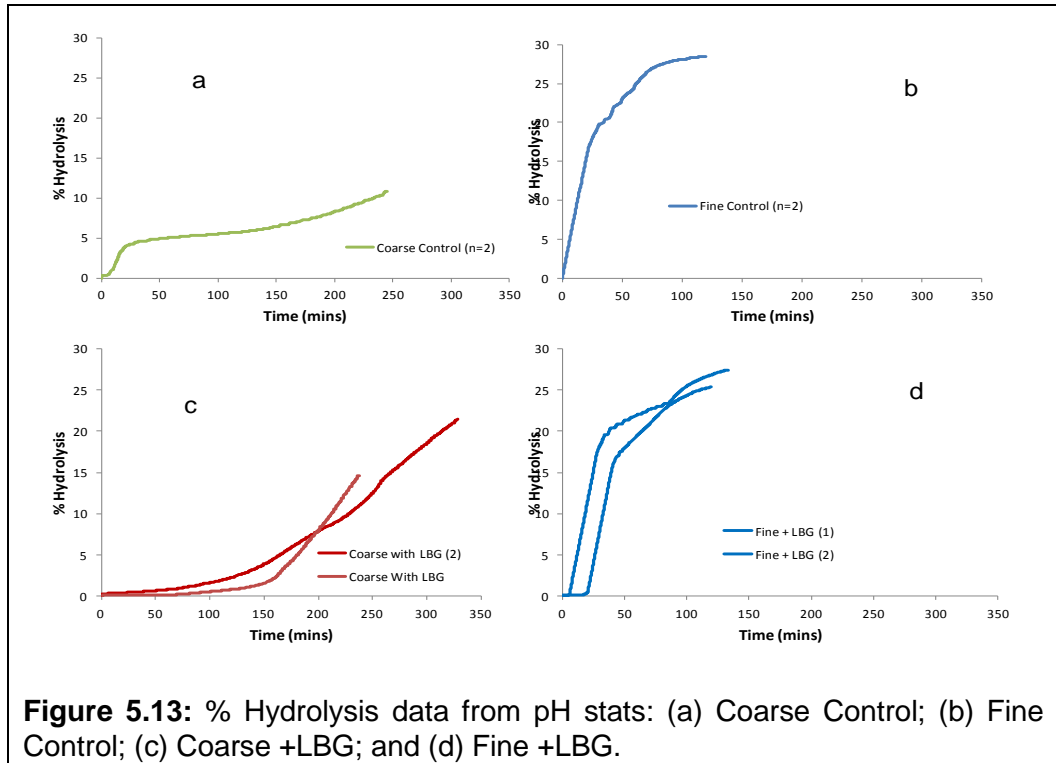


**Figure 5.12:** schematic diagram for pH stat adapted from McClements [53].

Some differences between the duplicates were observed and one of the samples was allowed to run for longer than the other, so they are plotted separately. The Fine + 0.5% LBG emulsion (Figure 5.13d) shows some differences between the two runs, one of which appeared to have a longer lag phase than the other. After this point (>20minutes) the hydrolysis has a rapid phase reaching approximately the same level of hydrolysis as the Fine emulsion without LBG.



### 5.3.5 Tributyrin experiment

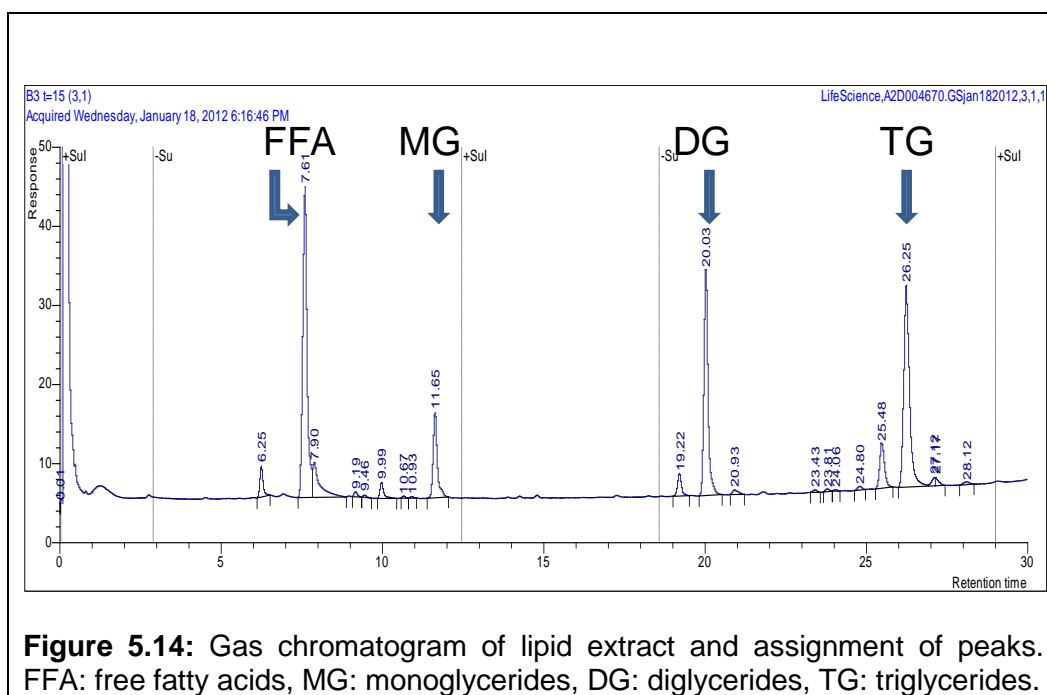
The tributyrin method was used in order to eliminate the possibility that LBG did not bind to the enzyme, thereby reducing its efficacy. The tributyrin is a solubilised lipid substrate. This was hydrolysed with and without LBG to check for possible difference in hydrolysis. The tributyrin method used followed established laboratory procedures. 0.016 g Tributyrin was weighed out into a 200ml bottle and 160 g of distilled water was added. The mixture was stirred for 24 hours by using a heated magnetic stirrer at 37°C. 3g of the 0.01% tributyrin solution (w/w) was weighed out and put into a 100 ml beaker. 53g of gastric solution was added into the emulsion and transferred into the sample holder of the pH stat titrator instrument. The sample holder with the mixture was attached to its position and the experiment was started by adjusting both the temperature ( $37.0 \pm 0.2^\circ\text{C}$ ) and pH ( $6 \pm 0.2$ ) for five minutes. After titration

optimisation was achieved, the pepsin solution was added in followed by the lipase solution. The above procedure was repeated using 0.01% Tributyrin solution (w/w) that contained 0.025% of LBG (w/w).

### 5.3.6 Gas chromatography

Gas Chromatography (GC) analysis was used to determine the relative quantity of different components of the hydrolysed products. The GC characterisation of lipids was conducted according to standard laboratory protocols. Briefly, during the lipolysis, a 1 mL aliquot was withdrawn from the emulsion mixture every 15 minutes and added to 10 mL of 2:1 chloroform/methanol mixture (prepared in advance), followed by the addition of 5 mL of a 1 % sodium chloride solution. After vigorous shaking, two phases separated with the upper layer constituting the aqueous solution and the bottom layer constituting the chloroform with extracted lipids. Three drops of concentrated HCl were then added to transfer any soap products to FFA. Following acid addition, the aqueous phase looked much clearer. A pH of approximately 2.0 was reached and pH paper was used to confirm this. The bottom phase was transferred into a new vial using a Fine glass pipette and placed on a heating block at 80 °C. The chloroform was removed by blowing nitrogen over the surface for 5-10 minutes. The lipid extract was then derivatised by adding 1 mL pyridine and 1 mL BSTFA (N,O-bis-(trimethylsilyl)trifluoroacetamide) reagent and heated on a heating block at 80 °C for 30 min. Silylation with BSTFA converts reactive hydroxyl and carboxyl groups to stable trimethylsilyl ethers, facilitating improved resolution, peak shape, and quantification. 200 µL of the derivatised extract were pipetted into a clean auto-sampler vial and 300 µL of toluene were added. This extract was then characterised by GC. GC analysis was performed on a Perkin Elmer

Autosystem XL. Lipids were separated on a 10 m, 0.53 mm I.D, 0.1  $\mu\text{m}$  film thickness Quadrex Methyl 5 % phenyl silicone bonded phase fused silica capillary column. The injection volume was 0.5  $\mu\text{L}$  and the carrier gas was helium set at 60 kPa. The GC column oven was programmed from an initial temperature of 120  $^{\circ}\text{C}$ , for 0.5 minutes, ramping to 325  $^{\circ}\text{C}$  at 10  $^{\circ}\text{C}/\text{minute}$ , followed by ramping from 325  $^{\circ}\text{C}$  to 350  $^{\circ}\text{C}$  at 5  $^{\circ}\text{C}/\text{minute}$  with a 2 minute hold at 350  $^{\circ}\text{C}$ . PTV injection was used, ramping from 70  $^{\circ}\text{C}$  to 350  $^{\circ}\text{C}$  at 200  $^{\circ}\text{C}/\text{minute}$  after 0.1 minutes, with a 3 minute hold at 350  $^{\circ}\text{C}$ . The detector temperature was set at 360  $^{\circ}\text{C}$ . An Agilent gas chromatograph, HP 6890 series (Agilent, Wokingham, UK) was used to separate different components in the extract. A typical chromatogram is displayed in Figure 5.14.



### 5.3.7 Analysis

- *Calculation of the molecular weight ( $M_w$ ) of triglycerides and average free fatty acids (FFA).*

The average molecular weight of the long chain triglyceride sunflower oil (SFO) sunflower oil was determined as 787.03g/mol according to the fatty acid composition of sunflower oil as listed in Table 5.4 below.

The average  $M_w$  of Triglyceride is thus calculated as follows:

$$3 * M_w (\text{FA}) + M_w (\text{Glycerol}) - 3 * M_w (\text{H}_2\text{O}) = 878.03 \text{ g/mol} , \quad [4.1]$$

and the average composition of fatty acid (FA) is calculated as:

$$\text{Total composition/\% of composition} = 27978.30/99.93 = 279.78 . \quad [4.2]$$

- *Calculation of % hydrolysis using pH stat*

The volume of added 0.1 M NaOH reflects the amount of FA released from lipolysis. The % hydrolysis as a function of time, was depicted as a measure of the hydrolysis of the TG by the lipase.

Since the enzyme specifically hydrolyses the ester bonds at 1 and 3 positions (Figure 5.15), 100 % hydrolysis was determined as when the lipase hydrolysed 2 free fatty acids (FFA) per triglyceride (TG) using the following equation:

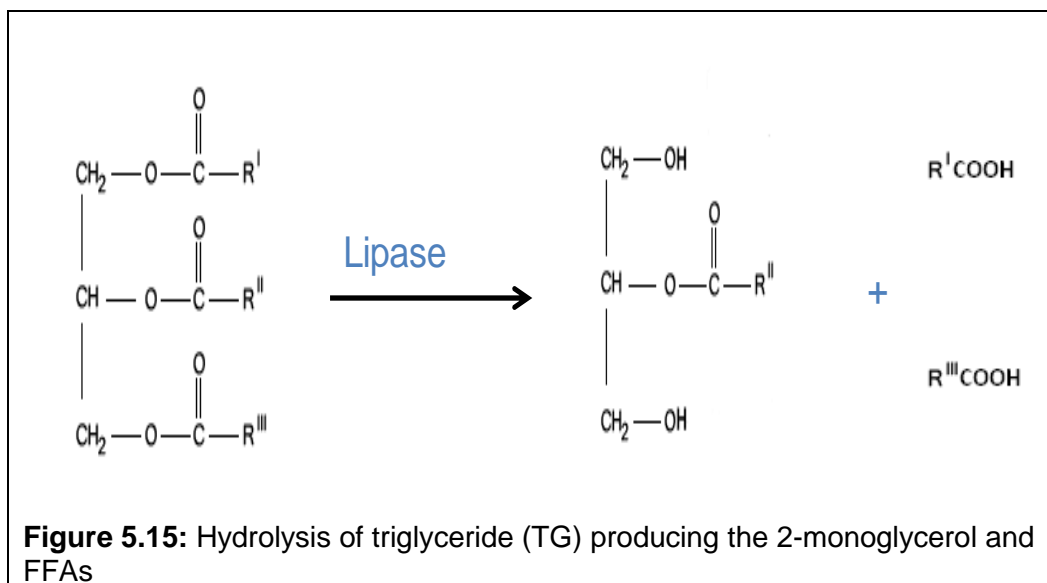
$$\text{Maximum volume of NaOH added} = X * 2 / (M_w \text{ TG} * [\text{NaOH}]) . \quad [4.3]$$

Where: X is the amount of oil in the emulsion (g) = 0.6 g. The factor 2 is required since every mole of TG produces 2 mol of FFAs.  $M_w \text{ TG}$  is the molecular weight of TG (g/mol); [NaOH] is the concentration of NaOH (0.1M) with  $M_w$  of Triglycerol (TG) = 878.03; Mass of TG in our emulsion 0.6 (g); Number of moles of TG (n) = Mass/ $M_w$  = 0.00068335

Number of moles of NaOH (n) = n of TG\*2 =0.0013667; the Vmax of NaOH = number of moles\*0.1 ([M] of NaOH) = 0.0013667\*0.1 = 0.01367L (converting this into ml by multiplying by 1000) =13.67ml.

<i>Fatty acid (FFA)</i>	<i>Mw (g/mol)</i>	<i>% composition</i>	<i>Total Composition</i>
16:0	228.37	0.2	45.67
16:1	256.42	6	1538.52
18:0	254.4	0.1	25.44
18:1	284.48	5.6	1593.09
18:2	282.46	17.8	5027.79
18:3	280.45	68.7	19266.92
20:0	178.43	0.2	35.69
20:1	312.53	0.3	93.76
22:00	310.51	0.1	31.05
24:00	340.58	0.8	272.46
Average Mw of FA	-	-	279.98
Average Mw of Triglycerides	-	-	878.03

**Table 5.4:** Fatty acid composition and molecular weight of soybean oil [86].



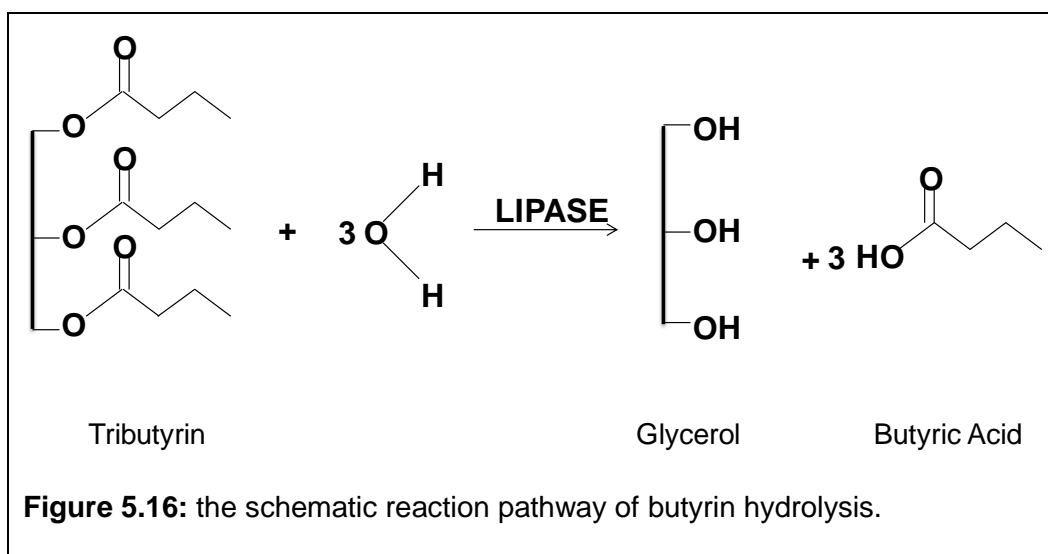
- *Calculation Vmax for tributyrin test*

The volume of added 0.1 M NaOH reflects the amount of butyric acid released from tributyrin lipolysis. The % hydrolysis as a function of time was depicted as a measure of the hydrolysis of the TG by the lipase. Since the enzyme specifically hydrolyses the ester bonds at 1 and 3 positions (Figure 5.16), 100 % hydrolysis was determined as when the lipase hydrolysed 3 butyric acid molecules per tributyrin using the following equation:

$$\text{Maximum volume of NaOH added} = \frac{X \cdot 3}{M_W \text{tributyrin} \cdot [\text{NaOH}]}, \quad [4.4]$$

where: X is the amount of tributyrin in the solution (g) = 0.006 g. The factor 3 is required since every mole of tributyrin produces 3 moles of butyric acids;  $M_W$  of tributyrin is the molecular weight of tributyrin = 302.36(g/mol); [NaOH] is the concentration of NaOH (0.1M).

With  $M_W$  of Tributyrin = 302.36; Mass of tributyrin in solution 0.006 (g); Number of moles of tributyrin (n) = Mass/ $M_W$  =  $1.984 \cdot 10^{-5}$ ; Number of moles of NaOH (n) = n of tributyrin \* 3 =  $1.984 \cdot 10^{-5} \cdot 3 = 5.95 \cdot 10^{-5}$ ; the Vmax of NaOH = number of moles \* 0.1 ([M] of NaOH) = 0.000595L (this can be converted into ml by multiplying by 1000) = 0.595ml.



- *Calculation of % hydrolysis for gas chromatography*

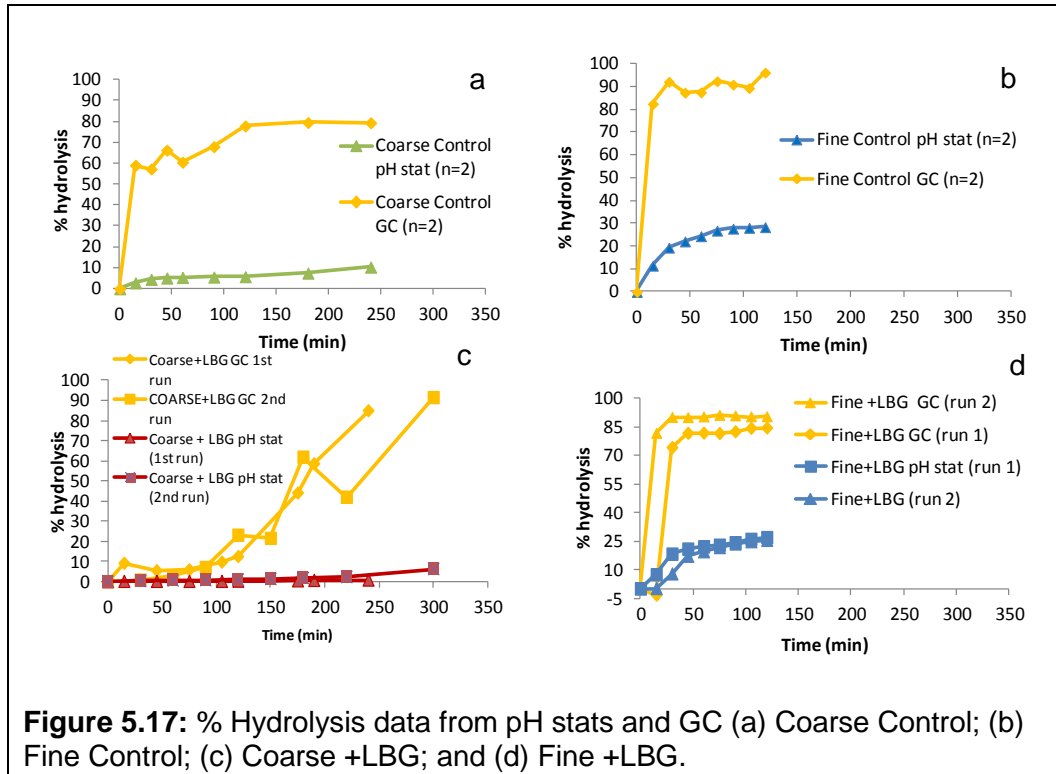
The area of each peak in Figure 5.14 directly corresponds to the mass ratio of individual lipid compounds. In order to have a direct comparison between pH stat and GC results, % FFA (w/w) was used instead of % hydrolysis. For GC, the % FFA, as a function of time, was depicted as a measure of actual hydrolysis. The relative ratio of % FFA detected by pH stat to % FFA characterised by GC was interpreted as a measure of FFA solubility in aqueous phase. From pH stat method, % FFA (w/w) was calculated as follows: first of all, the response factor (RF) was established as it depends on type of oil and its composition. The data of each peak (e.g. TG) was then normalised by multiplying the area of peak by the response factor which is 1 for FFA and 1.2 for TG. % hydrolysis of FFA =  $[(x_0 - x_i) * 100 / (x_0)]$ .

### 5.3.8 Results

#### 5.3.8.1 Comparison of pH stat and GC hydrolysis data

Figure 5.17 shows a direct comparison of the data from the pH stat experiments with the GC data.: The Coarse emulsion in Figure 5.17a shows a marked difference between the GC and pH stat calculated hydrolysis where the former shows much faster hydrolysis, reaching approximately 60% hydrolysis in 20 minutes and up to 80% at the end of the experiment. This is approximately a 70% increase in hydrolysis compared to the pH stat experiment. The Fine emulsion data is shown in Figure 5.17b and, again, there was a big difference in calculated hydrolysis between the 2 methods with GC data approximately 65% higher after 2 hours of hydrolysis. The Coarse + LBG in Figure 5.17c shows the duplicate data separately since the 2 runs could not be averaged due to different sampling times. Both pH stat and GC data show slow hydrolysis initially then at approximately 2 hours the data diverge with the GC data reaching much higher levels of hydrolysis. At ~5 hours the pH stat data reaches <10% hydrolysis whereas the GC data reaches approximately 90%. The Fine + LBG emulsion (Figure 5.17d) data shows that the GC-derived hydrolysis data (orange line) reaches between 70-80% after 20 minutes then plateaus whereas the pH stat data was again much lower in terms of hydrolysis, reaching <25% after 2 hours. There was some difference between the GC duplicates which are shown separately, one of which seemed to have a longer lag phase than the other. After that point, the hydrolysis again shows a rapid increase. Also, it is important to mention that the enzyme that was used for this study can only transform 1 TG into 2 FFA, so 100% hydrolysis represents 66% FFA in composition, and we have over

66% FFA composition which means 100% hydrolysis were achieved for all samples.



### 5.3.8.2 Tributyrin hydrolysis data

Figure 5.18 shows the raw data from the pH stat experiments using tributyrin: in Figure 5.18(a1) and Figure 5.18(a2) the data for the emulsion without LBG shows an initial fast hydrolysis followed by a step-like gradual increase throughout the 100 minute run. The raw data of the pH stat experiment for tributyrin + LBG are shown in figure 5.18(b1), with again an initial rapid hydrolysis followed by a step-like process. One of the two runs for the tributyrin + LBG experiment was terminated before the end point due to limited

time for the experiment to complete; therefore the two runs are showed separately.

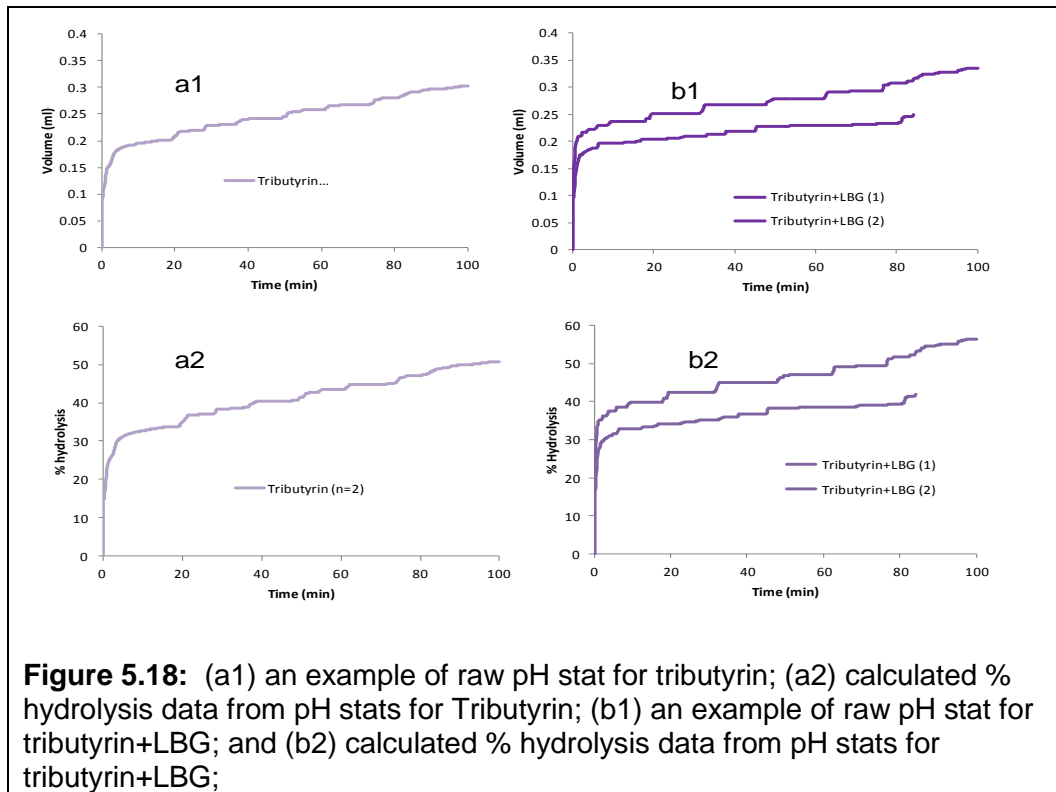


**Figure 5.18:** (a1) an example of raw pH stat for tributyrin; (a2) calculated % hydrolysis data from pH stats for Tributyrin; (b1) an example of raw pH stat for tributyrin+LBG; and (b2) calculated % hydrolysis data from pH stats for tributyrin+LBG;

#### 5.4 *In vivo* pilot studies without thickener

Having observed and characterised the fat emulsion systems *in vitro* the next logical step was to run small scale pilot studies *in vivo* using MRI. This was done with a view to gathering information on the gastrointestinal response to the fat emulsion meals and also to build experience on MRI and optimise methods and protocols. The pilot study was also used to gain experience with the  $^{13}\text{C}$  breath analysis.

Two healthy volunteers were used for this first pilot study. Each of them attended on two separate mornings, having fasted overnight. On each occasion their abdomens were imaged at 3T at baseline (fasted). Having completed the baseline scanning; the volunteers were asked to drink 300 ml of a flavoured 20% sunflower oil fat emulsion (Fine or Coarse) labelled with 100mg  $^{13}\text{C}$ -triolein. The volunteers therefore consumed 60g SFO in total.

After this, the postprandial scanning was carried out and they were imaged at intervals for up to 6 hours with a range of  $^1\text{H}$  MRI sequences (e.g.  $T_1$  and  $T_2$  weighted, water selective and fat selective images) to follow the journey of the emulsion meals along the GI tract. Additionally, breath samples were collected (2 at baseline and after feeding every 15 min for 6 hours) to measure the absorption and excretion of the label compound (100mg  $^{13}\text{C}$ -triolein). These breath samples were analysed using an IRIS®-Lab analyser (Wagner Analysen Technik, Bremen, Germany) calculating the change in delta over baseline  $^{13}\text{CO}_2/^{12}\text{CO}_2$  ratio in the breath samples from baseline and plotting it against time. From these breath-test time curves it will be possible to calculate the areas under the curve, the time to peak and the initial slope. This is of interest because the arrival of the  $^{13}\text{C}$  label in the breath of the subjects is a marker of digestion and absorption of the label in the fat. Differences in digestion caused by the different droplet sizes should reflect in differences in  $^{13}\text{C}$  label appearance in the breath.

#### **5.4.1 Gastric emptying**

Examples of the MRI images of the meal in the stomach of a volunteer are shown below in Figure 5.19. The water images are 3T axial TSE images (Echo time TE 59 ms, TR 1511 ms, 3 stacks of 15 slices with no gap between

them, reconstructed resolution  $0.78 \times 0.78 \times 7 \text{mm}^3$ ). The fat images are 3T, T1 weighted 3D FFE images (Echo time TE 3.6 ms, TR 9.9 ms, 64 slices with no gap between them, reconstructed resolution  $0.63 \times 0.62 \times 2.5 \text{mm}^3$ ). These show that the Fine emulsion remained stable in the stomach up to 4 hours, whereas the coarse emulsion creamed up in the stomach forming two layers (water at the bottom and fat on the top), which is in good agreement with the *in vitro* stability data shown at the beginning of this chapter.

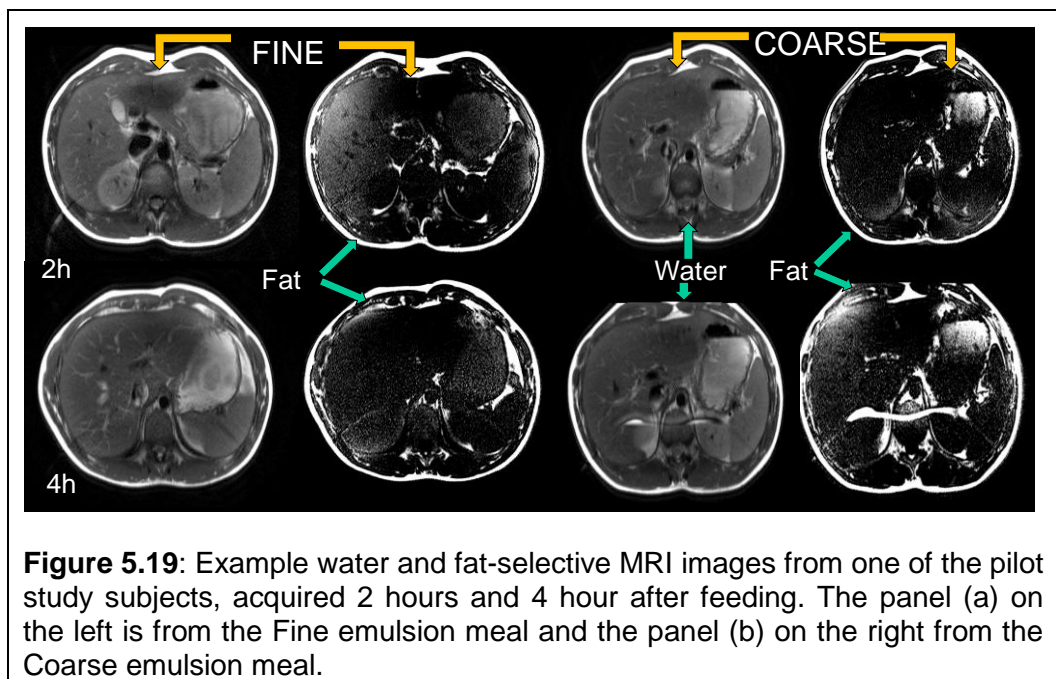
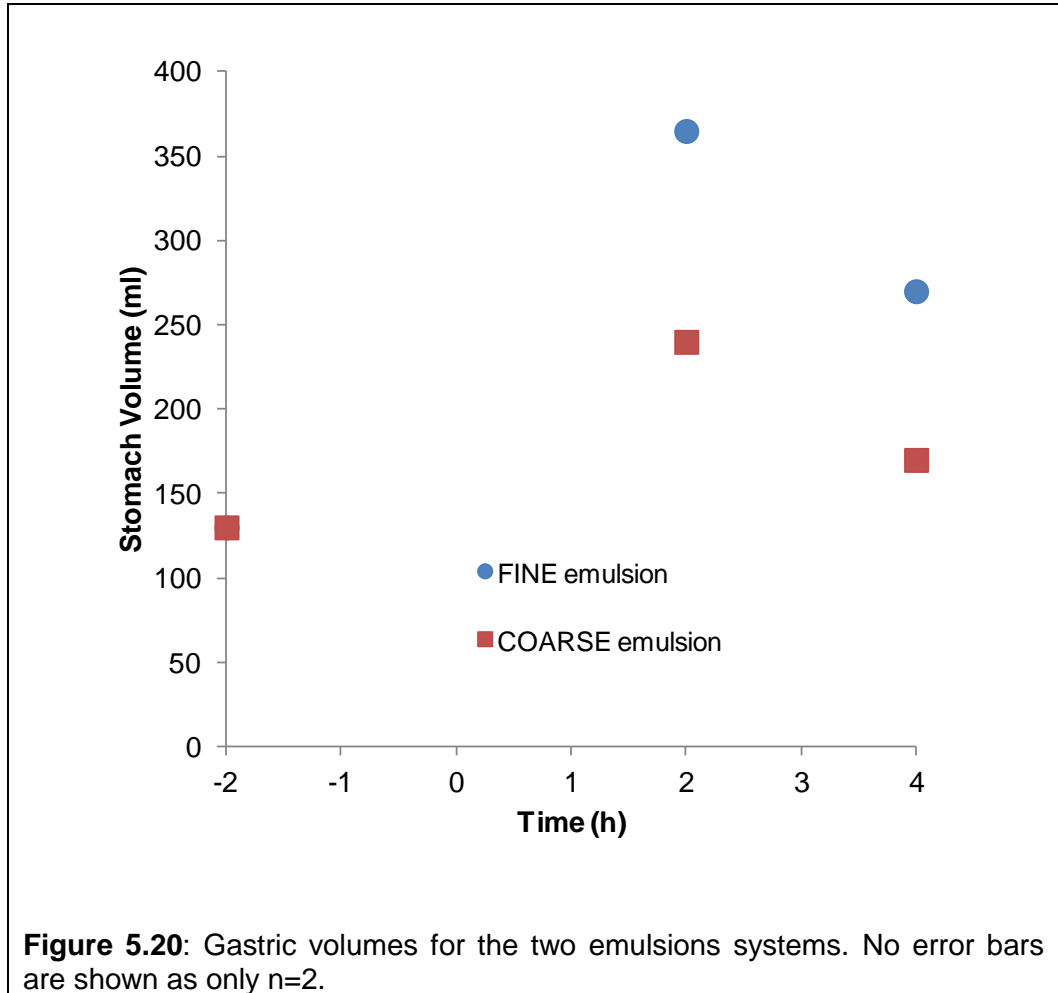


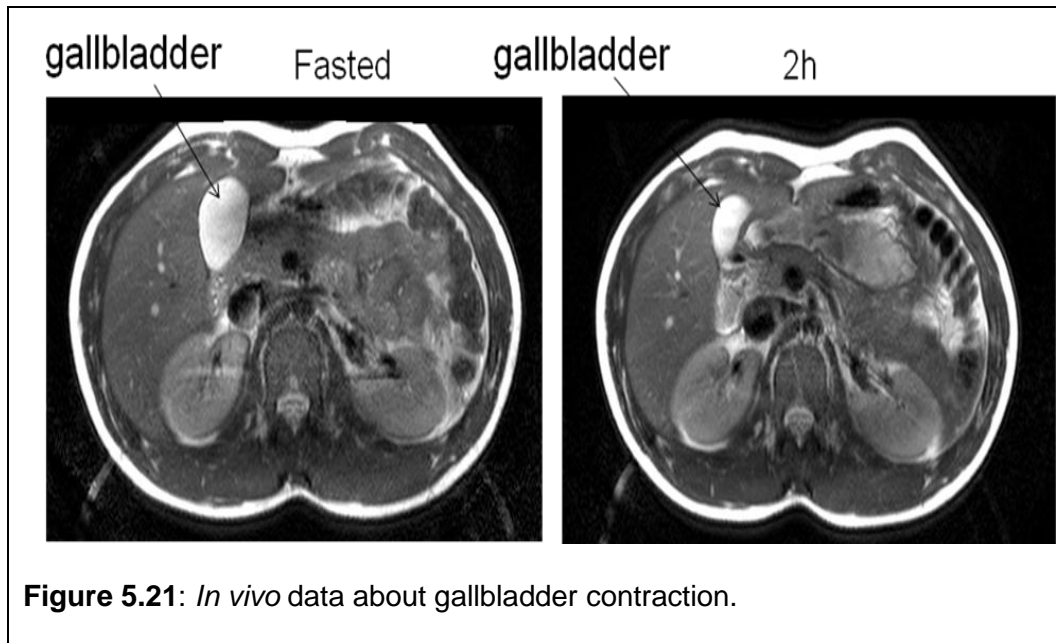
**Figure 5.19:** Example water and fat-selective MRI images from one of the pilot study subjects, acquired 2 hours and 4 hour after feeding. The panel (a) on the left is from the Fine emulsion meal and the panel (b) on the right from the Coarse emulsion meal.

The MRI gastric volume measurement in this thesis was done using balanced turbo field echo (bTFE) sequences. The gastric emptying/volume were processed using the Analyze9 software (MayoClinic, Rochester, MN, USA) by manually drawing around the contents of the stomach as regions of interests (ROI) and summing them. The final stage of data processing was done using Microsoft Excel to present the time courses graphically. The initial gastric emptying pilot data points for this study are shown in Figure 5.20. Although very preliminary, from this data it can be seen that the Coarse emulsion emptied faster than the Fine emulsion, with a large portion of the fat emulsion

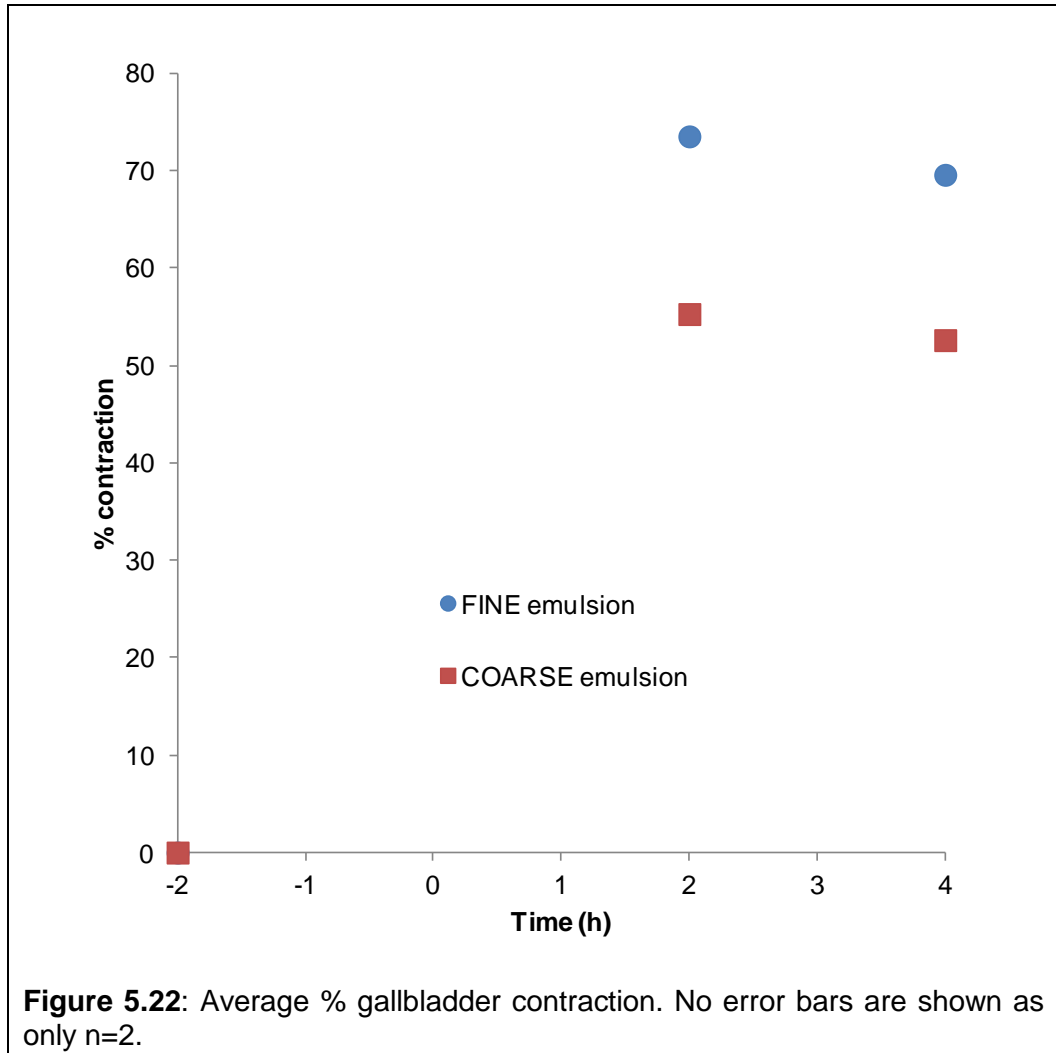
meal remaining in the stomach 4 hours after feeding. This is might be due to the Coarse emulsion creaming up in a layer on the top of the stomach and/or to droplet size effect of interest.



### 5.4.2 Gallbladder contraction



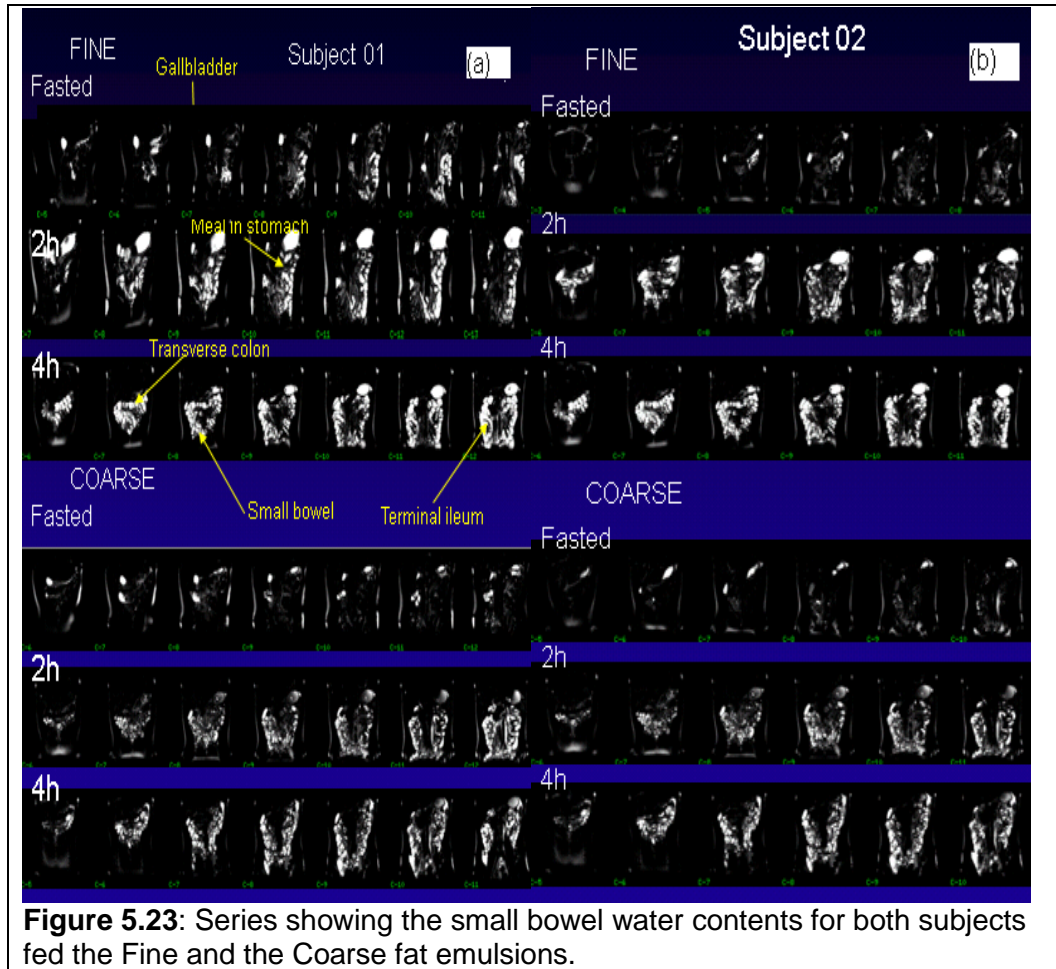
The gallbladder contracted in response to both fatty meals as shown in Figure 5.21 and Figure 5.22. The imaging sequence is the same TSE sequence as detailed for water images in the previous page. This is due to the release of CCK from mucosal cells which causes gallbladder contraction and releases the bile salt through the duct. The gallbladder seemed to respond differently for the two emulsions with the Coarse emulsion showing a smaller % gallbladder contraction. The % gallbladder contraction was calculated as  $[1 - \text{gallbladder volume at time } t / \text{gallbladder volume at baseline}] \times 100$  expressed in %.

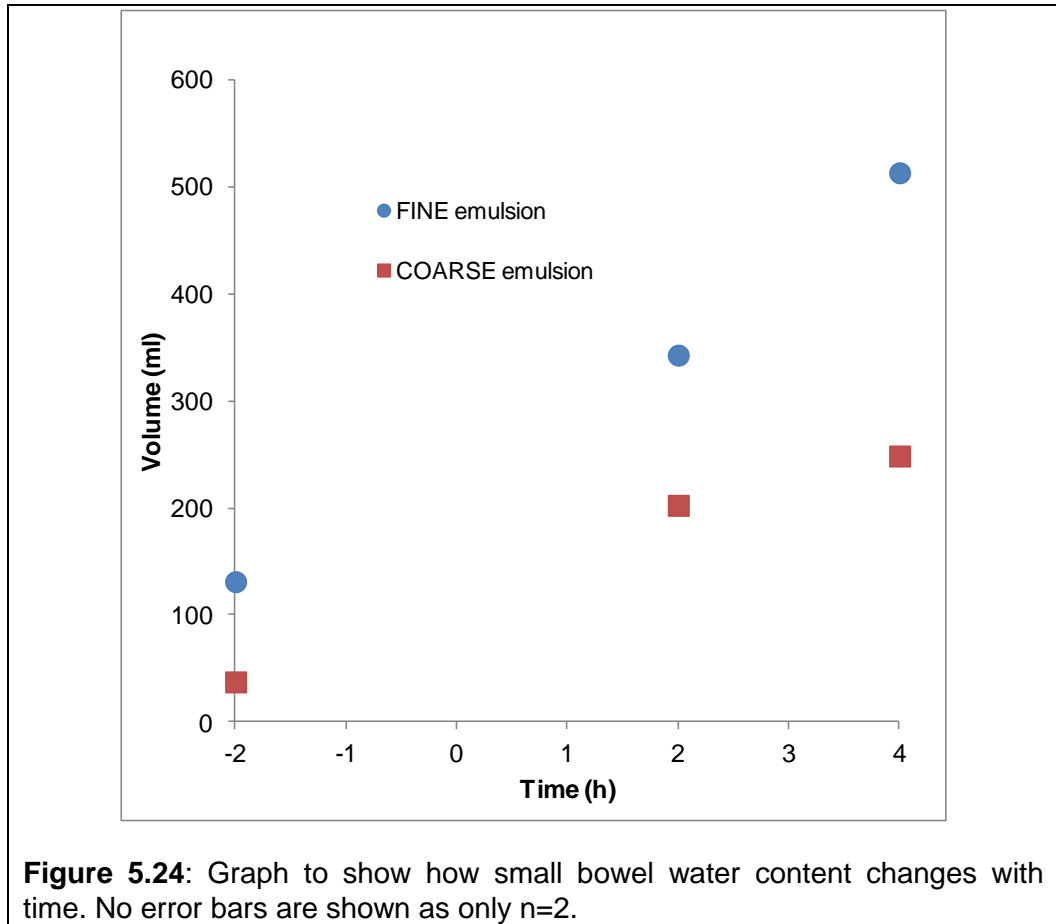


### 5.4.3 Small bowel water content

The small bowel water contents were calculated by using a method developed in this group [5] and showed substantial inflow of liquid into the small bowel (Figure 5.23). The Fine emulsion generated more SBWC than the Coarse emulsion as shown in Figure 5.24. The sequence was a coronal RARE sequence (Echo time TE 400 ms, TR 1511 ms, 2 stacks of 11 slices with no gap between them, reconstructed resolution  $0.78 \times 0.78 \times 7 \text{mm}^3$ ). There was a difference in initial baseline volumes of the order of 100 ml which makes the interpretation of differences between emulsions more difficult. The sources of the small bowel water content are normally considered to be a combination of gastric fluid, gallbladder secretion, pancreatic and small intestine fluid

secretions. Therefore there is a considerable amount of fluid/water fluxes through the small intestine which occur during the digestion of this kind of fat emulsion meal.





To rule out a systematic effect from the emulsifier Tween20 on enhancing small bowel water content a separate experiment feeding the meal system without the fat was carried out. Both the samples were prepared using the methods used for the Coarse emulsion formulation, although there was no fat added. A control sample with no fat and no Tween20 was also prepared. Two healthy volunteers were used in this pilot study where each one of them attended on two separate mornings, having fasted overnight. On each occasion their abdomens were imaged at 3T at baseline (fasted) and after drinking flavoured Tween20 and non-Tween20 formulations respectively.

This showed some presence of water in the small bowel, but not as a high volume as that observed in the study using fat and no difference between the drink with and without the emulsifier. Therefore, it was concluded that the high volume of SBWC was predominantly due to an effect of the emulsified

fat, with a greater effect for the Fine emulsion and not to an unknown effect of the emulsifier on its own.

Figure 5.25 shows an example HASTE MRI image (a) which indicates the content of stomach and coronal RARE image (b) at 3T to show the SBWC. The gastric emptying was fast as predicted due to the lack of fat as shown in. Figure 5.26. The mean small bowel water content volume (SBWC) measurements are shown in Figure 5.27. The SBWC is low (order of 50-100ml) compared to the values observed with the fat emulsions. Therefore it was concluded that the high volume of SBWC observed using the fat emulsions was predominantly due to an effect of fat on digestion with only a limited contribution from the bulk solution containing surfactant.

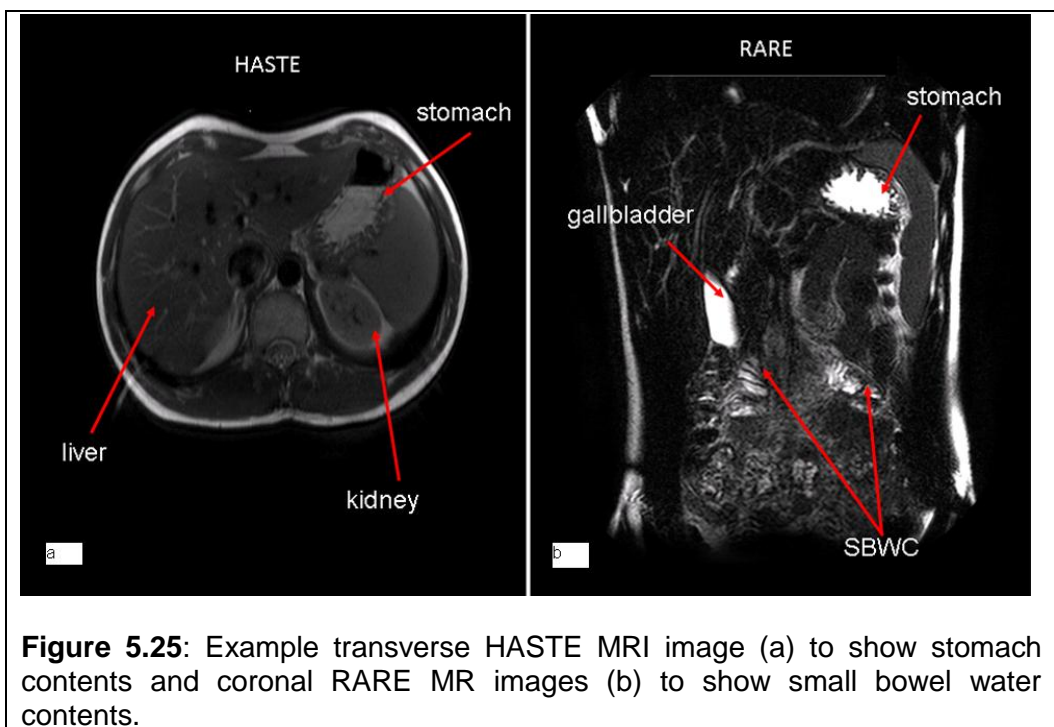


**Figure 5.25:** Example transverse HASTE MRI image (a) to show stomach contents and coronal RARE MR images (b) to show small bowel water contents.

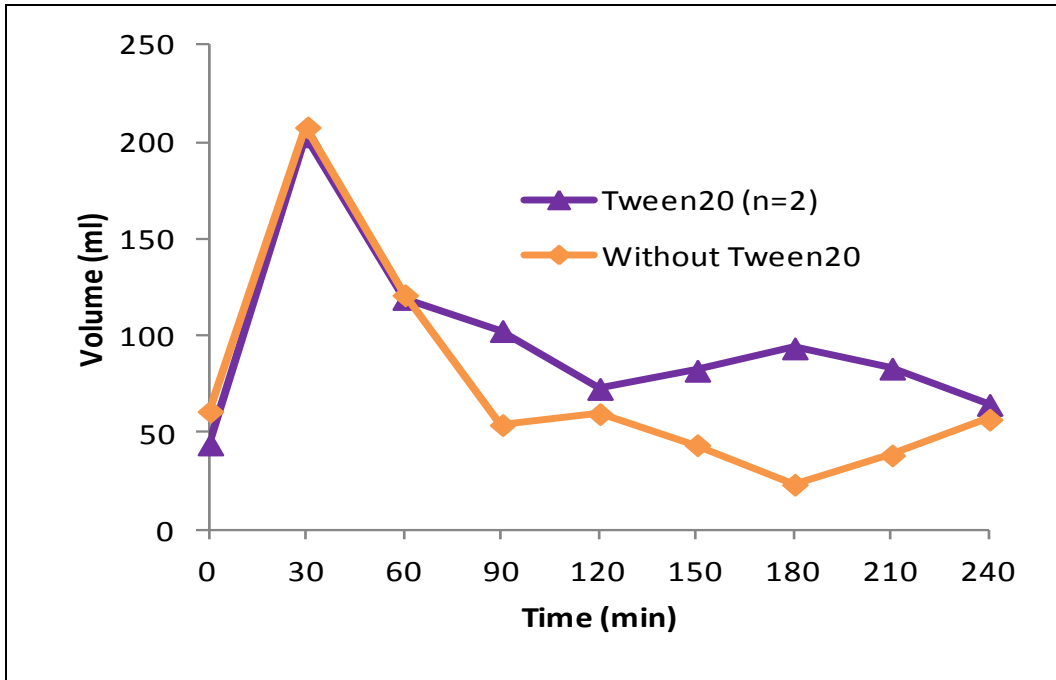


**Figure 5.26:** Gastric emptying for Tween20 emulsifier formulation with no fat and control sample with no fat and no Tween 20. No error bars are shown as only n=2.

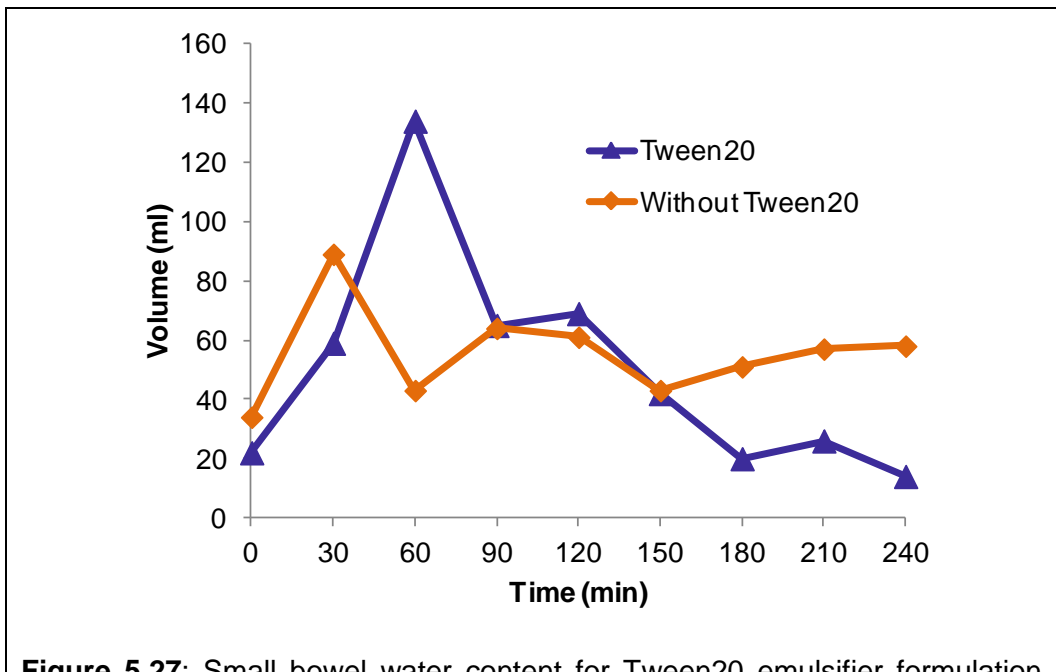
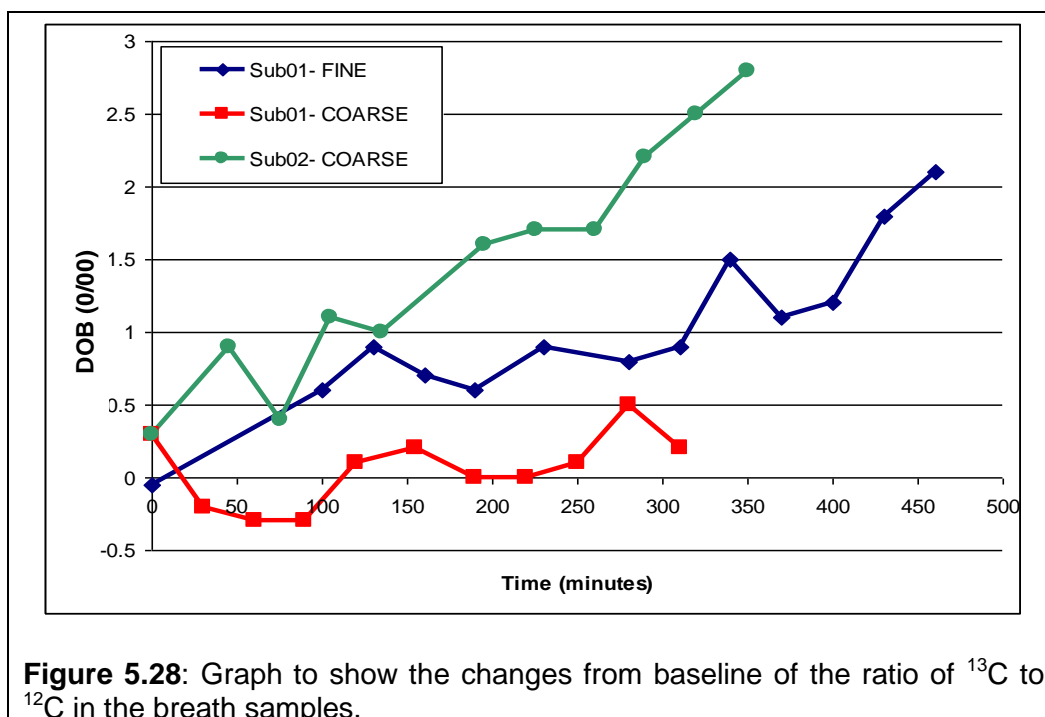


**Figure 5.27:** Small bowel water content for Tween20 emulsifier formulation with no fat and control sample with no fat and no Tween 20. No error bars are shown as only n=2.

#### 5.4.4 $^{13}\text{C}$ breath test

The  $^{13}\text{C}$  breath test results (Figure 5.28) showed that the label materials were absorbed, metabolised and became detectable in the breath, but the data appeared to be particularly noisy. It was found that unfortunately the IRIS machine was not calibrated correctly when this set of samples was analysed and one of the series (subject 02 Fine emulsion) was not run correctly for this technical reason so this comparison was inconclusive, however this technical problem was detected and solved for future analyses.



#### 5.4.5 Introducing a gum stabiliser in the emulsion

The pilot studies showed a possible effect of droplet size on gastrointestinal physiology but the observed creaming of the Coarse emulsion introduces a confounding factor. In order to investigate the role of droplet size one needs to

make both fat emulsions equally spatially stable in the stomach in terms of spatial distribution so that, for example, differences in gastric emptying may not be caused by simple layering [26]. One solution is the use of a food thickener in order to avoid the creaming effect.

A wide range of stabilizers or thickeners was considered to select the most appropriate. The thickeners that were looked at included Guar Gum, Citrus fiber and Locust Bean Gum (LBG) which all commonly added to foods. The aim was to obtain emulsions that are minimal thickened but spatially stable throughout the gastric emptying process. The choice fell on locust bean gum (LBG). Stability tests were carried out as detailed in section 5.3 suggesting that 0.5% was an optimal concentration to improve emulsion stability without making the solution too thick to drink. Another small pilot study was carried out using 0.5% LBG thickener in the bulk phase of the fat emulsion. The hypothesis was that addition of LBG makes the spatial distribution of a fat emulsion in the stomach more homogeneous (i.e. preventing creaming) which in turn also will enhance the gastrointestinal and satiety responses.

### **5.5 *In vivo* scouting pilot with thickener**

For this purpose a Coarse and Fine droplet size oil in water emulsions containing 20% SFO and 0.5% LBG as a thickener were prepared. To obtain a Fine emulsion with LBG the emulsion is passed through the Microfluidizer once, with a pressure of 2.6 bar at the inlet, which corresponds to 606 bar in the interaction chamber. Microbiological clearance was obtained for refrigerated storage up to 2 weeks. An *in vivo* pilot study was carried out. Two healthy volunteers visited on two separate occasions to consume 300 g of the emulsions. Gastric emptying, gall bladder contraction and small bowel water content were measured and compared to the previous pilot study (emulsions

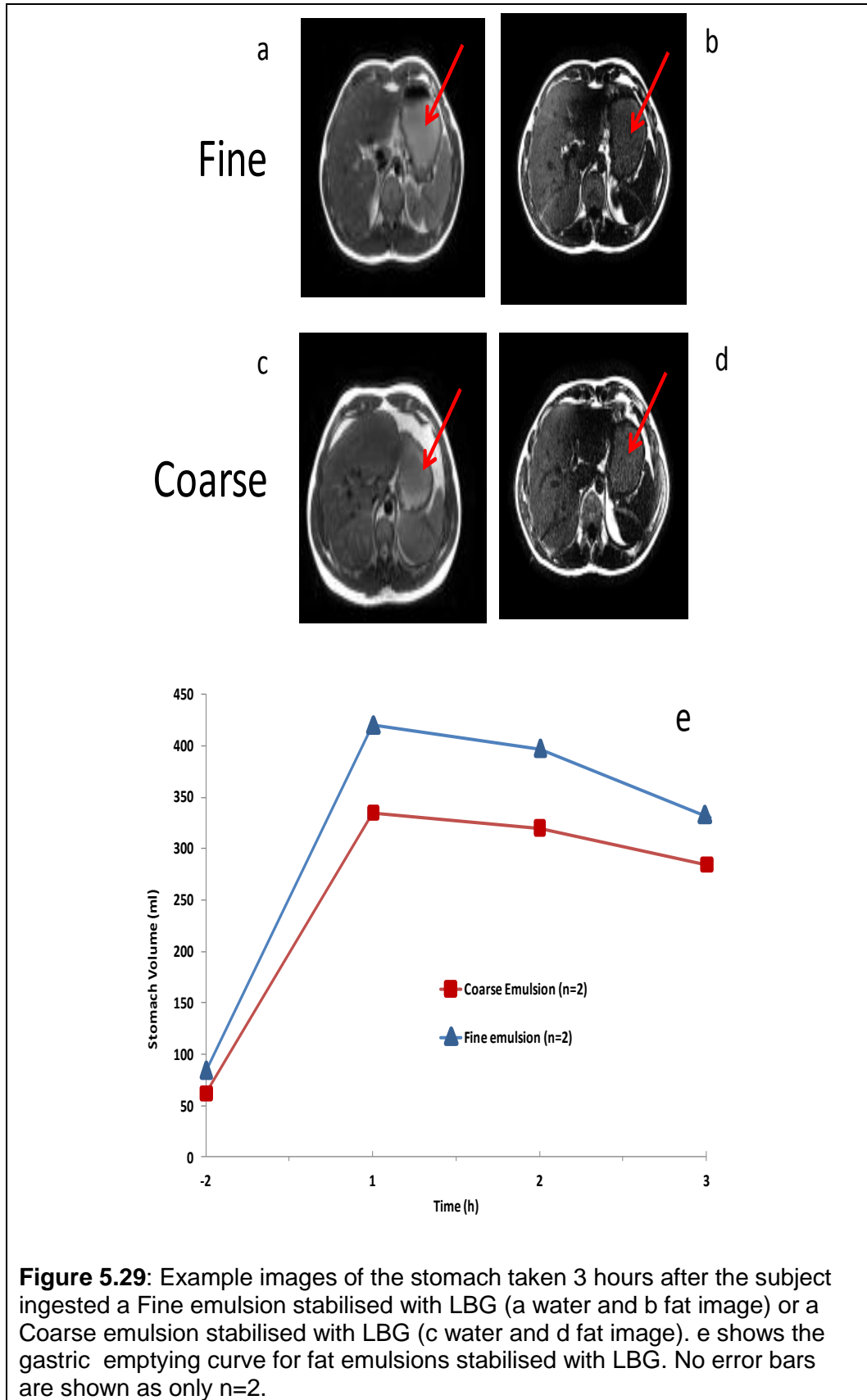
containing no LBG, Coarse emulsion creamed in the stomach). The timing of this protocol was shortened to 3 hours as more emphasis was put on the intragastric behaviour of the meals than on later small bowel effects.

The two emulsions prepared were:

- a) Fine+LBG - 350g o/w-emulsion with 20% sunflower oil (containing 100 mg <sup>13</sup>C-labelled octanoic acid), 1% Tween20, with 0.4µm mean droplet size with 0.5% Locust Bean Gum
- b) Coarse+LBG - 350g o/w-emulsion with 20% sunflower oil (containing 100 mg <sup>13</sup>C-labelled octanoic acid), 1% Tween20, with 10µm mean droplet size with 0.5% Locust Bean Gum

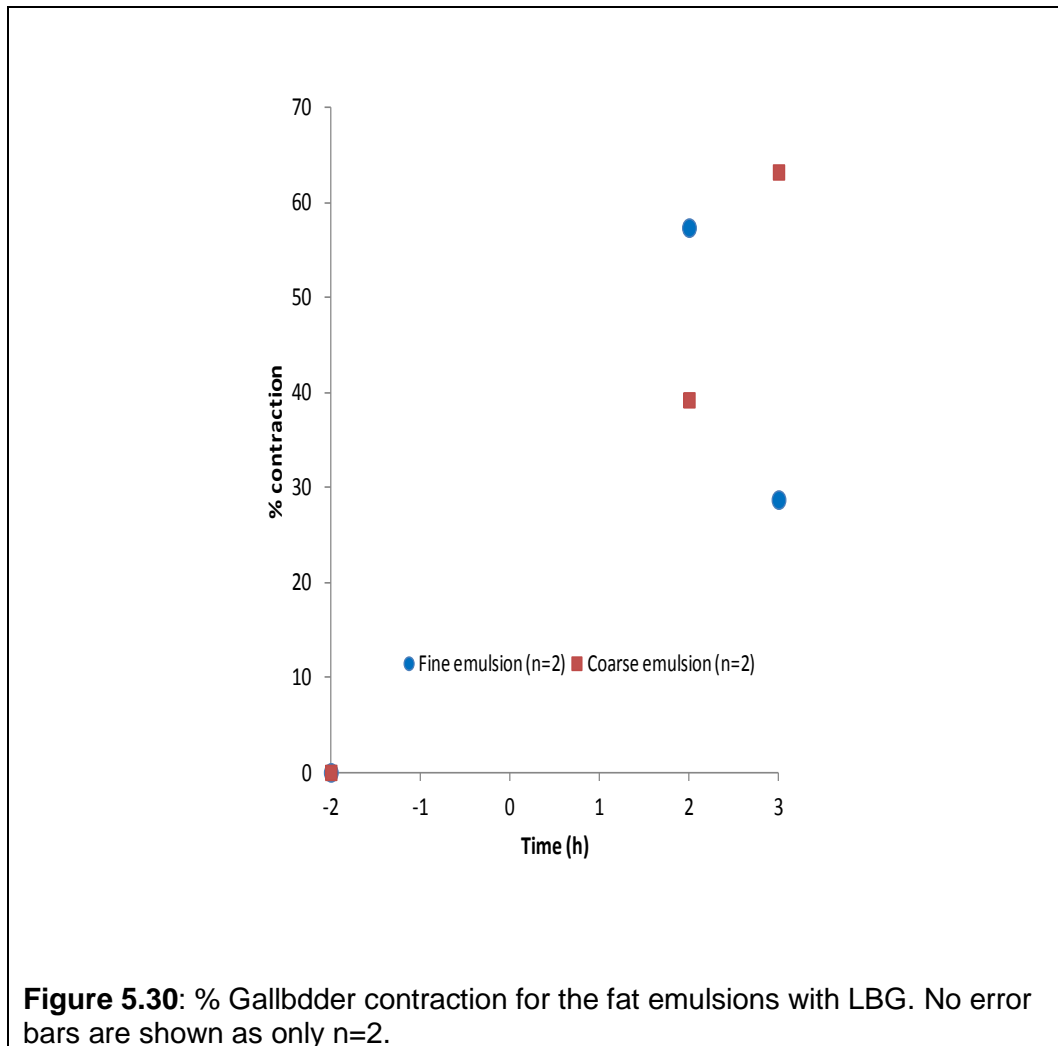
### 5.5.1 Gastric emptying

The MRI images (examples given in Figure 5.29 a-d) showed that the Coarse emulsion containing LBG was stable in the stomach for over three hours in agreement with the *in vitro* results. The gastric emptying for the Coarse emulsion with LBG appeared to be faster than for the Fine emulsion (Figure 5.29e) suggesting that the feedback from the duodenum depends on droplet size and that this experimental set up was appropriate to investigate the effects of fat droplet size on gastrointestinal responses.



### 5.5.2 Gallbladder contraction

This is expressed as % of baseline volume. The data in Figure 5.30 show contraction of the gallbladder but differences between formulations were not clearly shown because of small numbers and individual variations.



### 5.5.3 Small Bowel water content

Again, a high amount of freely mobile water was observed in the small bowel as shown in the images in Figure 5.31 and in the graph in Figure 5.32. The Coarse emulsion with LBG showed larger SBWC than that with no LBG (though the subjects were different).

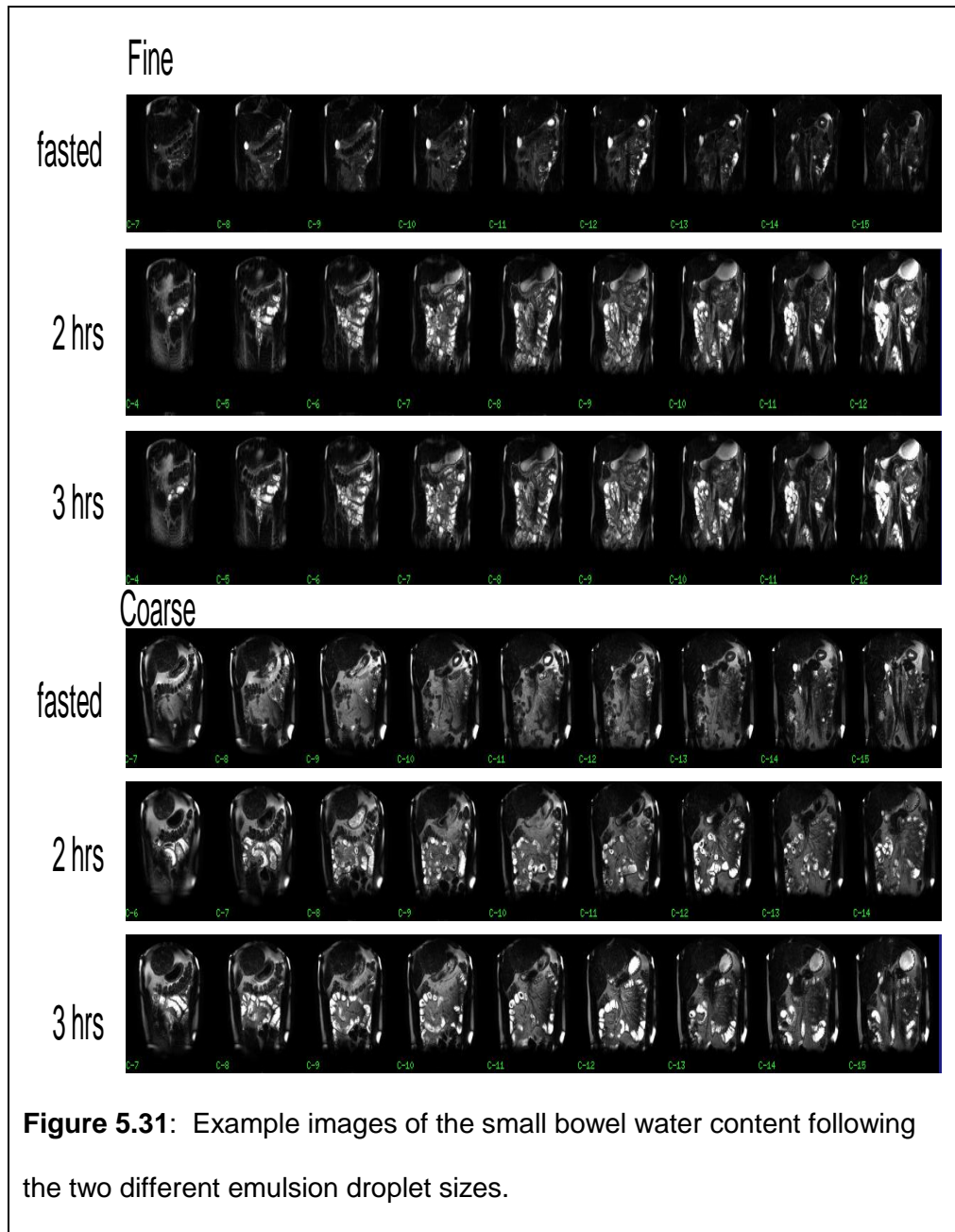
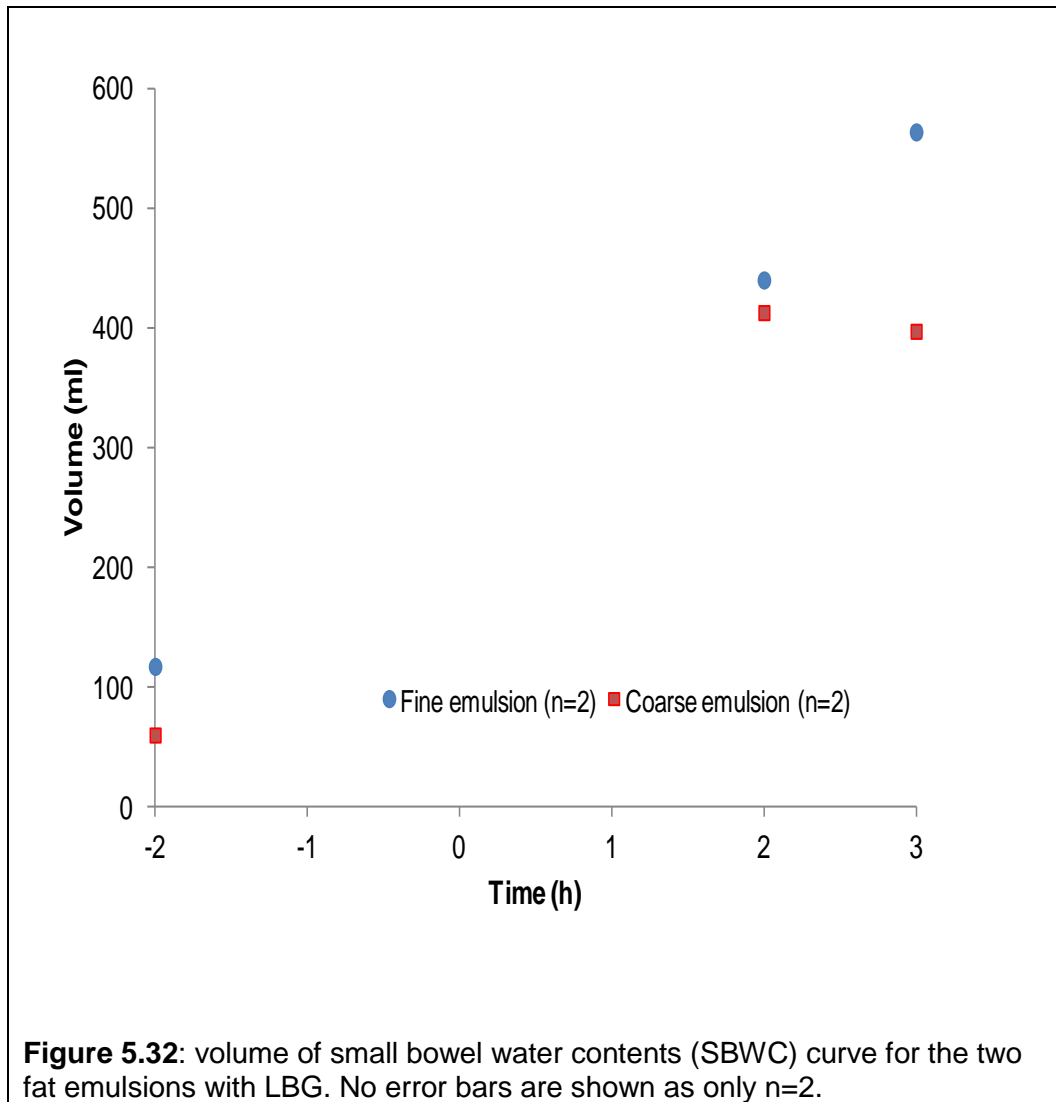


**Figure 5.31:** Example images of the small bowel water content following the two different emulsion droplet sizes.



## 5.6 Discussion

### 5.6.1 *In vitro* bench characterisation

The aim of this study was to mimic triglyceride hydrolysis in the stomach and observe the performance of the Fine and Coarse fat emulsions. It is well documented in the literature that only 10-40 % of lipolysis can be achieved in the stomach by the lipase enzyme, where this enzyme is inhibited by protonated free fatty acids [48, 50, 63, 87]. This occurs when free fatty acids

are produced and dominate the fat droplet interface preventing further access of lipase to the lipid substrate [88].

The % hydrolysis data obtained from the pH stats method for all 4 emulsions showed that the Coarse control emulsion displayed a slower hydrolysis compared to the Fine control emulsion. Similarly the Coarse +LBG emulsion showed very slow hydrolysis for greater than 2 hours compared to the Fine +LBG emulsion which was rapid. Both Coarse formulations reached 10-15% hydrolysis after 4 hours whereas the 2 Fine formulations reached >25% hydrolysis after approximately two hours. This indicates that there is a droplet surface area (size) effect on fat hydrolysis where the smaller droplet size hydrolyses faster than a larger droplet size. There are a number of studies showing that the droplet sizes of fat emulsion can influence triglyceride hydrolysis [63, 89, 90]. Similarly, Armand and co-workers [91] reported that their Fine emulsion changed its droplet size by 10 fold after digestion, whereas the Coarse emulsion did not change.

The pH stat data also showed that the LBG has a more significant effect on hydrolysis of the Coarse emulsion compared to the Fine emulsion. The duplicate data for the Coarse + LBG samples showed negligible hydrolysis for the first 2 hours whilst the duplicate runs for the Fine +LBG samples behaved very differently. There was a small (more noticeable for one of the duplicates) lag phase for both Fine +LBG duplicates, but overall the hydrolysis was rapid and behaved more or less like the Fine control emulsion. Although LBG addition appears to be able to slow the hydrolysis of an emulsion with reduced surface area, it has negligible effect on meals with large surface area. As both Coarse meals (with and without LBG) underwent less gastric hydrolysis compared to Fine counterparts, it can be concluded that there was an overall droplet size effect as well as the addition of LBG effect in reduced surface area emulsions only.

For all emulsions, the GC data showed much higher hydrolysis than the pH stat data (between 10-30% hydrolysis was achieved for pH stat), where 60-80% hydrolysis was achieved within the first hour for all formulations except the Coarse +LBG where only approximately 10% hydrolysis was achieved. The maximum % hydrolysis achieved from GC data were 87 % for Fine +LBG emulsion, 92% for Fine control emulsion; 78% for Coarse control emulsion (all for first hour) and 91% for Coarse with LBG emulsion (at 5th hour). The maximum % hydrolysis was achieved within first hour for all meals except the Coarse with LBG which was 91% at 5th hour. Again, this suggests that both the LBG and the reduced surface area of the Coarse emulsion resulted in a reduction in lipid hydrolysis. Both Fine emulsions (with and without LBG) showed a rapid hydrolysis and this may have been due to its greater surface area compared to the Coarse formulations.

However, the Coarse emulsion with LBG showed a period of limited activity or “lag phase”. The emulsions with bigger droplet sizes have less surface area compared to the Fine formulations, which have larger surface areas, therefore less surface area for enzyme, less enzyme-substrate interaction and ultimately less hydrolysis.

It was possible to get more than 66 % FFA as FA chains on monoglyceride can migrate from ester position 2 to 1 leading to higher hydrolysis. Dependant on their solubility (or hydrophobicity) fat or lipids may be in different phases and thus the hydrolysis measured using different techniques may depend on which phase particular fat/lipids exist in a mixture. The pH stat only titrates the FFAs that are in the aqueous phase and titratable by NaOH[53]. Pregent and colleagues (Personal Communication, 2011) have previously shown that the amount of FFA in the aqueous phase depends on the pH of the solution and that in the gastric condition used here (about pH 6) only about 30 % hydrolysis

is recorded because the rest of the FFA is in another phase, probably in the oil, or in lamellar phase [48, 92, 93]. This explains that pH stat data underestimates hydrolysis due to limited solubility of FFAs in aqueous phase and GC represents true hydrolysis obtained.

These experiments were very interesting and showed that droplet size was the main factor influencing lipid hydrolysis with the presence of LBG only influencing hydrolysis of emulsions with reduced surface area. These gastric model experiments can be used to help explain *in vivo* results.

In order to eliminate the possibility that LBG did not bind to the enzyme, thereby reducing its efficacy, the tributyrin test was used. This was a solubilised lipid substrate, hydrolysed with and without LBG. Since both results were similar this suggests that LBG did not bind to the lipase reducing tributyrin hydrolysis (tributyrin hydrolysis produces 3 butyric acid molecules plus 1 glycerol molecule). Therefore, the tributyrin data (soluble lipid substrate i.e. not emulsion droplets) did not show a clear effect of LBG in hydrolysis of tributyrin so the effect was probably at the emulsion droplet surface.

### **5.6.2 *In vivo* pilot MRI studies**

The purposes of this pilot study were to gain information on the intragastric behaviour of the two fat emulsion systems and to start assessing the physiological responses to them in healthy volunteers. The number of subjects studied was necessarily very small but the insights provided proved very useful for the planning for the subsequent work. The two emulsions seem to trigger a diverse gastrointestinal response which affected gastric emptying (Fine slower), gallbladder contraction (Fine greater) and small bowel secretion (Fine greater). A suspicion that the observed strong small bowel secretory responses could be caused by the emulsifier (Tween20 surfactant) used was

ruled out by carrying out pilot experiments *in vivo* using the same ingredients and preparation methods but no fat. The pilots were very informative. The fat emulsions provided good images *in vivo*. The pilot studies also indicated the need to stabilise the fat emulsions intragastrically so that the true effect of droplet size could be assessed. The gum-stabilised fat emulsion meals were minimally thickened and appeared stable throughout the gastric emptying process.

## **5.7 Conclusion**

The pilot studies on the bench and *in vivo* supported the initial hypothesis that there is an overall droplet size effect on gastrointestinal responses to emulsion meals. Although carried out in only two subjects the data informed the direction of the subsequent work which investigates the droplet size effect in more depth in the next chapter.

## **6 Effect of fat emulsion intragastric stability and droplet size on gastrointestinal responses**

This chapter describes a study aimed to monitor, in the gastrointestinal tract, the physiological effects of fat droplet size and intragastric stability by the combined use of magnetic resonance imaging and spectroscopy. The conclusion was that manipulating food microstructure, especially intragastric stability and fat emulsion droplet size, can influence human gastrointestinal physiology and satiety responses.

### **6.1 Background**

The information gathered from the pilot studies described in the previous Chapter was valuable and indicated that changes in fat emulsion droplet size seem to affect the gastrointestinal response. A hypothesis that the observed strong small bowel secretory responses could be caused by the emulsifier (surfactant) used to keep the fat emulsions together was ruled out by carrying out further pilot experiments *in vivo* using the same ingredients and preparation methods but no fat.

At this point, from the bench work and the MRI images of the stomach it was clear that the fat in the Coarse fat emulsion meal tended to cream upwards more than the Fine emulsion. Therefore this introduced a

confounding variable since the output from the stomach and, in turn, gastrointestinal and satiety responses, could be modulated by either intragastric creaming or droplet size. To control for this problem, together with colleagues from Unilever, development work was carried out to select the best possible thickener. The integration of the thickener into both fat emulsion meals was planned in order to stabilise the meal against creaming inside the stomach hence ruling out this variable for future studies. A wide range of properties had to be considered such as purity and solubility; the thickener had to be as inert as possible and also leave the droplet size profiles unchanged. This *in vitro* development work, described in Chapter 5, led to the selection of Locust Bean Gum (LBG) which is a common food thickener used for example in breads and icecreams. LBG was particularly suited to the task since it is quite resistant to the acidic environment of the stomach. The **Fine+LBG** and **Coarse+LBG** fat emulsion meals behaved as desired preventing fast creaming of the Coarse emulsion. This was also checked *in vivo* in the stomach in small scale pilot work. For this larger subsequent study the Coarse emulsion with no LBG (called **Coarse Control**) was also used. All this work allowed definition of the study design and protocol for the full *in vivo* study which is reported here.

The aim of this study was to monitor in the gastrointestinal tract the physiological effects of fat droplet size and intragastric stability by the combined use of MRI and MRS.

The main hypothesis was that a difference in oil droplet size of fat emulsion meals will modulate gastrointestinal handling of the fat emulsion as determined by MRI, MRS and <sup>13</sup>C breath test.

## 6.2 Specific methods and protocol

### 6.2.1 Fat emulsions

The three fat emulsions prepared were:

- a) **Fine+LBG** - 350g o/w-emulsion with 20% sunflower oil (containing 100 mg <sup>13</sup>C-labelled octanoic acid), 1% Tween 20, with 0.4µm mean droplet size with 0.5% Locust Bean Gum
- b) **Coarse+LBG** - 350g o/w-emulsion with 20% sunflower oil (containing 100 mg <sup>13</sup>C-labelled octanoic acid), 1% Tween 20, with 10µm mean droplet size with 0.5% Locust Bean Gum
- c) **Coarse Control** (without LBG) - 350g o/w-emulsion with 20% sunflower oil (containing 100 mg <sup>13</sup>C-labelled octanoic acid), 1% Tween 20, with 10µm mean droplet size without any Locust Bean Gum

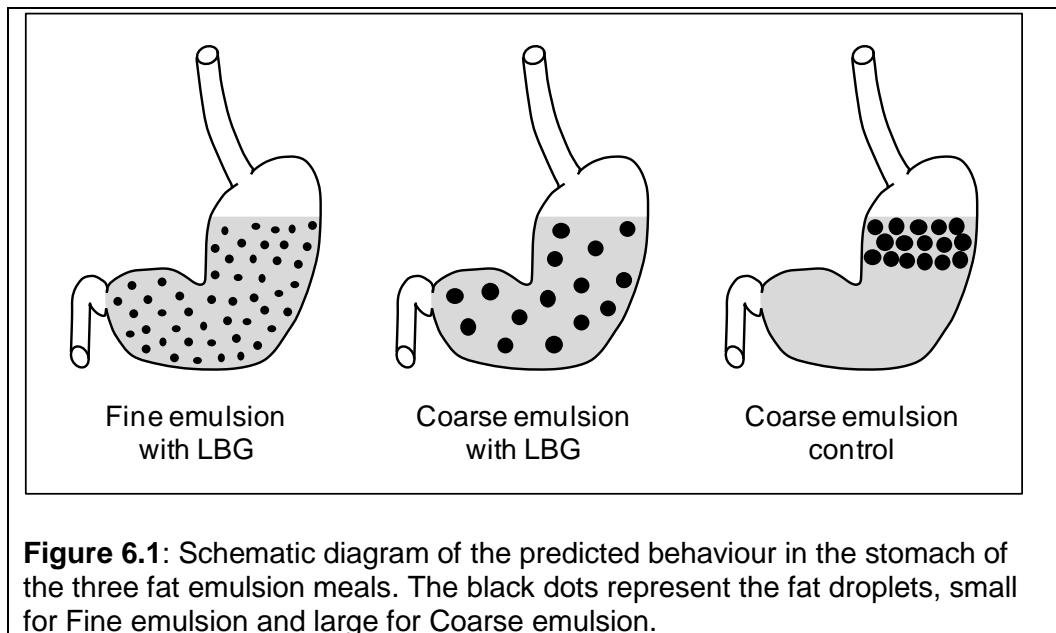
The predicted behaviour *in vivo* is represented schematically in Figure 6.1 below with the black dots representing fat droplets in the emulsion within the gastric lumen.

The fat emulsion meals were prepared in the Unilever Food laboratory (A104A) in Building 50 of Unilever Discovery Colworth. All ingredients and suppliers obtained Unilever Safety and Environmental Assurance Centre (SEAC) approval (reference number for this study was no 95724). The preparation procedures follow multiple checklist and Standard Operating Procedures (SOPs) and HACCP (Hazard Analysis and Critical Control Points) which were designed specifically for this study and were supervised by the

studentship collaborators there. Each emulsion had a unique identifier number and its preparation was recorded in a specially designed checklist.

Following the meal preparation, SOPs guaranteed that all prepared meals were free from microbial contamination for up to the expiry date from their prepared time as determined by the Microbiology department of Unilever Colworth.

An initial microbiology storage trial was carried out and this indicated the storage conditions and allowed length of storage limitations (i.e. expiry date of 4 weeks) to be adhered to. The emulsions were stored in a food grade fridge in the experimental kitchen room next to the MRI scanner and used within the expiry date. The temperature of the storage fridge was monitored routinely and the values logged in the Trial Master File. The acceptable range was  $5\pm 3^{\circ}\text{C}$ .



The droplet sizes were assessed for each sample (not batched, each sample was prepared individually and characterised individually for inclusion/rejection

from the study) as soon as they were prepared. LBG (0.5% w/w) was added into each of the Fine and the Coarse emulsions to stabilise the coarse emulsion and unify the Fine with the Coarse, therefore the viscosity of each meal including the Coarse control were obtained. The flavouring was added to improve palatability (1% coffee flavouring and 5 tablets of Hermesetas Gold sweetener).

The acceptable range of droplet size was 0.3-0.5  $\mu\text{m}$  for the Fine emulsion and 6-10  $\mu\text{m}$  for the Coarse emulsion. The measured D[3,2] range for droplet sizes for Fine+LBG emulsion was 0.402-0.389 (SD 0.0071), for the Coarse+LBG was 6.95-6.54 (SD 0.12) and for the Coarse Control was 7.5-5.58 (SD 44). The data for the droplet sizes measured for these emulsions are tabulated in Table 6.1.

Measurements	Fine+LBG		Coarse+LBG		Coarse Control	
	Mean (micron)	Standard deviation (+/-)	Mean (micron)	Standard deviation (+/-)	Mean (micron)	Standard deviation (+/-)
D [3, 2]	0.44	0.04	6.3	0.4	6.0	0.9
D [4, 3]	0.7	0.1	9	4	15	1
D(0.5)	0.52	0.06	7.0	0.5	14	1

**Table 6.1:** Summary of laser diffractometry data for Fine+LBG, Coarse+LBG and Coarse Control emulsions. The table reports the emulsion droplet size using the most commonly reported measures: D[3,2] (the surface area mean diameter), D[4, 3] (a volume mean diameter) and D[0,5] (a mass median diameter).

### 6.2.2 Subjects

Nineteen healthy volunteers aged 19-32 years, of normal height/body frame (Body Mass Index, BMI,  $23\pm 3$   $\text{kg/m}^2$ ) with no history of GI disease were

recruited from the University of Nottingham campus and asked to attend on 3 mornings each having fasted overnight. Details of the demographic data are given below in Table 6.2.

Initial baseline MRI scans were acquired and then the volunteers were given 300g of one of the 3 fat emulsion meals (60g fat in each meal) in random order. Scanning was performed hourly for 5 hours afterwards. 11 out of 19 subjects entered the final analysis. Equipment failure of the fridge where the test meals were stored meant that a batch of meals was inadvertently frozen causing 4 volunteers to be excluded. 2 subjects withdrew after the first visit whereas the other 2 completed 2 ways and could not make the 3rd visit appointment due to a change in their diary. The test meals were given to the volunteers following a latin square randomisation schedule to avoid order effects.

<b>N</b>	<b>Age yrs (sd)</b> <b>min-max</b>	<b>Height m (sd)</b> <b>min-max</b>	<b>Weight kg</b> <b>(sd)</b> <b>min-max</b>	<b>BMI</b> <b>kg/m<sup>2</sup>(sd)</b> <b>min-max</b>
19	24 (3) 19-32	1.7 (0.1) 1.49-1.91	71 (13) 50-102	23 (3) 19-30

**Table 6.2:** Demographic data for the volunteers

The study was approved by both the University of Nottingham local Medical School Research Ethics Committee and Unilever Critical Functional Capabilities Clinicals department. The study records were kept to a 'Good Clinical Practice' level of a phase 1 drug clinical trial, resulting in 19 Case

Report Forms and 4 large lever arch file folders, which were formally monitored by a Unilever representative who was not involved in this study. The records kept passed the monitoring session. All subjects gave written consent prior to any examination.

Volunteers were scanned when they arrived at the test centre to ensure an empty stomach and to acquire fasting baseline measurements of small bowel water content. All volunteers were asked to consume one meal of each type on 3 separate occasions. All meals were provided to the volunteer at a physiological temperature of 37°C to avoid rapid changes in relaxation times due to changes in temperature within the stomach. Volunteers were tilted slightly on their right hand side to encourage normal “upright” gastric emptying profile since previous research had shown that lying with the left side down (left lateral position) allows some fat of an oily meal to be delivered to the duodenum early resulting in delayed gastric emptying of the entire meal [85]. Volunteers were then given the test meal and they were then scanned every hour, for approximately 15 minutes, for five hours after the beginning of the meal ingestion. After each set of scans satiety visual analogue scores (VAS) were collected. At regular intervals (at baseline and, after feeding, every 15 min for 2 hours and subsequently every 30 min for up to 5 hours) the subjects were asked to blow in <sup>13</sup>C breath test bags which were stored for analysis. These breath samples were analysed using an IRIS®-Lab analyser (Wagner Analysen Technik, Bremen, Germany) calculating the change in <sup>13</sup>C breath signal from baseline and plotting it against time.

### **6.2.3 MRI methods**

MR data were acquired using the Philips 1.5T Achieva whole body scanner and the SENSE-body coil. A range of abdominal scans were acquired in ~15

minutes: bTFE to quantify gastric volumes: 40 transverse slices, 7 mm thick, acquired in 2 breath-holds 13 s acquisition time each, covering the whole abdomen, flip angle=80°, TR/TE 2.8/1.4 ms FOV=400 mm, in plane resolution 1.56x1.56 mm<sup>2</sup>, SENSE factor 2.0. Proton spectroscopy was acquired using STEAM (90°x90°x90°), TR 4s, TE 9ms, 2 dummies, voxel size 25x25x25 mm<sup>3</sup>, spectral bandwidth 1000 Hz, 512 samples, 4 repeats acquired in 24 s; acquired separately for 2 VOIs in the upper (top) and lower (bottom) parts of the gastric lumen corresponding to different components of the gastric contents due to layering in the supine position were identified on the bTFE images. The areas of the water and fat peaks were measured using in-house software written by Dr Mary Stephenson in Matlab®, and lipid/water ratios were calculated. To measure Small Bowel Water Content (SBWC): 24 coronal FSE images in a single breath-hold, in-plane resolution =1.56x2.83 mm<sup>2</sup>, SL=7 mm, with no gap between slices. The gastric and gallbladder volumes were calculated by using Analyze® software (Analyze9®, Biomedical Imaging Resource, Mayo Foundation, and Rochester, MN), where the volumes of individual regions of interest on individual slices were summed across. SBWC data were analysed with in-house methods and software developed by Dr. Caroline Hoad [5].

#### **6.2.4 Blood sampling**

The volunteers were cannulated in a forearm vein by a qualified research nurse. 9 serial (6.5ml each) blood samples were collected during the study day to correlate the MRI results with the relevant gut peptide CCK. CCK is one of the most likely candidates to mediate effects of fat on satiety. Its release correlates with immediate satiation; CCK antagonists inhibit post-prandial satiety and CCK alters taste preferences. The blood was immediately

separated and the plasma snap-frozen in liquid nitrogen. CCK plasma levels were measured using commercial radioimmunoassay by Dr Gulzar Singh in the UoN School of Biomedical Sciences.

### **6.2.5 Objective pasta meal**

Satiety was also measured objectively using an *ad libitum* weighed pasta meal buffet at the end of the study day. This is a standardized tomato and mozzarella pasta meal (purchased ready-made from Sainsbury's supermarket and heated using a microwave). The subjects are given a very large amount of pasta (1.2 Kg, so that they will not feel a small 'plate size' effect) and told to eat as much as they feel like. The final amount of pasta left over is weighed therefore yielding the real amount of food eaten to satisfaction. The pasta meal provides 127 kcal per 100 g (4.9 protein, 18.2 g carbohydrate and 13.8 g fat). This method has been used extensively in Unilever. The volunteers were presented with a very large amount of pasta (1.2 kg) and asked to eat as much as they felt like, with the remaining amount weighed again.

### **6.2.6 Statistics**

Statistical significance of differences was evaluated where appropriate using 2-way repeated measures ANOVA, 2-way repeated measures ANCOVA (analysis of covariance for the satiety VAS scores), 1-way ANOVA of the Areas Under the Curves (AUCs) followed by *post-hoc* individual t-tests corrected for multiple comparison or paired t-test. The software GraphPad Prism 5, SPSS and SAS 9.3 were used.

### 6.2.7 Safety and efficacy

The volunteers tolerated well the scanning and blood sampling procedures as well as the 3 test meals.

In terms of safety, all subjects filled in a MRI safety questionnaire on enrollment to ensure their suitability for the MRI scanner environment. Adverse events (AEs) were defined in the Protocol and monitored throughout the study and standard operating procedures (SOPs) were in place to deal with them, if any.

There were two adverse events in this study. One subject complained of headache before drinking the test meal. History of migraine was reported and this was a minor to moderate event judged to have no link with the study. Another subject reported that after the first study day felt nauseous, sweaty and had an episode of diarrhoea overnight. The subject was fine the following day, did not feel the need to report this immediately and classed this episode to us on the second occasion as a moderate severity (score 2). The subject was happy to come back for the other study days, which were completed with no further events. We classed the episode as possibly related to the study procedures (score 2) and took no action (score 1).

At the beginning of each study day the subjects were also asked a standard question “Are you well?” and the answer recorded in the case report form (CRF).

During each study day the investigator was always present and ready to monitor how the subjects were feeling in case there was need of any action. A medical expert was available to consult if needed.

This study used food grade fat emulsions as intervention, healthy volunteers as subjects and non-invasive magnetic resonance imaging as research methods hence the risk assessed by the investigators was very low.

In terms of efficacy, fat digestion activates gastrointestinal feedback that slows down gastric emptying, a mechanism mediated amongst other pathways by the duodenal release of cholecystokin (CCK). The efficacy of the test product was therefore assessed on gastric emptying (which was the main outcome of the study). This was also an imaging study so it is worth pointing out that good quality images of the fat emulsion meals in the stomach were obtained.

## **6.3 Results**

### **6.3.1 Bench checks on the test meals**

The Mastersizer laser diffractometer (Malvin Mastersizer 2000 particle size analyzer) was used again to analyse the droplet sizes of all individual test meals upon preparation since droplet size range was an acceptance/rejection criteria for meal preparation in the Unilever laboratory. Figure 6.2 shows the droplet size distributions.

The surface weighted mean  $D[3,2]$ , which reflects more the surface weight rather than volume was used here. The mean droplet sizes for Fine + LBG was 400nm, where the Coarse + LBG and Coarse Control were 7 and 8 microns respectively. The cup and bob geometry (Anton Paar, Physica MRC 501) consisting in coaxial cylinders configuration, smooth with 17mm diameter, was used to check the viscosity of the test meals.

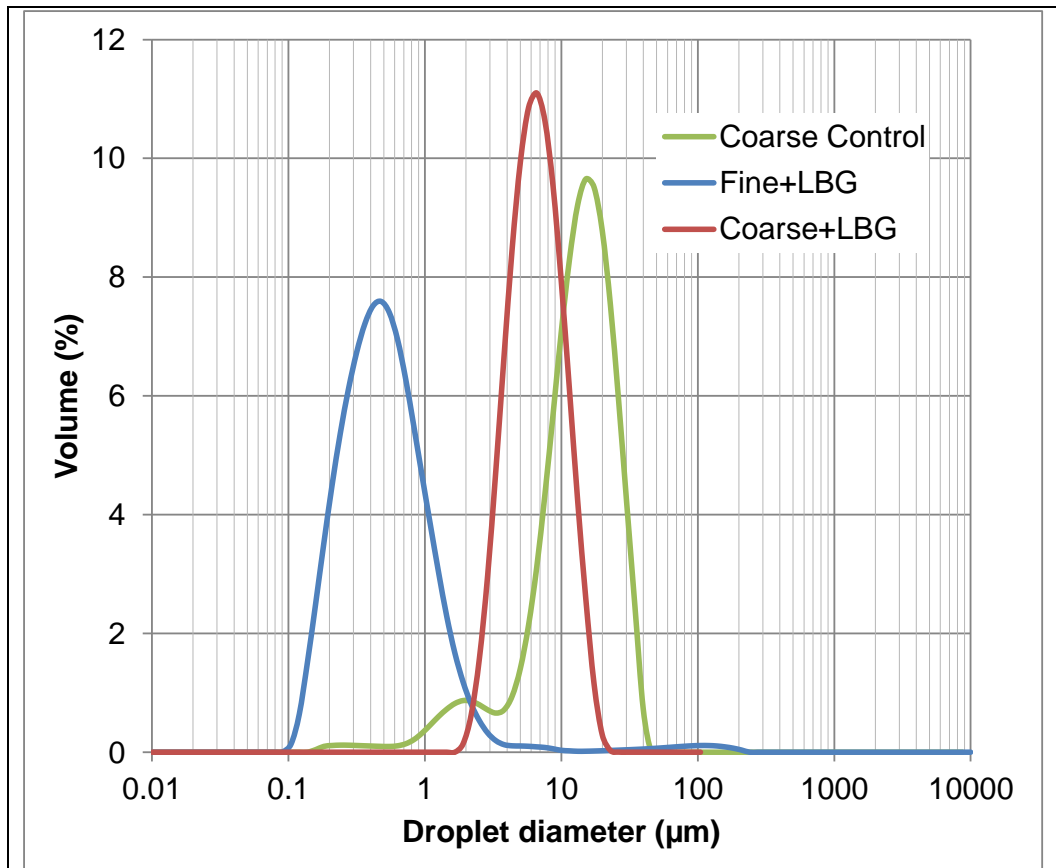
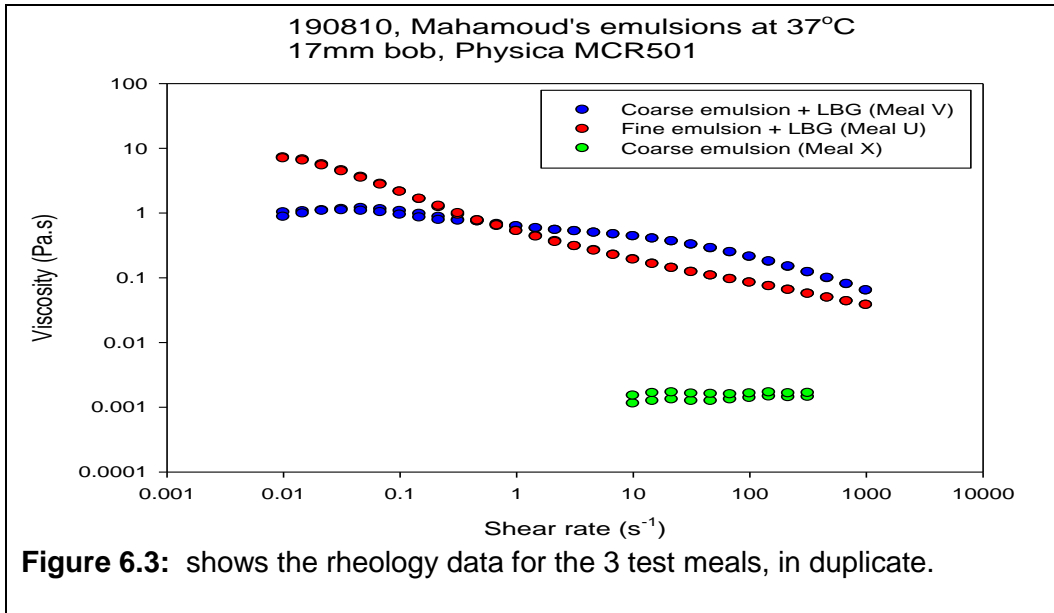


**Figure 6.2:** Example laser diffractometry Mastersizer data for the droplet size of the 3 meals.

The cup and bob geometry seemed to provide more reproducible profiles compared to other geometries. The duplicates and the data in Figure 6.3 show the good reproducibility. Due to sensitivity issues with the low viscosity Coarse Control (no LBG) sample, the initial readings at the low shear rate showed a number of negative torque values and the rheometer struggled until  $\sim 10\text{s}^{-1}$ . The Fine + LBG showed slightly higher viscosity at the lower shear rate. The Coarse + LBG had slightly higher viscosity at high shear rates compared to the Fine + LBG. Turbulent flow is often an issue when using this geometry at the high shear rates.



### 6.3.2 MRI imaging

Good quality images of the fat emulsion meals in the stomach were obtained as shown in Figure 6.4.

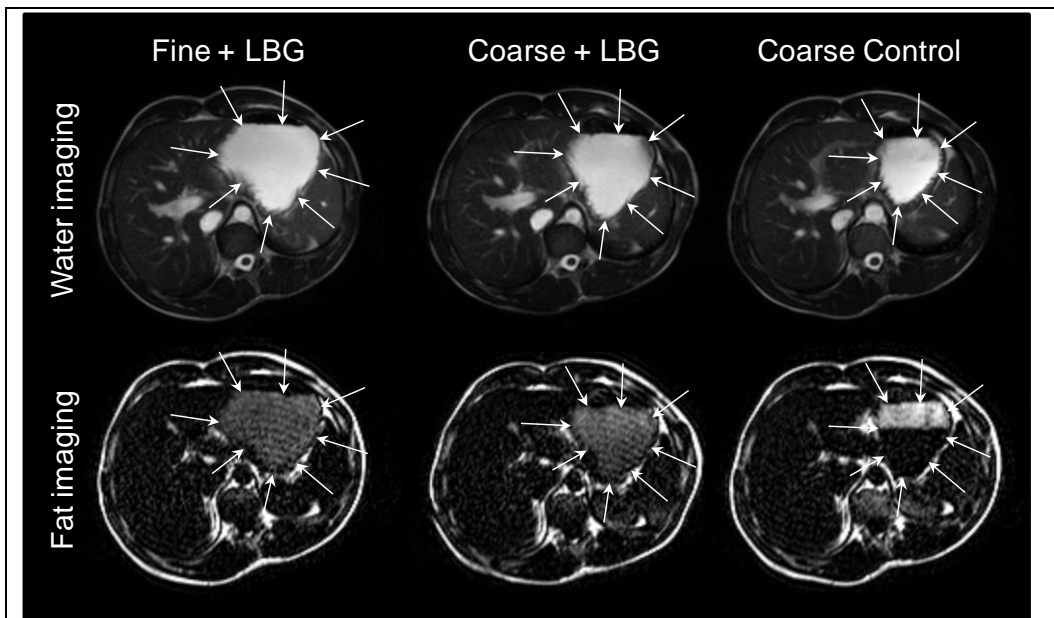
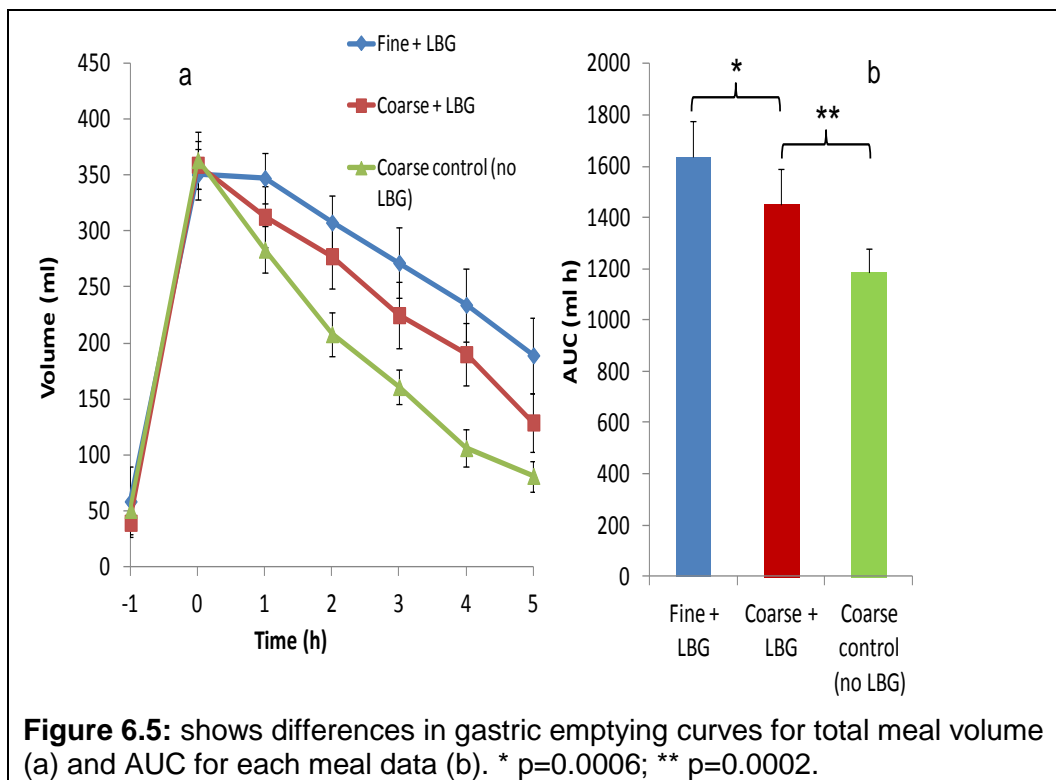


**Figure 6.4:** The upper panel shows typical bTFE (water) images taken across the stomach of the same subject at time t=2 hours after consumption of each test meal on the three separate study days. On the lower panel the corresponding fat-only images. These show that the LBG stabilised emulsions did not phase separate in the stomach whilst the Coarse Control shows a clear creamed fat layer on top of the stomach contents.

### 6.3.3 Gastric emptying

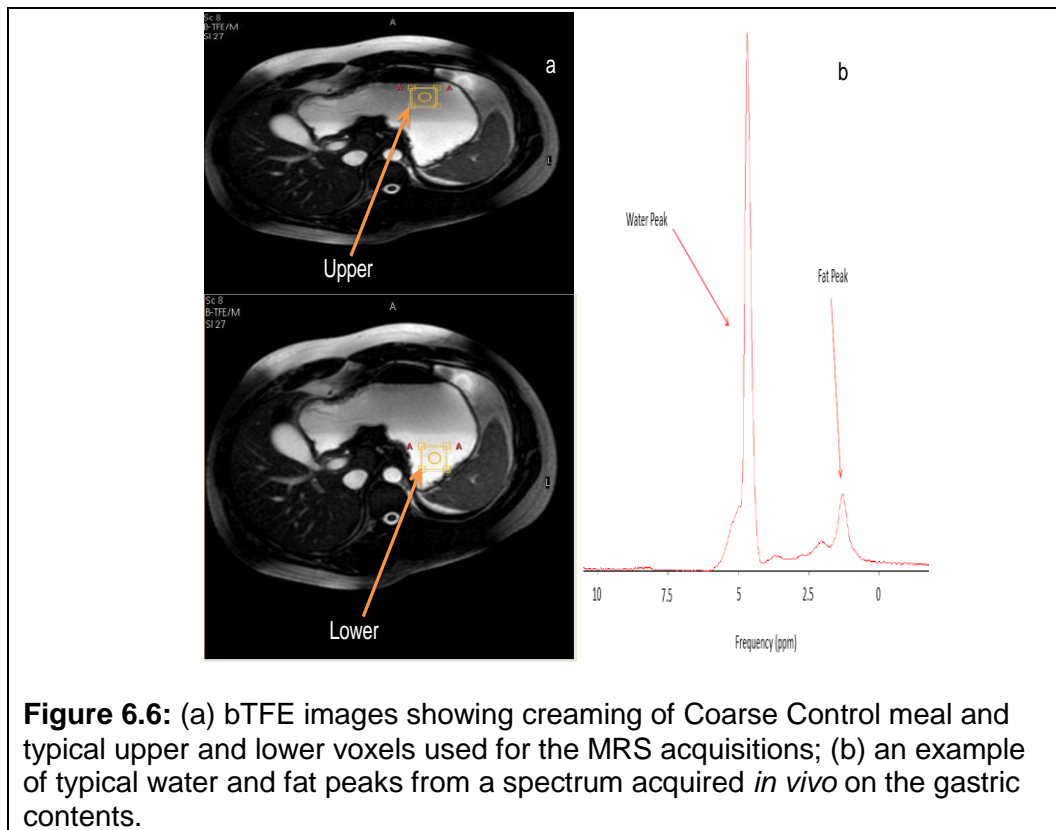
The time courses of mean meal intragastric volumes are shown in Figure 6.5a. It can be seen that the Fine emulsion with LBG emptied from the stomach slower and the Coarse Control faster. The corresponding mean AUCs are shown in Figure 6.5b. Adding LBG to the Coarse control emulsion significantly delayed gastric emptying (Coarse+LBG versus Coarse Control  $p=0.0002$ ). Reducing droplet size in the two meals containing LBG significantly delayed gastric emptying (Fine+LBG versus Coarse+LBG,  $p=0.0006$ ).

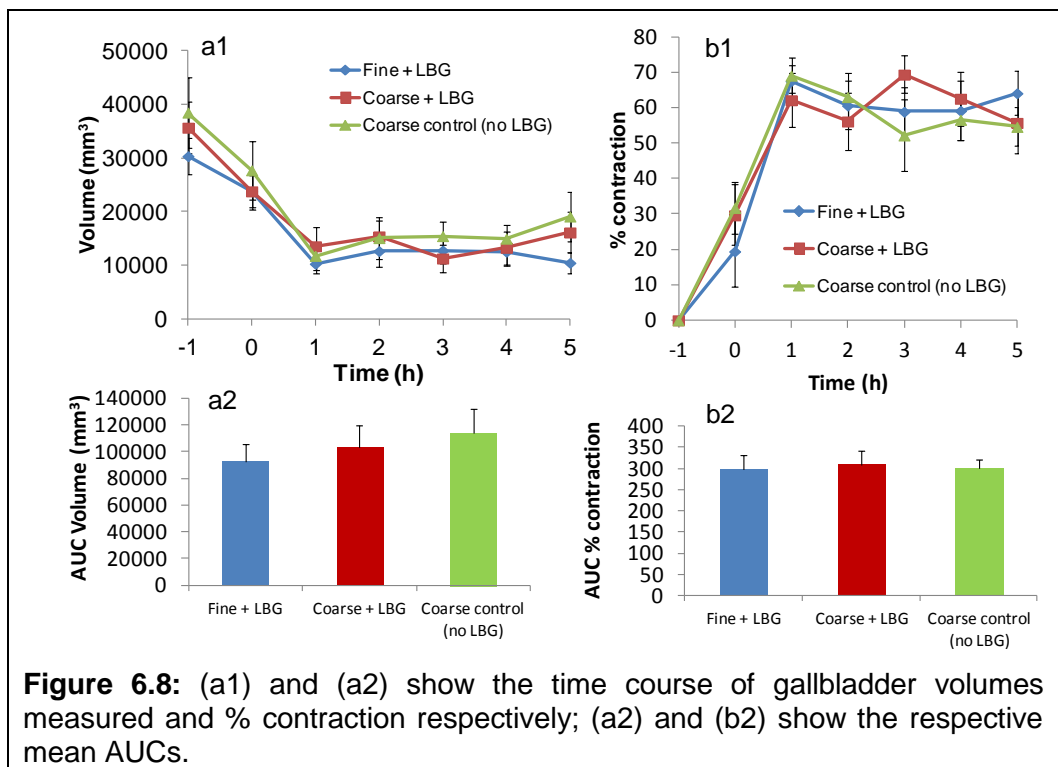
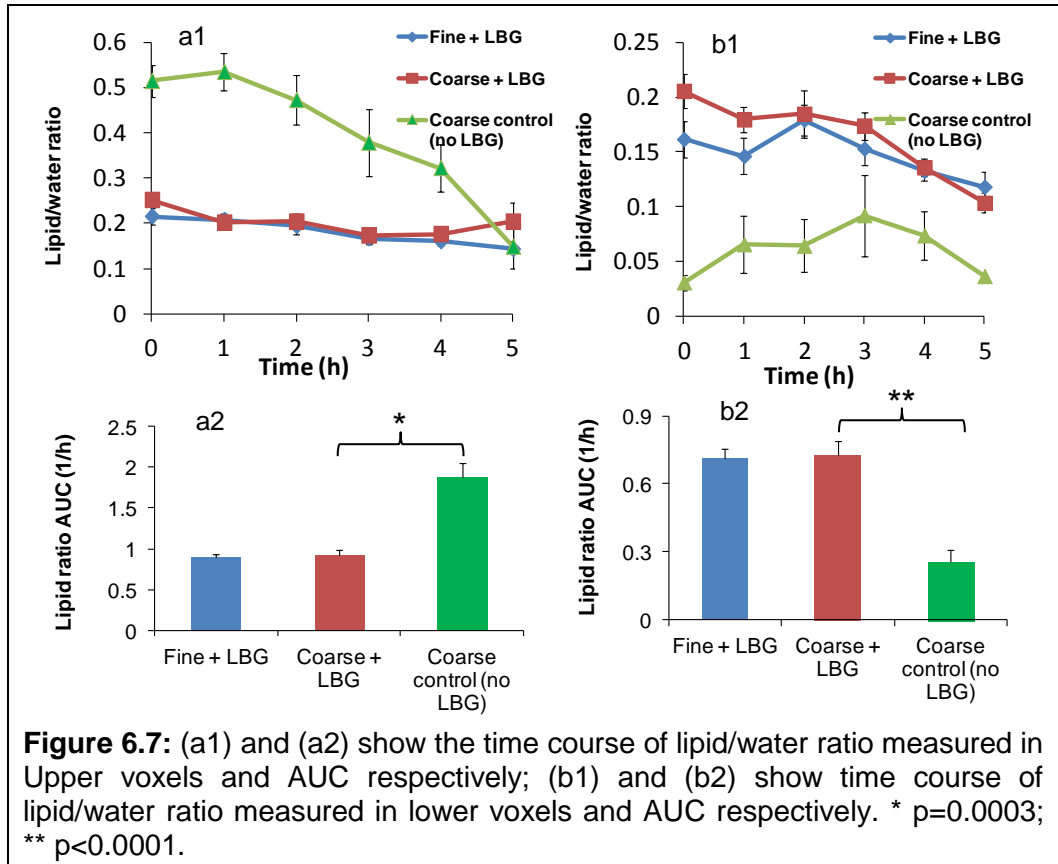


### 6.3.4 Fat/water ratio using MRS

Figure 6.6a shows a typical bTFE image of a fat emulsion in the stomach and Figure 6.6b shows a typical water and fat proton MRS spectrum obtained *in*

*in vivo* on the intragastric contents. Figure 6.7 shows the time courses of the processed lipid/water ratio MRS data including overall mean for upper voxel and lower voxel. The data show no significant difference over time in fat content for the Fine + LBG and Coarse+LBG emulsions. Conversely there was a significant difference between upper ( $p=0.0003$ ) and lower ( $p<0.0001$ ) voxel for Coarse+LBG versus Coarse Control with higher fat content in the upper voxel.



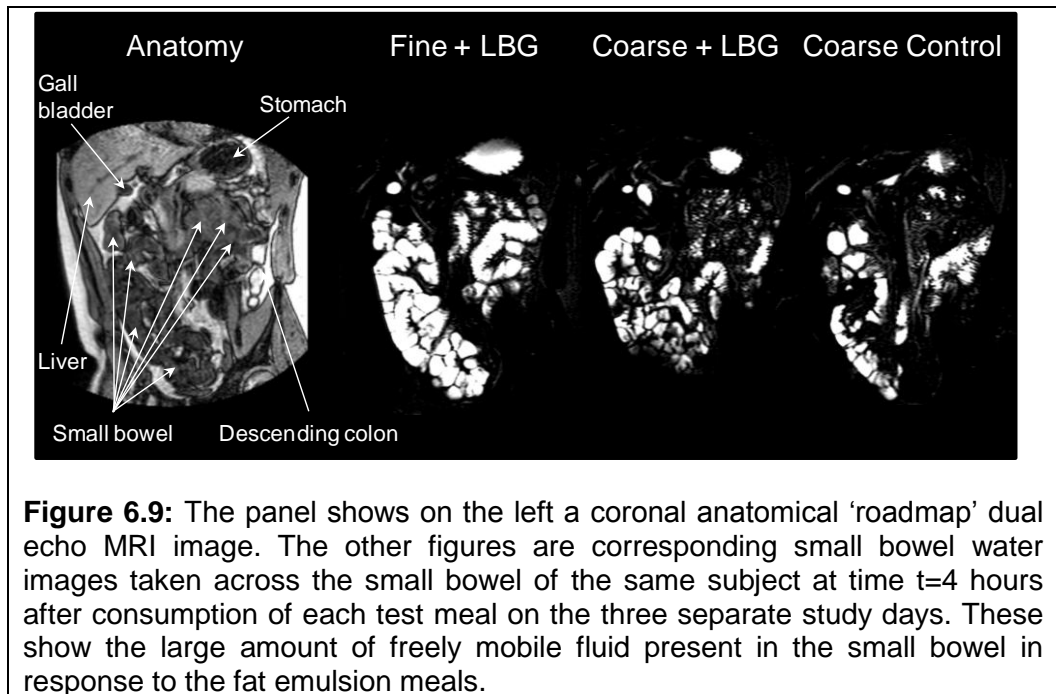


### 6.3.5 Gallbladder contraction

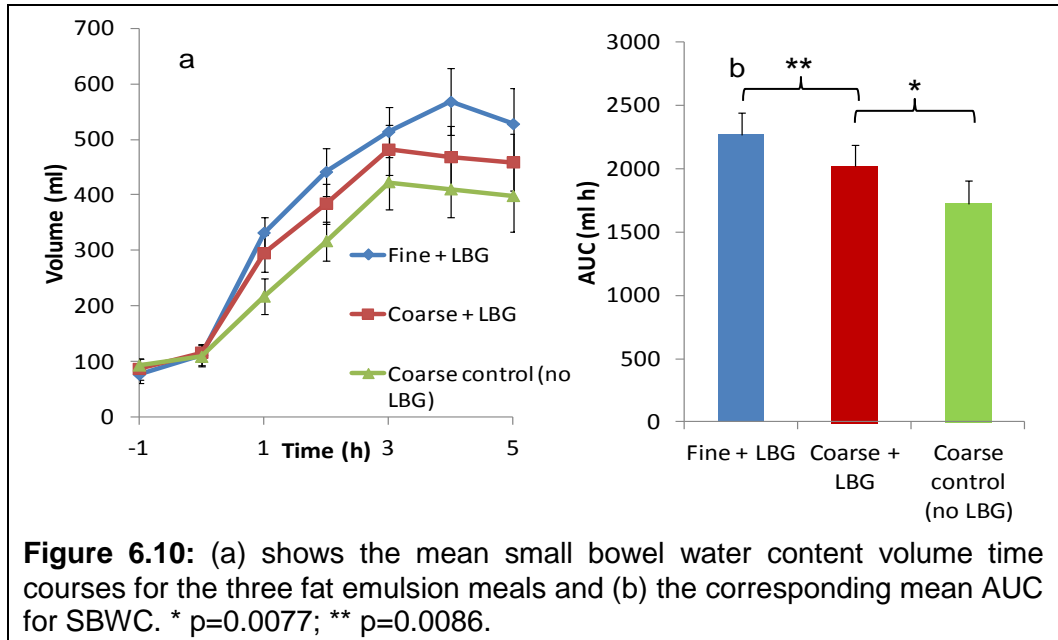
The mean gallbladder volumes and % contraction plus their AUCs are plotted in Figure 6.8. There were no significant differences between meals.

### 6.3.6 Small bowel water content

Figure 6.9 shows the small bowel water content images for the 3 tested meals and Figure 6.10 the mean SBWC volume time courses with their AUCs.

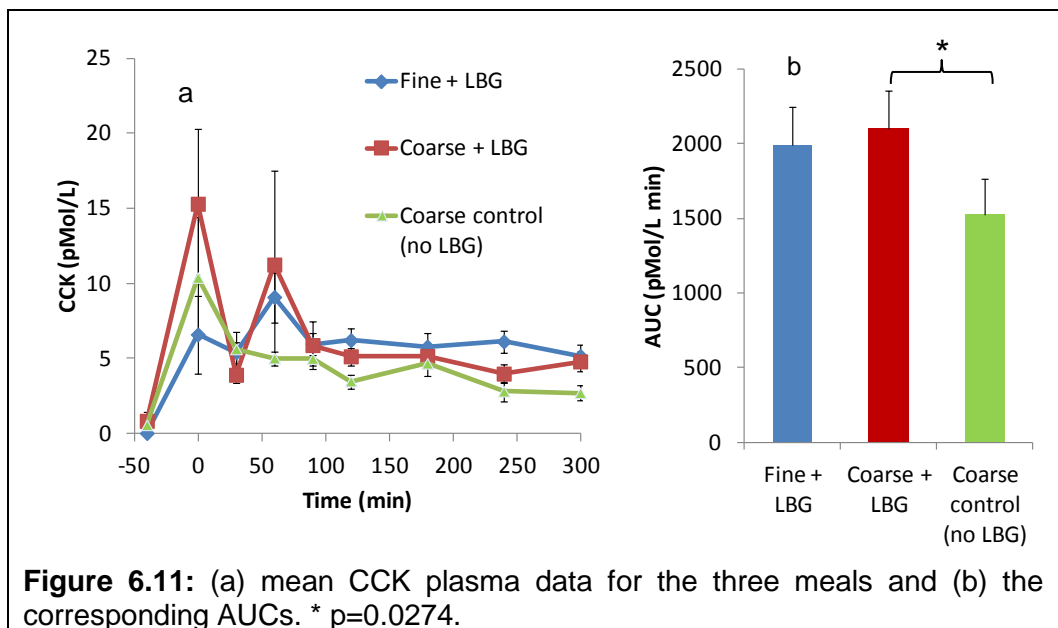


Adding LBG to the Coarse control emulsion significantly increased SBWC ( $p=0.0077$ ). Also, reducing droplet size significantly increased SBWC ( $p=0.0086$ ). The mean time to peak in the SBWC data, simply extracted manually from the spreadsheet data, showed a trend to be longer for the Fine+LBG meal (4 hours) and than for both the Coarse+LBG and the Coarse Control meals (3 hours).



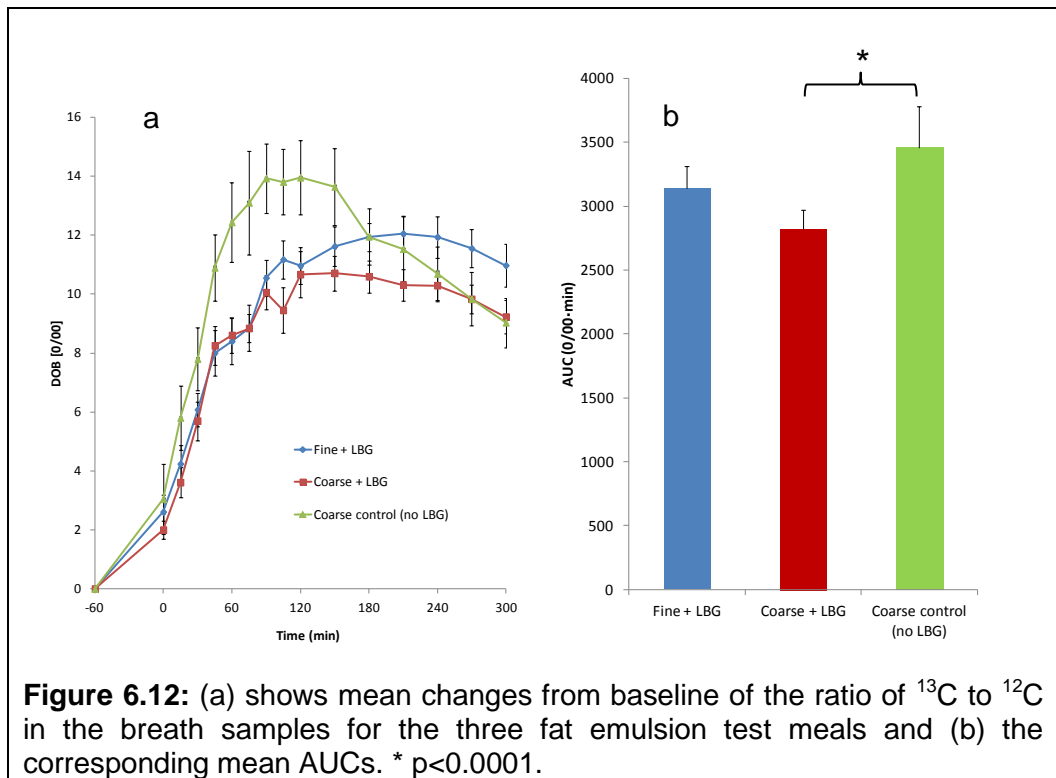
### 6.3.7 Plasma cholecystokinin

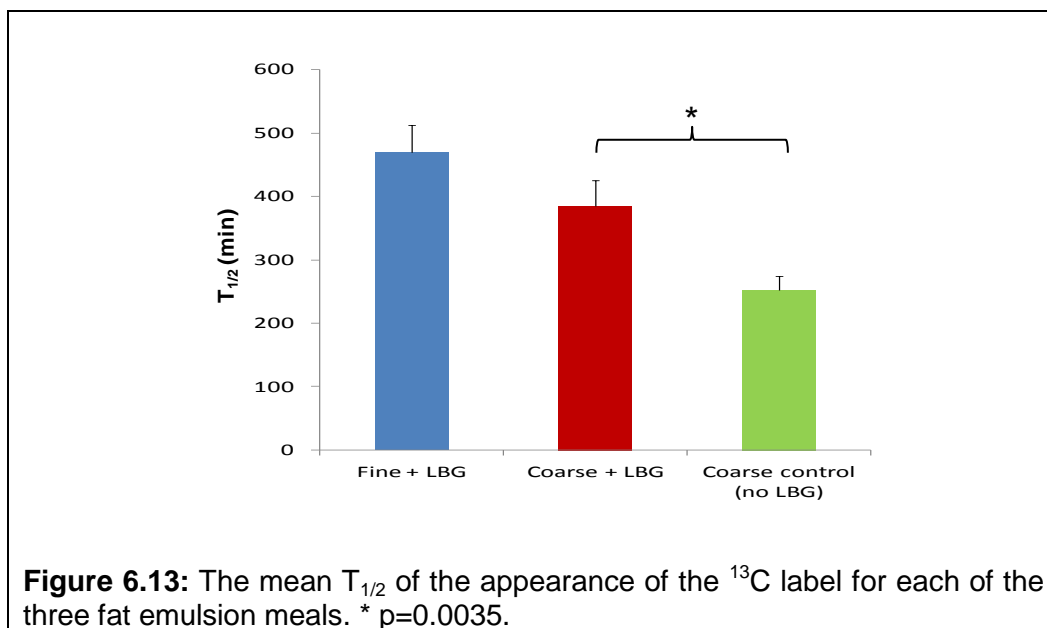
Figure 6.11 shows the mean CCK plasma level time courses. Adding LBG to the Coarse Control emulsion significantly increased plasma CCK ( $p=0.0274$ ). There were no significant differences in plasma CCK between Fine+LBG and Coarse+LBG.



### 6.3.8 Breath test

The mean changes from baseline (tracer appearance in the breath due to absorption from the gut and metabolism of the label) and the corresponding AUCs are shown below Figure 6.12. As the graph 6.12a shows, soon after ingestion the Delta Over Baseline (DOB) of the  $^{13}\text{C}$ -label in the breath appeared to be increased for the Coarse Control fat emulsion faster than for the LBG-stabilised meals in the first 2 hours. Figure 6.13 shows the  $^{13}\text{C}$  label  $T_{1/2}$  data across the 3 meals.





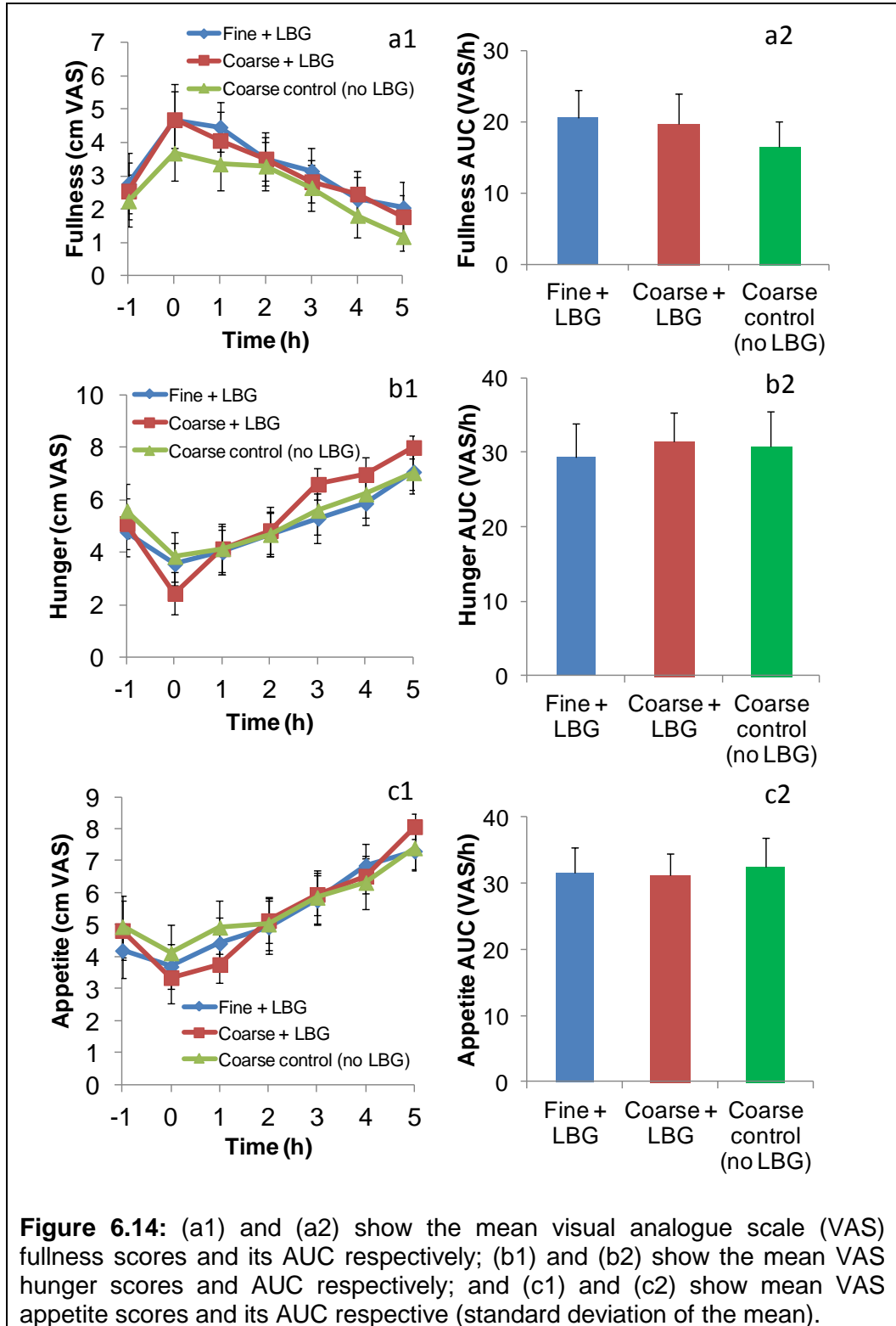
Adding LBG to the Coarse control emulsion significantly increased the  $^{13}\text{C}$  label  $T_{1/2}$  ( $p=0.0035$ ) and reduced delta over baseline ( $p<0.0001$ ). Also, reducing droplet size appeared to increase  $T_{1/2}$  though the change failed to reach statistical significance ( $p=0.127$ ). The delta over baseline appeared to be higher for the Fine + LBG emulsion but only after 3 hours post prandially as shown in Figure 6.12a.

### 6.3.9 Satiety questionnaires

The mean data of the fullness, hunger and appetite satiety scores are shown in Figure 6.14.

Fullness and hunger showed a trend appearing to be higher for the LBG containing meals; however, this failed to reach statistical significance (Fullness AUC versus Coarse control was  $p=0.1930$  for Coarse+LBG and  $p=0.1649$  for Fine+LBG; Hunger AUC  $p=0.8667$  and  $p=0.6783$  respectively). Analysis of the satiety VAS data using RM ANCOVA as recommended in the literature also

showed no significant differences between meals as summarized in the Table 6.3 below.

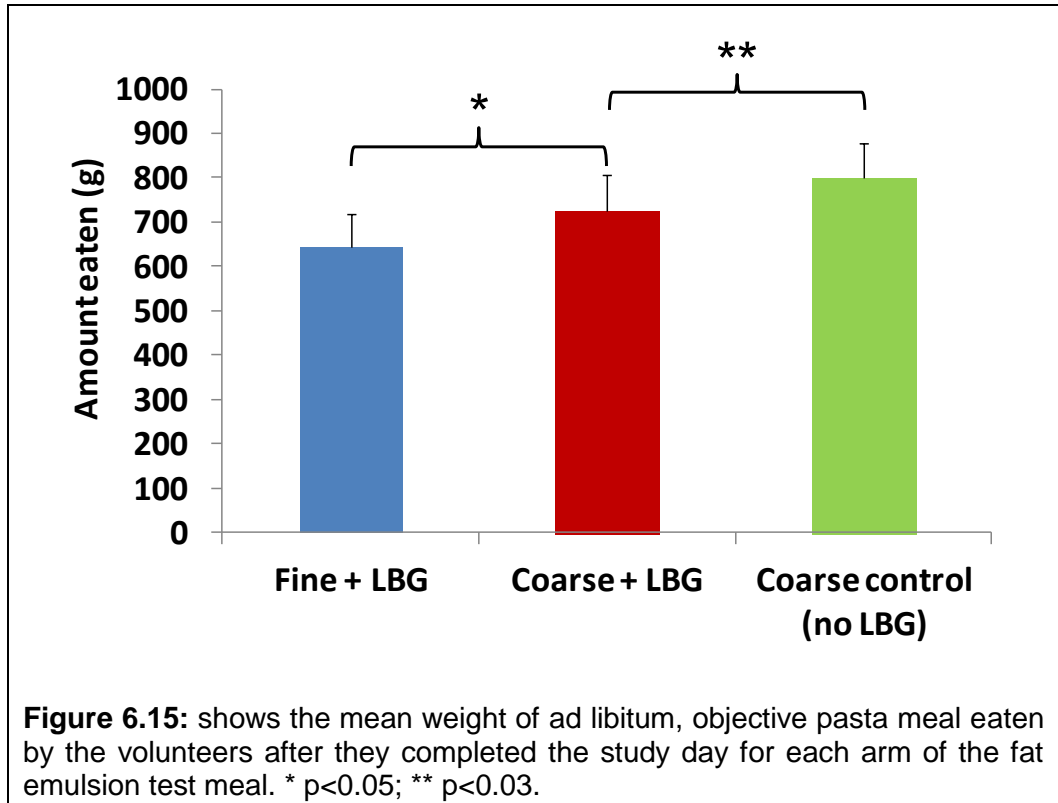


		Time	Time x Meal	Meal
<b>Fullness VAS</b>	Coarse Control versus Coarse LBG	P<0.0001	P<0.955	P<0.611
	Fine LBG versus Coarse LBG	P<0.0001	P<0.993	P<0.984
<b>Hunger VAS</b>	Coarse Control versus Coarse LBG	P<0.0001	P<0.203	P<0.656
	Fine LBG versus Coarse LBG	P<0.0001	P<0.125	P<0.767
<b>Appetite VAS</b>	Coarse Control versus Coarse LBG	P<0.0001	P<0.264	P<0.907
	Fine LBG versus Coarse LBG	P<0.0001	P<0.492	P<0.657

**Table 6.3:** ANOVA results for the satiety visual analogue scores.

### 6.3.10 Objective satiety assessment

Figure 6.15 shows the effects of feeding the 3 fat emulsion meals on a subsequent objective pasta meal to assess the satiety. Adding LBG to the Coarse Control emulsion significantly reduced the amount of pasta meal eaten afterwards ( $p<0.0293$ ). Reducing droplet size also significantly reduced the amount of pasta meal eaten afterwards ( $p<0.0417$ ).



## 6.4 Discussion

From the images and the spectroscopy data it can be seen that the LBG helped to stabilise the spatial distribution of the fat emulsions intragastrically, preventing creaming. This was the desired outcome since creaming of the larger droplet size emulsion was one of the limitations demonstrated by the previous pilot work. Having obtained an homogeneous spatial distribution in the stomach now allowed inferences to be drawn on the effect of droplet size on the gastrointestinal and satiety response to fat emulsion meals.

The choice of test meals and the study design allow two main effects to be investigated: (a) the effect of stabilizing the intragastric spatial distribution of a coarse fat emulsion and (b) the effect of decreasing droplet size in a gastric stabilized fat emulsion.

Gastric emptying was faster for the Coarse Control fat emulsion meal, which was predicted since creaming of fat to the top of the lumen away from the pylorus would lead to delivery to the small bowel of a fat-depleted watery phase during early gastric emptying, supported by the CCK data. The LBG-stabilised meals ensured steady delivery of fat to the duodenum during gastric emptying. This would trigger duodenal receptors which form part of the feedback loop that slow gastric emptying. Interestingly the Fine+LBG emulsion emptied slower than the matched Coarse+LBG emulsion possibly reflecting increased activation of duodenal fat receptors by the more finely emulsified droplets which therefore present a larger surface area for hydrolysis. This however was not reflected in the CCK data, which was likely due to the high variability and the relatively small number of subjects. Similar observations were reported by Armand et al [63]. The increased viscosity of the LBG-containing meal may have reduced gastric mixing and slowed enzyme-substrate interactions.

The gastric behaviour and gastric emptying response to these fat emulsions was analogous to that observed using acid-stable and acid-unstable fat emulsions [79].

There was substantial inflow of secretion into the small bowel. This was higher for the Fine+LBG meal, possibly reflecting again increased small bowel stimulation from the higher surface area offered to digestion by the smaller droplets. There are many factors driving SBWC and pancreatic secretion. A

direct vagal effect is possible or perhaps the coarse emulsion exerts inhibitory effects. Fat entering the ileum inhibits pancreatic secretion.

Initial gallbladder contraction differences which could be expected given the different intragastric behaviour of the meals may have been missed because of the hourly sampling frequency.

The  $^{13}\text{C}$  breath data also suggested that the different fat emulsion systems resulted in differences in availability of the fat to digestion and metabolism.

Ultimately, the combined effect of these different gastrointestinal responses to the test meals resulted in real differences in objective satiety (pasta meal) assessment. This is potentially important since it has been shown that small reductions in calorie intake can lead to significant improvements in weight management in obesity.

## 6.5 Conclusions

A highly emulsified intragastrically-stable emulsion leads to delayed gastric emptying, increased SBWC and reduced consumption of food at the end of the study day. Manipulating food microstructure especially intragastric stability and fat emulsion droplet size can influence human gastrointestinal physiology and satiety responses.

The work described in this chapter showed the importance of monitoring and quantifying fat fraction and spatial distribution *in vivo* in the gastric lumen to be able to relate fat emulsion performance to the gastrointestinal response and satiety. There is more work to be done to improve such methods and this is the subject of the next chapter using magnetic resonance imaging and spectroscopy methods.

## 7 Optimisation of fat quantification *in vivo*

This chapter describes the final part of the work. This required a deeper insight into the MRI characteristics of the fat emulsion systems including relaxometry, dilution, fat fraction quantification and cross-field experiments *in vitro*. Finally, imaging and spectroscopy methods were compared in a pilot study *in vivo*.

### 7.1 Background

The work described in the previous chapters showed the importance of the spatial distribution of fat in the stomach and of the droplet size delivered from the stomach to the duodenum as they both modulate gastrointestinal responses. The droplet size of a fat emulsion may also change in the stomach due to competing processes of coalescence [63] and gastric emulsification [87]. It would therefore be desirable to be able to monitor fat spatial distribution and fat droplet size in the stomach at different time points during digestion. The only method thus far available to assess fat fraction and droplet size is nasogastric aspiration, which is an invasive procedure and sampling is generally limited to a small volume of gastric contents around the catheter tip. Imaging methods would overcome both these limitations. The following two paragraphs describe the rationale for making such measurements in more detail.

### 7.1.1 Fat fraction quantification and m-DIXON method

Gastrointestinal function and satiety are strongly influenced by the spatial distribution of fat. Early studies using radiolabelling of the fat component of a meal [94, 95] made it possible to assess gastric emptying of fat with gamma scintigraphy [96]. Such studies have provided evidence that the isolated lipid component of a test meal empties much more slowly than the aqueous component of the meal [94, 95], whilst lipid integrated within the matrix of solid food particles empties with the solid phase of a meal [97]. MRI has an advantage in that the chemical shift between the resonances of the water and the fat protons can be exploited to image fat and water components separately by selectively exciting one or suppressing the signal arising from the other component. MRI studies have exploited the ability of MRI to discriminate between changes in the proton environment of water and fat components of a multiphase aqueous and oil meal to measure the emptying rates of oil and water components separately and to observe how posture altered gastric emptying [85]. When the subject was lying with the right side down, the lipid phase was observed to float in the fundus and emptying of the aqueous phase was rapid. With the subject lying with the right side up, the lipid layer filled the duodenum, where it could stimulate the duodenal receptors, and gastric emptying was significantly slower. It was also found that the longitudinal relaxation time  $T_1$  was relatively insensitive to droplet size and a method to assess the fat fraction in an oil-in-water emulsion both *in vitro* and *in vivo* within the gastric lumen using inversion recovery EPI and a two non-exchanging compartments empirical model was shown [25]. The intragastric behaviour of fat emulsions designed to be stable or break in the acidic gastric environment was shown to have an effect on the sense of satiety [23] and to stimulate greater cholecystokinin release which was associated with delayed

gastric emptying [26] compared to acid unstable emulsions in which the fat layer empties after the aqueous phase.

Established MR-based methods to quantify the fat fraction in a sample are magnetic resonance spectroscopy (MRS) and Dixon MR imaging sequences. MRS is widely used and validated across peer reviewed literature to determine the fat/water ratio of a sample or organ [98-106]. It is based on integrating the fat and the water peaks of the frequency spectrum obtained from a small volume of interest within the region of interest. We have used this method successfully to determine the fat fraction of the fat emulsions in the previous study described in Chapter 6. The MRS assessment of fat fraction has an inherently poor spatial resolution as the signal is collected from a large volume of interest (typically  $25 \times 25 \times 25 \text{ mm}^3$ ). Using an imaging method would provide fat fraction information at a much higher spatial resolution both in plane and in three dimensions on a multislice set. In 1984, Dixon introduced a technique for decomposing the fat and water components of the proton signal of a subject into two separate images [107]. This exploited the phase shift between water and fat signals and acquired two images, one with water and fat in-phase and one with opposite phase. By adding and subtracting the two images, water-only and fat-only images can be obtained. The method is elegant but suffers from signal to noise ratio problems, and issues related to shimming problems [108, 109]. The DIXON method has been constantly improved leading to the latest multi-echo (m-DIXON) methods [110]. The m-DIXON sequence collects data when the fat and water signals are in and out of phase. In a single breath hold of about 20 seconds the Philips 3D m-DIXON sequence can collect data to produce 4 image types using a simple algebraic manipulation: an in-phase image, an opposite phase image, a water only image and a fat only image. This has a clear advantage over previous methods which had to acquire 2

separate breath holds to obtain an in-phase image and an opposite phase image first and then a water only image. Unfortunately these fat and water images have signal that depends on the  $T_1$  and  $T_2$  weighing of the sequence for both fat and water as well as shimming effects which will change the absolute time for on and off resonance signals.

### **7.1.2 Droplet size measurements**

When fat is emptied from the stomach into the small bowel, long chain fatty acids trigger active responses from the GI tract [111] and the length and site of exposure of the small bowel can influence hunger and food intake [112]. However, it is not just the presence of fat that plays a key role in modulating the GI responses. In a recent review Golding stated that “The surface area of an emulsion is probably the key physicochemical parameter affecting the rate of fat digestion” [113]. There is substantial evidence supporting this conclusion, starting from early studies in a rat model [114]. Increasing the size of droplets in fat emulsions delivered directly to the small intestine reduced gastric antral pressure waves and attenuated plasma cholecystokinin (CCK) and peptide YY (PYY) and reduced hunger and energy intake [115]. Emulsified fat delivered, again intra-duodenally, in another study increased CCK, pancreatic polypeptide (PP) and gallbladder contraction compared to un-emulsified fat [116]. In another key study coarse (10  $\mu\text{m}$ ) and fine (0.7  $\mu\text{m}$ ) fat emulsions were delivered intra-gastrically and gastric and duodenal aspirates were taken at intervals to measure fat droplet size and lipase activities [63]. This showed a marked increase in the stomach in droplet size for the fine emulsions (2.75-6.20  $\mu\text{m}$ ) although the fine emulsion retained a higher gastro-duodenal lipolysis [63]. The ‘droplet size effect’ can be explained with the fact that a smaller droplet size for a given mass of fat offers a larger

lipid surface area [63]. The increased surface area will allow in turn a higher number of lipase molecules to bind at the oil-water interface because lipase is generally present in excess [63]. The body of evidence in the literature therefore shows the importance of the fat droplet size delivered from the stomach to the duodenum and that this may change in the stomach from the initial, ingested size due to competing processes of coalescence [63] and gastric emulsification [87].

It would therefore be desirable to be able to measure fat droplet size in the stomach at different time points during digestion, however the only method thus far available is nasogastric aspiration, which is an invasive procedure and sampling is generally limited to a small volume of gastric contents around the catheter tip.

MRI imaging could provide the solution to this problem. The transverse relaxation time  $T_2$  will depend on the size and distribution of any microscopic susceptibility perturber that gives rise to magnetic field gradients affecting the bulk water itself [117-119]. A distribution of fat droplets in solution will do this. Hence it should be possible to exploit this mechanism to measure fat droplet size. Indeed, an *in vitro* study showed that it is possible to measure fat droplet size non-invasively using MRI by measuring  $T_2$ . That study used 20% fat emulsions with droplet sizes ranging from 3  $\mu\text{m}$  to 12  $\mu\text{m}$ . Such measurements were in good agreement with predictions from Montecarlo simulations and analytical solutions [24].

Thus far there are no examples in the literature of *in vivo* intragastric fat emulsion fat fraction measurements using m-DIXON nor of fat emulsion droplet size measurements *in vivo* in the stomach using the transverse relaxation times  $T_2$ .

Building on the experience and samples described thus far, this Chapter describes work to gain familiarity *in vitro* on the methods and carry out an initial assessment *in vivo*.

## **7.2 *In vitro* studies**

This *in vitro* study was divided into 2 main experimental areas: (1) cross-field (X-Field) experiments to identify any field effect on the MRI parameters for these emulsion and (2) dilution studies, to establish calibration curves for the m-DIXON method and to evaluate possible droplet size effects on the observables.

### **7.2.1 Cross field experiment**

The relaxation times and also the susceptibility effects of the presence of the fat droplets in solution (as perturbers) are expected to be different at different static magnetic fields. Hence this study aimed at gaining a preliminary experience of these effects using two different magnetic fields (1.5T and 3T) and 6 different droplet sizes (for a fixed fat volume). In this experiment 6 emulsions with different droplet sizes ranging from 0.4  $\mu\text{m}$  to 10  $\mu\text{m}$  (named sample A, B, C, D, E and F) were scanned both on the Philips Achieva 1.5T and 3T MRI scanners. The sequences run on each sample at both fields were  $T_1$ ,  $T_2$ , MRS and m-DIXON. The sequence parameters were kept as much as possible the same both at 1.5T and 3T. The sequence used to measure  $T_1$  was an Inversion Recovery EPI using 15 inversion times from 0 to 4900 ms, scan duration was 8.5 minutes with a repetition time TR of 15 seconds and an echo time TE of 31 ms. The image resolution was 2mmx2mmx8mm, on a single slice acquired with a 96x96 matrix. The sequence used to measure  $T_2$

was a spin echo EPI using 12 echo times from 31 ms to 600 ms, the scan duration as approximately 2 minutes with a repetition time of 3 seconds. The image resolution was 2mm×2mm×8mm, on a single slice acquired with a 96×96 matrix. The m-DIXON sequence was a proprietary Philips 3D TFE double echo sequence, scan duration approximately 20 seconds with echo time one (TE1) 1.8 ms and echo time 2 (TE2) 4.0 ms and repetition time TR 5.4 ms (these values changed at 3T as follows: TE1 1.1 ms, TE2 2.4 ms, TR 3.9 ms). The image resolution was 1.49mm×1.95mm×3mm with 65 slices acquired in one average. The data were subsequently reconstructed to water only, fat only, in-phase and out of phase images automatically on the Philips platform.

Samples	Droplet size ( $\mu\text{m}$ )
A	0.42
B	0.55
C	2.25
D	7
E	8
F	10.25

**Table 7.1:** The droplet sizes of the six 20% fat emulsions that were scanned *in vitro*. Data on  $T_1$ ,  $T_2$ , MRS and m-DIXON was acquired for each sample A-F at both at 1.5T and 3T.

These emulsions were prepared using the same methods described in Section 5.2 and characterised by Malvern Mastersizer in order to measure their droplet size accurately. The differences in droplet sizes are simply obtained by varying the homogenising times.

### 7.2.2 Dilution experiment

In this experiment, batches of two emulsions with different droplet sizes (Fine and Coarse as described previously) were progressively diluted to lower fat fractions as described in Table 7.2. These samples *in vitro* were scanned both on the Philips Achieva 1.5T and 3T MRI scanners. In an initial series of experiments only 2.5%, 5%, 10% and 20% fat samples were used. In a second series of experiments (termed ‘repeat’) the 7.5% and 12.5% samples were also prepared after initial results showed it would have been beneficial to have additional data points in that range. The sequences run on each sample at both fields were  $T_1$ ,  $T_2$ , MRS and m-DIXON as detailed above.

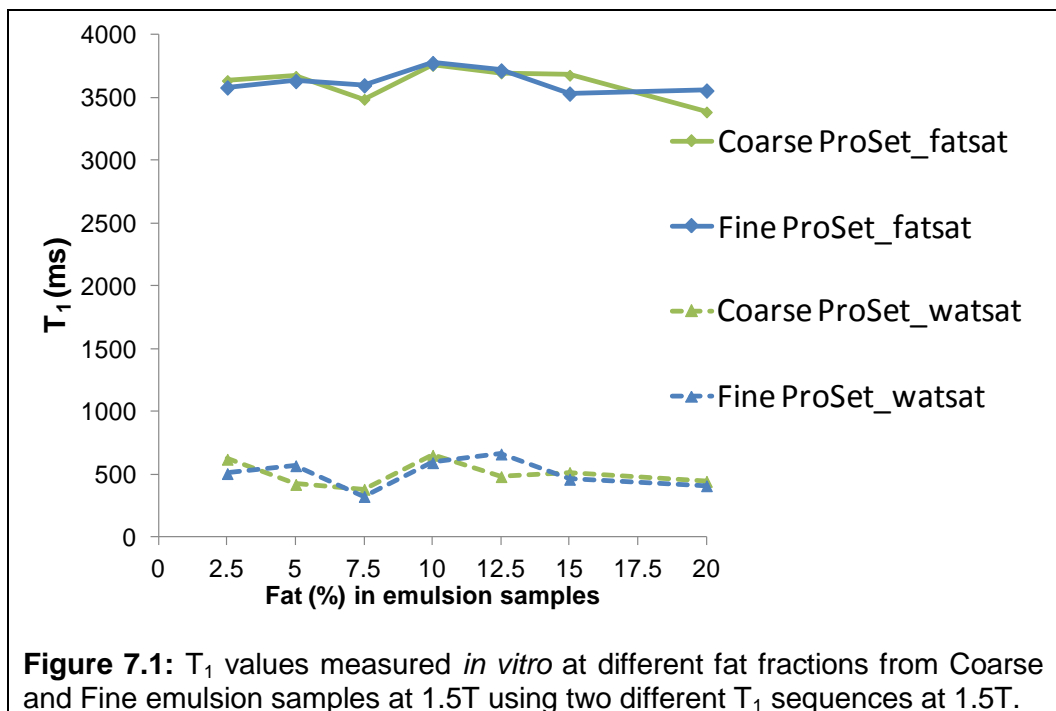
Fine emulsion samples	Coarse emulsion samples	Emulsion fat content (%)
G	O	20
H	P	12.5
I	Q	10
L	R	7.5
M	S	5
N	T	2.5

**Table 7.2:** The % fat content of the six progressive dilutions of fat emulsions prepared for both Fine and Coarse emulsions. Data on  $T_1$ ,  $T_2$ , MRS and m-DIXON was acquired for each sample G-N at both at 1.5T and 3T.

### 7.3 Results *in vitro*

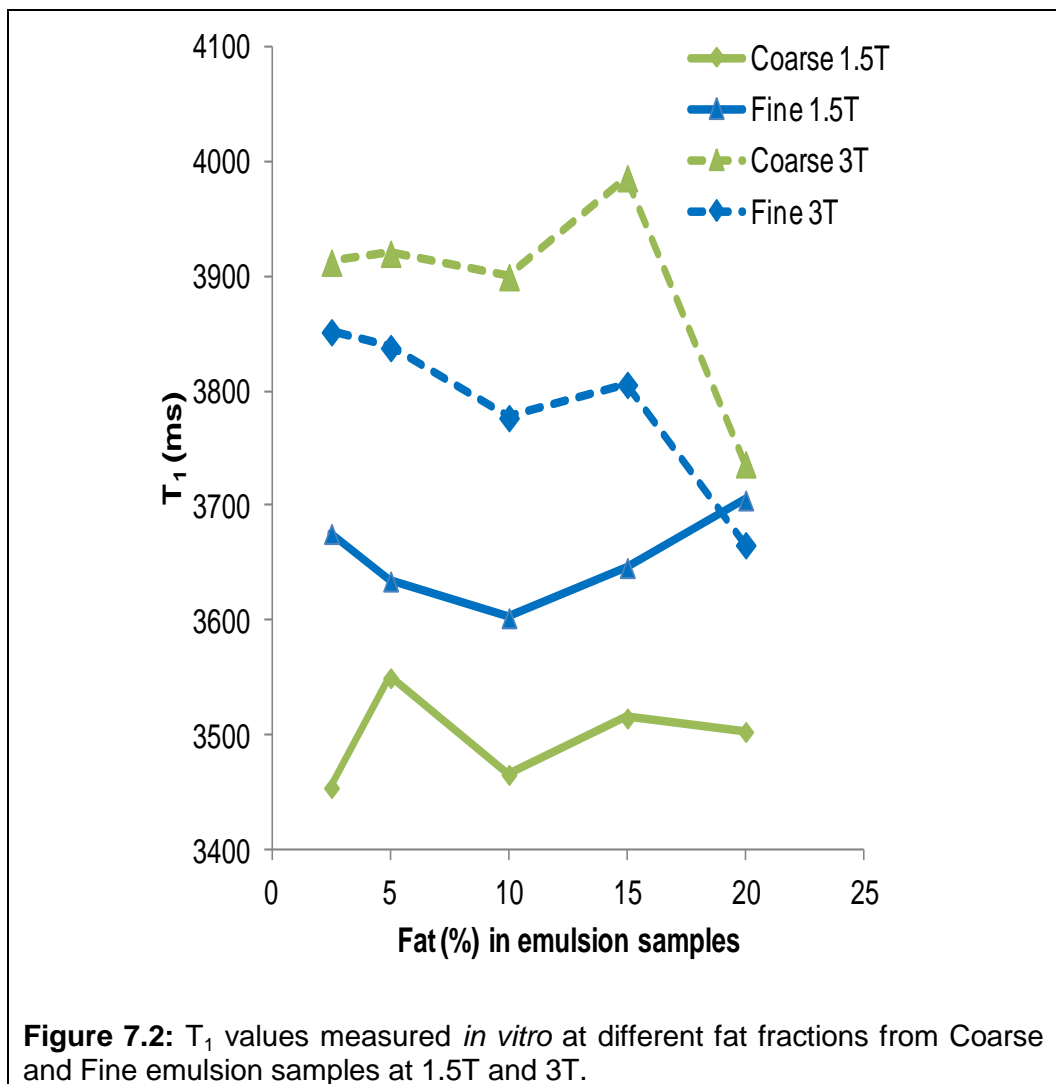
#### 7.3.1 Cross-field $T_1$ relaxation

Figure 7.1 shows a comparison of two different  $T_1$  sequences ProSet\_watsat and ProSet\_fatsat on both emulsion (Fine and Coarse) at 1.5T. The MRI sequence and scan parameters are the same as detailed above using a standard inversion pulse but using in the EPI readout a spectrally selective pulse to excite only the fat or water protons. This was set to be a 1-2-1 binomial pulse. The fat suppressed sequence showed high  $T_1$  for both samples and lower  $T_1$  was recorded for water suppressed sequences with no apparent effect of fat concentration.



$T_1$  relaxation showed an apparent effect of static magnetic field in that the Coarse and Fine  $T_1$  values were apparently higher at 3T than for 1.5T. No

effect of droplet size could be inferred from the data as shown in Figure 7.2 because the Coarse and Fine  $T_1$  values were in opposite directions for the two fields, probably due to experimental error (maybe temperature differences). No statistical analysis was attempted as  $n=1$  for each fat %. Also, the  $T_1$  relaxation times for these emulsion samples were apparently higher at lower field (1.5T) than at higher field (3T). The field effect on  $T_1$  is consistent on both Fine and Coarse emulsions. This data includes signal from both water and fat, so the reduction in  $T_1$  at high fat fraction is probably due to multiexponential relaxation and being fitted as a shorter  $T_1$ . Also, the fat signal may be suppressed in smaller droplets due to field inhomogeneities.

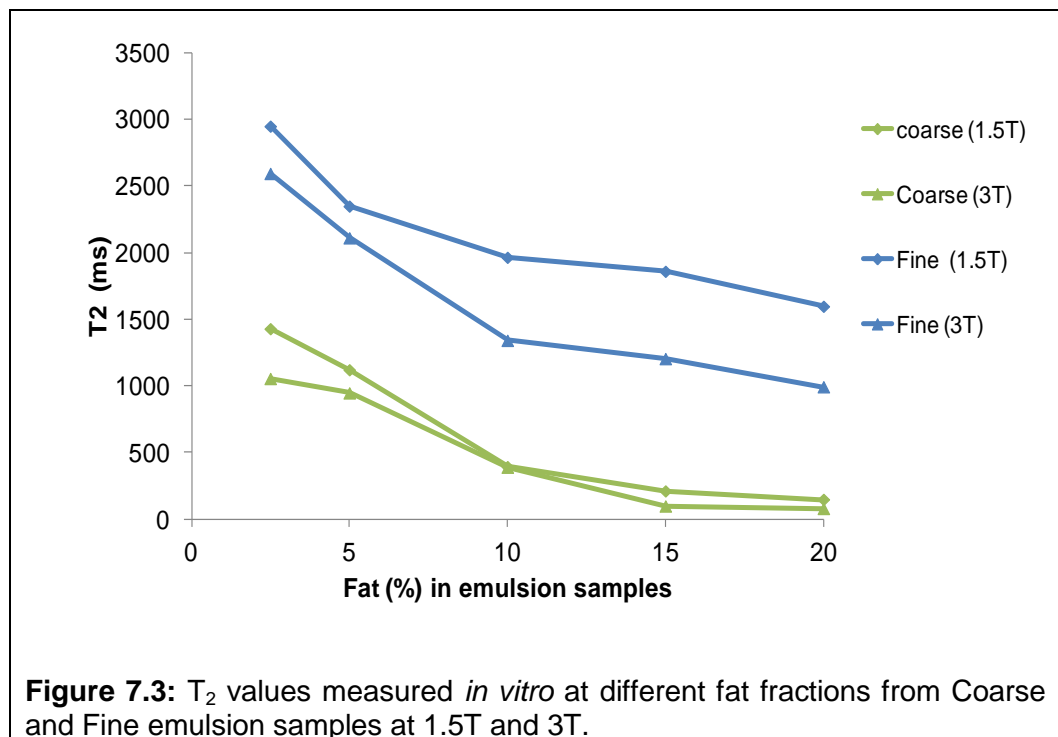


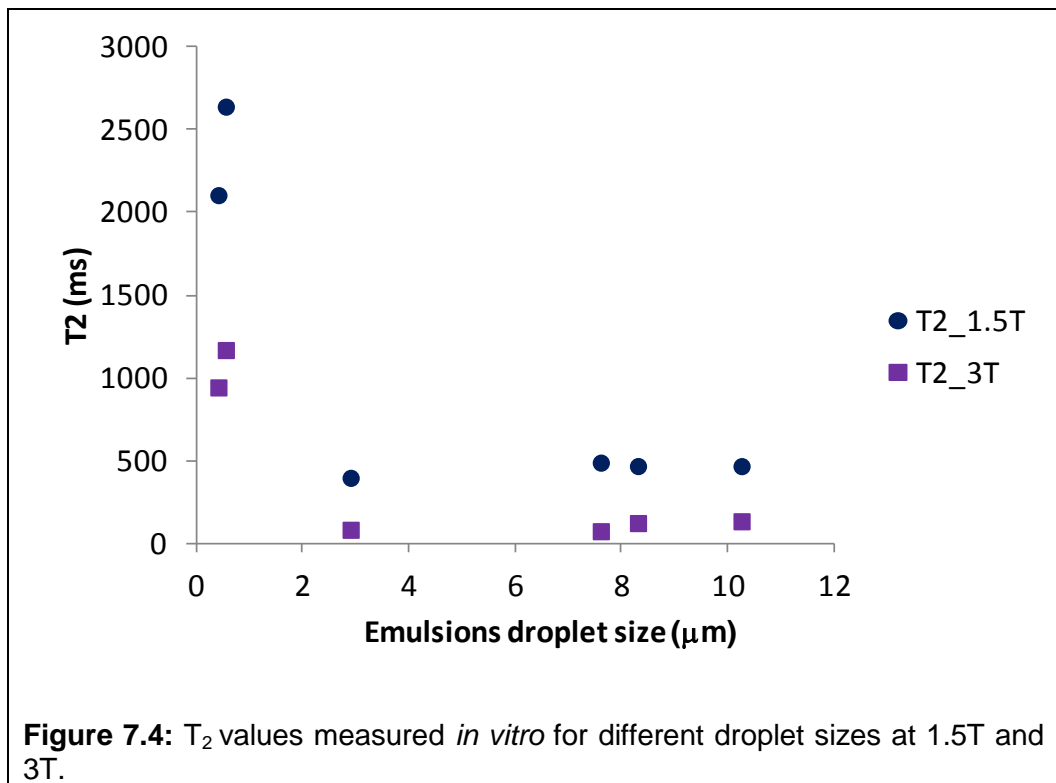
### 7.3.2 Cross-field $T_2$ relaxation

There were both apparent field effects as well as apparent droplet size effects on  $T_2$  relaxation as shown in Figure 7.3. The Fine emulsion showed a longer  $T_2$  compared to the Coarse emulsion at both 1.5T and 3T. The field dependence of  $T_2$  seemed to be greater for the Fine emulsion than for the Coarse. This was a n=1 sample for each dilution point so no statistical analysis was attempted.

Figure 7.4 shows that  $T_2$  was high for small droplet sizes at 1.5T (order of 2000 ms) but it was reduced by approximately a factor of 4 to the order of 500ms for droplet sizes greater than 3 microns. There was no further variation for droplet sizes larger than 3 microns.

There seemed to be also a field effect on  $T_2$  relaxation times with  $T_2$  values of the various emulsions consistently higher at 1.5T as one would expect because of reduced field distortions due to susceptibility effects.





### 7.3.3 Cross-field m-DIXON fat/water ratio

Figure 7.5 shows the m-DIXON fat/water ratio measurements for both Coarse and Fine emulsions. This is the initial signal intensity ratio before any calibration was attempted. The graph seem to show an apparent field effect on fat emulsion above 10% fat content, with a limited droplet size effect. The relationship between measured fat/water ratio and fat % seems to be non linear. It is possible that this deviation at low fat/water ration could be a limitation of the m-DIXON sequence at low fat fraction. Figure 7.6 indicates the reproducibility of the m-DIXON measurements with a test-retest on different batches on different days.

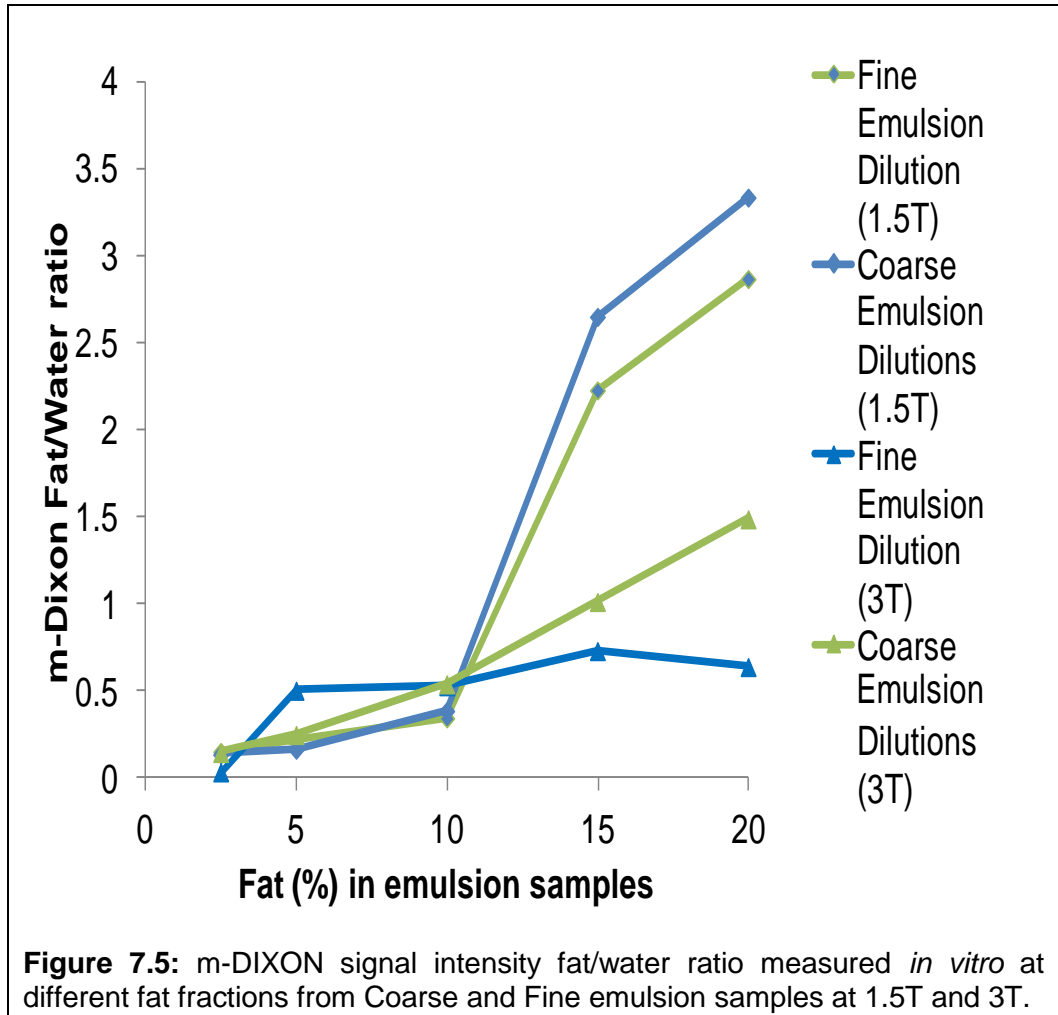
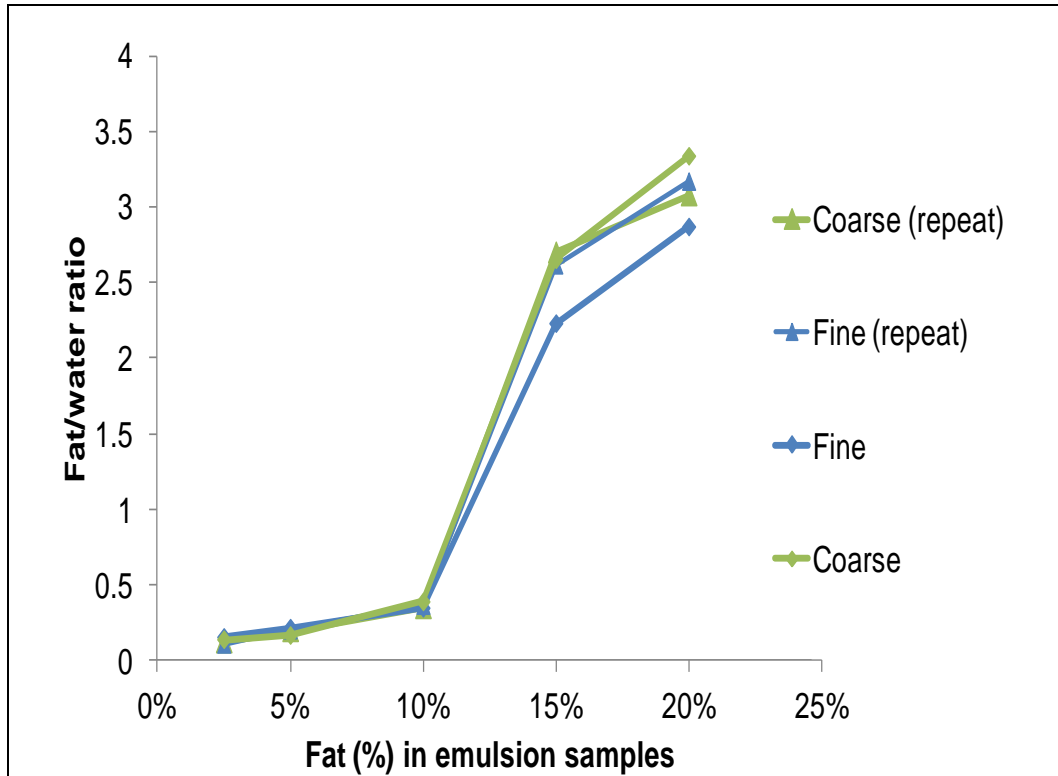
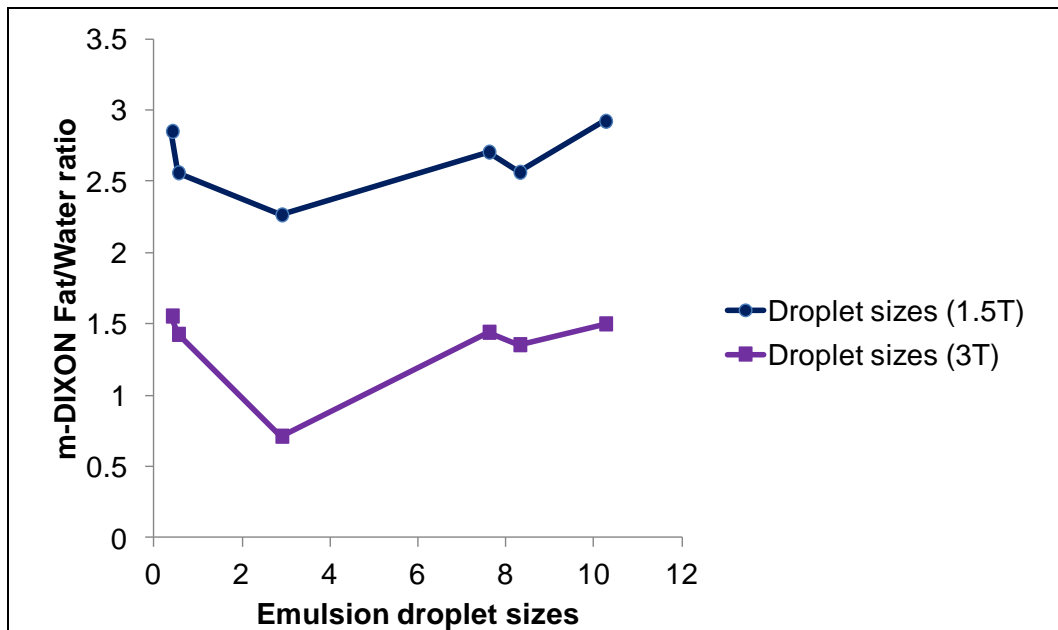


Figure 7.7 confirms that with the m-DIXON sequence a higher fat/water ratio is obtained at lower field. However the graph also shows no marked differences in m-DIXON fat/water ratio with varying droplet sizes at both fields.



**Figure 7.6:** Test-retest on two different batches of samples for the m-DIXON signal intensity fat/water ratio measured *in vitro* at different fat fractions from Coarse and Fine emulsion samples at 1.5T.



**Figure 7.7:** m-DIXON signal intensity fat/water ratio measured *in vitro* (n=1 for each sample) at different droplet sizes at 1.5T and 3T.

### 7.3.4 m-DIXON calibration for *in vivo* study

The data shown in the previous paragraph are based on a simple ratio of signal intensity between corresponding regions of interest drawn on the fat-only and water-only m-DIXON images. These ratios do not correspond to fat fractions imaged because the m-DIXON sequence is  $T_1$ -weighted and the water and fat samples have an inherently large difference in  $T_1$ . The signal depends also on  $T_2$ . It would be desirable to be able to convert these to actual fat fraction and this can be done simply by calibrating, at a given field, the signal intensity ratios measured with the known fat fractions in the samples.

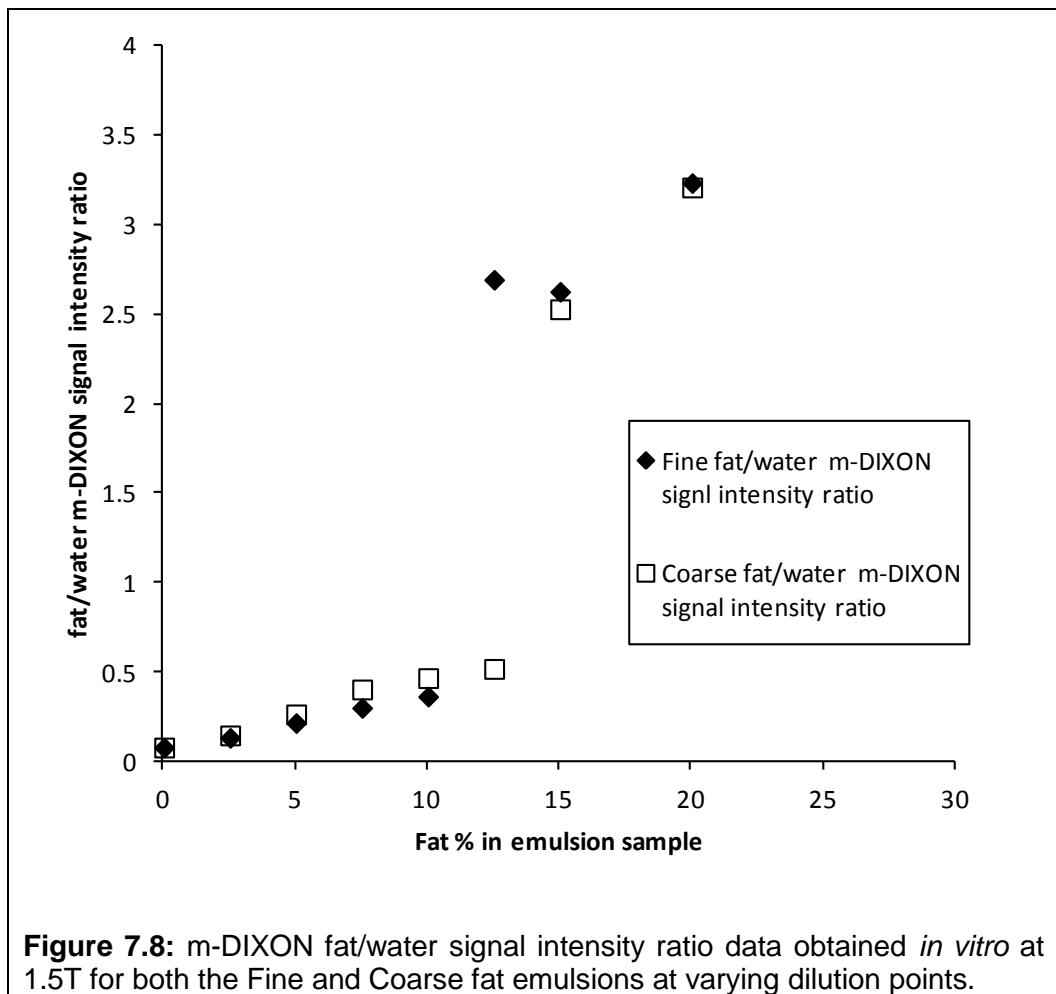
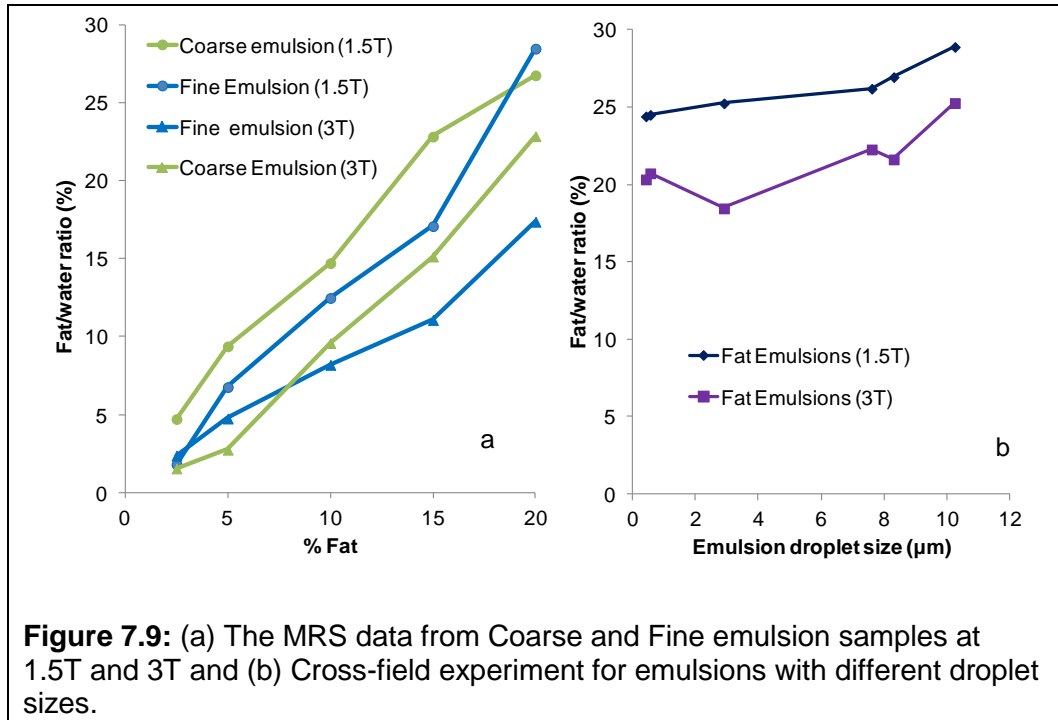


Figure 7.8 shows the m-DIXON fat/water signal intensity ratio data obtained *in vitro* at 1.5T for both the Fine and Coarse fat emulsions at varying dilution points. The Fine and Coarse data for each dilution were close to each other indicating that droplet size does not introduce a systematic variation in the m-DIXON fat/water ratio data. Based on this observation the data were all pooled together for the fit. The linear fit of the data is poor but assuming linearity of the data across this dilution interval is a simple option and the linear fit has an  $R^2$  value of 0.7895. This yields a calibration curve for the *in vivo* data as:

$$\text{Emulsion fat fraction} = (\text{m-DIXON fat water SI ratio} + 0.8213) / 19.719 . \quad [7.1]$$

### 7.3.5 MRS fat fraction

Figure 7.9 shows the MRS fat fraction data for both Coarse and Fine emulsion dilutions (i.e. different fat fractions). The data showed good correspondence of the MRS method with known fat fraction. There was an apparent field effect on fat/water ratio measured by MRS but there was no marked variation in the MRS fat fraction data with varying droplet sizes. Figure 7.10 shows repeated experiments with a larger number of fat fractions at 1.5T.



**Figure 7.9:** (a) The MRS data from Coarse and Fine emulsion samples at 1.5T and 3T and (b) Cross-field experiment for emulsions with different droplet sizes.

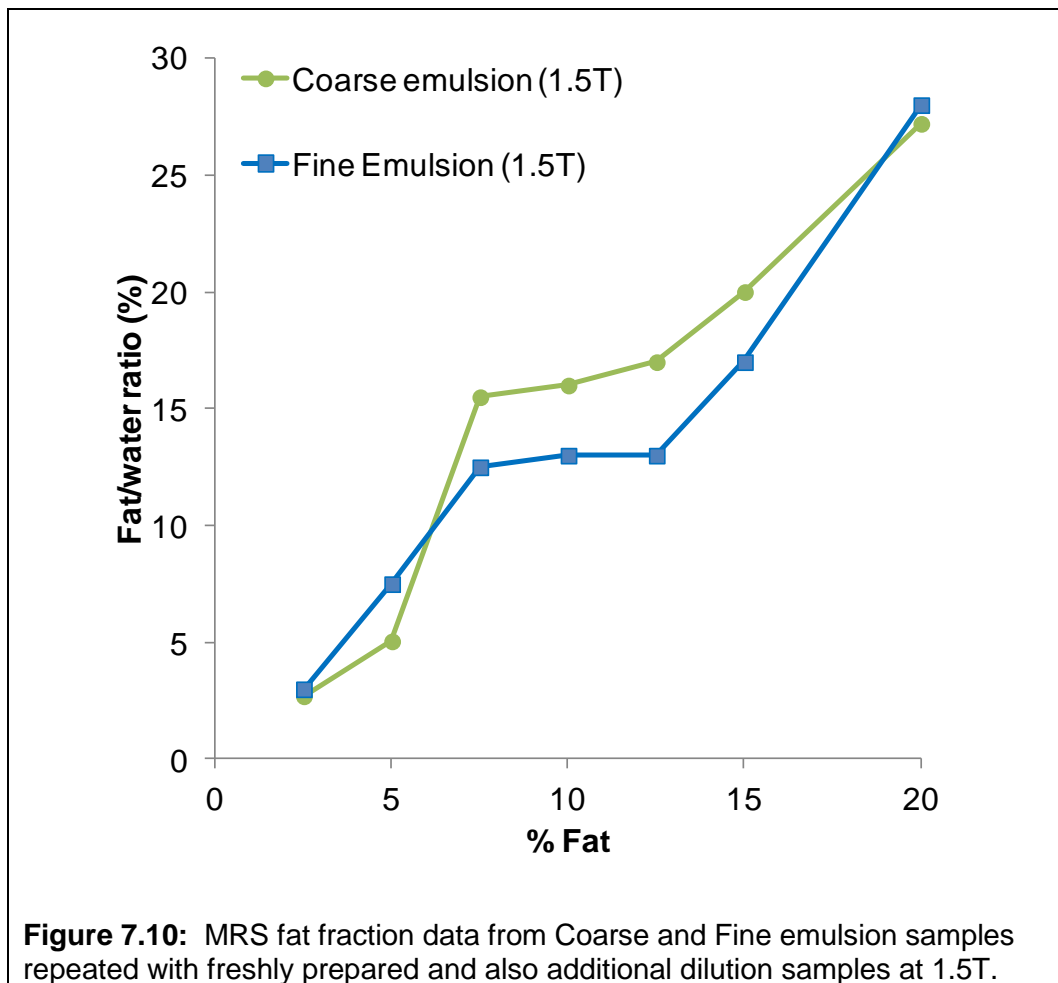


**Figure 7.10:** MRS fat fraction data from Coarse and Fine emulsion samples repeated with freshly prepared and also additional dilution samples at 1.5T.

#### 7.4 Discussion: *in vitro* study

As hypothesised there were both field and droplet size effects on  $T_2$  relaxation times of the Fine and the Coarse emulsions with the Fine emulsion having  $T_2$  values much longer than the Coarse at both 1.5T and 3T fields. The differences in  $T_2$  values between the 20% fat Fine and Coarse emulsions was encouraging and should be possible to detect *in vivo* as the effect size would likely be greater than increased variation due to imaging the gastrointestinal environment and motion although this remains to be assessed. For droplets sized greater than 3 microns there was not much difference in  $T_2$  at a given field which would make it difficult to detect changes in droplet size in that range. There was also an effect of fat fraction on  $T_2$ . These effects could be due to two mechanisms. One mechanism is droplet size effects whereby different size of the droplets results in different perturbation of the bulk water signal.  $T_2$  is changed by local field effects due to susceptibility and also because the  $T_2$  data are fitted to a single exponential when the relaxation is in effect multiexponential. This means that when the single exponential  $T_2$  of water is greater than the single exponential  $T_2$  of fat, if fat fraction increases then bulk  $T_2$  decreases. This was indeed seen in the *in vitro* data.

The  $T_1$  sequence that was used for this experiment was ProSet-fatsat (fat suppression). Comparison of two different  $T_1$  sequences saturating fat or water (ProSet\_watsat and ProSet\_fatsat) on both Fine and Coarse emulsions at 1.5T showed as expected a marked difference in  $T_1$  values between sequences but no droplet size effect.

The MRS data on fat/water ratio for both Coarse and Fine emulsion dilutions showed good correlation with known fat fraction and a field effect. In Figure

7.10 the MRS-derived fat fraction data seem to show a plateau at around 10% fat content for both Coarse and Fine emulsions. The reason for this plateau is unclear. These sample dilutions were all made individually from a 20% sample stock and following a printed (and re-checked) Excel file dilution plan, hence a systematic dilution mistake is unlikely. This plateau could reflect changes in field inhomogeneities created by fat droplet concentration (not size) and warrants further investigation as it could also be an artifact generated by a couple of points with high noise. Adding further dilution points either side of the 10% fat fraction would be beneficial to investigate this further. There is no major variation between the fat/fraction of these two emulsions, therefore there was no droplet size effect. However, it seemed the 1.5T was slightly over estimating the fat/water ratio whereas the 3T seemed to have more accurate fat fraction. Comparing this MRS data to the m-DIXON data *in vitro*, it can be concluded that MRS was more accurate to estimate the fat fraction of these fat emulsion samples than the m-DIXON data, although the MRS method lacks the 3D spatial resolution that is offered by the m-DIXON method. One possible explanation for discrepancies is also that the m-DIXON method may need a more sophisticated calibration using more data points.

## **7.5 *In vivo* study**

### **7.5.1 Aims and objectives**

The data gathered *in vitro* showed the complex interplay of fat fraction, field and droplet size effects on the MRI and MRS parameters. Based on this experience the next logical step was to evaluate these methods *in vivo* in the gastric environment. The small scale pilot study described below was designed primarily to assess feasibility of measurement methods. It aimed to

measure the spatial location and fraction of fat in the stomach comparing the m-DIXON high resolution MR imaging method with the standard MRS method. It also aimed to measure  $T_2$  relaxation times on the stomach contents to evaluate changes in  $T_2$  due to ingested (Fine and Coarse) droplet size and due to predicted changes in emulsification of the fine emulsion with time of digestion

### **7.5.2 Specific methods**

The two emulsions used for this study were the 20% fat Coarse (droplet size Mass Median Diameter range 12-15  $\mu\text{m}$ ) and Fine (droplet size Mass Median Diameter range 0.4-0.6  $\mu\text{m}$ ) emulsions with no gum stabiliser as described in Chapter 5. The LBG stabiliser was not added to these samples as the aim of this study was not to make physiological measurements requiring intragastric stability.

The study samples were previously approved by Unilever Safety and Environmental Assurance Centre (SEAC), approval reference number 95724. The composition here was the same as the previous study with only a change in the “off the shelf” food flavour (coffee flavouring) in concentrations below 1%. These samples have been deemed “low risk” by a SEAC expert for this study. Full Ethics approval was obtained from the local Ethics Committee and all subjects gave informed written consent.

Eight healthy male subjects with age  $25\pm 1$  years and Body Mass Index  $22.0\pm 0.4$   $\text{kg}/\text{m}^2$  were recruited. One subject was withdrawn as he presented with a stomach full of liquid and particulate at baseline as shown by fasted baseline MRI, despite stating at baseline checklist that he had not eaten any food or drunk any drink apart from water since 10pm the evening before. Another subject vomited the test meal on his first visit. The event was mild in

nature, possibly related to study procedures and was resolved quickly. Therefore the data presented are from N=6 subjects. A simple randomisation schedule was employed to avoid test product order effects. The two study days were approximately one week apart. The data for processing was renamed in a randomized way by a study-independent member of the investigator team according to standard operating procedures used also in the previous study. Hence following these procedures the author processed all data blind. The blind code was broken only when the study was finished and all data processed had undergone a blind data review.

On each study day MRI was carried at fasted baseline, immediately following consumption of the fat emulsion drink and every hour for the following 3 hours. All scans were acquired across the abdomen using the Philips 1.5T Achieva MR scanner and the 16-channel parallel imaging body receiver coil. The duration of each postprandial scan including set up was about 12 minutes. Two or three subjects were alternated throughout the test day. After each scan they were taken out of the scanner and asked to sit quietly in the volunteers' lounge.

At each time point the following scans were acquired:

Standard scouts scan to locate the abdominal organs. This was acquired during free-breathing and lasted less than a minute. A calibration scan to allow automated calibration of the parallel imaging was acquired during free-breathing and lasted 1 minute. One bTFE sequence across the stomach (as located from the scout scan) to measure gastric volumes: 40 transverse slices acquired in two 13s breath-holds, flip angle=80°, TR/TE=2.8/1.4ms, FOV=400mm, in plane resolution 1.56x1.56mm, slice thickness 7mm, SENSE factor 2.0. This sequence also helped planning the position of the subsequent volumes of interest for the spectroscopy. Proton spectroscopy (MRS) to determine intra-gastric fat fraction: one STEAM sequence (90°x90°x90°),

TR=4s, TE=9ms, 2 dummies, resolution =25x25x25mm<sup>3</sup>, spectral bandwidth 1000 Hz, 512 samples, 4 repeats in 24 s. This was acquired twice, once in the upper and once in the lower regions of the gastric lumen as identified on the bTFE images. Transverse m-DIXON sequence to determine intra-gastric fat fraction across whole stomach: 3D TFE double echo sequence with 400x370x150 mm<sup>3</sup> coverage, slice thickness 3 mm, in-plane resolution 1.49x1.95 mm<sup>2</sup>, FA = 15, TE1=1.8 ms TE2=4.0 ms TR = 5.4 ms, 1 average. Data were acquired in a single breath-hold (<20s). Data was then reconstructed to water-only, fat-only, in-phase and out-of-phase images. A single-slice T<sub>2</sub>-prepared bTFE sequence [120] to measure the relaxation time T<sub>2</sub> of the gastric contents: TR/TE = 3.0/1.5 ms, TEprep values (ms): 20, 29, 43, 63, 93, 137, 201, 295, 434, 637, resolution 2.00 mm x 1.56 mm and a slice thickness of 7 mm. For this sequence the volunteers held their breath only for a few seconds for each TEprep value, the whole measurement lasting a couple of minutes.

Measurements of gastric volumes and gallbladder volumes were carried out as described in previous chapters.

Within this section of this chapter the regions of interest drawn on different spatial locations in the gastric lumen will be referred to as:

- UP voxel = a region of interest drawn in the upper layer of the gastric contents
- DOWN voxel = a region of interest drawn in the lower layer of the gastric contents

For the spectroscopic data, the areas of the water and fat peaks were measured using in-house software written by Dr. Mary Stephenson, and lipid/water fat fraction ratios were calculated. Briefly, the operator corrects the baseline of the spectrum and marks the peaks to be integrated and the software yields the two integral values for the area under the peak of fat and

water. The m-DIXON provided water and fat only images. On these images regions of interest can be drawn using Analyze9 software (Biomedical Imaging Resource, Mayo Foundation, Rochester, MN, USA) summing across all the slices to determine the fat and water volume distribution at each time point.  $T_2$  data sets were processed, firstly using Analyze9 to generate a region of interest in the stomach contents. Then using the mean of this region at all the different echo times to calculate the  $T_2$  of the tissue using a in-house program written by Dr. Caroline Hoad which models the effect of the  $T_2$ -prepared scheme and subsequent imaging sequence for the  $T_2$  -prepared bTFE sequence as described and used previously [120, 121]. Briefly, the software fits the mean signal intensities in the regions of interest for  $T_2$  using a program which models the evolution of the magnetisation after each radiofrequency pulse used in the MRI sequence. The parameters fitted are  $T_2$ ,  $T_1$ ,  $M_0$  and an additional parameter  $\alpha$  (which is a measure of radiofrequency pulse imperfections).

The statistical analysis was carried out using GraphPad Prism version 5 (GraphPad software Inc., San Diego,CA, USA). The sample size is very small so non parametric Wilcoxon's matched paired signed rank test was used to test differences between areas under the curves (AUCs).

### **7.5.3 Emulsions characterisation**

Following the initial microbiological storage trial, the production process was cleared and subsequently the emulsions were prepared according to these approved SOPs. The droplet sizes were assessed for each sample (not batched, each sample was prepared individually and characterised individually for inclusion/rejection from the study) as soon as they were prepared. No rheology test was carried out during this preparation phase. Figure 7.11 below

shows the laser diffractometry profiles of Fine and Coarse emulsions. Droplet size data are reported in the Table 7.3 below.

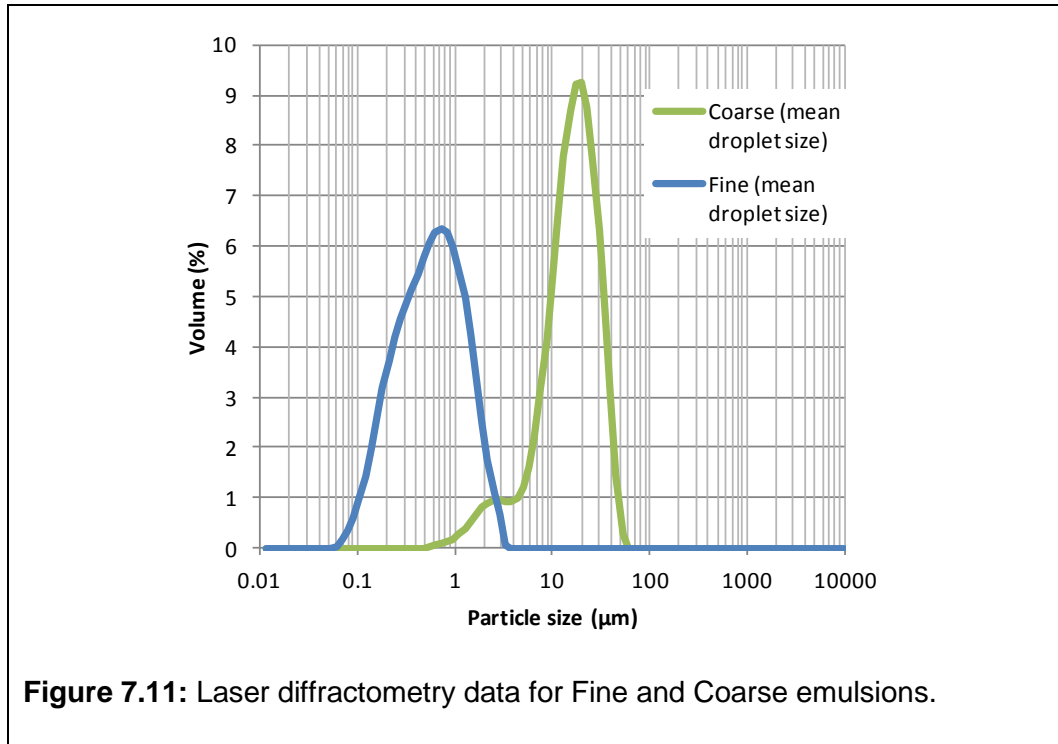
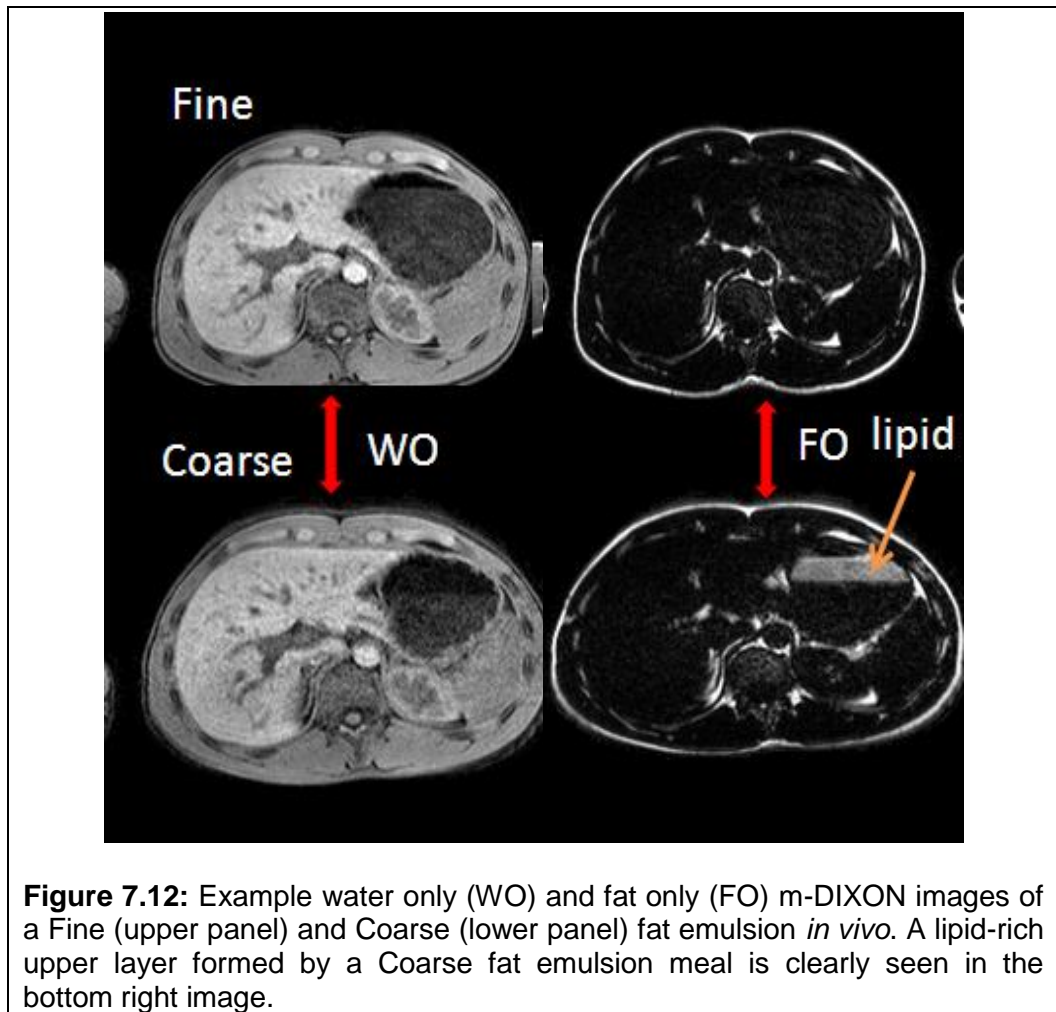


**Figure 7.11:** Laser diffractometry data for Fine and Coarse emulsions.

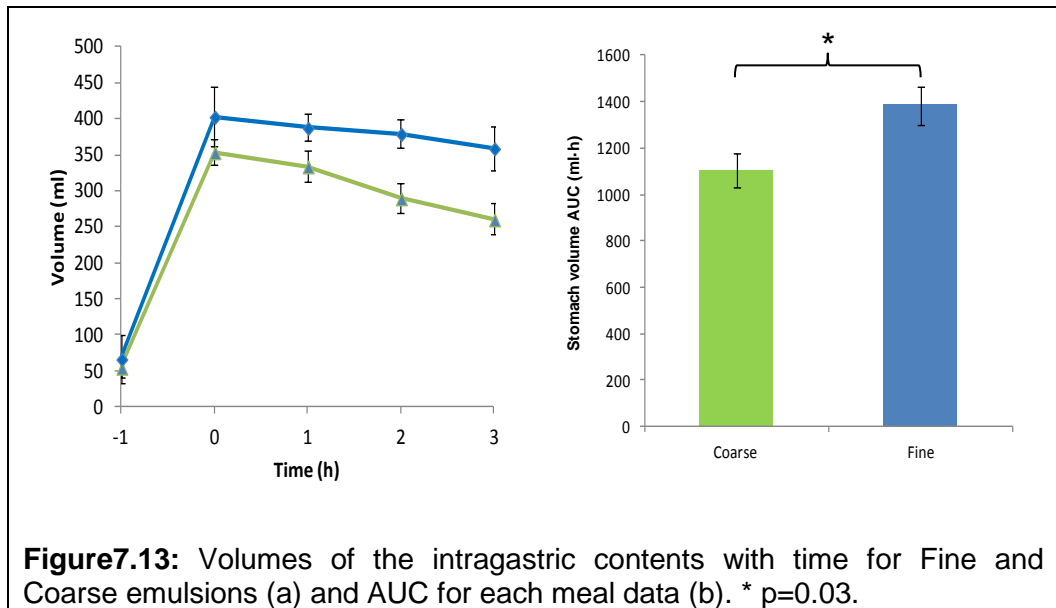
Measurements	Fine		Coarse	
	Mean (micron)	Standard deviation (+/-)	Mean (micron)	Standard deviation (+/-)
D [3, 2]	0.79	0.06	15.1	0.5
D [4, 3]	0.39	0.02	8.3	0.3
D [0, 5]	0.58	0.03	14.0	0.5

**Table 7.3:** Summary of laser diffractometry data for Fine and Coarse emulsions. The table reports the emulsion droplet size using the most commonly reported measures: D[3,2] (the surface area mean diameter), D[4, 3] (a volume mean diameter) and D[0,5] (a mass median diameter).



#### 7.5.4 Gastric emptying

Good quality images of the fat emulsion meals in the stomach were obtained as shown in Figure 7.12. The time courses of mean meal intragastric volumes are shown in Figure 7.13. It can be seen that the Fine emulsion emptied from the stomach slower than the Coarse. The corresponding mean AUCs are shown on the right panel. The AUCs were  $1104 \pm 72$  ml·h for the Coarse emulsion and  $1383 \pm 84$  ml·h for the Fine emulsion. The Fine emulsion significantly delayed gastric emptying ( $p=0.03$ ).



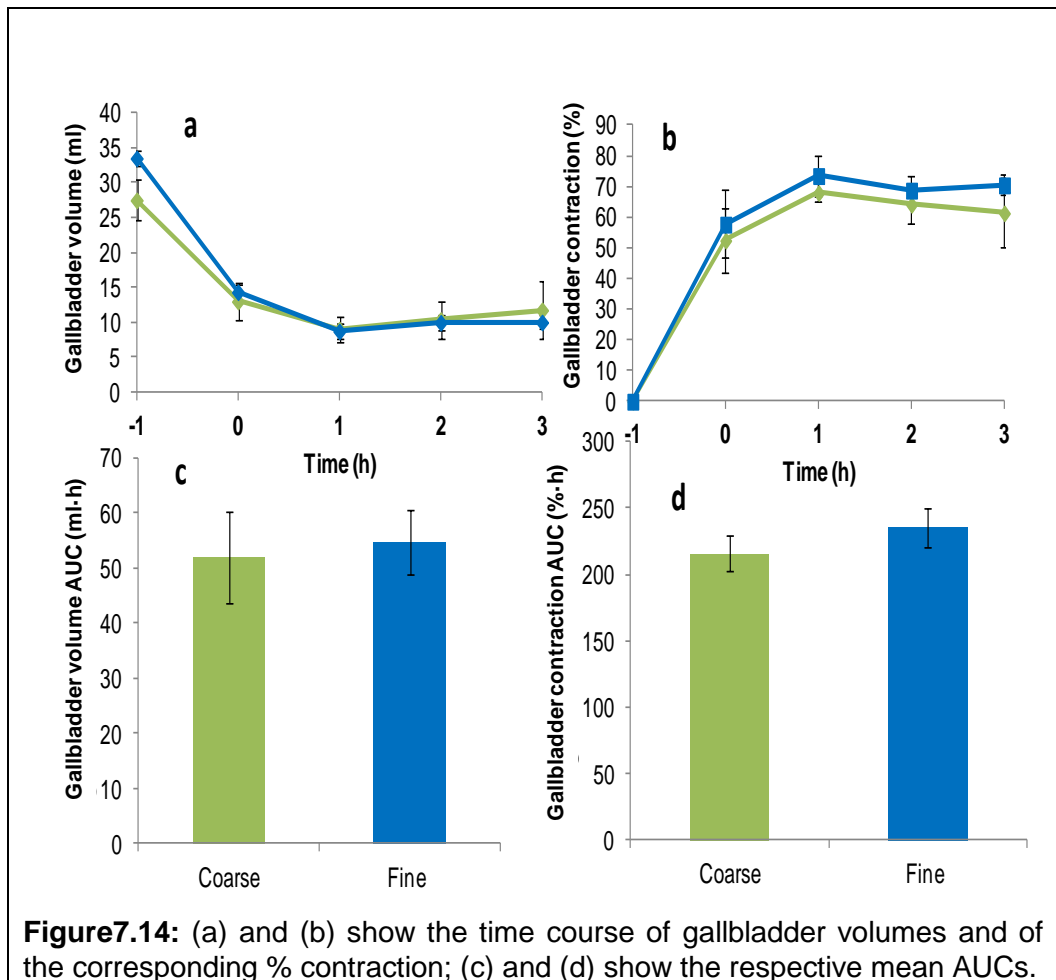
### 7.5.5 Gallbladder contraction

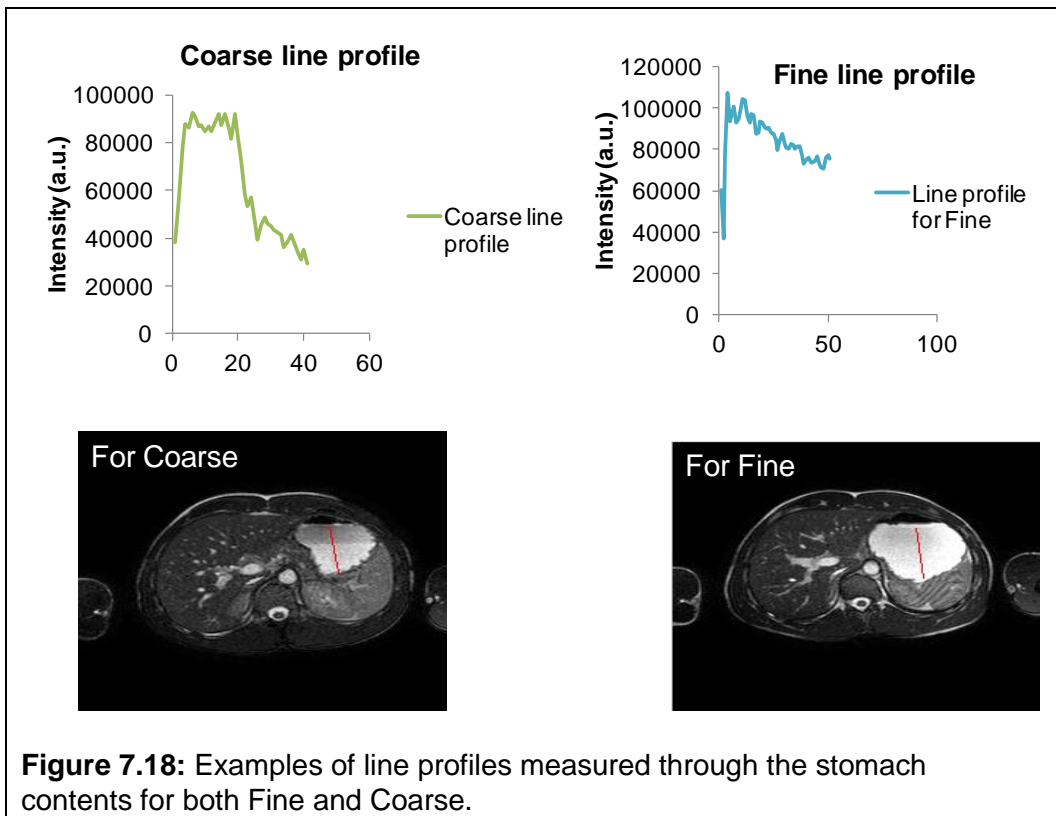
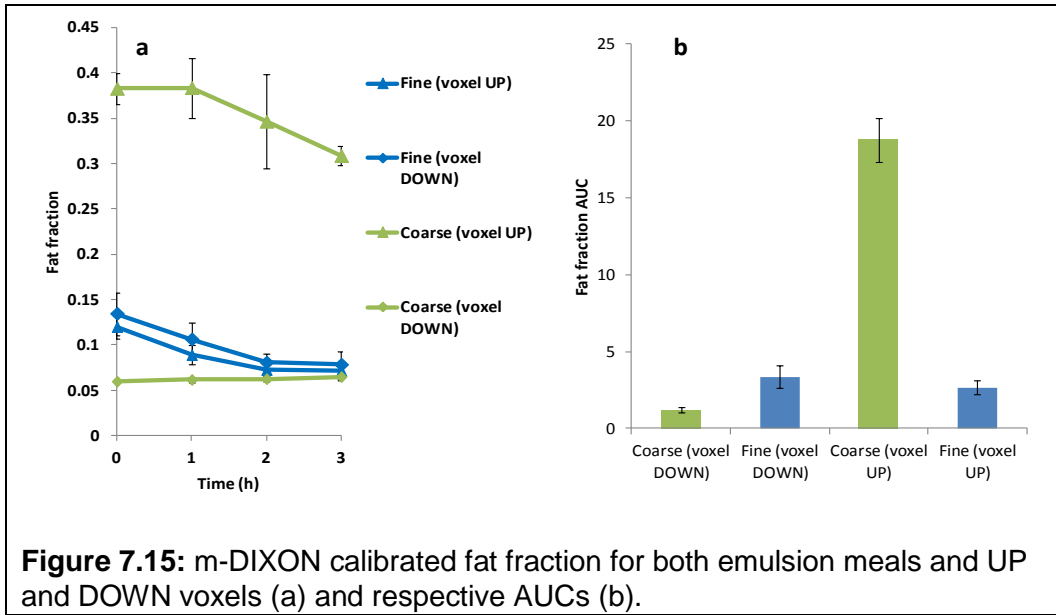
Although this was not a planned secondary outcome, the gallbladder volumes were measured in keeping with the previous study. The mean gallbladder volumes and % contraction plus their AUCs are plotted in Figure 7.14. The AUCs for gallbladder volumes were  $52 \pm 8$  ml·h for the Coarse emulsion and  $55 \pm 6$  ml·h for the Fine emulsions. There were no significant differences between meals ( $p=0.69$ ).

### 7.5.6 m-DIXON fat fraction

The m-DIXON fat fraction measurement was calibrated using *in vitro* data as reported in Appendix. There was a clear difference between the m-DIXON fat fraction for Fine and Coarse as shown in Figure 7.15. The pattern is very similar to the MRS data. The Coarse emulsion meal showed an immediate separation in an UP (upper) layer of high lipid/water ratio compared to a DOWN lower voxel at  $t=0$  whereby the fat fraction DOWN has markedly reduced (but it is not zero) ( $p=0.03$ ). There is no difference between Fine UP

and Fine DOWN ( $p=0.2$ ). There are significant differences between Fine and Coarse UP voxels ( $p=0.03$ ) and Fine and Coarse DOWN voxels ( $p=0.03$ ). THE m-DIXON datasets cover the whole stomach and allow not only region of interest but also line profile analysis as shown in Figure 7.18. Interestingly the line profiles (drawn from the bottom of the stomach upwards) seem to show a gradient for the Fine emulsion, which appears moderately darker towards the top. This could reflect a mild creaming effect whereby the upper parts of the stomach contain a more concentrated fat than the bottom. By contrast the Coarse profile showed a clear jump between the two phases.

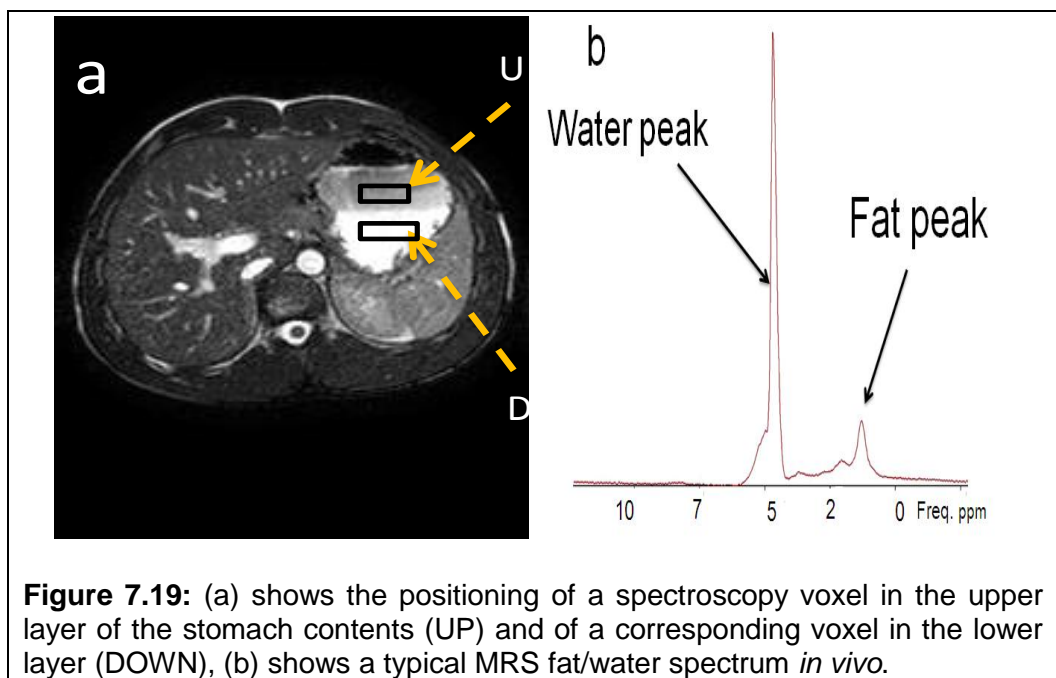




### 7.5.7 MRS fat fraction

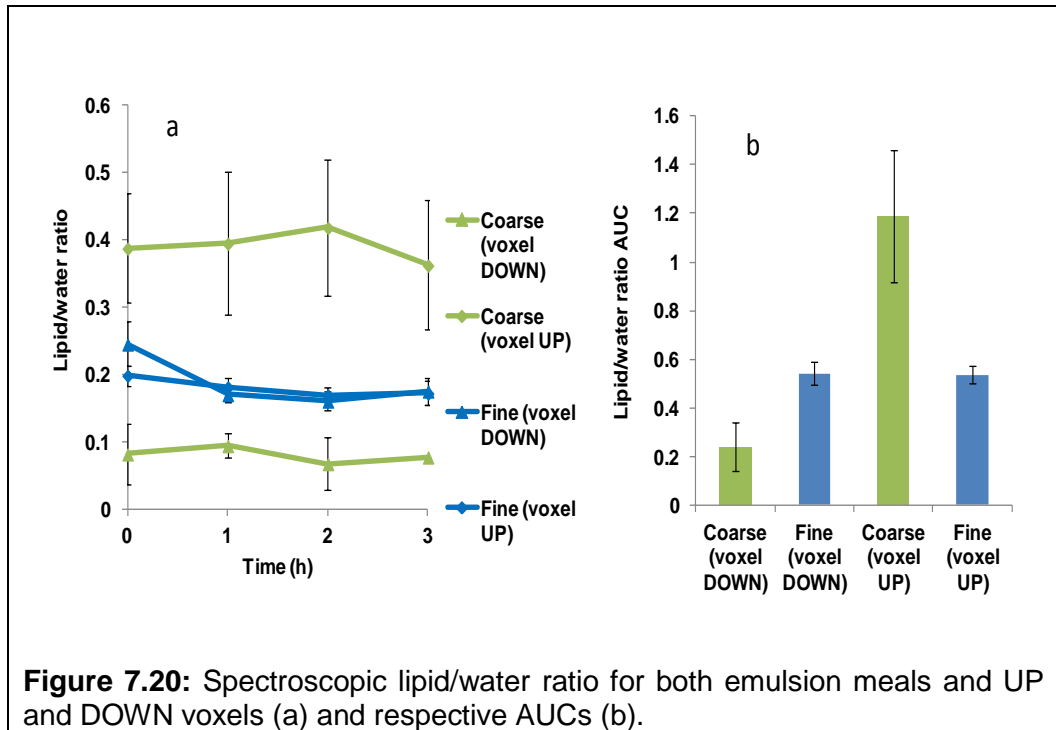
Figure 7.19 shows on the left an image of the stomach of a volunteer who had eaten a Coarse emulsion and the positioning of the UP and DOWN voxels in

the upper and lower layer of the stomach contents respectively. There was a clear difference in lipid/water ratio between Fine and Coarse as shown in Figure 7.20. The Coarse emulsion meal showed an immediate separation in an UP (upper) layer of high lipid/water ratio (around 0.4 which is double that of the original drink at 0.2) compared to a DOWN lower voxel whereby the fat fraction has more than halved (but it is not zero), the difference is just outside the significant threshold probably due to higher variability of the UP voxel values ( $p=0.06$ ). The fine emulsion fat fraction values remain close to 0.2 throughout with no difference between UP and DOWN voxels ( $p=1$ ). There are differences between Fine and Coarse UP voxels ( $p=0.09$ ) and Fine and Coarse DOWN voxels ( $p=0.09$ ) but these are outside the significance level.



The large error bars for the Coarse UP voxel have to be noted. This large variability is probably due to the fact that positioning the fixed size voxel in thinner upper layers could have been more difficult. Also, differences in holding the breath after the positioning axial images were taken could have

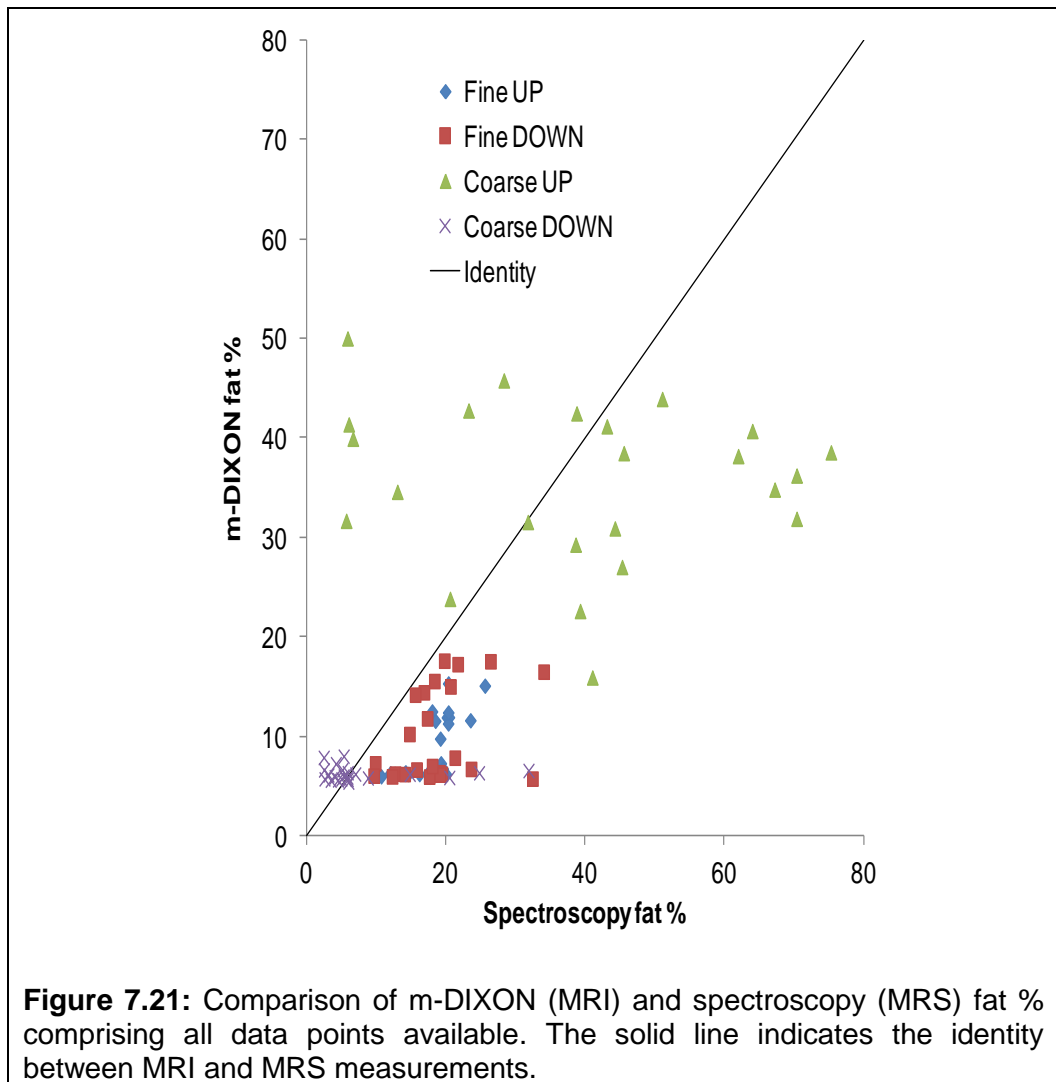
contributed to this variability. The size of the DOWN layer was usually greater therefore minimising these possibilities.

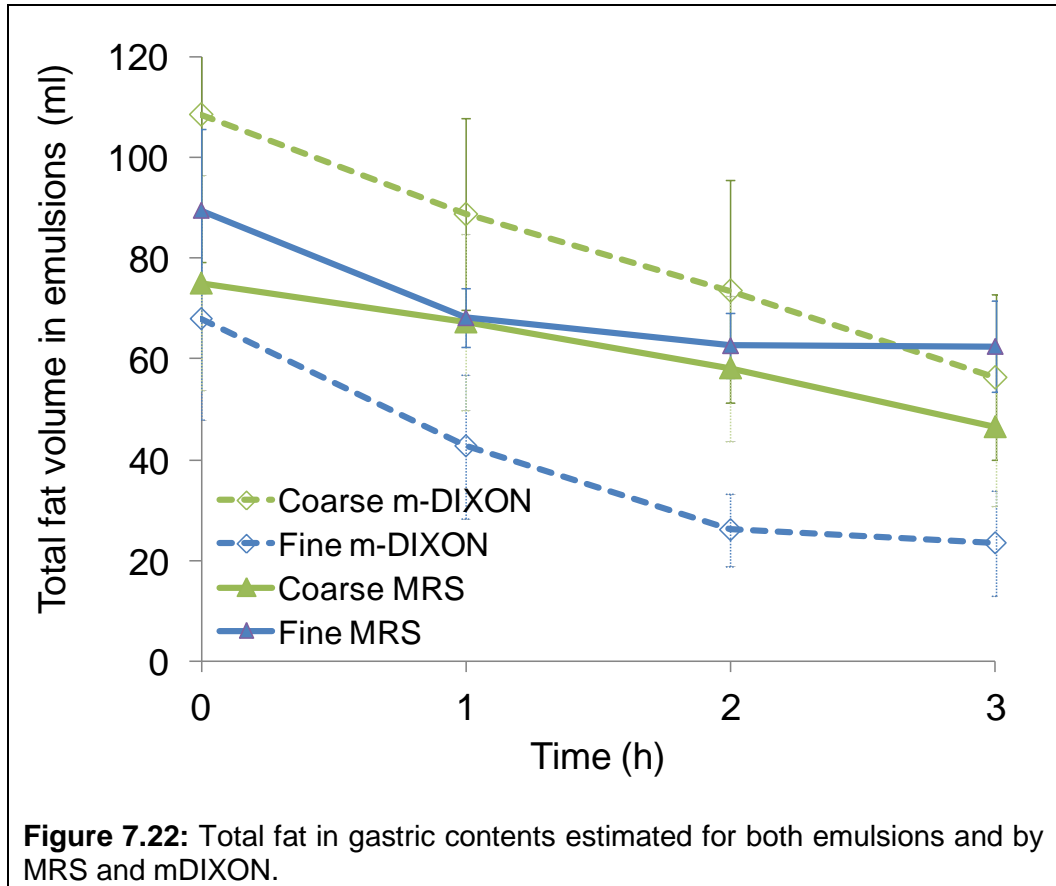


### 7.5.8 Comparison m-DIXON and MRS fat fractions

Plotting all m-DIXON fat % values against the corresponding spectroscopy data points as shown in Figure 7.21 yields a good correlation between the two methods (Spearman's  $r=0.6038$ ,  $p<0.0001$ ). A cluster of m-DIXON values around fat fraction 0.05 can be seen. These belong mostly to Coarse DOWN regions of interest but removing them does not improve greatly the correlation. Overall the graph suggests that at low fat % MRS was better at discriminating differences between voxels whilst m-DIXON was less sensitive. At higher fat % the data for Coarse UP are largely scattered which confirms once again the variability of that measurement on the MRS side, probably due to difficulties in positioning the acquisition voxel in the first place. At  $t=0$  the MRS measures of

total fat content of the stomach and the average fat fraction of the emulsion (Figure 7.22) agreed better with fat in ingested meal (assuming only small meal dilution at  $t=0$ ) than mDIXON measures. Interestingly the net rate of emptying of fat (calculated from volumes and MRS fat fractions) was fairly similar for both meals. Considering the different intragastric spatial distributions of these two emulsions without the LBG stabiliser this is not contradicting the difference in gastric (volume) emptying whereby the Coarse emulsion tends to empty more quickly a fat-depleted lower layer thus reducing gastric emptying times compared to a more stable Fine emulsion.





### 7.5.9 $T_2$ relaxation times *in vivo*

An example of the single slice images used to measure the  $T_2$  relaxation time on the gastric contents is shown in Figure 7.23. The mean transverse relaxation data for both Fine and Coarse and voxels UP and DOWN are shown in Figure 7.24. This shows that the DOWN voxels (e.g. the lower layers of the stomach contents for both emulsions) have much longer  $T_2$ s than the UP voxels (e.g. the upper layers of the stomach contents). The AUCs for the Fine emulsion were  $2600 \pm 500$  ms·h for the UP voxel and  $3600 \pm 400$  ms·h for the DOWN voxel ( $p=0.03$ ).

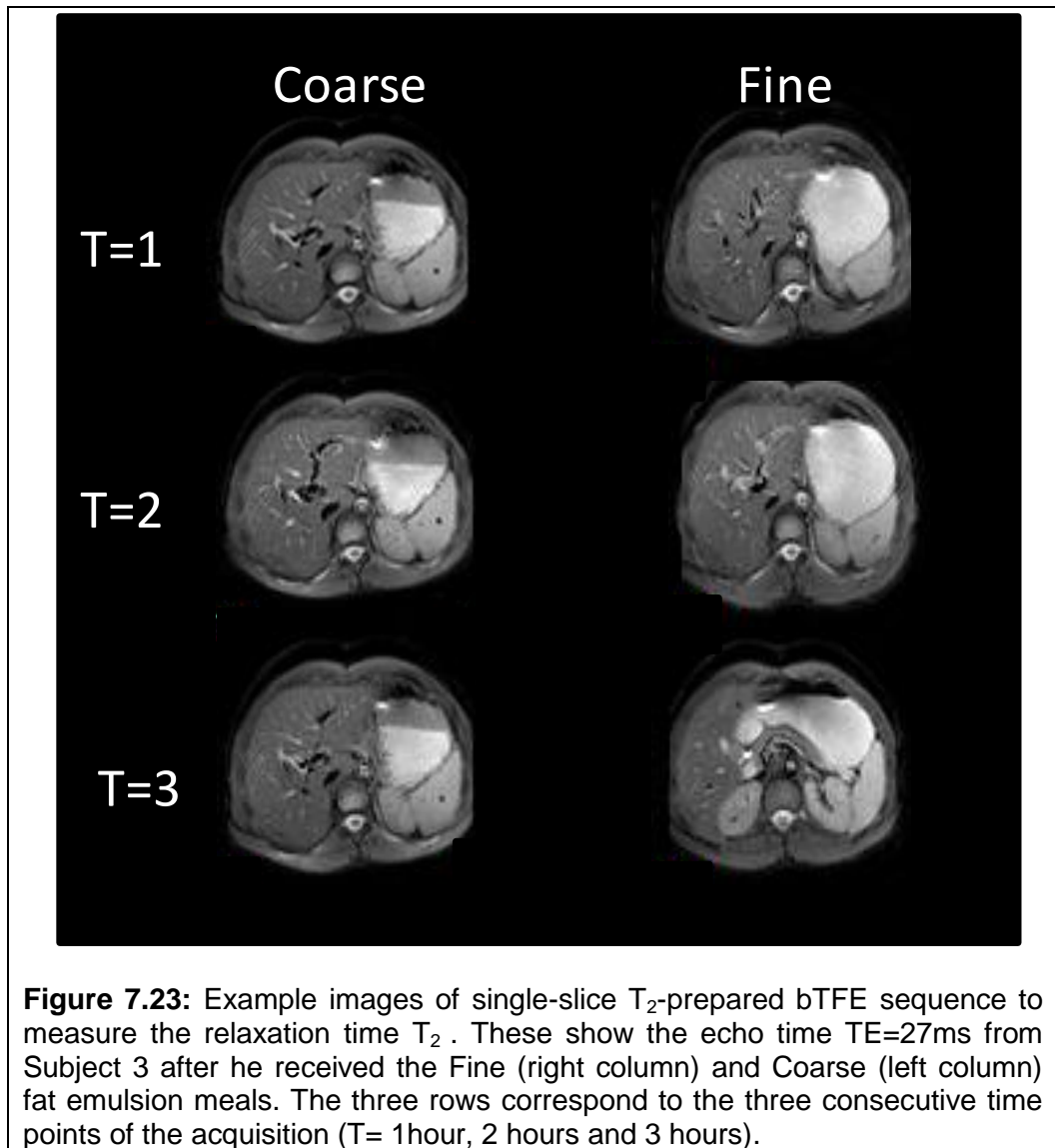
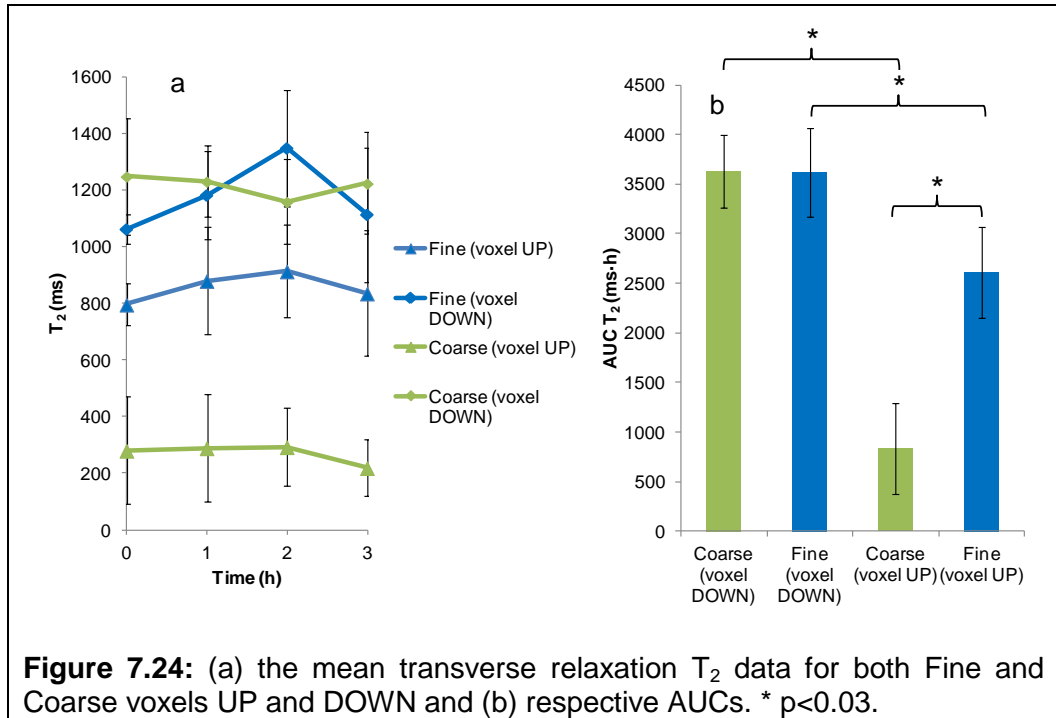


**Figure 7.23:** Example images of single-slice  $T_2$ -prepared bTFE sequence to measure the relaxation time  $T_2$ . These show the echo time  $TE=27ms$  from Subject 3 after he received the Fine (right column) and Coarse (left column) fat emulsion meals. The three rows correspond to the three consecutive time points of the acquisition ( $T= 1$ hour, 2 hours and 3 hours).

The AUCs for the Coarse emulsion were  $800\pm 500$  ms·h for the UP voxel and  $3600\pm 400$  ms·h for the DOWN voxel ( $p=0.03$ ). There was no difference between DOWN voxels ( $p=1$ ) for the two meals, whereas the main visible difference is between the UP voxels ( $p=0.03$ ), with the UP Coarse emulsion having a  $T_2$  of  $270\pm 80$  ms (average of all time points and all subjects) four times shorter than the UP Fine emulsion  $T_2$  of  $860\pm 80$  ms. The corresponding average  $T_2$  values DOWN were  $1180\pm 90$  ms for Fine and  $1220\pm 80$  ms for Coarse. There are no marked temporal changes in  $T_2$  for both emulsion meals and voxel positions.



## 7.6 Discussion: *in vivo* study

The overall aims of this pilot feasibility study were to compare MRS and m-DIXON fat fraction estimates *in vivo* and to observe variations in relaxation time  $T_2$  of the emulsions in the gastric lumen.

Gastric emptying was faster for the Coarse fat emulsion meal than for the Fine emulsion. This was predicted and it is in keeping with the results of the previous studies. This may be explained with both creaming of the Coarse emulsion fat to the top of the lumen away from the pylorus (leading to delivery to the small bowel of a fat-depleted watery phase during early gastric emptying) and to an effect of droplet size on gastric emptying (possibly reflecting increased activation of duodenal fat receptors by the more finely emulsified droplets which present a larger surface area for hydrolysis).

The m-DIXON measurement was successful in that it provided information on the 3D distribution of fat in the gastric lumen as opposed to MRS which has to use a single large voxel. It has to be noted that for m-

DIXON the errors on the Coarse UP measurement are much smaller than the corresponding spectroscopy error bars. This is likely due to the fact that the m-DIXON post-processing ROI can be aimed much more precisely than positioning *in vivo* a large spectroscopy voxel, which sometimes may include (due to motion or limited stomach volumes) other layers different from the desired one. High fat fractions are determined with the same calibration which did not have such concentrated samples to use so it is a linear assumption which may well be slightly inaccurate though the substance remains.

The MRS assessment of fat fraction was successful and showed large differences between the two emulsion meals. The Coarse emulsion results are very much in keeping with the 'Coarse Control' (exactly the same sample) results from the previous study described in Chapter 6.

A reasonable correlation between MRI m-DIXON method to determine fat fraction and the 'gold-standard' MRS spectroscopic method was found. A closer look at the cluster of low values measured on m-DIXON shows they mostly belong to DOWN region of interest measurements for the Coarse emulsion. The fact that these are lower than the MRS values may be due to the fact that the m-DIXON ROI on Analyze was smaller in size than the MRS voxel and on post-hoc processing on screen could be placed accurately just in the lower, fat depleted layer, thereby reflecting a much lower fat value than the MRS. In this respect the m-DIXON imaging method has advantages since it allows positioning of ROIs in the gastric lumen.

Additional information can be gained by comparing gastric emptying and fat fraction data. Gastric emptying of the Fine emulsion was significantly delayed compared to the coarse emulsion although the differential volume measurements showed that both the upper and lower layers of the gastric contents emptied steadily and MRS showed the fat content of the upper layer gradually reduced over 3 hours. Interestingly the net rate of emptying of fat

(calculated from volumes and MRS fat fractions) was similar for both meals (Figure 7.22).

The measurement of the transverse relaxation time  $T_2$  as a measure of droplet size was another endpoint for this study. The study was successful in detecting different relaxation times for different droplet sizes of 20% fat emulsions *in vitro*. There was little subsequent change, suggesting no marked changes in droplet size, but any changes were difficult to separate from creaming effects *in vivo*. Both fat emulsification (smaller droplet sizes) and emulsion dilution (smaller fat fractions) increase  $T_2$  making it difficult to separate clearly these effects from just relaxometry measures. It was possible to detect differences in  $T_2$  values between each emulsion between the upper and lower layer of the stomach contents. The relaxation times of the 'DOWN' voxels for both the Fine and the Coarse emulsions are higher than the 'UP' voxels. This is likely to be because of creaming of the emulsions. A higher fraction of mobile water (high water proton density) with lower fraction of oil would indeed yield a higher  $T_2$  value. Interestingly a marked difference in  $T_2$  values for the 'UP' voxels between emulsions was detected, with the Fine having  $T_2$  values 4 times longer than Coarse. This could be due to two mechanisms. One mechanism is droplet size effects whereby different size of the droplets results in different perturbation of the bulk water signal. Another mechanism is fat concentration whereby both the proton density (reduced amount of bulk water) and the effect of the more concentrated perturbers (fat droplets) will reduce  $T_2$ . The *in vitro* studies indeed showed an effect of increasing droplet size on reducing  $T_2$  and an effect of increasing fat fraction in reducing  $T_2$ . Overall therefore the study was successful in detecting intragastric  $T_2$  differences between the two emulsion meals. However the fact that the Coarse emulsion creamed up more than the Fine emulsion made it more difficult to separate *in vivo* the effect of creaming from the effect of

droplet size on  $T_2$ . No clear time trend in changing  $T_2$  with time of digestion was detected for either emulsion nor UP or DOWN voxels which suggests it was not possible here to detect effects of emulsification *in vivo*.

## 7.7 Conclusions

This chapter describes a pilot study aimed at evaluating *in vitro* and *in vivo* MRI imaging methods to assess fat fraction and relaxation times of two fat emulsion meals of different droplet size. The m-DIXON imaging method to determine the intragastric fat fraction of fat emulsion meals compared well with the 'gold standard' spectroscopic method but gave more spatial information since it provided three dimensional data on the whole stomach and allowed more flexible post-processing. The relaxometry data showed *in vitro* expected apparent differences in  $T_2$  between Fine and Coarse droplet size. Such differences were difficult to interpret *in vivo* due to combined effects of intragastric dilution and creaming. Further work is needed to achieve a comprehensive MRI based measurement package capable of monitoring both fat fraction and fat droplet size *in vivo* in the stomach. This would enable in the future to relate the microstructure and location of different fatty food formulations with, for example, the time it takes to empty from the stomach, the levels of hormones in the blood and the sensation of satiety, thus aiding the design of foods with desired health promoting characteristics and check their performance *in vivo*.

## 8 Conclusions

### 8.1 Brief summary of main findings

The main hypothesis underpinning this work was that fat emulsion droplet size has a profound effect on fat digestion and, in turn, on the gastrointestinal and satiety responses. To test this hypothesis two fat emulsion meal systems were used. The two fat emulsions had exactly the same composition but a small or a large emulsified fat droplet size was achieved using different homogenising methods. The two emulsions were termed the Fine emulsion (with a droplet size of 400 nm) and the Coarse emulsion (with a droplet size of 8 µm). The two fat emulsion systems were characterised using a range of bench techniques, *in vitro* digestion models and MRI techniques *in vitro*.

The microstructure difference caused, as predicted, different temporal creaming characteristics for the emulsions and different percentage hydrolysis profiles in a gastric digestion model *in vitro*. The Fine emulsion showed initial rapid hydrolysis whilst the Coarse emulsion showed an initial slow hydrolysis phase with the hydrolysis rate increasing at later stages. This indicated that there was indeed a droplet surface area (size) effect on fat hydrolysis whereby the smaller droplet size hydrolysed faster than a larger droplet size.

The emulsions' performance was finally tested *in vivo* in healthy volunteers using MRI in a series of pilot studies leading to a main physiological study. The fat emulsions provided good images *in vivo*. The pilot studies also indicated that creaming differences in the gastric lumen were a confounding factor that made the physiological responses more difficult to

dissect mechanistically. The two emulsion systems were therefore redesigned using a locust bean gum (LBG) thickener to stabilise them intragastrically so that the true effect of droplet size could be assessed. The gum-stabilised fat emulsion meals were characterized once again on the bench and in small pilot studies *in vivo* and they appeared stable throughout the gastric emptying process. This initial phase suggested that there was indeed an overall droplet size effect on hydrolysis and gastrointestinal responses to fat emulsion meals.

This was investigated in more depth in a major physiological and satiety study in healthy volunteers. This was a three-way study that used Coarse emulsion meals without and with LBG (i.e. emulsions with different intragastric creaming stability) and Fine+LBG emulsion meals (i.e. small droplet size compared to Coarse+LBG but same stability). In this complex study serial MR imaging and spectroscopy, blood sampling, <sup>13</sup>C breath test and also a final objective weighed meal satiety assessment were used. The results showed that a highly emulsified, intragastrically stable emulsion delayed gastric emptying, increased small bowel water content and reduced consumption of food at the end of the study day. The clear conclusion was that manipulating food microstructure especially intragastric stability and fat emulsion droplet size can influence human gastrointestinal physiology and satiety responses.

The final part of this work aimed to explore further magnetic resonance imaging, spectroscopy and relaxometry techniques to assess fat emulsion parameters *in vitro* and *in vivo* in the gastric lumen. Main static magnetic field and droplet size effects on T<sub>2</sub> relaxation times of the Fine and the Coarse emulsions were observed. T<sub>1</sub> was higher for the Coarse emulsion compared to the Fine emulsion, possibly due to surface area effects. T<sub>1</sub> values varied depending on imaging sequence used but showed no droplet size effect. There was reasonable correlation between m-DIXON and spectroscopy

methods to quantify fat fraction both *in vitro* and *in vivo*. Differences in  $T_2$  relaxation times for different droplet sizes of 20% fat emulsions were detected *in vitro*. These changes were however difficult to separate from creaming effects *in vivo* with a view of draw meaningful inferences on droplet sizes.

## **8.2 Advantages**

This work had clear advantages. One of the main strengths was the industrial and academic collaboration whereby leading food science research and development worked alongside state-of-the art in-body MRI imaging to generate novel insights on the gastrointestinal fate of foods. Another advantage was the use of MRI as imaging technique. MRI uses non-ionising radiation, has multi-planar, three dimensional, high resolution capability, an excellent contrast for tissue and liquid food components, and the capability to 'tune' this contrast differently depending on the sample of interest and to quantitate many different parameters in the same study session. The human studies were generally well tolerated and recruitment from the large campus population was never a problem.

## **8.3 Limitations**

This work also had some limitations. One limitation is the physiological variability of individual human healthy subjects. The studies were powered appropriately for the main outcomes however secondary outcomes would have benefitted from larger numbers of subjects due to variability. Another limitation is the horizontal imaging position which is necessary due to scanner configuration. In the supine position there is a risk that large floating creamed

fat layers may enter the duodenum first. Imaging the subjects moderately tilted helped prevent this. The high cost of these MRI serial studies was also an issue since the experimental design became more demanding as the project developed dramatically increasing the cost of the programme of work.

#### **8.4 Future directions**

As pointed out above, this project provided exceptional synergy between using model food systems developed and characterised with the unique know-how and laboratory equipment of a major food manufacturer's research department on the one side and cutting edge, in-body MRI imaging on the other. This needs to be further exploited to generate novel insights on mechanisms of digestion and satiety of food actives and novel food microstructures. Such insights could ultimately help manipulate food products microstructure (and monitor product performance) to enhance desired health-promoting effects.

The use of relaxometry to measure intragastric droplet size needs further exploration, possibly using fat emulsion systems that are more resistant to creaming such as the ones stabilised using LBG as shown in Chapter 6. However, intragastric dilution of the gum could itself affect  $T_2$  [11] so more work to find a more relaxation-independent intragastric stabilizer would also be needed.

From the MRI point of view the use of MRS to monitor gastrointestinal fate of foods is novel and should be pursued, possibly further along the gastrointestinal tract beyond the stomach. The availability of scanners with ultra-high field strength (7T) could then provide increased signal and enhanced contrast mechanisms (e.g. magnetic susceptibility or chemical exchange saturation transfer or CEST [122-124]) well worth exploring though

practical limitations such as the current difficulties with whole-body imaging at such high resonance frequencies, still need to be overcome fully.

## 9 References

1. Mansfield, P. and P.K. Grannell, NMR diffraction in solids. *Journal of Physics C: solid state physics*, 1973. 6: p. L422.
2. Lauterbur, P.C., Image formation by induced local interactions: examples employing nuclear magnetic resonance. *Nature*, 1973. 242(5394): p. 190-191.
3. Richardson, J.C., R.W. Bowtell, K. Mader, and C.D. Melia, Pharmaceutical applications of magnetic resonance imaging (MRI). *Advanced drug delivery reviews*, 2005. 57(8): p. 1191-1209.
4. Li, S.K., M. J Lizak, and E.K. Jeong, MRI in ocular drug delivery. *NMR in biomedicine*, 2008. 21(9): p. 941-956.
5. Hoad, C.L., L. Marciani, S. Foley, J.J. Totman, J. Wright, D. Bush, E.F. Cox, E. Campbell, R.C. Spiller, and P.A. Gowland, Non-invasive quantification of small bowel water content by MRI: a validation study. *Physics in Medicine and Biology*, 2007. 52(23): p. 6909-6922.
6. Lobo, D.N., P.O. Hendry, G. Rodrigues, L. Marciani, J.J. Totman, J.W. Wright, T. Preston, P. Gowland, R.C. Spiller, and K.C.H. Fearon, Gastric emptying of three liquid oral preoperative metabolic preconditioning regimens measured by magnetic resonance imaging in healthy adult volunteers: A randomised double-blind, crossover study. *Clinical Nutrition*, 2009. 28(6): p. 636-641.
7. Marciani, L., D. Bush, P. Wright, M. Wickham, B. Pick, J. Wright, R. Faulks, A. Fillery-Travis, R.C. Spiller, and P.A. Gowland, Monitoring of

## References

- gallbladder and gastric coordination by EPI. *Journal Of Magnetic Resonance Imaging*, 2005. 21(1): p. 82-85.
8. Marciani, L., E.F. Cox, C.L. Hoad, S. Pritchard, J.J. Totman, S. Foley, A. Mistry, S. Evans, P.A. Gowland, and R.C. Spiller, Postprandial changes in small bowel water content in healthy subjects and patients with irritable bowel syndrome. *Gastroenterology*, 2010. 138(2): p. 469-477.
  9. Marciani, L., P.A. Gowland, A. Fillery-Travis, P. Manoj, J. Wright, A. Smith, P. Young, R. Moore, and R.C. Spiller, Assessment of antral grinding of a model solid meal with echo- planar imaging. *American Journal of Physiology*, 2001. 280(5): p. G844-G849.
  10. Marciani, L., P.A. Gowland, R.C. Spiller, P. Manoj, R.J. Moore, P. Young, S. Al-Sahab, D. Bush, J. Wright, and A.J. Fillery-Travis, Gastric response to increased meal viscosity assessed by echo- planar magnetic resonance imaging in humans. *Journal of Nutrition*, 2000. 130(1): p. 122-127.
  11. Marciani, L., P.A. Gowland, R.C. Spiller, P. Manoj, R.J. Moore, P. Young, and A.J. Fillery-Travis, Effect of meal viscosity and nutrients on satiety, intragastric dilution, and emptying assessed by MRI. *American Journal of Physiology*, 2001. 280(6): p. G1227-G1233.
  12. Marciani, L., S.L. Little, J. Snee, N.S. Coleman, D.J. Tyler, J. Sykes, I.G. Jolliffe, P.W. Dettmar, R.C. Spiller, and P.A. Gowland, Echo-planar magnetic resonance imaging of Gaviscon alginate rafts in-vivo. *Journal of Pharmacy and Pharmacology*, 2002. 54(10): p. 1351-1356.
  13. Marciani, L., P. Manoj, B.P. Hills, R.J. Moore, P. Young, A. Fillery-Travis, R.C. Spiller, and P.A. Gowland, Echo-planar imaging relaxometry to measure the viscosity of a model meal. *Journal of Magnetic Resonance*, 1998. 135(1): p. 82-86.

## References

14. Marciani, L., P. Young, J. Wright, R. Moore, N. Coleman, P.A. Gowland, and R.C. Spiller, Antral motility measurements by magnetic resonance imaging. *Neurogastroenterology and Motility*, 2001. 13(5): p. 511-518.
15. Totman, J.J., L. Marciani, S. Foley, E. Campbell, C.L. Hoad, I.A. Macdonald, R.C. Spiller, and P.A. Gowland, Characterization of the time course of the superior mesenteric, abdominal aorta, internal carotid and vertebral arteries blood flow response to the oral glucose challenge test using magnetic resonance imaging. *Physiological Measurement*, 2009. 30(10): p. 1117-1136.
16. Hoad, C., P. Rayment, E. Cox, P. Wright, M. Butler, R. Spiller, and P. Gowland, Investigation of alginate beads for gastro-intestinal functionality, Part 2: In vivo characterisation. *Food Hydrocolloids*, 2009. 23(3): p. 833-839.
17. Hoad, C.L., P. Rayment, R.C. Spiller, L. Marciani, B.D. Alonso, C. Traynor, D.J. Mela, H.P.F. Peters, and P.A. Gowland, In vivo imaging of intragastric gelation and its effect on satiety in humans. *Journal of Nutrition*, 2004. 134(9): p. 2293-2300.
18. De Celis Alonso, B., P. Rayment, E. Ciampi, S. Ablett, L. Marciani, R.C. Spiller, I.T. Norton, and P.A. Gowland, NMR relaxometry and rheology of ionic and acid alginate gels. *Carbohydrate Polymers*, 2010. 82(3): p. 663-669.
19. Eldeghaidy, S., L. Marciani, F. McGlone, T. Hollowood, J. Hort, K. Head, A.J. Taylor, J. Busch, R.C. Spiller, P.A. Gowland, and S.T. Francis, The cortical response to the oral perception of fat emulsions and the effect of taster status. *Journal of Neurophysiology*, 2011. 105(5): p. 2572-2581.

## References

20. Hollowood, T., S. Bayarri, L. Marciani, J. Busch, S. Francis, R. Spiller, A. Taylor, and J. Hort, Modelling sweetness and texture perception in model emulsion systems. *European Food Research and Technology*, 2008. 227(2): p. 537-545.
21. Hort, J., S. Redureau, T. Hollowood, L. Marciani, S. Eldeghaidy, K. Head, J. Busch, R.C. Spiller, S. Francis, P.A. Gowland, and A.J. Taylor, The effect of body position on flavor release and perception: implications for fMRI studies. *Chemosensory Perception*, 2008. 1(4): p. 253-257.
22. Wright, P.J., E. Ciampi, C.L. Hoad, A.C. Weaver, M. van Ginkel, L. Marciani, P. Gowland, M.F. Butler, and P. Rayment, Investigation of alginate gel inhomogeneity in simulated gastro-intestinal conditions using magnetic resonance imaging and transmission electron microscopy. *Carbohydrate Polymers*, 2009. 77(2): p. 306-315.
23. Marciani, L., R. Faulks, M.S.J. Wickham, D. Bush, B. Pick, J. Wright, E.F. Cox, A. Fillery-Travis, P.A. Gowland, and R.C. Spiller, Effect of intragastric acid stability of fat emulsions on gastric emptying, plasma lipid profile and postprandial satiety. *British Journal of Nutrition*, 2009. 101(6): p. 919-928.
24. Marciani, L., C. Ramanathan, D.J. Tyler, P. Young, P. Manoj, M. Wickham, A. Fillery-Travis, R.C. Spiller, and P.A. Gowland, Fat emulsification measured using NMR transverse relaxation. *Journal of Magnetic Resonance*, 2001. 153(1): p. 1-6.
25. Marciani, L., M. Wickham, B.P. Hills, J. Wright, D. Bush, R. Faulks, A. Fillery-Travis, R.C. Spiller, and P.A. Gowland, Intragastric oil-in-water emulsion fat fraction measured using inversion recovery echo-planar magnetic resonance imaging. *Journal of Food Science*, 2004. 69(6): p. E290-E296.

## References

26. Marciani, L., M. Wickham, G. Singh, D. Bush, B. Pick, E. Cox, A. FilleryTravis, R. Faulks, C. Marsden, P.A. Gowland, and R.C. Spiller, Enhancement of intragastric acid stability of a fat emulsion meal delays gastric emptying, increases cholecystinin release and gallbladder contraction. *American Journal of Physiology*, 2007. 292: p. G1607-G1613.
27. Abragam, A., *Principles of nuclear magnetism*. 1961, Oxford: Oxford University Press.
28. Slichter, C.P., *Principles of magnetic resonance*. 1963, New York: Harper and Row.
29. Callaghan, P.T., *Principles of Nuclear Magnetic Resonance Microscopy*. 1993, Oxford: Oxford University Press.
30. Kumar, A., D. Welti, and R.R. Ernst, NMR Fourier zeugmatography. *Journal of Magnetic Resonance*, 1975. 18(1): p. 69-83.
31. Mansfield, P., Multi-planar image formation using NMR spin echoes. *Journal of Physics C: solid state physics*, 2001. 10(3): p. L55.
32. McRobbie, D.W., E.A. Moore, M.J. Graves, and M.R. Prince, *MRI from Picture to Proton*. 2002: Cambridge University Press.
33. Macfarlane, G.T. and S. Macfarlane, Human colonic microbiota: ecology, physiology and metabolic potential of intestinal bacteria. *Scandinavian Journal of Gastroenterology-Supplements*, 1997. 32(222): p. 3-9.
34. Morris, P.G., *Nuclear magnetic resonance imaging in medicine and biology*. 1986: Clarendon Press Oxford, UK.
35. Robitaille, P.M. and L. Berliner, *Ultra high field magnetic resonance imaging*. Vol. 26. 2006: Springer.

## References

36. Haacke, E.M., R.W. Brown, M.R. Thompson, and R. Venkatesan, *Magnetic resonance imaging: physical principles and sequence design*. Vol. 82. 1999: Wiley-Liss New York:.
37. Bernstein, M.A., K.F. King, and X.J. Zhou, *Handbook of MRI pulse sequences*. 2004: Academic Press.
38. Burtscher, I.M. and S. Holtas, Proton MR spectroscopy in clinical routine. *Journal of Magnetic Resonance Imaging*, 2001. 13(4): p. 560-567.
39. Fischbach, F. and H. Bruhn, Assessment of in vivo <sup>1</sup>H magnetic resonance spectroscopy in the liver: A review. *Liver International*, 2008. 28(3): p. 297-307.
40. Frahm, J., K.D. Merboldt, and W. Hanicke, Localized proton spectroscopy using stimulated echoes. *Journal of Magnetic Resonance*, 1987. 72(3): p. 502-508.
41. Brown, M.A. and R.C. Semelka, *MRI basic principles and applications*. 2010: Wiley-Blackwell.
42. Sanz, T. and H. Luyten, In vitro evaluation of genistein bioaccessibility from enriched custards. *Food Hydrocolloids*, 2007. 21(2): p. 203-211.
43. Bilt, A., D.J. McClements, and E.A. Decker, Oral physiology, mastication and food perception. *Designing functional foods: measuring and controlling food structure breakdown and nutrient absorption*, 2009: p. 3-37.
44. Vingerhoeds, M.H., T.B.J. Blijdenstein, F.D. Zoet, and G.A. van Aken, Emulsion flocculation induced by saliva and mucin. *Food Hydrocolloids*, 2005. 19(5): p. 915-922.
45. Sanz, T. and H. Luyten, Release, partitioning and stability of isoflavones from enriched custards during mouth, stomach and

## References

- intestine in vitro simulations. *Food Hydrocolloids*, 2006. 20(6): p. 892-900.
46. Michalski, M.C., Specific molecular and colloidal structures of milk fat affecting lipolysis, absorption and postprandial lipemia. *European Journal of Lipid Science and Technology*, 2009. 111(5): p. 413-431.
  47. Lundin, L., M. Golding, and T.J. Wooster, Understanding food structure and function in developing food for appetite control. *Nutrition & Dietetics*, 2008. 65: p. S79-S85.
  48. Kalantzi, L., K. Goumas, V. Kalioras, B. Abrahamsson, J.B. Dressman, and C. Reppas, Characterization of the human upper gastrointestinal contents under conditions simulating bioavailability/bioequivalence studies. *Pharmaceutical Research*, 2006. 23(1): p. 165-176.
  49. Ekmekcioglu, C., A physiological approach for preparing and conducting intestinal bioavailability studies using experimental systems. *Food Chemistry*, 2002. 76(2): p. 225-230.
  50. Pafumi, Y., D. Lairon, P.L. de la Porte, C. Juhel, J. Storch, M. Hamosh, and M. Armand, Mechanisms of inhibition of triacylglycerol hydrolysis by human gastric lipase. *Journal of Biological Chemistry*, 2002. 277(31): p. 28070-28079.
  51. Armand, M., Lipases and lipolysis in the human digestive tract: where do we stand? *Current Opinion in Clinical Nutrition & Metabolic Care*, 2007. 10(2): p. 156.
  52. Barrett, K.E. and S.J. Keely, Integrative physiology and pathophysiology of intestinal electrolyte transport. *Physiology of the Gastrointestinal Tract*, 2006. 4: p. 1931-1951.
  53. McClements, D.J. and Y. Li, Review of in vitro digestion models for rapid screening of emulsion-based systems. *Food & Function*. 1(1): p. 32-59.

## References

54. Cummings, J.H. and G.T. Macfarlane, The control and consequences of bacterial fermentation in the human colon. *Journal of Applied Microbiology*, 1991. 70(6): p. 443-459.
55. Cummings, J.H., Short chain fatty acids in the human colon. *Gut*, 1981. 22(9): p. 763-779.
56. Singh, H., A. Ye, and D. Horne, Structuring food emulsions in the gastrointestinal tract to modify lipid digestion. *Progress in Lipid Research*, 2009. 48(2): p. 92-100.
57. Gabriele, D., M. Migliori, R. Di Sanzo, C.O. Rossi, S.A. Ruffolo, and B. De Cindio, Characterisation of dairy emulsions by NMR and rheological techniques. *Food Hydrocolloids*, 2009. 23(3): p. 619-628.
58. Leal-Calderon, F., V. Schmitt, and J. Bibette, Double emulsions. *Emulsion Science-Basic Principles*, 2007: p. 173-199.
59. Brennan, I.M., K.L. Feltrin, M. Horowitz, A.J.P.M. Smout, J.H. Meyer, J. Wishart, and C. Feinle-Bisset, Evaluation of interactions between CCK and GLP-1 in their effects on appetite, energy intake, and antropyloroduodenal motility in healthy men. *American Journal of Physiology-Regulatory, Integrative and Comparative Physiology*, 2005. 288(6): p. R1477-R1485.
60. Feinle, C., T. Rades, B. Otto, and M. Fried, Fat digestion modulates gastrointestinal sensations induced by gastric distention and duodenal lipid in humans. *Gastroenterology*, 2001. 120(5): p. 1100-1107.
61. Feinle-Bisset, C., M. Patterson, M.A. Ghatei, S.R. Bloom, and M. Horowitz, Fat digestion is required for suppression of ghrelin and stimulation of peptide YY and pancreatic polypeptide secretion by intraduodenal lipid. *American Journal of Physiology-Endocrinology And Metabolism*, 2005. 289(6): p. E948-E953.

## References

62. Little, T.J. and C. Feinle-Bisset, Oral and gastrointestinal sensing of dietary fat and appetite regulation in humans: modification by diet and obesity. *Frontiers in neuroscience*. 4.
63. Armand, M., B. Pasquier, M. Andre, P. Borel, M. Senft, J. Peyrot, J. Salducci, H. Portugal, V. Jaussan, and D. Lairon, Digestion and absorption of 2 fat emulsions with different droplet sizes in the human digestive tract. *American Journal of Clinical Nutrition*, 1999. 70(6): p. 1096-1106.
64. Marciani, L., R. Faulks, M.S.J. Wickham, D. Bush, B. Pick, J. Wright, E.F. Cox, A. Fillery-Travis, P.A. Gowland, and R.C. Spiller, Effect of intragastric acid stability of fat emulsions on gastric emptying, plasma lipid profile and postprandial satiety. *British Journal of Nutrition*, 2009. 101(6): p. 919.
65. Hillery, A.M., A.W. Lloyd, and J. Swarbrick, *Drug delivery and targeting for pharmacists and pharmaceutical scientists*. 2001: Taylor & Francis.
66. Wilson, C.G. and N. Washington, The stomach: its role in oral drug delivery. *Physiological Pharmaceutical: Biological Barriers to Drug Absorption*. Chichester, UK: Ellis Horwood, 1989: p. 47-70.
67. Krupey, J., P. Gold, and S.O. Freedman, Physicochemical studies of the carcinoembryonic antigens of the human digestive system. *The Journal of experimental medicine*, 1968. 128(3): p. 387-398.
68. Bechgaard, H. and F.N. Christensen, Physiological factors and controlled release dosage forms. *Pharm. J*, 1982. 229: p. 373-376.
69. Stehling, M.K., D.F. Evans, G. Lamont, R.J. Ordidge, A.M. Howseman, B. Chapman, R. Coxon, P. Mansfield, J.D. Hardcastle, and R.E. Coupland, Gastrointestinal tract: dynamic MR studies with echo-planar imaging. *Radiology*, 1989. 171(1): p. 41-46.

## References

70. Evans, D.F., G. Lamont, M.K. Stehling, A.M. Blamire, P. Gibbs, R. Coxon, J.D. Hardcastle, and P. Mansfield, Prolonged monitoring of the upper gastrointestinal tract using echo planar magnetic resonance imaging. *Gut*, 1993. 34(6): p. 848-852.
71. Evans, D.F., M.K. Stehling, G. Lamont, R. Coxon, A.M. Howseman, R.J. Ordridge, J.D. Hardcastle, and P. Mansfield, Investigation of gastrointestinal motility with echo-planar magnetic resonance imaging (EPI). *Gut*, 1988. 29(10): p. A1452.
72. Evans, D.F., G. Lamont, M.K. Stehling, A.M. Blamire, P. Gibbs, R. Coxon, J.D. Hardcastle, and P. Mansfield, Prolonged Monitoring of the Upper Gastrointestinal-Tract Using Echo-Planar Magnetic-Resonance-Imaging. *Gut*, 1993. 34(6): p. 848-852.
73. Schwizer, W., R. Fraser, H. Maecke, K. Siebold, R. Funck, and M. Fried, Gd<sup>3+</sup>•DOTA as a gastrointestinal contrast agent for gastric emptying measurements with MRI. *Magnetic resonance in medicine*, 1994. 31(4): p. 388-393.
74. Boulby, P., P. Gowland, V. Adams, and R.C. Spiller, Use of echo planar imaging to demonstrate the effect of posture on the intragastric distribution and emptying of an oil/water meal. *Neurogastroenterology & Motility*, 1997. 9(1): p. 41-47.
75. Marciani, L., R. Faulks, M.S.J. Wickham, D. Bush, B. Pick, J. Wright, E.F. Cox, A. Fillery-Travis, P.A. Gowland, and R.C. Spiller, Effect of intragastric acid stability of fat emulsions on gastric emptying, plasma lipid profile and postprandial satiety. *British Journal of Nutrition*, 2009. 101(06): p. 919-928.
76. Marciani, L., P.A. Gowland, A. Fillery-Travis, P. Manoj, J. Wright, A. Smith, P. Young, R. Moore, and R.C. Spiller, Assessment of antral grinding of a model solid meal with echo-planar imaging. *American*

## References

- Journal of Physiology-Gastrointestinal and Liver Physiology, 2001. 280(5): p. G844-G849.
77. Marciani, L., P.A. Gowland, R.C. Spiller, P. Manoj, R.J. Moore, P. Young, S. Al-Sahab, D. Bush, J. Wright, and A.J. Fillery-Travis, Gastric response to increased meal viscosity assessed by echo-planar magnetic resonance imaging in humans. *The Journal of nutrition*, 2000. 130(1): p. 122-127.
78. Marciani, L., D. Bush, P. Wright, M. Wickham, B. Pick, J. Wright, R. Faulks, A. Fillery-Travis, R.C. Spiller, and P.A. Gowland, Monitoring of gallbladder and gastric coordination by EPI. *Journal of Magnetic Resonance Imaging*, 2005. 21(1): p. 82-85.
79. Marciani, L., M. Wickham, G. Singh, D. Bush, B. Pick, E. Cox, A. Fillery-Travis, R. Faulks, C. Marsden, and P.A. Gowland, Enhancement of intragastric acid stability of a fat emulsion meal delays gastric emptying and increases cholecystokinin release and gallbladder contraction. *American Journal of Physiology-Gastrointestinal and Liver Physiology*, 2007. 292(6): p. G1607-G1613.
80. Buffa, R., E. Solcia, and V.L. Go, Immunohistochemical identification of the cholecystokinin cell in the intestinal mucosa. *Gastroenterology*, 1976. 70(4): p. 528-532.
81. Dubois, P.M., C. Paulin, and J.A. Chayvialle, Identification of gastrin-secreting cells and cholecystokinin-secreting cells in the gastrointestinal tract of the human fetus and adult man. *Cell and tissue research*, 1976. 175(3): p. 351-356.
82. Liddle, R.A., Cholecystokinin cells. *Annual Review of Physiology*, 1997. 59(1): p. 221-242.
83. Hoad, C.L., L. Marciani, S. Foley, J.J. Totman, J. Wright, D. Bush, E.F. Cox, E. Campbell, R.C. Spiller, and P.A. Gowland, Non-invasive

## References

- quantification of small bowel water content by MRI: a validation study. *Physics in medicine and biology*, 2007. 52: p. 6909.
84. Marciani, L., Assessment of gastrointestinal motor functions by MRI: a comprehensive review. *Neurogastroenterology and Motility*, 2011. 23(5): p. 399-407.
85. Boulby, P., P. Gowland, V. Adams, and R.C. Spiller, Use of echo planar imaging to demonstrate the effect of posture on the intragastric distribution and emptying of an oil/water meal. *Neurogastroenterology and Motility*, 1997. 9(1): p. 41-47.
86. Gunstone, F.D., *Determination of the structure of fatty acids*, in *Recent Advances in the Chemistry and Biochemistry of Plant Lipids*, T. Galliard and E.I. Mercer, Editors. 1975, London Academic Press: London. p. 21-42.
87. Armand, M., P. Borel, B. Pasquier, C. Dubois, M. Senft, M. Andre, J. Peyrot, J. Salducci, and D. Lairon, Physicochemical characteristics of emulsions during fat digestion in human stomach and duodenum. *American Journal of Physiology-Gastrointestinal and Liver Physiology*, 1996. 271(1): p. G172-G183.
88. van Aken, G.A., Relating Food Emulsion Structure and Composition to the Way It Is Processed in the Gastrointestinal Tract and Physiological Responses: What Are the Opportunities? *Food Biophysics*. 5(4): p. 258-283.
89. Seimon, R.V., T. Wooster, B. Otto, M. Golding, L. Day, T.J. Little, M. Horowitz, P.M. Clifton, and C. Feinle-Bisset, The droplet size of intraduodenal fat emulsions influences antropyloroduodenal motility, hormone release, and appetite in healthy males. *The American journal of clinical nutrition*, 2009. 89(6): p. 1729-1736.

## References

90. Borel, P., M. Armand, P. Ythier, G. Dutot, C. Melin, M. Senft, H. Lafont, and D. Lairon, Hydrolysis of emulsions with different triglycerides and droplet sizes by gastric lipase in vitro. Effect on pancreatic lipase activity. *The Journal of Nutritional Biochemistry*, 1994. 5(3): p. 124-133.
91. Armand, M., B. Pasquier, M. Andre, P. Borel, M. Senft, J. Peyrot, J. Salducci, H. Portugal, V. Jaussan, and D. Lairon, Digestion and absorption of two fat emulsions with different droplet sizes in the human digestive tract. *American Journal of Clinical Nutrition*, 1999. 70(6): p. 1096-1106.
92. Cistola, D.P., J.A. Hamilton, D. Jackson, and D.M. Small, Ionization and phase behavior of fatty acids in water: application of the Gibbs phase rule. *Biochemistry*, 1988. 27(6): p. 1881-1888.
93. Reis, P., K. Holmberg, H. Watzke, M.E. Leser, and R. Miller, Lipases at interfaces: a review. *Advances in colloid and interface science*, 2009. 147: p. 237-250.
94. Cunningham, K.M., R.J. Baker, M. Horowitz, A.F. Maddox, M.A.L. Edelbroek, and B.E. Chatterton, Use of technetium-99m(V)thiocyanate to measure gastric emptying of fat. *Journal of Nuclear Medicine*, 1991. 32(5): p. 878-881.
95. Jian, R., N. Vigneron, Y. Najean, and J.J. Bernier, Gastric emptying and intragastric distribution of lipids in man - a new scintigraphic method of study. *Digestive Diseases and Sciences*, 1982. 27(8): p. 705-711.
96. Horowitz, M., K. Jones, M.A.L. Edelbroek, A. Smout, and N.W. Read, The effect of posture on gastric emptying and intragastric distribution of oil and aqueous meal components and appetite. *Gastroenterology*, 1993. 105(2): p. 382-390.

## References

97. Edelbroek, M., M. Horowitz, A. Maddox, and J. Bellen, Gastric emptying and intragastric distribution of oil in the presence of a liquid or a solid meal. *Journal of Nuclear Medicine*, 1992. 33(7): p. 1283-1290.
98. Boesch, C., J. Decombaz, J. Slotboom, and R. Kreis, Observation of intramyocellular lipids by means of H-1 magnetic resonance spectroscopy. *Proceedings of the Nutrition Society*, 1999. 58(4): p. 841-850.
99. Boesch, C., J. Machann, P. Vermathen, and F. Schick, Role of proton MR for the study of muscle lipid metabolism. *NMR in Biomedicine*, 2006. 19(7): p. 968-988.
100. Boesch, C., J. Slotboom, H. Hoppeler, and R. Kreis, In vivo determination of intra-myocellular lipids in human muscle by means of localized H-1-MR-spectroscopy. *Magnetic Resonance in Medicine*, 1997. 37(4): p. 484-493.
101. Howald, H., C. Boesch, R. Kreis, S. Matter, R. Billeter, B. Essen-Gustavsson, and H. Hoppeler, Content of intramyocellular lipids derived by electron microscopy, biochemical assays, and H-1-MR spectroscopy. *Journal of Applied Physiology*, 2002. 92(6): p. 2264-2272.
102. Schrauwen-Hinderling, V.B., M.K.C. Hesselhik, P. Schrauwen, and M.E. Kooij, Intramyocellular lipid content in human skeletal muscle. *Obesity*, 2006. 14(3): p. 357-367.
103. Torriani, M., B.J. Thomas, M.A. Bredella, and H. Ouellette, Intramyocellular lipid quantification: comparison between 3.0-and 1.5-T H-1-MRS. *Magnetic Resonance Imaging*, 2007. 25(7): p. 1105-1111.
104. Torriani, M., B.J. Thomas, E.F. Halpern, M.E. Jensen, D.I. Rosenthal, and W.E. Palmer, Intramyocellular lipid quantification: Repeatability with H-1 MR spectroscopy. *Radiology*, 2005. 236(2): p. 609-614.

## References

105. Weis, J., L. Johansson, F. Ortiz-Nieto, and H. Ahlstrom, Assessment of lipids in skeletal muscle by high-resolution spectroscopic imaging using fat as the internal standard: Comparison with water referenced spectroscopy. *Magnetic Resonance in Medicine*, 2008. 59(6): p. 1259-1265.
106. Weis, J., L. Johansson, F. Ortiz-Nieto, and H. Ahstrom, Assessment of Lipids in Skeletal Muscle by LCMoel and AMARES. *Journal of Magnetic Resonance Imaging*, 2009. 30(5): p. 1124-1129.
107. Dixon, W.T., Simple proton spectroscopic imaging. *Radiology*, 1984. 153(1): p. 189-194.
108. Bley, T.A., O. Wieben, C.J. Francois, J.H. Brittain, and S.B. Reeder, Fat and water magnetic resonance imaging. *Journal of Magnetic Resonance Imaging*, 2010. 31(1): p. 4-18.
109. Ma, J., Dixon techniques for water and fat imaging. *Journal of Magnetic Resonance Imaging*, 2008. 28(3): p. 543-558.
110. Eggers, H., B. Brendel, A. Duijndam, and G. Herigault, Dual-Echo Dixon Imaging with Flexible Choice of Echo Times. *Magnetic Resonance in Medicine*, 2011. 65(1): p. 96-107.
111. McLaughlin, J., Long-chain fatty acid sensing in the gastrointestinal tract. *Biochemical Society Transactions*, 2007. 35: p. 1199-1202.
112. Maljaars, P.W.J., H.P.F. Peters, A. Kodde, M. Geraedts, F.J. Troost, E. Haddeman, and A.A.M. Masclee, Length and site of the small intestine exposed to fat influences hunger and food intake. *British Journal of Nutrition*, 2011. 106(10): p. 1609-1615.
113. Golding, M., T.J. Wooster, L. Day, M. Xu, L. Lundin, J. Keogh, and P. Clifton, Impact of gastric structuring on the lipolysis of emulsified lipids. *Soft Matter*, 2011. 7(7): p. 3513-3523.

## References

114. Borel, P., M. Armand, B. Pasquier, M. Senft, G. Dutot, C. Melin, H. Lafont, and D. Lairon, Digestion and absorption of tube feeding emulsions with different droplet sizes and composition in the rat. *Journal of Parenteral and Enteral Nutrition*, 1994. 18(6): p. 534-543.
115. Seimon, R.V., T. Wooster, B. Otto, M. Golding, L. Day, T.J. Little, M. Horowitz, P.M. Clifton, and C. Feinle-Bisset, The droplet size of intraduodenal fat emulsions influences antropyloroduodenal motility, hormone release, and appetite in healthy males. *American Journal of Clinical Nutrition*, 2009. 89(6): p. 1729-1736.
116. Ledebøer, M., A.A.M. Masclee, I. Biemond, and C. Lamers, Differences in cholecystokinin release and gallbladder contraction between emulsified and nonemulsified long-chain triglycerides. *Journal of Parenteral and Enteral Nutrition*, 1999. 23(4): p. 203-206.
117. Kennan, R.P., J.H. Zhong, and J.C. Gore, Intravascular susceptibility contrast mechanisms in tissues. *Magnetic Resonance in Medicine*, 1994. 31(1): p. 9-21.
118. Muller, R.N., P. Gillis, F. Moyny, and A. Roch, Transverse relaxivity of particulate MRI contrast media: from theories to experiments. *Magnetic Resonance in Medicine*, 1991. 22(2): p. 178-182.
119. Weisskoff, R.M., C.S. Zuo, J.L. Boxerman, and B.R. Rosen, Microscopic susceptibility variation and transverse relaxation: theory and experiment. *Magnetic Resonance in Medicine*, 1994. 31(6): p. 601-610.
120. Hoad, C.L., E.F. Cox, and P.A. Gowland, Quantification of T2 in the abdomen at 3.0 T using a T2-prepared Balanced Turbo Field Echo sequence. *Magnetic Resonance in Medicine*, 2010. 63(2): p. 356-364.
121. Pregent, S., C.L. Hoad, E. Ciampi, M. Kirkland, E.F. Cox, L. Marciani, R.C. Spiller, M.F. Butler, P. Gowland, and P. Rayment, Investigation of

## References

- the behaviour of chitosan microparticles as pH responsive hydrogels in the gastro-intestinal tract using magnetic resonance imaging. *Food Hydrocolloids*, 2012. 26(1): p. 187-196.
122. Regatte, R.R. and M.E. Schweitzer, Novel contrast mechanisms at 3 Tesla and 7 Tesla. *Seminars in Musculoskeletal Radiology*, 2008. 12(3): p. 266-280.
123. van Zijl, P.C.M. and N.N. Yadav, Chemical Exchange Saturation Transfer (CEST): What is in a Name and What Isn't? *Magnetic Resonance in Medicine*, 2011. 65(4): p. 927-948.
124. Zhang, S.R., M. Merritt, D.E. Woessner, R.E. Lenkinski, and A.D. Sherry, PARACEST agents: Modulating MRI contrast via water proton exchange. *Accounts of Chemical Research*, 2003. 36(10): p. 783-790.

## 10 Appendix

### 10.1 Specific list of materials and equipment used in Unilever

- Sunflower Oil (KTC Edibles, cholesterol free) supplied by Anglian Oils Ltd, Bexwell, Norfolk, U.K.
- Distilled water (Food lab (A104A))
- Coffee Flavouring: Dr. Oetker (UK) Ltd., Sherburn-in-Elmet, Leeds LS25 6JA, England.
- Sweetener: Hermesetas gold (Sodium saccharin) (E 954), Tesco supermarket U.K.
- Tween20: Sigma Aldrich, Gillingham, U.K.
- LBG: GENU® GUM type RL-200Z locust bean gum, CP Kelco, Leatherhead, U.K.
- <sup>13</sup>C Octanoic acid: Octanoic acid (<sup>13</sup>C-marked) Euriso-Top, Parc des Algorithmes, Bâtiment Homère, Route de l'Orme, F-91194 Saint Aubin cedex, France .
- Balance: Sartorius Model LC4800P (Asset number: C910300)
- Silverson: Model L5R (Serial no: 20281)
- Ultra-Turrax: Model IKA T25BS2 (Serial no: 10.011161)
- Microfluidiser: Model 110S (Asset number: C2007072)
- Medi-Wipes, a hard surface disinfectant containing chlorhexidine (Boston Healthcare, Bedford, U.K).
- Glassware (Beakers, flask and bottles)

## **10.2 Detailed methods for preparation of emulsions**

### **10.2.1 Area and equipment cleaning**

The bench area used for the preparation of the emulsions is wiped down using Medi-Wipes, a hard surface disinfectant containing chlorhexidine (Boston Healthcare, Bedford, U.K.).

All glassware is checked for damage before use. Any damaged glassware is discarded immediately. If the glassware becomes damaged during the preparation of the emulsion, this will be discarded, the area will be cleaned and the emulsion re-prepared.

The ultra-turrax and Silverson heads are sterilised in boiling water before use.

The microfluidiser is cleaned according the relative SOP before use.

### **10.2.2 Preparation of 1% LBG Solution**

All glassware and utensils are sterilised using boiling water before use.

A weighing boat is wiped using Premi-wipes, a food safe, non-toxic disinfectant wipe (Shermond, Brighton, UK) and allowed to dry. 16 g LBG powder is weighed in a weighing boat.

The Operator boils ~2 litres of water and uses thermal gloves when handling hot objects. 1584g boiled water is weighed in a 2000ml plastic beaker.

The LBG is dispersed in 1584g boiling water whilst stirring using Silverson at full speed. The beaker is covered with aluminium foil whilst using the Silverson. Any aggregates are manually dissolved using clean spatula and

dispersed whilst stirring for 10 minutes with Silverson. The final solution concentration is 1% w/w LBG/water.

1600ml of this 1% LBG solution will be stored in a 2000ml Borosil bottle

The operator cools the glass bottle down rapidly by placing in an ice bath and then stores the glass bottle in the A104 fridge until use for a maximum of 4 weeks.

### **10.2.3 Preparation of coarse emulsion with no LBG (Coarse Control)**

- 1 All glassware and utensils are sterilised using boiling water before use
- 2 H<sub>2</sub>O (276.5g) +Tween0 (3.5g)
- 3 Using a dedicated precision pipette (serviced and calibrated on an annual basis by an external contractor), 117 mg <sup>13</sup>C-octanoic acid is added to the SFO (70g) and the bottle is swirled gently to ensure the label is well mixed with the SFO.
- 4 The beaker is covered with a foil and the mixture is ultra-turraxed for 20 minutes at speed 3
- 5 The emulsion is transferred to a labelled 500ml new glass bottle.
- 6 3.5g of coffee flavour and 5 sweetener tablets was added to this emulsion and mixed well by shaking if necessary.
- 7 The emulsion is then stored in the A104 fridge located in the food laboratory for a maximum 4 days until it is shipped to Nottingham.

### **10.2.4 Preparation of the fine emulsion**

To obtain a fine emulsion steps (1-4 as above) to prepare coarse emulsion, then step (5) was used where the emulsion is passed through the Microfluidizer once, with a pressure of 2.6 bars at the inlet, which corresponds

to 605.8 bars in the interaction chamber and steps (6 and 7) was repeated as above coarse.

### 10.2.5 Preparation of the coarse emulsion with 0.5% LBG

- 1 All glassware and utensils are sterilised using boiling water before use.
- 2 H<sub>2</sub>O (241.5g) + Tween20 (3.5g) + 1% LBG stock solution (175g) solution are placed in 600ml glass beaker and mixed well using a spatula (due to thickness of the solution).

Materials	Weight	%
Distilled water	276.5g	79
Sunflower Oil	70g	20
Tween20	3.5g	1
Coffee flavour	3.5g	1
sweetener	5 tablets	-
<sup>13</sup> C-octanoic acid	117 mg	-

**Table 10.1:** Summary of the ingredients of coarse emulsion with no LBG

- 3 Using a precision pipette (serviced and calibrated on an annual basis by an external contractor), 117 mg <sup>13</sup>C-octanoic acid is added to the SFO (70g) and the bottle is swirled gently to ensure the label is well mixed with the SFO

Materials	Weight	%
Distilled water	101.50g	29
1% LBG solution	175.0g	50
Sunflower Oil	70g	20
Tween20	3.5g	1
Coffee flavour	3.5g	1
sweetener	5 tablets	-
<sup>13</sup> C-octanoic acid	117 mg	-

**Table 10.2:** Summary of the ingredients of coarse emulsion with 0.5% LBG and fine emulsion with LBG

- 4 The beaker is covered with a foil and the mixture is ultra-turraxed for 5 minutes at speed 2.
- 5 The emulsion is transferred to a labelled 500ml new glass bottle
- 6 3.5g of coffee flavour and 5 sweetener tablets is added to this emulsion and mixed well by shaking.
- 7 The emulsion is then stored in the A104 fridge (for a maximum of 4 days) until it is shipped to Nottingham.

#### 10.2.6 Preparation of the fine emulsion with 0.5% LBG (Fine+LBG)

To obtain a fine emulsion with LBG steps (1-4 as above) to prepare coarse emulsion with LBG, then step (5) was used where the emulsion is passed through the Microfluidizer once, with a pressure of 2.6 bars at the inlet, which corresponds to 605.8 bars in the interaction chamber and steps (6 and 7) was repeated as above coarse with LBG prep.

Appendix

More specifically, the Table 10.3 below shows a comprehensive list of contents of the study products:

Ingredient	Concentration in sample (%)	Weight per emulsion	Additional Information	Supplier
Octanoic acid ( <sup>13</sup> C-marked)	0.03%	100mg	<i>In vivo</i> breath test labels	Euriso-Top Parc des Algorithmes Bâtiment Homère, Route de l'Orme F-91194 Saint Aubin cedex France
Sunflower oil	20%	60g	Food ingredient.	Anglian Oils Ltd, Bexwell, Norfolk, U.K.
Supercook coffee flavour	1%	3g	Flavour; food ingredient. Ingredients: Water, Alcohol, colour: Plain	Dr. Oetker (UK) Ltd., Sherburn-in-Elmet, Leeds LS25 6JA, England

## Appendix

			caramel; Flavouring.	
Locust Bean Gum (GENU® GUM type RL-200Z)	0.5%	1.5g	Food thickener	CPKelco, Leatherhead, U.K.
Hermestas gold (Sodium saccharin) (E 954)	5 tablets in 350 g		Sweetener (sodium saccharin)	Tesco Supermarkets UK
Tween 20 (Polysorbat 20) (E 432)	1%	3g	Emulsifier	Sigma Aldrich, Gillingham, U.K.
Water		237 g for emulsion without LBG and 235.5g for emulsion with LBG	De-ionised water (Elga water purification system)	

**Table 10.3:** list of ingredients contained in the study products